REGULATION OF LIPID METABOLISM IN ADIPOSE TISSUE AND SKELETAL MUSCLE

EDITED BY: Zhihao Jia, Seung-Hyun Ro and Tizhong Shan
PUBLISHED IN: Frontiers in Physiology and Frontiers in Endocrinology

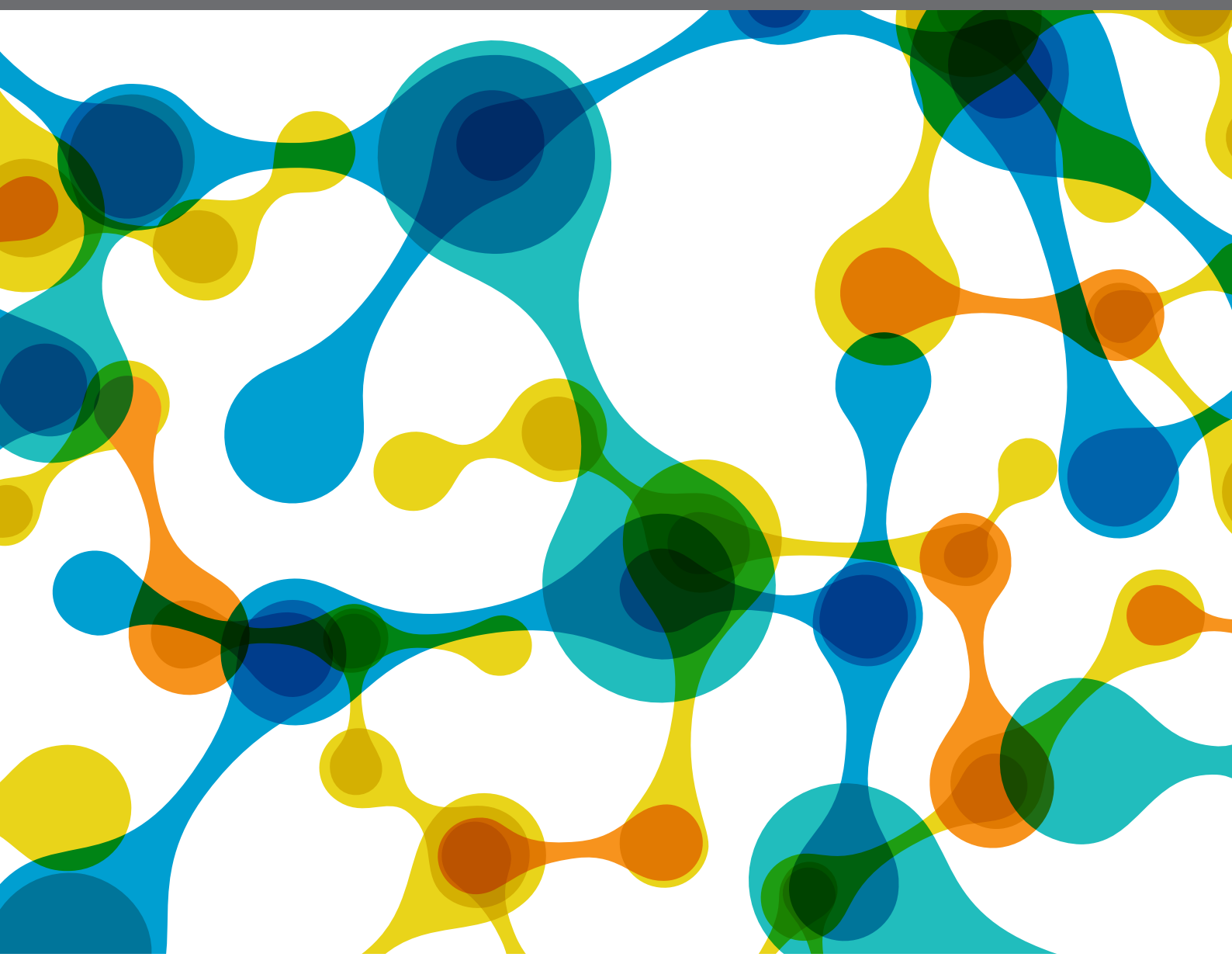

frontiers Research Topics

frontiers

Frontiers eBook Copyright Statement

The copyright in the text of individual articles in this eBook is the property of their respective authors or their respective institutions or funders. The copyright in graphics and images within each article may be subject to copyright of other parties. In both cases this is subject to a license granted to Frontiers.

The compilation of articles constituting this eBook is the property of Frontiers.

Each article within this eBook, and the eBook itself, are published under the most recent version of the Creative Commons CC-BY licence. The version current at the date of publication of this eBook is CC-BY 4.0. If the CC-BY licence is updated, the licence granted by Frontiers is automatically updated to the new version.

When exercising any right under the CC-BY licence, Frontiers must be attributed as the original publisher of the article or eBook, as applicable.

Authors have the responsibility of ensuring that any graphics or other materials which are the property of others may be included in the CC-BY licence, but this should be checked before relying on the CC-BY licence to reproduce those materials. Any copyright notices relating to those materials must be complied with.

Copyright and source acknowledgement notices may not be removed and must be displayed in any copy, derivative work or partial copy which includes the elements in question.

All copyright, and all rights therein, are protected by national and international copyright laws. The above represents a summary only. For further information please read Frontiers' Conditions for Website Use and Copyright Statement, and the applicable CC-BY licence.

ISSN 1664-8714
ISBN 978-2-83250-762-9
DOI 10.3389/978-2-83250-762-9

About Frontiers

Frontiers is more than just an open-access publisher of scholarly articles: it is a pioneering approach to the world of academia, radically improving the way scholarly research is managed. The grand vision of Frontiers is a world where all people have an equal opportunity to seek, share and generate knowledge. Frontiers provides immediate and permanent online open access to all its publications, but this alone is not enough to realize our grand goals.

Frontiers Journal Series

The Frontiers Journal Series is a multi-tier and interdisciplinary set of open-access, online journals, promising a paradigm shift from the current review, selection and dissemination processes in academic publishing. All Frontiers journals are driven by researchers for researchers; therefore, they constitute a service to the scholarly community. At the same time, the Frontiers Journal Series operates on a revolutionary invention, the tiered publishing system, initially addressing specific communities of scholars, and gradually climbing up to broader public understanding, thus serving the interests of the lay society, too.

Dedication to Quality

Each Frontiers article is a landmark of the highest quality, thanks to genuinely collaborative interactions between authors and review editors, who include some of the world's best academicians. Research must be certified by peers before entering a stream of knowledge that may eventually reach the public - and shape society; therefore, Frontiers only applies the most rigorous and unbiased reviews.
Frontiers revolutionizes research publishing by freely delivering the most outstanding research, evaluated with no bias from both the academic and social point of view. By applying the most advanced information technologies, Frontiers is catapulting scholarly publishing into a new generation.

What are Frontiers Research Topics?

Frontiers Research Topics are very popular trademarks of the Frontiers Journals Series: they are collections of at least ten articles, all centered on a particular subject. With their unique mix of varied contributions from Original Research to Review Articles, Frontiers Research Topics unify the most influential researchers, the latest key findings and historical advances in a hot research area! Find out more on how to host your own Frontiers Research Topic or contribute to one as an author by contacting the Frontiers Editorial Office: frontiersin.org/about/contact

REGULATION OF LIPID METABOLISM IN ADIPOSE TISSUE AND SKELETAL MUSCLE

Topic Editors:
Zhihao Jia, Purdue University, United States
Seung-Hyun Ro, University of Nebraska-Lincoln, United States
Tizhong Shan, Zhejiang University, China

Citation: Jia, Z., Ro, S.-H., Shan, T., eds. (2022). Regulation of Lipid Metabolism in Adipose Tissue and Skeletal Muscle. Lausanne: Frontiers Media SA.
doi: 10.3389/978-2-83250-762-9

Table of Contents

frontiers | Frontiers in Physiology

TYPE Editorial
PUBLISHED 04 November 2022
DOI 10.3389/fphys.2022.1010578

Check for updates

OPEN ACCESS

EDITED AND REVIEWED BY
John D. Imig,
University of Arkansas for Medical Sciences, United States

*CORRESPONDENCE
Zhihao Jia,
zhjia@suda.edu.cn
Tizhong Shan,
tzshan@zju.edu.cn

SPECIALTY SECTION
This article was submitted to Lipid and Fatty Acid Research, a section of the journal Frontiers in Physiology

RECEIVED 03 August 2022
ACCEPTED 13 October 2022
PUBLISHED 04 November 2022

CITATION
Jia Z and Shan T (2022), Editorial: Regulation of lipid metabolism in adipose tissue and skeletal muscle. *Front. Physiol.* 13:1010578. doi: 10.3389/fphys.2022.1010578

COPYRIGHT
© 2022 Jia and Shan. This is an open-access article distributed under the terms of the Creative Commons Attribution License (CC BY). The use, distribution or reproduction in other forums is permitted, provided the original author(s) and the copyright owner(s) are credited and that the original publication in this journal is cited, in accordance with accepted academic practice. No use, distribution or reproduction is permitted which does not comply with these terms.

Editorial: Regulation of lipid metabolism in adipose tissue and skeletal muscle

Zhihao Jia[1,2]* and Tizhong Shan[3,4,5]*

[1]Cambridge-Suda Genomic Resource Center, Suzhou Medical College, Soochow University, Suzhou, China, [2]Department of Animal Sciences, Purdue University, West Lafayette, IN, United States, [3]College of Animal Sciences, Hangzhou, China, [4]Key Laboratory of Molecular Animal Nutrition, Ministry of Education, Zhejiang University, Hangzhou, China, [5]Key Laboratory of Animal Feed and Nutrition of Zhejiang Province, Hangzhou, China

KEYWORDS

lipid metabolism, adipose tissue, skeletal muscle, metabolic disorder, T2D

Editorial on the Research Topic
Regulation of lipid metabolism in adipose tissue and skeletal muscle

Introduction

Obesity due to excessive deposition of lipids in adipose tissue (AT) has become a global epidemic. Obesity and its increased risks of chronic diseases including Type 2 Diabetes (T2D), chronic inflammation, hypertension, and cancer have posed formidable challenges to human health. Adipocytes are highly plastic and can uptake, esterificate, and store excess lipids in the form of triacylglycerols (TAG) within lipid droplets (LDs), as well as undergo lipolysis to provide energy when nutrition is limited. Non-AT such as skeletal muscle, which has a comparatively high capacity for fatty acid oxidation to generate energy, becomes dysfunctional with "lipid overload". Thus, the dysregulation of lipid metabolism in skeletal muscle highly contributes to obese-related insulin resistance. Thus, understanding how lipid storage and utilization are regulated in AT and skeletal muscle is critical for the development of therapeutics to overcome obesity. Indeed, interventions that increase AT/muscle fatty acid oxidation and/or limit lipid storage have been postulated as therapies for treating obesity-related conditions. Besides, lipid metabolism in AT and skeletal muscle are also closely associated with growth performance, meat quality, and reproduction in livestock farming. Therefore, this Research Topic aims to compile articles that expand our understanding of the lipid metabolism processes within the AT and skeletal muscle.

Beige/brown adipocyte thermogenesis

There are three types of adipocytes: brown adipocyte, white adipocyte, and beige adipocyte. Brown and beige adipocyte dissipate glucose and fatty acid (FA) to generate heat and play important roles in cold- and diet-induced thermogenesis (Kajimura et al., 2015). Therefore, genetically and pharmaceutically activation of beige/brown adipocyte has drawn great attention in the treatment of metabolic diseases. Li et al. analyze and compare the transcriptomics of AT after chronic cold exposure and β3-AR agonist CL316,243 (CL) administration. The results reveal that cold and CL treatment both upregulates genes in lipid metabolism and TCA cycle pathways. CL treatment uniquely activates genes in carbohydrate mobilization, while cold uniquely promotes genes in glycolipid and specific amino acids metabolism. In addition, cold and CL treatment could separately suppress different inflammatory pathways. In particular, cold specifically inhibits fibrotic programs.

Lipoprotein lipase (LPL) expressed by brown adipocyte play a central role in lipid metabolism by processing triglyceride-rich lipoproteins (TRL). Thiemann et al. observe that *Lpl* is also expressed by endothelial cells in cold-activated brown adipose tissue (BAT). By using a VE-cadherin (*Cdh5*)-Cre to drive the knockout of *lpl*, they demonstrate that endothelial *Lpl* is dispensable for lipoprotein handling and adaptive thermogenesis. The authors hypothesize that a compensatory high expression of LPL in brown adipocyte may enhance BAT TRL disposal in this model, but the mechanism remains unclear.

In another interesting review, Bruder et al. discuss the potential physiological purposes of postnatal AT remodeling. They state that postnatal AT remodeling is an ideal model process to investigate beige/brown adipocyte thermogenesis since there is less external manipulation.

Epigenetic regulation

In the condition of overnutrition, AT is able to expand in two ways: Hyperplasia that is dependent on increasing adipocyte number through adipogenesis and hypertrophy by enlargement of adipocyte cell size (Ghaben and Scherer, 2019). Notably, targeting adipogenesis is now emerging for the treatment of obesity. Interest in the epigenetic roles of non-coding RNAs during adipogenesis has been growing rapidly (Sun et al., 2013). Zhang et al. review the recent advances in long non-coding RNAs (lncRNAs) that regulate AT development and metabolism. In particular, they summarize the potential involvement of lncRNAs in metabolic disorders and prospect the potential of targeting lncRNAs in the treatment of obesity and metabolic diseases by using antisense oligonucleotides (ASO). Besides non-coding RNA, RNA m6A methylation (m6A) also plays many aspects in various diseases (He and He, 2021). Wang et al. introduce the up-to-date research advances between m6A and lipid metabolism, especially those within non-alcoholic fatty liver disease (NAFLD), diabetes, and cardiovascular diseases. This review provides insights into the possibilities that modify RNA m6A methylation in the fight against metabolic diseases.

Circular RNA (circRNA) is a newly discovered type of non-coding RNAs that participates in numerous cellular processes. Zhang et al. perform RNA-sequencing and identify 3,711 circRNAs at different stages of adipogenesis (preadipocyte, differentiating preadipocyte, and mature adipocyte). They find that many circRNAs share similar expression patterns with their parental genes. In addition, they discover multiple microRNA (miRNA) binding sites from the differential expressed circRNAs, which indicates that crircRNAs may act as miRNA sponges. However, the function of circRNA during adipogenesis requires to be further evaluated.

Disease-relevant study

Besides its role in energy storage, AT also contributes to systemic metabolism as an endocrine organ, especially through the secretion of adipokines (Fasshauer and Blüher, 2015). Ji et al. review the role of retinol-binding protein 4 (RBP4) in lipid metabolism and highlight the emerging importance of RBP4 with cardiovascular diseases (CVDs). By comparing published datasets, they predict that RBP4 might not only be a new biomarker for CVD, but targeting RBP4 preserves therapeutic potentials.

For years, scientists have been investigating antihyperglycemic drugs to protect against tissue damage in T2D (Verma and McMurray, 2018). The administration of a sodium-glucose cotransporter 2 inhibitor (SGLT2i) has been proven as a candidate therapy for hyperglycemia in T2D patients (Chao and Henry, 2010). Nagayama et al. extend the application of SGLT2i to incomplete acquired lipodystrophy. They report a case wherein a patient is treated with a combination of metreleptin supplementation and SGLT2i to improve hyperglycemia and insulin sensitivity. This study provides the potential benefits of using SGLT2i for non-obese diabetic patients.

Skeletal muscle metabolism

The skeletal muscle is the largest metabolic organ in the body and is extremely important for energy homeostasis (Sheffield-Moore and Urban, 2004). Antony et al. investigate the role of UCHL1 in skeletal muscle lipid metabolism. They observe that in fasting or glucose starvation conditions, UCHL1 protein levels are decreased in both skeletal muscle and differentiated myotubes. Muscle-specific *Uchl1* knockout reduces lipid

content and improves glucose tolerance, which may be correlated with the stabilization of Perilipin 2. In another research article on patients with spinal cord injury (SCI), Goldsmith et al. show that increased visceral adiposity, and inflammatory signaling, as well as reduced testosterone levels, predict mitochondrial dysfunction in these patients. However, due to the restriction in patient size of the current study, it remains unclear the complex causal relationships among those factors with chronic SCI. To better address the limitations more effectively, a large multi-centered trial is highly warranted.

Comparative studies

In addition to its association with human health, lipid metabolism in AT and skeletal muscle are also extremely popular among non-medical researchers, especially for those working in agriculture. Conserved signaling pathways that govern adipose and skeletal muscle development and metabolism have been investigated in agricultural animals, such as liver kinase B1 (LKB1) (Shan et al., 2014; Shan et al., 2016). Xiong et al. report a role of LKB1 in goat intramuscular preadipocytes differentiation *via* the focal adhesion kinase (FAK) pathway. The results indicate that targeting LKB1 might be a potential strategy to manipulate intramuscular fat deposition to improve the meat quality of goat. Pig farming requires stale temperature control as piglets lack the ability for thermogenesis. For this purpose, Xu et al. explore the effect of acute cold exposure on carcass indicators, enzyme activity, fatty acid composition, and gene expression profiles in the longissimus dorsi muscle (LDM) of growing-finishing pigs. The results suggest that chronic cold exposure significantly changes fatty acid profile and lipid metabolism, which emphasizes the importance of pre-slaughter temperature conditions in the fatty acid metabolism of pork. However, no difference is found in the content of amino acids, which needs to be further investigated in a longer time of cold treatment.

Conclusion

In sum, the 12 articles in this Research Topic are representative of the depth content of lipid metabolism in AT and skeletal muscle, as well as their application in metabolic diseases. Results from the aforementioned articles could help better unravel the selective and specific biomarkers and therapeutic targets of various metabolic diseases.

Author contributions

All authors listed have made a substantial, direct, and intellectual contribution to the work and approved it for publication.

Conflict of interest

The authors declare that the research was conducted in the absence of any commercial or financial relationships that could be construed as a potential conflict of interest.

Publisher's note

All claims expressed in this article are solely those of the authors and do not necessarily represent those of their affiliated organizations, or those of the publisher, the editors and the reviewers. Any product that may be evaluated in this article, or claim that may be made by its manufacturer, is not guaranteed or endorsed by the publisher.

References

Chao, E. C., and Henry, R. R. (2010). SGLT2 inhibition—A novel strategy for diabetes treatment. *Nat. Rev. Drug Discov.* 9, 551–559. doi:10.1038/nrd3180

Fasshauer, M., and Blüher, M. (2015). Adipokines in health and disease. *Trends Pharmacol. Sci.* 36, 461–470. doi:10.1016/j.tips.2015.04.014

Ghaben, A. L., and Scherer, P. E. (2019). Adipogenesis and metabolic health. *Nat. Rev. Mol. Cell Biol.* 20, 242–258. doi:10.1038/s41580-018-0093-z

He, P. C., and He, C. (2021). m6A RNA methylation: from mechanisms to therapeutic potential. *EMBO J.* 40, e105977. doi:10.15252/embj.2020105977

Kajimura, S., Spiegelman, B. M., and Seale, P. (2015). Brown and beige fat: Physiological roles beyond heat generation. *Cell Metab.* 22, 546–559. doi:10.1016/j.cmet.2015.09.007

Shan, T., Xiong, Y., Zhang, P., Li, Z., Jiang, Q., Bi, P., et al. (2016). Lkb1 controls Brown adipose tissue growth and thermogenesis by regulating the intracellular localization of CRTC3. *Nat. Commun.* 7, 12205–12211. doi:10.1038/ncomms12205

Shan, T., Zhang, P., Liang, X., Bi, P., Yue, F., and Kuang, S. (2014). Lkb1 is indispensable for skeletal muscle development, regeneration, and satellite cell homeostasis. *Stem cells* 32, 2893–2907. doi:10.1002/stem.1788

Sheffield-Moore, M., and Urban, R. J. (2004). An overview of the endocrinology of skeletal muscle. *Trends Endocrinol. Metab.* 15, 110–115. doi:10.1016/j.tem.2004.02.009

Sun, L., Goff, L. A., Trapnell, C., Alexander, R., Lo, K. A., Hacisuleyman, E., et al. (2013). Long noncoding RNAs regulate adipogenesis. *Proc. Natl. Acad. Sci. U. S. A.* 110, 3387–3392. doi:10.1073/pnas.1222643110

Verma, S., and McMurray, J. J. (2018). SGLT2 inhibitors and mechanisms of cardiovascular benefit: A state-of-the-art review. *Diabetologia* 61, 2108–2117. doi:10.1007/s00125-018-4670-7

frontiers in Physiology

ORIGINAL RESEARCH
published: 04 May 2021
doi: 10.3389/fphys.2021.667698

Comparative Transcriptome Profiling of Cold Exposure and β3-AR Agonist CL316,243-Induced Browning of White Fat

Yu Li†, Xiaodan Ping†, Yankang Zhang†, Guoqiang Li, Ting Zhang, Geng Chen, Xinran Ma, Dongmei Wang* and Lingyan Xu**

Shanghai Key Laboratory of Regulatory Biology, School of Life Sciences, Institute of Biomedical Sciences, East China Normal University, Shanghai, China

OPEN ACCESS

Edited by:
Tizhong Shan, Zhejiang University, China

Reviewed by:
Zhuoxian Meng, Zhejiang University, China
Yong Chen, Tongji Hospital, Huazhong University of Science and Technology, China
Lenan Zhuang, Zhejiang University, China

***Correspondence:**
Xinran Ma
xrma@bio.ecnu.edu.cn
Dongmei Wang
dmwang@bio.ecnu.edu.cn
Lingyan Xu
lyxu@bio.ecnu.edu.cn

†These authors have contributed equally to this work

Specialty section:
This article was submitted to Lipid and Fatty Acid Research, a section of the journal Frontiers in Physiology

Received: *14 February 2021*
Accepted: *06 April 2021*
Published: *04 May 2021*

Citation:
Li Y, Ping X, Zhang Y, Li G, Zhang T, Chen G, Ma X, Wang D and Xu L (2021) Comparative Transcriptome Profiling of Cold Exposure and β3-AR Agonist CL316,243-Induced Browning of White Fat. Front. Physiol. 12:667698. doi: 10.3389/fphys.2021.667698

Beige adipocytes are newly identified thermogenic-poised adipocytes that could be activated by cold or β3-adrenergic receptor (β3-AR) signaling and offer therapeutic potential for treating obesity and metabolic diseases. Here we applied RNA-sequencing analysis in the beige fat of mice under cold exposure or β3-AR agonist CL316,243 (CL) treatment to provide a comparative and comprehensive analysis for the similarity and heterogeneity of these two stimulants. Importantly, via KEGG analysis, we found that cold and CL commonly induced oxidative phosphorylation. Meanwhile, cold increased glycerolipid and amino acids metabolism while CL treatment triggered a broader spectrum of metabolic responses including carbohydrate metabolism. Besides, cold or CL treatment featured greater heterogeneity in downregulated gene programs. Of note, the top changed genes in each category were confirmed by qPCR analysis. Overall, our analysis provided a better understanding of the heterogeneity of differential models for beige adipocytes activation and a possible clue for optimizing β3-AR agonists in the future.

Keywords: browning of white fat, cold exposure, β3-AR agonist, heterogeneity analysis, transcriptomics

INTRODUCTION

Obesity, manifested as excess fat accumulation caused by the imbalance between energy intake and expenditure, is a severe public health crisis throughout the world since it is the major risk factor for metabolic diseases including type 2 diabetes, hypertension, cardiovascular disease, and certain types of cancers (Harms and Seale, 2013). Fat tissues are divided into three categories. White fat stores energy in the form of triglyceride and classic brown fat dissipates chemical energy as heat via uncoupling protein 1 (UCP1). Recently, beige adipocytes have been discovered and characterized by their high thermogenic and energy dissipating capacity upon cold exposure or β3-adrenergic signaling (Himms-Hagen et al., 1994; Rosell et al., 2014), which is called the "browning of white fat." Of note, the browning phenomenon was also observed in cold-exposed human adults in the supraclavicular region revealed by PET-CT scans with characteristics resembling beige/brown adipocytes in rodents (Nedergaard et al., 2007; Sharp et al., 2012). The existence of beige/brown fat in human adults has attracted great attention and has been considered a novel peripheral target to treat obesity and metabolic diseases.

Under cold exposure, norepinephrine (NE) release from sympathetic nerves is critical for the induction of white fat browning through the β3-adrenergic receptor (β3-AR) since β3-AR loss in mice almost abolished the cold-induced browning in WAT (Galitzky et al., 1995; Jimenez et al., 2003; Collins, 2011). In detail, NE binds to β3-AR and triggers a signal transduction cascade involving cyclic AMP (cAMP)-PKA-CREB signaling, which eventually activates the transcriptions of mitochondrial, lipolytic, lipid oxidative, and thermogenic gene programs (Harms and Seale, 2013; Bargut et al., 2017). CL316,243 (CL), one kind of β3-adrenergic activator, is widely used in cellular models and rodents to mimic cold stimulation with potent effects on metabolic rate and thermogenic effects at least partially via activating browning of white fat since the thermogenic effects of CL still exist in mice lacking brown adipose tissues (Lowell et al., 1993).

Due to the importance of β3-AR signaling in the browning of white fat, the β3-AR agonists are considered a potential therapeutic strategy to combat obesity and metabolic diseases. However, compared to cold, distinct β3-AR agonists featured different efficacies in thermogenic activation and side effects, which complicated its wide and safe use. For example, the applications of various β3-AR agonists have been hindered in clinical use due to their potential adverse effects on the cardiovascular system, which call for continuous efforts for developing novel and safer β3-AR agonists (Arch, 2011). Besides, previous studies have shown that β3-AR stimulation with sympathomimetic ephedrine had no thermogenic effect on human BAT, while mirabegron, a β3-AR agonist used to treat an overactive bladder, was effective in activating BAT as compared to placebo but may have adverse impacts on glucose homeostasis (Cypess et al., 2012, 2015). Moreover, it has been reported that cold exposure and β3-AR agonists may activate distinct cellular populations that express different β-adrenergic receptors (Jiang et al., 2017). Overall, this evidence suggested the obvious heterogeneity of cold exposure and β3-AR agonists on the process of white fat browning, while the detailed differences between two stimulants are not well clarified. A detailed comparative study would offer previously unappreciated mechanisms and strategies for better β3-AR agonists development.

In the present study, via analyzing the transcriptomics of chronic cold exposure or CL administration, we revealed the commonalities and heterogeneity of these two powerful instigators of white fat browning, which may provide novel insights into the theoretical basis in order to optimize β3-AR agonists for the treatment of obesity and metabolic diseases.

MATERIALS AND METHODS

Animals

All of the procedures involving mice were performed according to guidelines of East China Normal University. Male C57BL/6J mice were purchased from Shanghai Model Organisms Center and housed under standard experimental environments controlled at room temperature (22°C) with a 12 h light/dark cycle and free access to food and water. For the establishment of the animal model, mice were housed at either 22°C or 4°C for 7 days in a temperature-controlled incubator (LP-LED, NK system, Japan), or injected daily with 1 mg/kg of PBS or CL316,243 (Sigma-Aldrich) for 7 days. Mice were subsequently sacrificed and inguinal fat was dissected and frozen immediately in liquid nitrogen and stored at −80°C for further analysis. To monitor the effect of the cold or CL treatment, body weight and food intake were measured after 7 days. Serum triglyceride (TG) and total cholesterol (TC) were determined according to the manufacturer's instructions (Sigma).

Hematoxylin & Eosin (H&E) and Immunohistochemical (IHC) Staining

Inguinal fat (iWAT) from room temperature (RT) and cold-exposed mice or PBS and CL treated mice were fixed in 10% formalin (Sigma Aldrich). The tissues were embedded into paraffin, blocked, and cut at 5 μm for H&E staining. For UCP1 IHC staining, 5-μm-thick iWAT sections were incubated with 3% H_2O_2 to inactivate the endogenous peroxidase and blocked with 5% goat serum for 2 h. Afterward, the slides were incubated with UCP1 antibody (1:200, Abcam) overnight at 4°C and followed with goat-anti rabbit IgG HRP for 1 h. The chromogen DAB was used to detect the immunoreactivity peroxidase. These images were acquired using a microscope (Nikon) and adipocyte sizes were quantified. Briefly, ImageJ software was used to calculate the total area and the number of adipocytes in the whole field of vision, then the sizes were calculated by dividing the total area by the number of adipocytes. Five random fields per section per mouse were analyzed.

Total RNA Extraction, RNA-Sequencing, and Quantitative Real-Time PCR

Total RNA was extracted from the iWAT of mice with TRIzol (Takara). The RNA library was generated and RNA sequencing (RNA-seq) was performed on an Illumina Hiseq instrument (Cloud-Seq Biotechnology, Shanghai). Reverse transcription and quantitative real-time PCR (qPCR) were performed to confirm the RNA sequencing results. A total of 1 μg of RNA was reversely transcribed using SuperScript™ III Reverse Transcriptase (Takara) for cDNA synthesis, and Universal SYBR Green Master Mix (Yeasen, Shanghai) was used to perform qPCR on the Light cycler 480II machine (Roche, United States). After normalization to 36b4, the relative expression level of RNA was calculated by using the $2^{-\Delta\Delta Ct}$ method.

The sequences of primers are listed in **Supplementary Table 2**.

RNA-Seq Analysis of In-House and NCBI Gene Expression Omnibus (GEO) Datasets

A unified method was adopted for all datasets. EdgeR was used to find differentially expressed genes. All sequencing reads were mapped to the mouse reference genome (UCSC mm10) using hisat2 (Kim et al., 2015), and StringTie was used to calculate the read counts (Pertea et al., 2015). EdgeR was used to identify the differentially expressed genes (Robinson et al., 2010). A gene was considered as differentially expressed with the

following criteria: *adjusted p*-value < 0.05 and log2| fold change| ≥ 1. Raw datasets have been uploaded to the Gene Expression Omnibus (GSE164219).

To avoid bias or randomization of datasets, we cross-analyzed RNA-seq data from our in-house data GSE164219 and GEO datasets GSE86338 both containing iWAT under room temperature or cold exposure for 7 days, as well as GSE86338 and GSE129083 datasets both for PBS or CL treatment chronologically (Bai et al., 2017; Wang et al., 2019).

Pathway Enrichment Analysis (KEGG) and Gene Ontology (GO) Analysis

The gene set enrichment analysis (GSEA) was performed to identify the significant pathways and functions using clusterprofiler (Yu et al., 2012). Kyoto Encyclopedia of Genes and Genomes (KEGG) pathway analysis identifies significantly enriched metabolic pathways or signal transduction pathways enriched in differentially expressed genes (DEGs) compared to those with reference gene background using the hypergeometric test. The functional enrichment analysis was carried out to map the DEGs to genes in the GO terms list. The GO terms and KEGG pathways were considered as significantly enriched if *p*-value < 0.05.

Statistical Analyses

The data analysis was performed with GraphPad Prism 7. The normalcy of data was examined by the Shapiro–Wilk normality test. Statistical comparisons between two groups were made by a two-tailed unpaired student *t*-test. Data are presented as mean ± SEM. Differences between groups were considered statistically significant when *p*-value < 0.05.

RESULTS

Chronic Cold Exposure or CL316,243 Administration Induce Browning of White Fat and Thermogenic Marker UCP1 Expression to a Similar Extent in Mice

To confirm the effects of cold exposure or β3-AR agonist stimulation on the browning of white fat, two groups of mice at 8 weeks old were kept under either room temperature (RT, 22°C) or 4°C for 7 days, while the other two groups of mice of a similar age were intraperitoneally (IP) administrated with PBS or CL316,243 (CL) at RT for 7 days (**Figure 1A**). To explore the effect of the cold or CL treatment on whole-body energy metabolism, we monitored the body weights and food intake changes during cold or CL treatment, as well as triglyceride and cholesterol level after cold or CL treatment. These data showed that both cold and CL treatment reduced body weight and serum lipid parameters (**Supplementary Figures 1A–D**). Interestingly, cold exposure also exhibited strong effects on increasing food intake compared to CL treatment, which was consistent with previous reports (Yoshida et al., 1996; Jia et al., 2016; Xu et al., 2019). At the end of interventions, inguinal white adipose tissues (iWAT) were dissected from these mice for histological and gene expression analysis (**Figure 1A**). The hematoxylin & eosin (H&E) staining of iWAT showed reduced adipocyte sizes upon either cold or CL treatment, compared to their respective controls (**Figure 1B**). In addition, cold and CL both led to a similar strong induction of UCP1, the marker for thermogenesis, at mRNA and protein levels compared to their controls, as shown by qPCR, UCP1 immunohistochemical staining, and western blot analysis (**Figures 1C–E**). Thus, these results indicated that, physiologically, both cold and CL treatment strongly induced the browning of white fat to a similar extent in mice.

We then set out to analyze the common and differential changes in gene transcriptome during the browning process induced by cold or CL treatment in mice iWAT. Of note, to avoid biased results from a single dataset, we cross-analyzed RNA-seq data using our in-house data GSE164219 and dataset GSE86338 from the GEO database which both analyzed the changes in mRNA landscapes in iWAT under cold exposure or room temperature for 7 days, while the other cross-analysis was performed between datasets GSE86338 and GSE129083 which both evaluated iWAT mRNA changes upon chronic CL or PBS administration (**Figure 2**). Consistent with a critical role for energy expenditure and thermogenesis in these two browning models, GSEA revealed that cold exposure and CL treatment commonly induced DEGs strongly correlated with fatty acid metabolism and the tricarboxylic acid (TCA) cycle in mitochondria in all datasets (**Figures 3A–D**).

Overall, these data indicated that cold and CL induced white fat browning featured common characterizations in both fat physiology and critical gene pathways, though the reported differences in functionality and side effects of cold or CL treatment may lie in their individual distinct gene expressions.

Cold Exposure Enhances Metabolism While Inhibits Inflammatory and Fibrotic Pathways in iWAT

We thus set out to investigate if cold or CL treatment induce different patterns of gene expressions and pathway enrichments in iWAT. We overlapped two datasets (GSE164219 and GSE86338) to highlight the commonly regulated gene sets upon cold exposure and performed bioinformatic analysis (Overlap-Cold). The results revealed 120 upregulated genes and 204 downregulated genes commonly regulated by cold in both datasets (**Figures 4A,B**). KEGG analysis revealed that cold stimulated classic metabolic pathways including the adipocyte differentiation-related PPAR signaling pathway, energy homeostasis related carbon metabolism, and TCA cycle (**Figure 4C**). This was in accordance with GO analysis showing that the lipid metabolic process and mitochondrial regulation were upregulated (**Supplementary Figure 2A**). Notably, in our analysis, cold exposure induced gene programs enriched in cardiac muscle contraction, suggesting that chronic cold may also pose potential threats to the cardiovascular system. Meanwhile, KEGG analysis also revealed that cold exposure inhibited complement and coagulation cascades, ECM-receptor interaction, and the TGF-β signaling pathway (**Figure 4D**), and GO analysis highlighted that the regulated genes were

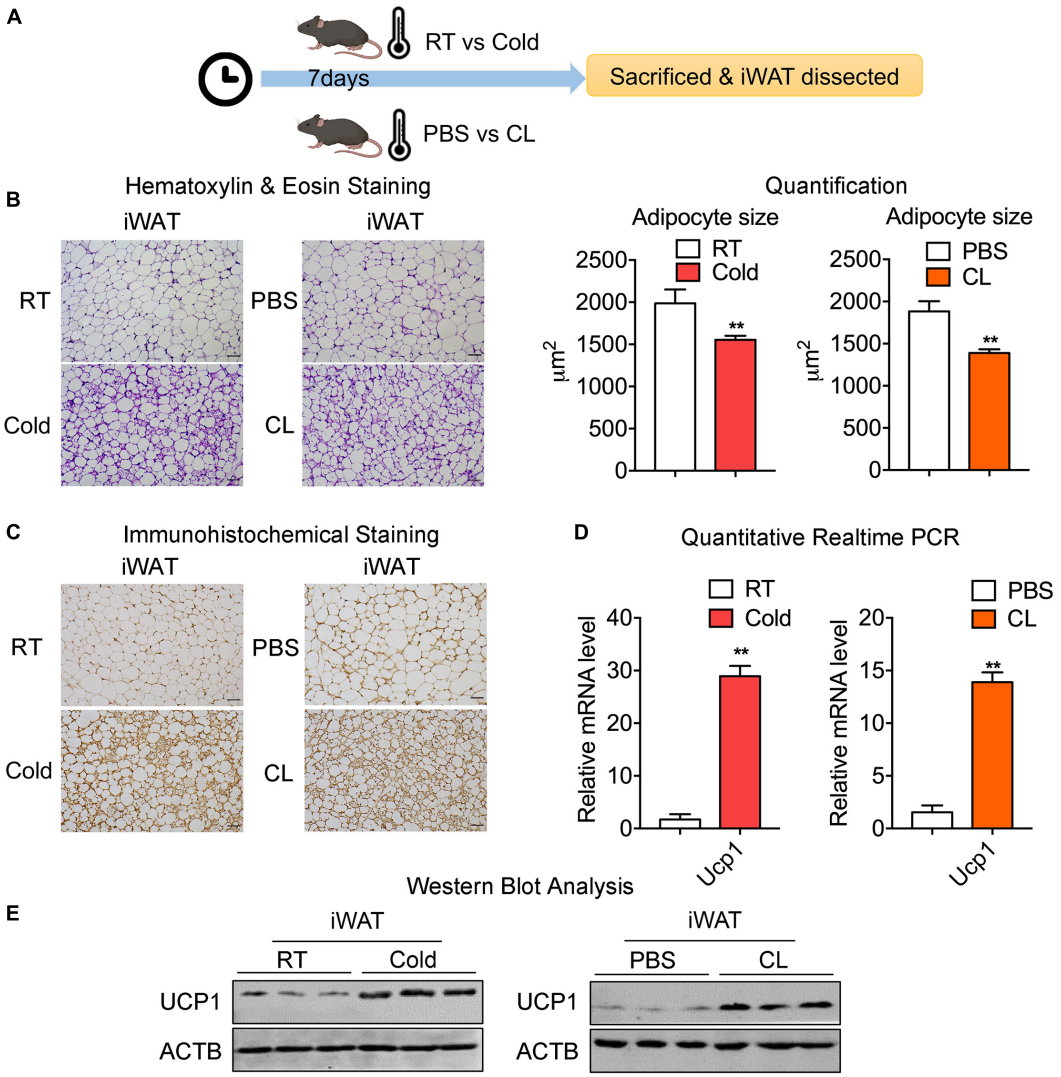

FIGURE 1 | Chronic old exposure and CL316,243 administration induce browning of white fat and thermogenic marker UCP1 levels in mice. **(A)** Schematic illustration of the browning of white fat induced by 7-day cold exposure or β-adrenergic agonist CL316,243 (CL) administration. **(B)** Representative H&E staining of adipocyte size quantification from iWAT of mice treated with RT or cold and PBS or CL. Scale bars: 50 μm. **(C–E)** Representative immunohistochemical images of UCP1 staining **(C)**, mRNA **(D)**, and protein levels of UCP1 **(E)** in iWAT from mice treated with RT or cold and PBS or CL. Scale bars: 50 μm. $N = 6$ per group. Data are presented as mean ± SEM and $^{**}P < 0.01$ compared to control group.

involved in extracellular matrix organization (**Supplementary Figure 2B**), which potentially contributed to adipose tissue fibrosis (Sun et al., 2013).

Taken together, these transcriptional data suggested that cold exposure promoted classic energy metabolism while it suppressed the inflammatory and fibrotic pathways in iWAT.

CL Stimulates a Broader Spectrum of Metabolic Gene Pathways and Decreases Immune Responses

We also overlapped genes from two datasets (GSE86338 and GSE129083) that study CL treatment, which rendered 664 commonly upregulated and 63 commonly downregulated genes (Overlap-CL, **Figures 5A,B**). Interestingly, the counts of commonly upregulated genes treated with CL were far more than those found in cold, suggesting that CL may cause changes to a broader spectrum of gene programs in iWAT (**Figures 5A,C**). Indeed, in addition to fatty acid metabolism and TCA cycle, KEGG analysis uncovered that CL positively regulated peroxisome and pyruvate metabolism, suggesting other cellular organelles and glucose metabolism were mobilized by CL treatment (**Figure 5C**). Consistently, GO analysis also showed that the upregulated DEGs were associated with lipid and carbohydrate metabolism (**Supplementary Figure 3A**). In comparison, only 5% of commonly downregulated genes were affected, including immune response pathways such as the toll-like receptor signaling pathway and NF-kappa B signaling

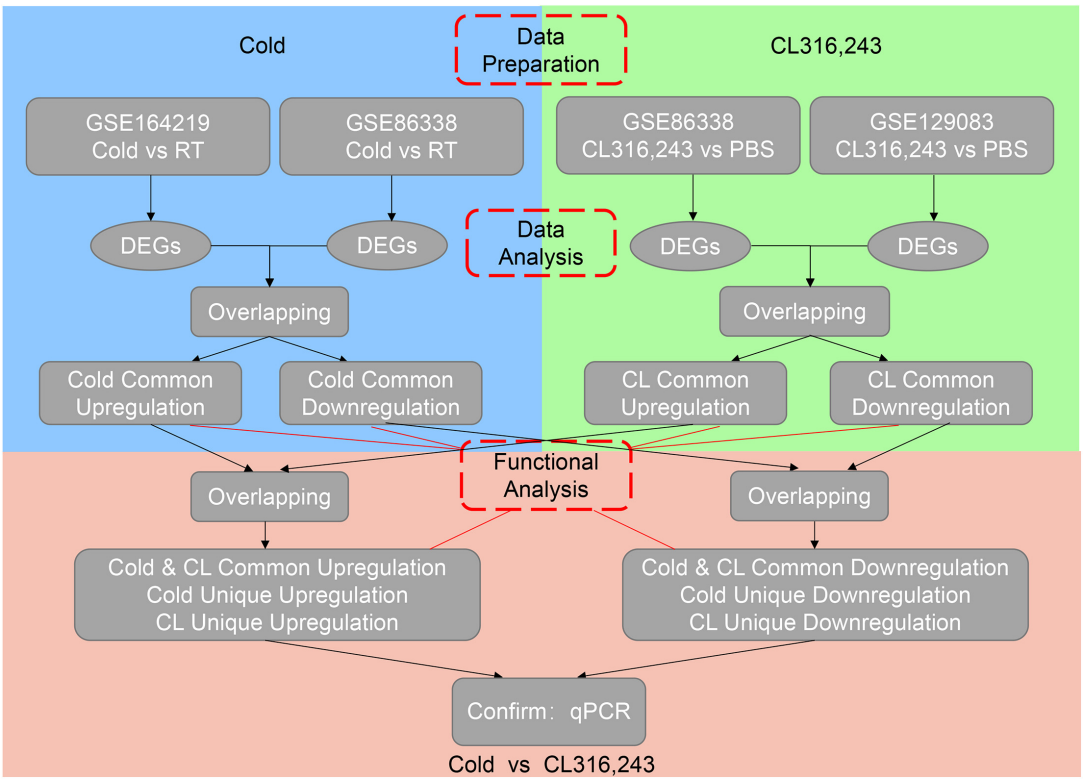

FIGURE 2 | Flow chart of RNA-sequencing data processing.

pathway (**Figure 5D**), which were consistent with GO analysis results showing a suppressed acute inflammatory response and IL-8 production (**Supplementary Figure 3B**).

Therefore, our transcriptional analysis revealed that aside from the classic energy metabolism observed in cold stimulation, CL treatment also induced peroxisomal and pyruvate metabolism, while subduing classic immune responses.

Comparative Analysis Revealed That Cold and CL Exposure Commonly Increase Oxidative Phosphorylation and Metabolic Pathways and Decrease Complement and Coagulation Cascades

Subsequently, we investigated the commonality between cold and CL treatment by further cross-analyzing the overlap-cold and overlap-CL datasets. Intriguingly, the majority of upregulated genes under the cold condition were covered by DEGs set under CL treatment (**Figure 6A**). The 98 genes commonly upregulated by cold and CL were majorly involved in oxidative phosphorylation and the metabolic pathways required for thermogenesis as revealed by KEGG analysis (**Figures 6B,C**). Furthermore, among the top enriched genes were classic thermogenic and mitochondrial genes including Ucp1, Cpt1b, and Cox7a1, which were confirmed by qPCR analysis (**Supplementary Table 1** and **Figures 1D**, **6D**). On the contrary, only nine genes, mainly related to complement and coagulation cascades, were commonly downregulated by cold and CL, with complement components C2 and C4b confirmed by qPCR (**Figures 6E–H**). Complement components are a critical part of the innate immune system and contribute to excessive inflammatory responses (Lin et al., 2018; Lung et al., 2019).

These results indicated that both cold and CL treatment promoted thermogenesis and energy metabolism via oxidative phosphorylation, while they suppressed complement and coagulation cascades.

Analysis of Unique Gene Programs of Cold Exposure and CL Treatment Suggest Distinct Energy Substrates Utilization and Physiological Events

Lastly but most importantly, we explored the heterogeneity in gene expression patterns between cold exposure and CL treatment during iWAT browning. Notably, after overlapping datasets, we found that 3.2% of DEGs (22 genes) were uniquely upregulated by cold, while 82.5% of DEGs (566 genes) were uniquely upregulated by CL (**Figure 6A**). These results suggested that though cold and CL both strongly induce white fat browning, CL regulates a unique set of gene programs compared to cold, which may explain the different functionality and side effects induced by these two stimulations.

Kyoto Encyclopedia of Genes and Genomes analysis revealed a significant enrichment of glycerolipid metabolism, as well

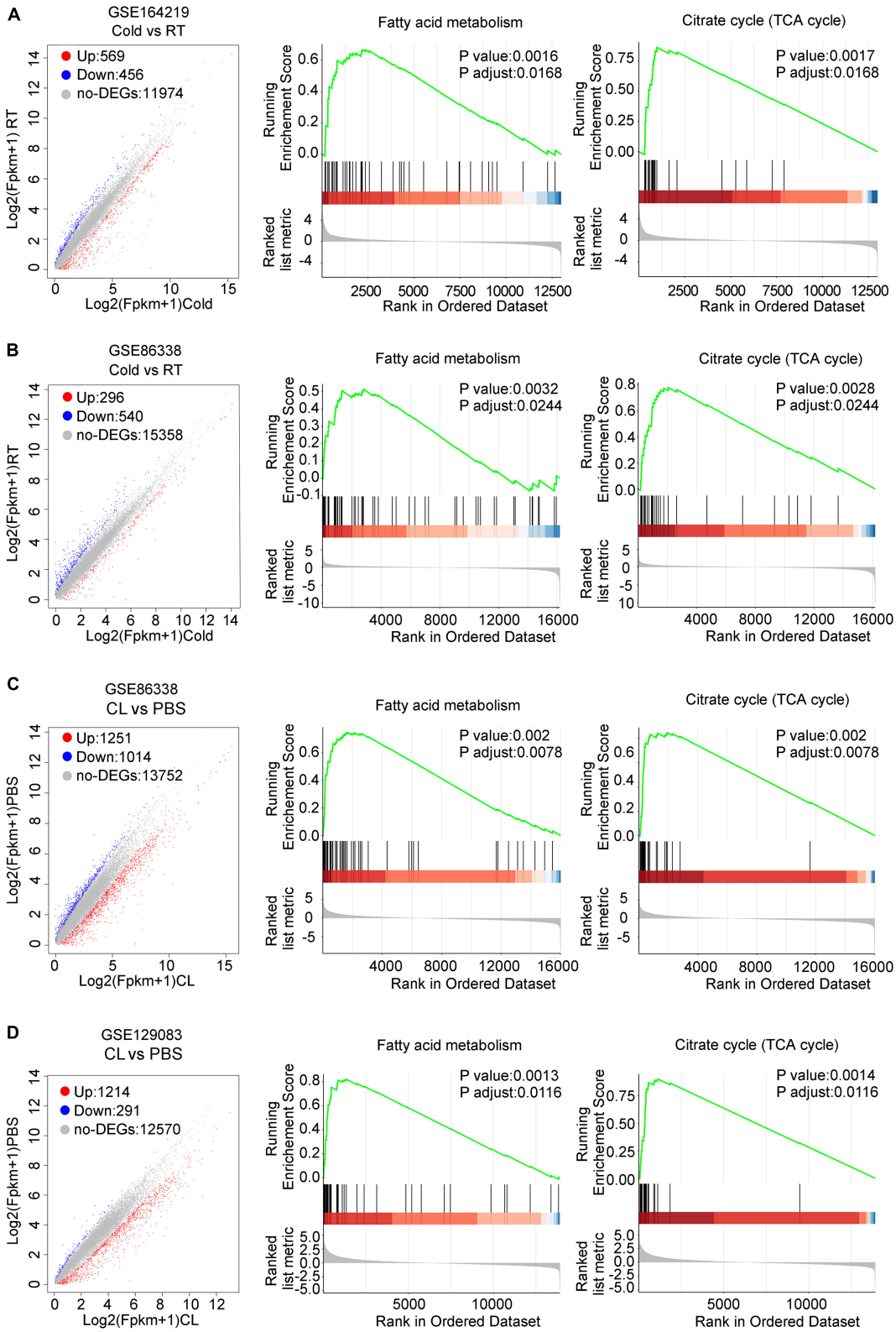

FIGURE 3 | DEGs and GSEA of RNA-seq datasets for iWAT under cold exposure or CL administration in mice. **(A–D)** Volcano plots for DEGs and GSEA of different datasets. **(A)** GSE164219 and **(B)** GSE86338: Cold vs. RT; **(C)** GSE86338 and **(D)** GSE129083: CL316,243 vs. PBS. Red dots for upregulated genes, blue dots for downregulated genes, and gray dots for non-DEGs.

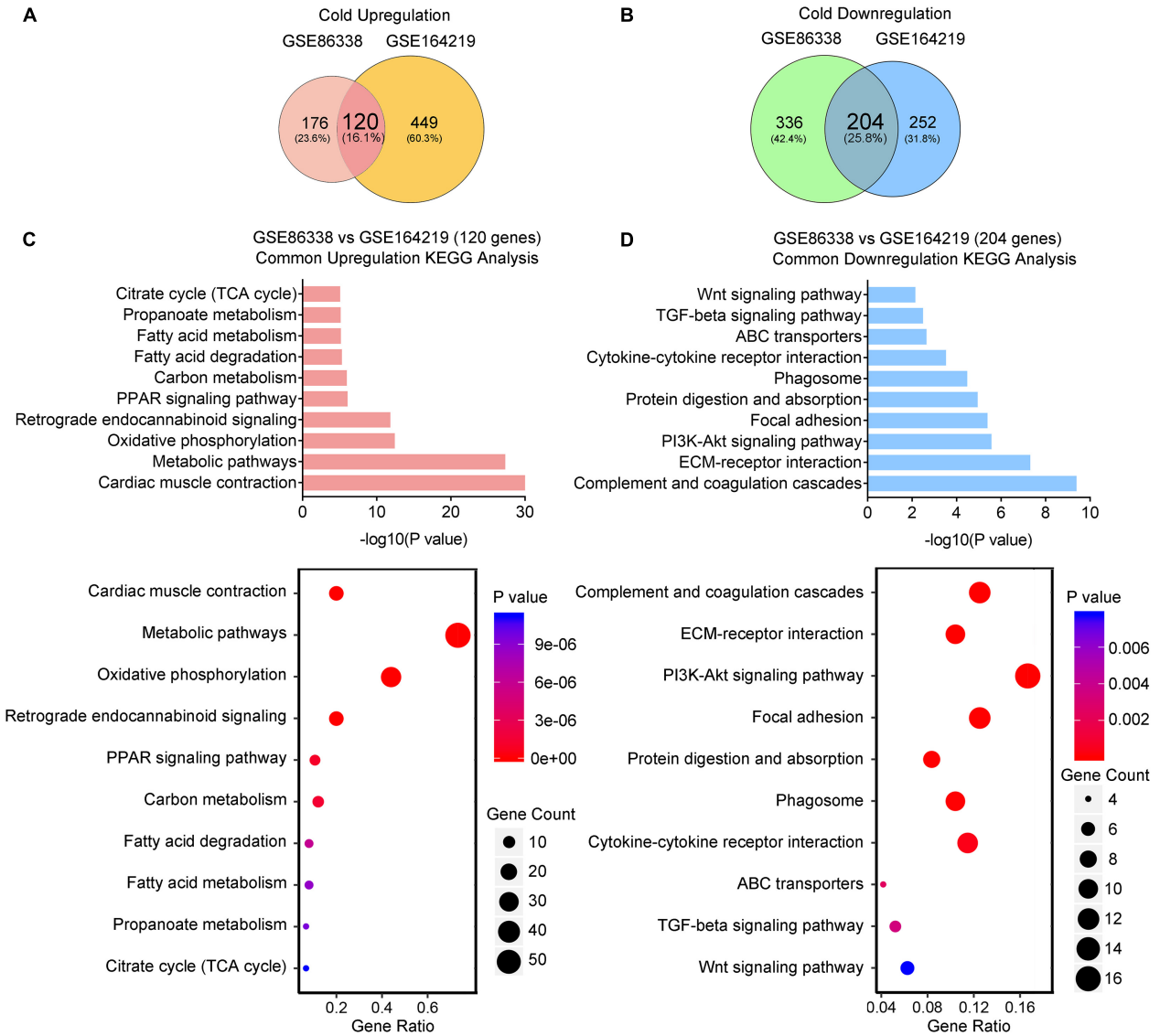

FIGURE 4 | Cold exposure enhances metabolism and inhibits inflammatory and fibrotic pathways in iWAT. **(A,B)** Venn diagram of overlapped upregulated **(A)** and downregulated **(B)** genes from iWAT of mice exposed to cold shown in the GSE86338 and GSE164219 datasets. **(C,D)** KEGG analysis for the DEGs of common upregulated 120 genes **(C)** shown in **(A)** and downregulated 204 genes **(D)** shown in **(B)**.

as glycine, serine, and threonine metabolism as a feature of cold-induced gene patterns (**Figure 7A**). qPCR analysis confirmed the increase in mRNA levels of aminolaevulinic acid synthase 2 (ALAS2), the rating-limiting enzyme in heme synthesis which can maintain the mitochondrial function in brown adipocytes (Galmozzi et al., 2019), as well as glycerol kinase (Gyk), which catalyzes the phosphorylation of glycerol to glycerol 3-phosphate and is reported to be involved in UCP1 level induction (Iwase et al., 2020), in cold-treated iWAT versus CL treatment (**Figure 7C**). Meanwhile, we noted that pyruvate metabolism, carbon metabolism, and glycolysis were uniquely enriched in CL treatment, suggesting that in addition to oxidative phosphorylation, fatty acid metabolism, and TCA cycle that were commonly regulated by cold and CL, CL treatment features active glucose mobilization for energy demands (**Figure 7B**). Among the top regulated genes, qPCR analysis confirmed enhanced expression of acetyl-CoA carboxylase alpha (ACACA), hydroxyacylglutathione hydrolase (HAGH), and acyl-CoA synthetase short chain family member 2 (ACSS2) in the pyruvate catabolism (**Figure 7C**) in CL-treated iWAT versus cold. These results suggested that cold uniquely regulated glycerolipid metabolism and specific amino acids metabolism, while compared to cold, CL treatment tended to mobilize both carbon and lipid substrates for the browning of white fat.

Besides, 75.6% of DEGs (195 genes) were uniquely downregulated upon cold exposure while 20.9% of DEGs (54 genes) were uniquely suppressed by CL treatment (**Figure 6E**),

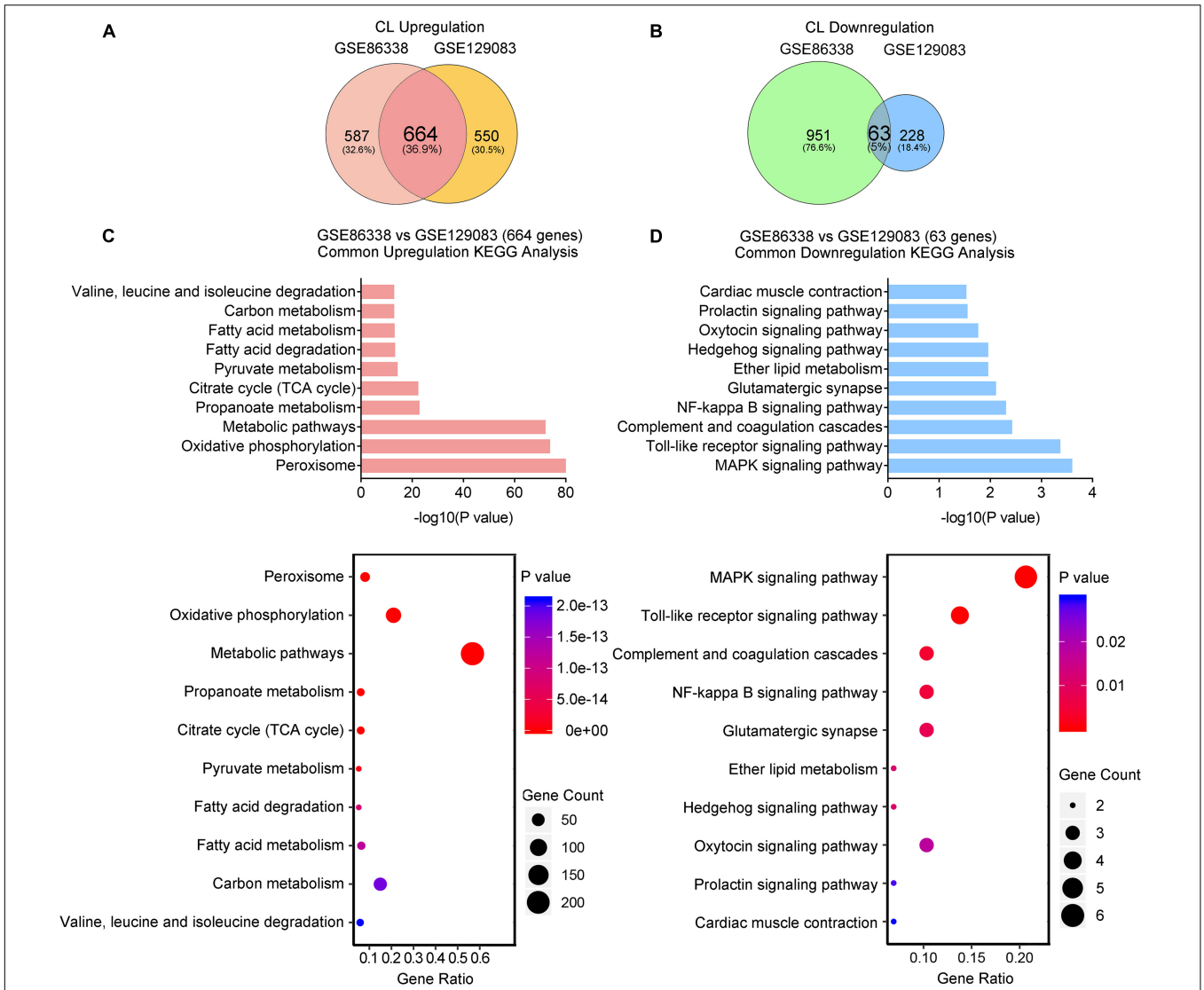

FIGURE 5 | CL stimulates a broader spectrum of metabolic gene pathways and decreases immune responses. **(A,B)** Venn diagram of overlapped upregulated **(A)** and downregulated **(B)** genes from iWAT of mice administrated with CL shown in GSE86338 and GSE129083 datasets. **(C,D)** KEGG analysis for the DEGs of common upregulated 664 genes **(C)** shown in **(A)** and downregulated 63 genes **(D)** shown in **(B)**.

suggesting that cold suppressed a large number of distinct genes compared to CL. KEGG analysis showed that cold exposure mainly inhibited ECM-receptor interaction and focal adhesion, while CL inhibited pathways included the MAPK signaling pathway, toll-like receptor signaling pathway, and glutamatergic synapse (**Figures 8A,B**). Besides, the unique genes suppressed by cold or CL treatment were confirmed by qPCR, including fibrotic and collagen related genes Fn1, Col6a6 regulated by cold, as well as Fos and proinflammatory cytokine IL-1b regulated by CL (**Figure 8C**). These results indicated that cold treatment tended to downregulate ECM-related pathways, while CL treatment decreased specific intracellular and receptor signaling pathways.

Altogether, our analyses revealed different energy substrates utilization and specific physiological events induced by cold or CL stimulated in beige adipocytes.

DISCUSSION

Chronic cold exposure and β3-AR treatment induce transcriptional signaling pathways in beige adipocytes for thermogenesis. In the present study, we examined the transcriptomic alterations that occur in the iWAT of mice during cold exposure or CL treatment by analyzing overlapped RNA-seq datasets and revealed that these two triggers of browning commonly drove lipid metabolism and TCA cycle in mitochondria for thermogenesis. Interestingly, we found differences between datasets generated from mice under similar treatment, which may be caused by multiple factors behind this phenomenon. First, the mice strains used by different labs may have differences due to sub-strains formed by long-term inbreeding in different facilities. Second, it has been more and

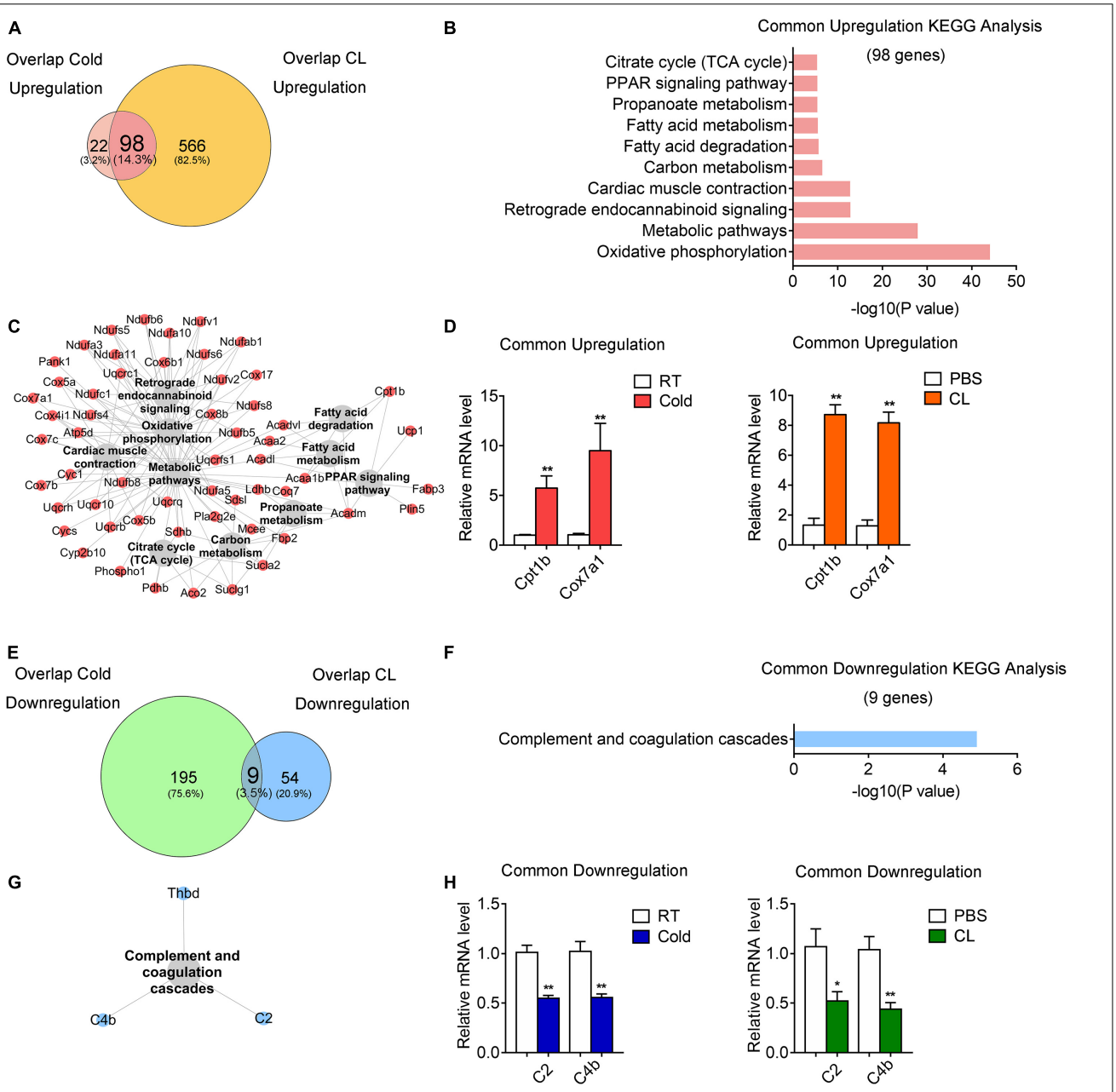

FIGURE 6 | Comparative analysis of commonly regulated genes by cold and CL exposure. Analysis of overlapped DEGs between cold (commonly regulated genes from GSE86338 and GSE164219 datasets) and CL (commonly regulated genes from GSE86338 and GSE129083 datasets). **(A,E)** Venn diagrams for commonly upregulated **(A)** and downregulated **(E)** DEGs between cold and CL treatment. **(B,C,F,G)** KEGG analysis and pathway-gene network for the upregulated 98 genes **(B,C)** shown in **(A)** and downregulated 9 genes **(F,G)** shown in **(E)**. **(D,H)** mRNA levels of top ranked upregulated **(D)** genes from **(A)** and downregulated **(H)** genes from **(E)**. *N* = 6 per group. Data are presented as mean ± SEM and $^{*}P < 0.05$, $^{**}P < 0.01$ compared to control group.

more recognized that housing environments may have a major influence on experimental outcomes, including different diet formula and bedding materials that the mice are kept on, distinct circadian rhythm due to different lighting schedules in the facility, or different times when the experiments were performed, etc. Last but not least, gut microbiota in animals from different facilities are different, which may contribute to the different metabolic performances and responsive gene programs under cold or CL treatment. To circumvent this factor, we overlapped different datasets to identify the stable alternations of gene programs between datasets under cold or CL treatment. Of note, CL treatment uniquely activated carbohydrates mobilization for energy demands, and cold uniquely promoted glycerolipid and specific amino acids metabolism. Meanwhile, we found that cold and CL treatment each suppressed different inflammatory events, while cold additionally downregulated fibrotic programs.

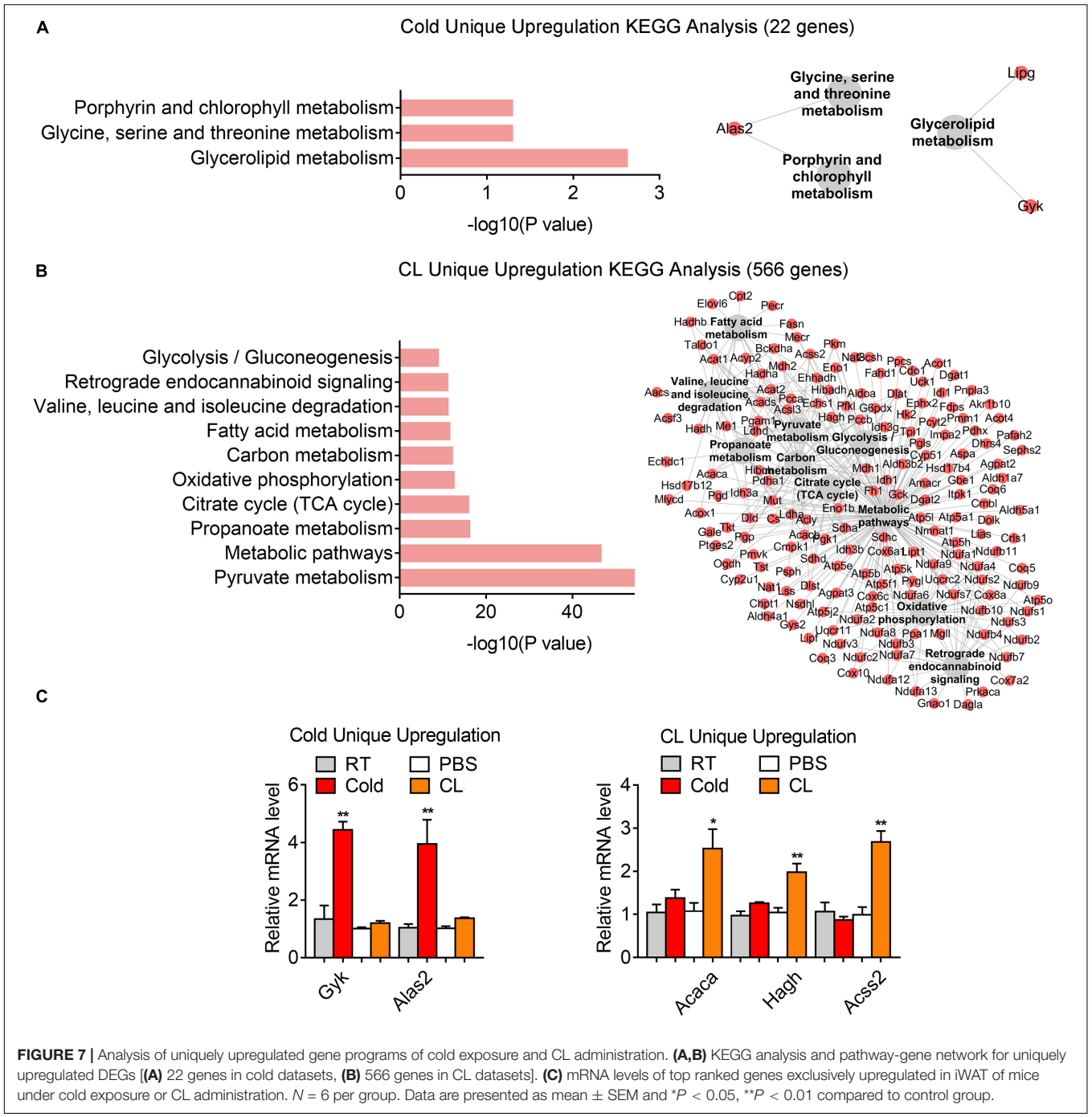

FIGURE 7 | Analysis of uniquely upregulated gene programs of cold exposure and CL administration. **(A,B)** KEGG analysis and pathway-gene network for uniquely upregulated DEGs [**(A)** 22 genes in cold datasets, **(B)** 566 genes in CL datasets]. **(C)** mRNA levels of top ranked genes exclusively upregulated in iWAT of mice under cold exposure or CL administration. $N = 6$ per group. Data are presented as mean ± SEM and $^{*}P < 0.05$, $^{**}P < 0.01$ compared to control group.

These results may provide novel insights for understanding the molecular mechanisms behind the functional differences and distinct side effects caused by cold or β3-AR agonist stimulation in the browning process.

We found that both cold and CL stimulation on beige fat significantly enhanced pathways related to oxidative phosphorylation for energy metabolism. White adipose tissue mainly stores energy in the form of triglycerides (TG). In the face of energy demand, for example, during cold or CL stimulation, TG breaks into glycerol and fatty acid (Beale et al., 2002) to provide energy substrates. Via transcriptome data and qPCR confirmation, we confirmed that Gyk, an enzyme critical for glycerol/fatty acid metabolism and UCP1 induction partially through the β3AR-cAMP-CREB pathway (Iwase et al., 2020), was upregulated upon cold exposure, indicating a critical role of lipid metabolism in cold-stimulated browning. Besides, we found that compared to CL treatment, cold exposure specifically promoted glycerolipid metabolism that is an integral part of the glycerolipid/FFA cycle essential for maintaining body temperature by releasing heat at the expense

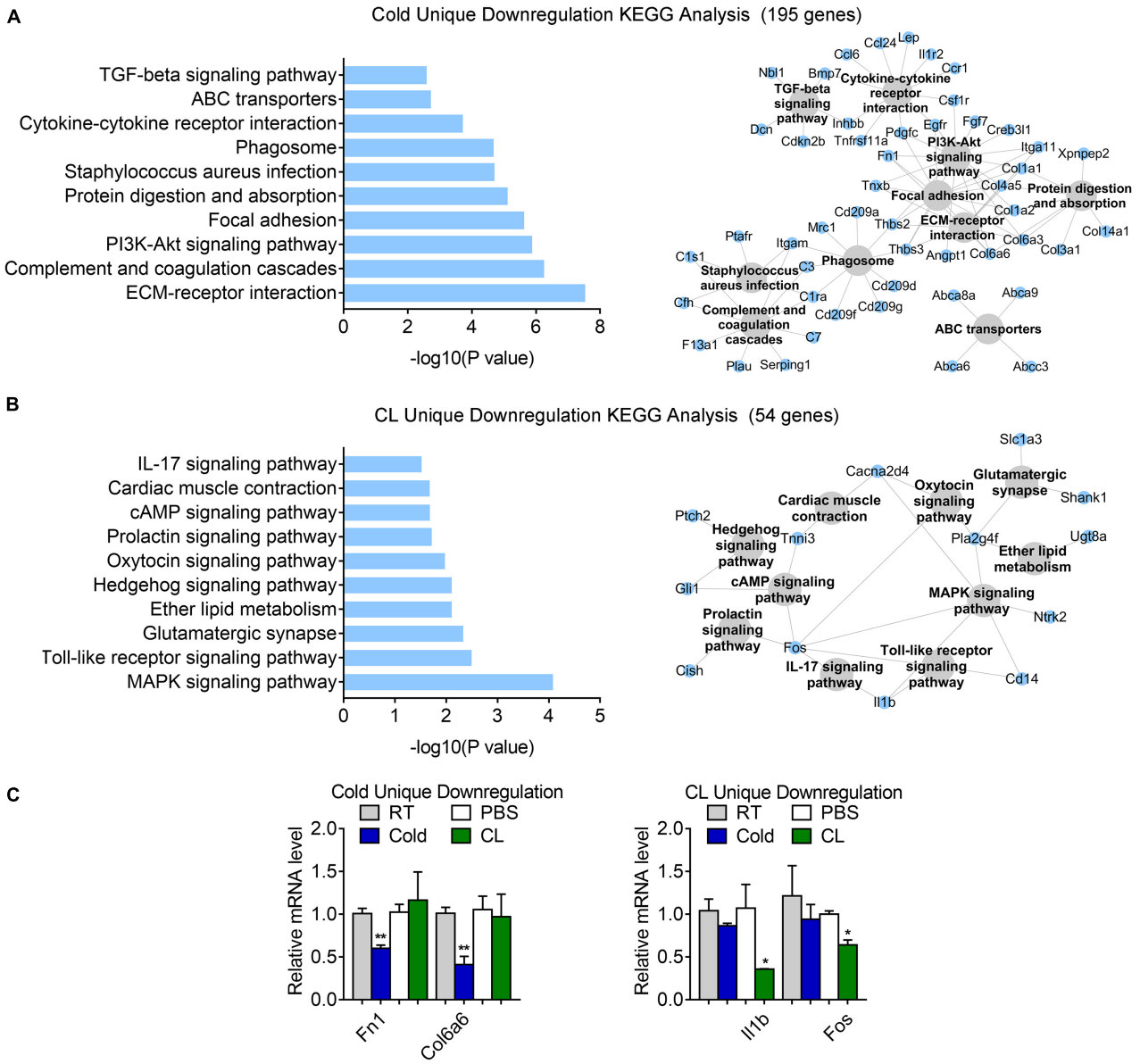

FIGURE 8 | Analysis of uniquely downregulated gene programs of cold exposure and CL administration. **(A,B)** KEGG analysis and pathway-gene network for uniquely downregulated DEGs [**(A)** 195 genes in cold datasets, **(B)** 54 genes in CL datasets]. **(C)** mRNA levels of top ranked genes exclusively downregulated in iWAT of mice under cold exposure or CL administration. $N = 6$ per group. Data are presented as mean ± SEM and $^{*}P < 0.05$, $^{**}P < 0.01$ compared to control group.

of ATP (Prentki and Madiraju, 2008). Since we found changes in glycerolipid metabolism uniquely in cold treatment but not CL treatment, it is possible that cold exposure also promoted thermogenesis by enhancing glycerolipid metabolism in a β3-AR-independent way. In addition, an interesting observation from our transcriptome data was that the upregulated DEGs in CL-induced browning included the majority of upregulated DEGs of cold-induced browning, while CL also featured unique DEGs, i.e., pyruvate metabolism among the top ranking pathway categories by KEGG analysis. This indicates that cold and CL activated an array of similar gene pathways, i.e., lipid metabolism for substrate consumption, while CL additionally promoted multiple substrate utilization, for example, glucose metabolism for enhanced oxidation phosphorylation, suggesting that CL was more prone to mobilize both carbohydrate and lipids for adequate heat production.

It is well known that proinflammatory macrophages infiltrate adipose tissues in obese mice, which leads to chronic low-grade systemic inflammation and obesity-related metabolic syndrome (Weisberg et al., 2003; Lumeng and Saltiel, 2011; Nguyen et al., 2011). This local pro-inflammatory environment in fat tissues directly impairs thermogenic activity, which also impacts brown-versus-white plasticity in subcutaneous adipose tissue (Villarroya et al., 2018). Meanwhile, thermogenic stimuli such as cold

exposure and β3-AR agonists treatment, have been reported to protect against metabolic derangements in obesity partially via triggering anti-inflammatory responses during tissue remodeling and beige adipogenesis (Lee et al., 2013; Hui et al., 2015; Burl et al., 2018). In our study, among the uniquely downregulated gene pathways in cold, we found that fibrotic genes, such as the fibronectin Fn1 and Col family involved in ECM-receptor interaction, were highlighted in the top ranking gene list (**Supplementary Table 1**), indicating that tissue remodeling is a critical event during cold-induced white fat browning. It is known that adipocytes undergo dramatic expansion during strong obesogenic insults, whereas collagen families are key factors in maintaining ECM integrity and promoting ECM remodeling (Khan et al., 2009; Mariman and Wang, 2010; Villarroya et al., 2018). Col4a5, Col6a6, and Fn1 genes in charge of producing collagen of ECM components and markers of iWAT fibrosis, were discovered to be uniquely decreased in cold (Zhang et al., 2020). Therefore, our results indicated that cold exposure could relieve adipose tissue fibrosis, which is one of the major characteristics for adipose tissue aging, thus offering a potential therapeutic method for treating aging-associated metabolic decline. Besides, the adaptive immune system is activated along with the development of adipose tissue inflammation during adipocytes hypertrophy (Kintscher et al., 2008). In this study, we found that interleukin family member IL-1b and Fos, a nucleoprotein transcription factor reported to orchestrate the functions of interleukin-family such as IL-17 and IL-1b for inflammatory responses (Frohnert et al., 2014; Camarena et al., 2017), were downregulated upon CL administration. It is thus interesting that although both cold and CL inhibit inflammation in iWAT, they impact different immune signaling pathways and inflammatory genes, which may provide a theoretical basis for studies on the interactions between obesity and inflammation.

Recently, single cell RNA sequencing (scRNA-seq) and single nucleus RNA-seq (snRNA-seq) have emerged as powerful tools to dissect tissue heterogeneity, which have been applied to the studies of development and function of adipose tissue (Burl et al., 2018; Rajbhandari et al., 2019; Henriques et al., 2020; Sun et al., 2020). These studies characterize various cell populations in SVF or mature adipocytes of iWAT as well as changes in immune cells including the upregulated expression of IL-10 and increased ratio of M2/M1 macrophages during iWAT browning process via scRNA-seq and snRNA-seq, which was similar to our result that both cold exposure and CL treatment affected the immune response pathways (Rajbhandari et al., 2019; Henriques et al., 2020). However, few single-nuclei transcriptome analyses have focused on the different impacts between cold and CL treatment on iWAT, which warrants further study. Besides, epigenetic modification has been demonstrated to play a critical role in regulating the development and function of adipose tissue. For example, upon activating β3-AR signaling, JMJD1A-mediated H3K9me2 demethylation promotes beige fat adipogenesis and KMT5c-mediated H4K20 methylation activates thermogenic gene program in iWAT (Abe et al., 2018; Zhao et al., 2020). In addition, studying different protein characteristics would offer additional dimensions in interpreting the differential responses caused by cold or CL stimulation. In this study, we explored the commonalities and heterogeneity of cold exposure and CL administration on iWAT transcriptome during the induction of beige fat browning. Future studies on how different stimuli convey different changes in epigenetic regulation, cell subsets, or proteomics within iWAT remain to be further explored.

Besides adipose tissues, liver, and skeletal muscle may also play important roles in regulating systemic energy homeostasis in response to cold or CL treatments (Baskin et al., 2015). In acute cold, muscles provide heat for body temperature defenses through shivering and non-shivering thermogenesis. For example, Sarcolipin (Sln) has been shown to be an important mediator in muscle-based non-shivering thermogenesis. Under acute cold exposure, Sln knock-out mice failed to maintain their core body temperatures (Bal et al., 2012). Meanwhile, CL treatment has been shown to promote the expression of uncoupling proteins such as UCP2 and UCP3 in skeletal muscle (Nagase et al., 1996; Nakamura et al., 2001). Besides, it has been reported that cold stimulation promoted FFA release from white adipocytes, which caused a metabolic switch in the liver by activating the nuclear receptor HNF4α and producing acylcarnitines (Simcox et al., 2017). Here, we aimed to explore the commonalities and heterogeneity of cold exposure and CL administration on iWAT transcriptome during the induction of beige fat browning, though contributions from other metabolic organs may also play a role in the overall outcomes.

CONCLUSION

In summary, our results specify both common and unique features of the molecular signatures in white fat brown activated by cold exposure or CL treatment. They commonly activate mitochondrial gene programs. Moreover, both stimulations inhibit inflammation and cause physiological changes in cellular components, though with different preferences. In terms of substrate utilization, both stimulants mobilize lipid metabolism for heat production, while CL is additionally prone to utilize carbohydrates for energy demands. Overall, our data offer novel insights toward the complex molecular events induced by various thermogenic stimulants, and provides further understanding of the thermogenic mechanism and physiological application of β3-AR agonists.

DATA AVAILABILITY STATEMENT

The datasets presented in this study can be found in online repositories. The names of the repository/repositories and accession number(s) can be found in the article/**Supplementary Material**.

ETHICS STATEMENT

The animal study was reviewed and approved by the East China Normal University.

AUTHOR CONTRIBUTIONS

XM, DW, and LX conceived and designed the experiments, and wrote and revised the manuscript. YL, XP, and YZ performed the bioinformatic analysis and established the animal models. GL and TZ assisted in the experiments. GC assisted in data analysis. All authors have read and agreed to the published version of the manuscript.

FUNDING

This project was supported by funds from the National Natural Science Foundation of China (31770840, 31800989, 32071148, 32022034, and 81902980), National Key Research and Development Program of China (2019YFA0904500 and 2018YFC1313803), and ECNU Public Platform for Innovation (011).

SUPPLEMENTARY MATERIAL

The Supplementary Material for this article can be found online at: https://www.frontiersin.org/articles/10.3389/fphys.2021.667698/full#supplementary-material

Supplementary Figure 1 | Effect of chronic cold exposure and CL316,243 administration on systemic energy homeostasis. **(A–D)** Body weight gain, food intake, serum triglyceride (TG), and total cholesterol (TC) levels of mice treated with RT or cold **(A,B)** and PBS or CL **(C,D)**. $N = 6$ per group. Data are presented as mean ± SEM and $^{**}P < 0.01$ compared to control group.

Supplementary Figure 2 | Gene ontology (GO) biological process analysis of commonly regulated genes in iWAT of mice upon cold exposure from two RNA-seq datasets. **(A,B)** GO enrichment analysis for overlapped upregulated **(A)** and downregulated **(B)** DEGs from iWAT of mice under cold exposure as shown in GSE86338 and GSE164219 datasets.

Supplementary Figure 3 | Gene ontology (GO) biological process analysis of commonly regulated genes in iWAT of mice upon CL administration from two RNA-seq datasets. **(A,B)** GO analysis for overlapped upregulated **(A)** and downregulated **(B)** DEGs from iWAT of mice under CL administration as shown in GSE86338 and GSE129083 datasets.

REFERENCES

Abe, Y., Fujiwara, Y., Takahashi, H., Matsumura, Y., Sawada, T., Jiang, S., et al. (2018). Histone demethylase JMJD1A coordinates acute and chronic adaptation to cold stress via thermogenic phospho-switch. *Nat. Commun.* 9:1566. doi: 10.1038/s41467-018-03868-8

Arch, J. R. (2011). Challenges in beta(3)-Adrenoceptor agonist drug development. *Ther. Adv. Endocrinol. Metab.* 2, 59–64. doi: 10.1177/2042018811398517

Bai, Z., Chai, X. R., Yoon, M. J., Kim, H. J., Lo, K. A., Zhang, Z. C., et al. (2017). Dynamic transcriptome changes during adipose tissue energy expenditure reveal critical roles for long noncoding RNA regulators. *PLoS Biol.* 15:e2002176. doi: 10.1371/journal.pbio.2002176

Bal, N. C., Maurya, S. K., Sopariwala, D. H., Sahoo, S. K., Gupta, S. C., Shaikh, S. A., et al. (2012). Sarcolipin is a newly identified regulator of muscle-based thermogenesis in mammals. *Nat Med* 18, 1575–1579. doi: 10.1038/nm.2897

Bargut, T. C. L., Souza-Mello, V., Aguila, M. B., and Mandarim-de-Lacerda, C. A. (2017). Browning of white adipose tissue: lessons from experimental models. *Horm. Mol. Biol. Clin. Investig.* 31:1. doi: 10.1515/hmbci-2016-0051

Baskin, K. K., Winders, B. R., and Olson, E. N. (2015). Muscle as a "mediator" of systemic metabolism. *Cell Metab.* 21, 237–248. doi: 10.1016/j.cmet.2014.12.021

Beale, E. G., Hammer, R. E., Antoine, B., and Forest, C. (2002). Glyceroneogenesis comes of age. *FASEB J.* 16, 1695–1696. doi: 10.1096/fj.02-0407rev

Burl, R. B., Ramseyer, V. D., Rondini, E. A., Pique-Regi, R., Lee, Y. H., and Granneman, J. G. (2018). Deconstructing adipogenesis induced by beta3-Adrenergic receptor activation with single-cell expression profiling. *Cell Metab.* 28, 300–309.e304. doi: 10.1016/j.cmet.2018.05.025

Camarena, V., Sant, D., Mohseni, M., Salerno, T., Zaleski, M. L., Wang, G., et al. (2017). Novel atherogenic pathways from the differential transcriptome analysis of diabetic epicardial adipose tissue. *Nutr. Metab. Cardiovasc. Dis.* 27, 739–750. doi: 10.1016/j.numecd.2017.05.010

Collins, S. (2011). beta-Adrenoceptor signaling networks in adipocytes for recruiting stored fat and energy expenditure. *Front. Endocrinol. (Lausanne)* 2:102. doi: 10.3389/fendo.2011.00102

Cypess, A. M., Chen, Y. C., Sze, C., Wang, K., English, J., Chan, O., et al. (2012). Cold but not sympathomimetics activates human brown adipose tissue in vivo. *Proc. Natl. Acad. Sci. U.S.A.* 109, 10001–10005. doi: 10.1073/pnas.1207911109

Cypess, A. M., Weiner, L. S., Roberts-Toler, C., Franquet Elia, E., Kessler, S. H., Kahn, P. A., et al. (2015). Activation of human brown adipose tissue by a beta3-adrenergic receptor agonist. *Cell Metab.* 21, 33–38. doi: 10.1016/j.cmet.2014.12.009

Frohnert, B. I., Long, E. K., Hahn, W. S., and Bernlohr, D. A. (2014). Glutathionylated lipid aldehydes are products of adipocyte oxidative stress and activators of macrophage inflammation. *Diabetes* 63, 89–100. doi: 10.2337/db13-0777

Galitzky, J., Carpene, C., Bousquet-Melou, A., Berlan, M., and Lafontan, M. (1995). Differential activation of beta 1-, beta 2- and beta 3-adrenoceptors by catecholamines in white and brown adipocytes. *Fundam. Clin. Pharmacol.* 9, 324–331. doi: 10.1111/j.1472-8206.1995.tb00506.x

Galmozzi, A., Kok, B. P., Kim, A. S., Montenegro-Burke, J. R., Lee, J. Y., Spreafico, R., et al. (2019). PGRMC2 is an intracellular haem chaperone critical for adipocyte function. *Nature* 576, 138–142. doi: 10.1038/s41586-019-1774-2

Harms, M., and Seale, P. (2013). Brown and beige fat: development, function and therapeutic potential. *Nat. Med.* 19, 1252–1263. doi: 10.1038/nm.3361

Henriques, F., Bedard, A. H., Guilherme, A., Kelly, M., Chi, J., Zhang, P., et al. (2020). Single-Cell RNA profiling reveals adipocyte to macrophage signaling sufficient to enhance thermogenesis. *Cell Rep.* 32:107998. doi: 10.1016/j.celrep.2020.107998

Himms-Hagen, J., Cui, J., Danforth, E. Jr., Taatjes, D. J., Lang, S. S., Waters, B. L., et al. (1994). Effect of CL-316,243, a thermogenic beta 3-agonist, on energy balance and brown and white adipose tissues in rats. *Am. J. Physiol.* 266, R1371–R1382. doi: 10.1152/ajpregu.1994.266.4.R1371

Hui, X., Gu, P., Zhang, J., Nie, T., Pan, Y., Wu, D., et al. (2015). Adiponectin enhances cold-induced browning of subcutaneous adipose tissue via promoting M2 macrophage proliferation. *Cell Metab.* 22, 279–290. doi: 10.1016/j.cmet.2015.06.004

Iwase, M., Tokiwa, S., Seno, S., Mukai, T., Yeh, Y. S., Takahashi, H., et al. (2020). Glycerol kinase stimulates uncoupling protein 1 expression by regulating fatty acid metabolism in beige adipocytes. *J. Biol. Chem.* 295, 7033–7045. doi: 10.1074/jbc.RA119.011658

Jia, R., Luo, X. Q., Wang, G., Lin, C. X., Qiao, H., Wang, N., et al. (2016). Characterization of cold-induced remodelling reveals depot-specific differences across and within brown and white adipose tissues in mice. *Acta Physiol. (Oxf.)* 217, 311–324. doi: 10.1111/apha.12688

Jiang, Y., Berry, D. C., and Graff, J. M. (2017). Distinct cellular and molecular mechanisms for beta3 adrenergic receptor-induced beige adipocyte formation. *Elife* 6:e30329. doi: 10.7554/eLife.30329

Jimenez, M., Barbatelli, G., Allevi, R., Cinti, S., Seydoux, J., Giacobino, J. P., et al. (2003). Beta 3-adrenoceptor knockout in C57BL/6J mice depresses the occurrence of brown adipocytes in white fat. *Eur. J. Biochem.* 270, 699–705. doi: 10.1046/j.1432-1033.2003.03422.x

Khan, T., Muise, E. S., Iyengar, P., Wang, Z. V., Chandalia, M., Abate, N., et al. (2009). Metabolic dysregulation and adipose tissue fibrosis: role of collagen VI. *Mol. Cell. Biol.* 29, 1575–1591. doi: 10.1128/MCB.01300-08

Kim, D., Langmead, B., and Salzberg, S. L. (2015). HISAT: a fast spliced aligner with low memory requirements. *Nat. Methods* 12, 357–360. doi: 10.1038/nmeth.3317

Kintscher, U., Hartge, M., Hess, K., Foryst-Ludwig, A., Clemenz, M., Wabitsch, M., et al. (2008). T-lymphocyte infiltration in visceral adipose tissue: a primary event in adipose tissue inflammation and the development of obesity-mediated insulin resistance. *Arterioscler. Thromb. Vasc. Biol.* 28, 1304–1310. doi: 10.1161/ATVBAHA.108.165100

Lee, Y. H., Petkova, A. P., and Granneman, J. G. (2013). Identification of an adipogenic niche for adipose tissue remodeling and restoration. *Cell Metab.* 18, 355–367. doi: 10.1016/j.cmet.2013.08.003

Lin, C. J., Hu, Z. G., Yuan, G. D., Lei, B., and He, S. Q. (2018). Complements are involved in alcoholic fatty liver disease, hepatitis and fibrosis. *World J. Hepatol.* 10, 662–669. doi: 10.4254/wjh.v10.i10.662

Lowell, B. B., S-Susulic, V., Hamann, A., Lawitts, J. A., Himms-Hagen, J., Boyer, B. B., et al. (1993). Development of obesity in transgenic mice after genetic ablation of brown adipose tissue. *Nature* 366, 740–742. doi: 10.1038/366740a0

Lumeng, C. N., and Saltiel, A. R. (2011). Inflammatory links between obesity and metabolic disease. *J. Clin. Invest.* 121, 2111–2117. doi: 10.1172/JCI57132

Lung, T., Sakem, B., Risch, L., Wurzner, R., Colucci, G., Cerny, A., et al. (2019). The complement system in liver diseases: Evidence-based approach and therapeutic options. *J. Transl. Autoimmun.* 2:100017. doi: 10.1016/j.jtauto.2019.100017

Mariman, E. C., and Wang, P. (2010). Adipocyte extracellular matrix composition, dynamics and role in obesity. *Cell. Mol. Life Sci.* 67, 1277–1292. doi: 10.1007/s00018-010-0263-4

Nagase, I., Yoshida, T., Kumamoto, K., Umekawa, T., Sakane, N., Nikami, H., et al. (1996). Expression of uncoupling protein in skeletal muscle and white fat of obese mice treated with thermogenic beta 3-adrenergic agonist. *J. Clin. Invest.* 97, 2898–2904. doi: 10.1172/JCI118748

Nakamura, Y., Nagase, I., Asano, A., Sasaki, N., Yoshida, T., Umekawa, T., et al. (2001). Beta 3-adrenergic agonist up-regulates uncoupling proteins 2 and 3 in skeletal muscle of the mouse. *J. Vet. Med. Sci.* 63, 309–314. doi: 10.1292/jvms.63.309

Nedergaard, J., Bengtsson, T., and Cannon, B. (2007). Unexpected evidence for active brown adipose tissue in adult humans. *Am. J. Physiol. Endocrinol. Metab.* 293, E444–E452. doi: 10.1152/ajpendo.00691.2006

Nguyen, K. D., Qiu, Y., Cui, X., Goh, Y. P., Mwangi, J., David, T., et al. (2011). Alternatively activated macrophages produce catecholamines to sustain adaptive thermogenesis. *Nature* 480, 104–108. doi: 10.1038/nature10653

Pertea, M., Pertea, G. M., Antonescu, C. M., Chang, T. C., Mendell, J. T., and Salzberg, S. L. (2015). StringTie enables improved reconstruction of a transcriptome from RNA-seq reads. *Nat. Biotechnol.* 33, 290–295. doi: 10.1038/nbt.3122

Prentki, M., and Madiraju, S. R. (2008). Glycerolipid metabolism and signaling in health and disease. *Endocr. Rev.* 29, 647–676. doi: 10.1210/er.2008-0007

Rajbhandari, P., Arneson, D., Hart, S. K., Ahn, I. S., Diamante, G., Santos, L. C., et al. (2019). Single cell analysis reveals immune cell-adipocyte crosstalk regulating the transcription of thermogenic adipocytes. *Elife* 8:e49501. doi: 10.7554/eLife.49501

Robinson, M. D., McCarthy, D. J., and Smyth, G. K. (2010). edgeR: a Bioconductor package for differential expression analysis of digital gene expression data. *Bioinformatics* 26, 139–140. doi: 10.1093/bioinformatics/btp616

Rosell, M., Kaforou, M., Frontini, A., Okolo, A., Chan, Y. W., Nikolopoulou, E., et al. (2014). Brown and white adipose tissues: intrinsic differences in gene expression and response to cold exposure in mice. *Am. J. Physiol. Endocrinol. Metab.* 306, E945–E964. doi: 10.1152/ajpendo.00473.2013

Sharp, L. Z., Shinoda, K., Ohno, H., Scheel, D. W., Tomoda, E., Ruiz, L., et al. (2012). Human BAT possesses molecular signatures that resemble beige/brite cells. *PLoS One* 7:e49452. doi: 10.1371/journal.pone.0049452

Simcox, J., Geoghegan, G., Maschek, J. A., Bensard, C. L., Pasquali, M., Miao, R., et al. (2017). Global analysis of plasma lipids identifies liver-derived acylcarnitines as a fuel source for brown fat thermogenesis. *Cell Metab.* 26, 509–522.e506. doi: 10.1016/j.cmet.2017.08.006

Sun, K., Tordjman, J., Clement, K., and Scherer, P. E. (2013). Fibrosis and adipose tissue dysfunction. *Cell Metab.* 18, 470–477. doi: 10.1016/j.cmet.2013.06.016

Sun, W., Dong, H., Balaz, M., Slyper, M., Drokhlyansky, E., Colleluori, G., et al. (2020). snRNA-seq reveals a subpopulation of adipocytes that regulates thermogenesis. *Nature* 587, 98–102. doi: 10.1038/s41586-020-2856-x

Villarroya, F., Cereijo, R., Gavalda-Navarro, A., Villarroya, J., and Giralt, M. (2018). Inflammation of brown/beige adipose tissues in obesity and metabolic disease. *J. Intern. Med.* 284, 492–504. doi: 10.1111/joim.12803

Wang, W., Ishibashi, J., Trefely, S., Shao, M., Cowan, A. J., Sakers, A., et al. (2019). A PRDM16-Driven Metabolic Signal from Adipocytes Regulates Precursor Cell Fate. *Cell Metab.* 30, 174–189.e175. doi: 10.1016/j.cmet.2019.05.005

Weisberg, S. P., McCann, D., Desai, M., Rosenbaum, M., Leibel, R. L., and Ferrante, A. W. Jr. (2003). Obesity is associated with macrophage accumulation in adipose tissue. *J. Clin. Invest.* 112, 1796–1808. doi: 10.1172/JCI19246

Xu, Z., You, W., Zhou, Y., Chen, W., Wang, Y., and Shan, T. (2019). Cold-induced lipid dynamics and transcriptional programs in white adipose tissue. *BMC Biol.* 17:74. doi: 10.1186/s12915-019-0693-x

Yoshida, T., Umekawa, T., Sakane, N., Yoshimoto, K., and Kondo, M. (1996). Effect of CL316,243, a highly specific beta3-adrenoceptor agonist, on sympathetic nervous system activity in mice. *Metabolism* 45, 787–791. doi: 10.1016/s0026-0495(96)90147-x

Yu, G., Wang, L. G., Han, Y., and He, Q. Y. (2012). clusterProfiler: an R package for comparing biological themes among gene clusters. *OMICS* 16, 284–287. doi: 10.1089/omi.2011.0118

Zhang, H., Chen, X., Xue, P., Ma, X., Li, J., and Zhang, J. (2020). FN1 promotes chondrocyte differentiation and collagen production via TGF-beta/PI3K/Akt pathway in mice with femoral fracture. *Gene* 769:145253. doi: 10.1016/j.gene.2020.145253

Zhao, Q., Zhang, Z., Rong, W., Jin, W., Yan, L., Jin, W., et al. (2020). KMT5c modulates adipocyte thermogenesis by regulating Trp53 expression. *Proc. Natl. Acad. Sci. U.S.A.* 117, 22413–22422. doi: 10.1073/pnas.1922548117

Conflict of Interest: The authors declare that the research was conducted in the absence of any commercial or financial relationships that could be construed as a potential conflict of interest.

Copyright © 2021 Li, Ping, Zhang, Li, Zhang, Chen, Ma, Wang and Xu. This is an open-access article distributed under the terms of the Creative Commons Attribution License (CC BY). The use, distribution or reproduction in other forums is permitted, provided the original author(s) and the copyright owner(s) are credited and that the original publication in this journal is cited, in accordance with accepted academic practice. No use, distribution or reproduction is permitted which does not comply with these terms.

frontiers in Endocrinology

CASE REPORT
published: 31 May 2021
doi: 10.3389/fendo.2021.690996

Case Report: Metreleptin and SGLT2 Inhibitor Combination Therapy Is Effective for Acquired Incomplete Lipodystrophy

Ayako Nagayama[1], Kenji Ashida[1], Miki Watanabe[1], Kanoko Moritaka[1], Aya Sonezaki[1], Yoichiro Kitajima[2], Hirokazu Takahashi[3], Satoko Yoshinobu[1], Shimpei Iwata[1], Junichi Yasuda[1], Nao Hasuzawa[1], Shuichi Ozono[4], Seiichi Motomura[1] and Masatoshi Nomura[1]*

[1] Division of Endocrinology and Metabolism, Department of Internal Medicine, Kurume University School of Medicine, Kurume, Japan, [2] Eguchi Hospital, Ogi, Japan, [3] Division of Hepatology, Diabetes Mellitus, and Endocrinology, Department of Internal Medicine, Saga University, Saga, Japan, [4] Department of Pediatrics and Child Health, Kurume University School of Medicine, Kurume, Japan

OPEN ACCESS

Edited by:
Seung-Hyun Ro,
University of Nebraska-Lincoln, United States

Reviewed by:
Hirofumi Hitomi,
Kansai Medical University, Japan
Adela Penesova,
Slovak Academy of Sciences, Slovakia
Tomoki Maeda,
Oita University, Japan

***Correspondence:**
Kenji Ashida
ashida@med.kurume-u.ac.jp

Specialty section:
This article was submitted to Obesity, a section of the journal Frontiers in Endocrinology

Received: *05 April 2021*
Accepted: *13 May 2021*
Published: *31 May 2021*

Citation:
Nagayama A, Ashida K, Watanabe M, Moritaka K, Sonezaki A, Kitajima Y, Takahashi H, Yoshinobu S, Iwata S, Yasuda J, Hasuzawa N, Ozono S, Motomura S and Nomura M (2021) Case Report: Metreleptin and SGLT2 Inhibitor Combination Therapy Is Effective for Acquired Incomplete Lipodystrophy. Front. Endocrinol. 12:690996. doi: 10.3389/fendo.2021.690996

Childhood cancer survivors (CCSs) who have undergone bone marrow transplantation with systemic chemotherapy and whole-body irradiation often experience impaired glucose tolerance with marked insulin resistance. Incomplete acquired diabetic lipodystrophy should be considered as a late complication of bone marrow transplantation. A 24-year-old Japanese female patient with incomplete acquired lipodystrophy, a CCS of acute lymphocytic leukemia at the age of 3 years, was treated for diabetes mellitus and dyslipidemia at our hospital. Administration of multiple daily insulin injections (70 units/day), and oral administration of 500 mg/day metformin, 15 mg/day pioglitazone, and 200 mg/day bezafibrate had proven ineffective for her metabolic disorders. Subcutaneous administration of metreleptin improved her insulin resistance and hypertriglyceridemia within a month; however, it failed to maintain adequate plasma glucose levels in the long term. When oral administration of 10 mg/day empagliflozin was added to the metreleptin supplementation, her HbA1c value (National Glycohemoglobin Standardization Program) improved from 11% to 8%, which was maintained for an additional 18 months. This is the first case report of incomplete lipodystrophy that shows efficacy of a combination therapy with metreleptin and a sodium glucose cotransporter 2 (SGLT2) inhibitor for the treatment of diabetes and dyslipidemia. An SGLT2 inhibitor attenuates hyperglycemia through urinary glucose excretion and has been suggested to enhance lipid catabolism in the extra-adipose tissues, especially in the liver and skeletal muscles. Furthermore, metreleptin supplementation could enhance the action of the SGLT2 inhibitor by promoting satiety and lipolysis through the central nervous system. Combination therapy with metreleptin and an SGLT2 inhibitor was suggested to recover the volume of adipose tissue, possibly through improvement of insulin resistance in the adipose tissue. This report highlights the pathophysiological mechanism of an SGLT2 inhibitor in the improvement of glucose metabolism in non-healthy lean CCSs with insulin

resistance. Administration of SGLT2 inhibitor, along with metreleptin supplementation, could be a good alternative therapy for diabetic lipodystrophy observed in CCSs.

Keywords: lipodystrophy, SGLT2 inhibitor, metreleptin, hypertriglyceridemia, diabetes mellitus

INTRODUCTION

Childhood cancer survivors (CCS) are at a high risk of cardiovascular events and mortality (1, 2), even after they have overcome their critical malignancies. CCSs often experience impaired glucose tolerance with marked insulin resistance as a late complication of hematopoietic stem cell transplantation and whole-body irradiation during childhood (3). Acquired incomplete lipodystrophy is considered as the pathogenesis for these conditions (4). Accordingly, supplementation with recombinant leptin, metreleptin, is a reasonable therapy for CCS for the improvement of their lipid and blood glucose profiles (5–7), and for the prevention of critical cardiovascular complications.

Disturbance in both white and brown adipose tissues has been suggested to occur during radiation therapy-related acquired incomplete lipodystrophy (4), although white adipose tissue abnormalities are the predominant disorder in congenital generalized lipodystrophy (8). Administration of a sodium glucose cotransporter 2 (SGLT2) inhibitor has been suggested as a candidate therapy for glucose impairment in a patient with congenital generalized lipodystrophy (9). SGLT2 inhibitor administration reduces hyperglycemia and fat accumulation in adipose tissues by increasing urinary glucose excretion in patients with type 2 diabetes mellitus (T2DM) (10). Additionally, an SGLT2 inhibitor has been suggested to improve glucose impairment through changes in glucose and lipid metabolisms in both adipose and extra-adipose tissues (11, 12). However, the precise mechanism of the beneficial effects of the SGLT2 inhibitor on lipodystrophy remains to be clarified.

We present a case of acquired incomplete diabetic lipodystrophy wherein the patient was treated with a combination of metreleptin supplementation and an SGLT2 inhibitor. We have previously reported the effect of metreleptin administration on lipid and glucose metabolisms in this case (5). An additional 2-year observation revealed dysregulation of hyperglycemia and continuous amelioration of hyperlipidemia. Herein, we observed that SGLT2 inhibitor administration in addition to metreleptin supplementation could regulate the patient's hyperglycemia and hyperlipidemia. An improvement was observed in her glucose and lipid profiles for an additional 18 months. Furthermore, recovery of adipose accumulation in the subcutaneous and visceral adipose tissues was demonstrated. SGLT2 inhibitor administration has the potential to be a suitable alternative for the treatment of major abnormalities in glucose and lipid metabolism and body composition in CCSs.

CASE DESCRIPTION

A 24-year-old Japanese female patient presented to our endocrinology center with hyperglycemia, and a 13-year history of acquired incomplete diabetic lipodystrophy with hypertriglyceridemia and non-alcoholic fatty liver disease (5). Systemic chemotherapy and whole-body irradiation before allogeneic stem cell transplantation for acute lymphocytic leukemia at 3 years of age were considered as possible reasons for lipodystrophy development (3, 5). Administration of 500 mg/day metformin and 15 mg/day pioglitazone, along with multiple daily subcutaneous injections of high-dose insulin (70 units/day)

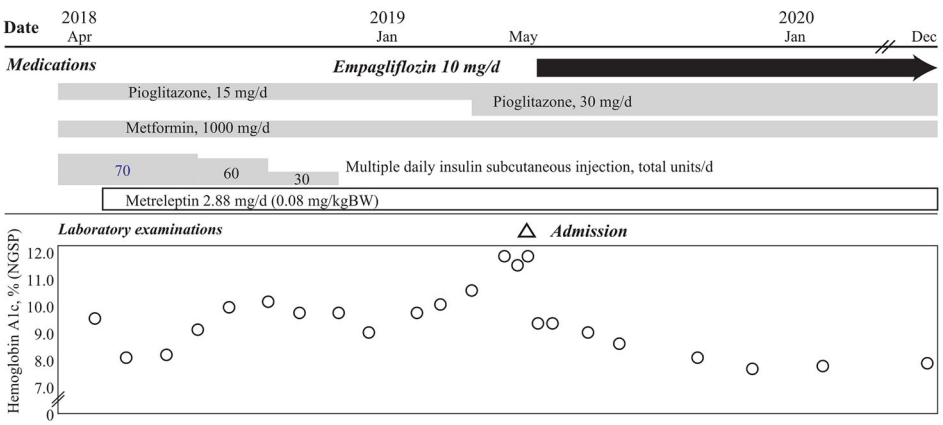

FIGURE 1 | Clinical course of the patient in this case. Hemoglobin A1c levels of the patient in this case show rapid reduction after oral administration of empagliflozin, with continuation of 15 mg/day pioglitazone and 1000 mg/day metformin, and 2.88 mg/day of subcutaneous metreleptin supplementation, with termination of insulin injection. The HbA1c level is maintained at ~8.0%, 18 months after empagliflozin initiation.

had failed to improve her hyperglycemia (**Figure 1**). Moreover, oral administration of 200 mg/day bezafibrate had failed to improve the hypertriglyceridemia. However, subcutaneous administration of metreleptin (0.08 mg/kg bodyweight/day) markedly improved her hypertriglyceridemia from 3897 mg/dL to 1828 mg/dL (reference range, 30–149 mg/dL) and the insulin resistance; the glucose infusion rate (GIR) during euglycemic glucose clamp examination (<5.7 mg/kg/min indicates insulin resistance) increased from 2.1 mg/kg bodyweight/min to 3.2 mg/kg bodyweight/min in 1 month. Her glycemic control improved, and the HbA1c value attenuated rapidly from 9.6% to 8.1% (National Glycohemoglobin Standardization Program: NGSP) (reference range, 4.6–6.2%) (5); however, no further consistent improvement was observed, and her HbA1c levels increased to 11.3% before empagliflozin initiation (**Figure 1** and **Table 1**).

After 1 year of metreleptin administration, oral administration of 10 mg/day empagliflozin was initiated, as her HbA1c level was still high at 11% (NGSP). Her glycemic control improved immediately, and the HbA1c level decreased to ~8% (NGSP). On physical examination, her bodyweight and body mass index of 30.5 kg and 15.6 kg/m^2, respectively, before administration of metreleptin and empagliflozin, had reduced to 28.6 kg and 14.6 kg/m^2, respectively, following 18 months from empagliflozin initiation and continuous metreleptin supplementation. The area under the curve and fluctuations in the daily plasma glucose, measured using a flash glucose monitoring (FGM) system, demonstrated significant improvements (**Supplementary Figure 1**). Notably, body composition analysis using computed tomography imaging disclosed an increase in visceral and subcutaneous fat accumulation, with reduced liver steatosis and unchanged muscle areas (**Figure 2**). Additionally, her insulin resistance and liver steatosis, evaluated using proton density fat fraction and T1 subtraction imaging on magnetic resonance imaging, improved (13) (**Figure 2**). Furthermore, her triglyceride level had decreased to 652 mg/dL (**Table 2**). For an additional 18 months from SGLT2 inhibitor initiation, her HbA1c level remained steady at 7.8% (NGSP); no specific adverse events, including urinary tract infection, were observed (**Figure 1** and **Table 1**). Evaluations using a questionnaire that comprised a visual analogue scale analysis revealed enhanced satiety in the patient; her appetite had reduced to 70% of what it was prior to metreleptin administration. Based on the ideal body mass index for the patient and her routine activities, a diet therapy with an intake of 1380 kcal/day was recommended (14). Administration of the SGLT2 inhibitor did not alter her satiety or adherence to the therapies. Her adherence to the combination therapy was well-preserved and her vigor had increased.

TABLE 1 | Laboratory findings of glucose metabolisms evaluated pre- and post-treatment with an SGLT2 inhibitor.

Variables, unit	Value		Reference range
	Pre-treatment	Post-treatment	
Diabetes mellitus profile			
Plasma glucose, mg/dL	215	98	73–109
HbA1c, % (NGSP)	11.3	7.8	4.9–6.0
Serum C-peptide, ng/dL	3.9	3.3	0.8–2.5
3-OHBA, μmol/L	66	90	0–74.0
HOMA-IR	6.37	2.46	
Glucagon loading test[†]			
ΔC-peptide, ng/dL	2.92	2.10	
Urinalysis			
Albumin, mg/day	1963.5	1051.5	
Glucose, g/day	29.14	24.64	

[†]ΔC-peptide is defined as an elevated value of the serum C-peptide level measured 6 minutes after the administration of 1-mg glucagon intravenous injection when compared with the baseline level.

HbA1c, hemoglobin A1c; 3-OHBA, 3-hydroxybutyric acid; GIR, glucose infusion rate; NGSP, National Glycohemoglobin Standardization Program.

DISCUSSION

We observed the first case of acquired diabetic lipodystrophy in which hyperglycemia improved with administration of SGLT2 inhibitor in addition to subcutaneous metreleptin supplementation. Additionally, combination therapy with metreleptin and empagliflozin decreased adipose accumulation in the extra-adipose tissues, and increased it in the adipose tissues. This study revealed the potential benefits of using SGLT2 inhibitors for non-obese patients with diabetes, especially in CCSs with lipodystrophy.

Combination therapy with SGLT2 inhibitor and metreleptin supplementation has the potential to improve glycemic control in patients with acquired diabetic lipodystrophy. The role of ectopic adipose accumulation in insulin resistance has been indicated in both complete and incomplete lipodystrophies, which is consistent with the findings of previous literature (9). Administration of an SGLT2 inhibitor increased urinary glucose excretion, and significantly improved the daily plasma glucose fluctuation and fasting plasma glucose levels (**Table 1**, **Figure 1**, and **Supplementary Figure 1**) (12, 15). Administration of an SGLT2 inhibitor promotes glucagon secretion. Chronic promotion of glucagon secretion activates mitochondrial oxidative phosphorylation, which leads to the attenuation of liver steatosis and insulin resistance (16). Moreover, a previous study has described a case of complete diabetic lipodystrophy wherein hyperglycemia rapidly improved after SGLT2 inhibitor administration (9). The glucose metabolism impairment in our case improved to approximately the same level as that in the complete lipodystrophy case; the HbA1c level of our patient changed from 11.3% to 7.6% in 7 months, and in the previously reported case (9), from 9.3% to 6.9% in 6 months. We confirmed consistent improvement in the glucose metabolism with regard to insulin resistance and plasma glucose variability, evaluated by GIR and the homeostasis model assessment of insulin resistance (HOMA-IR), and FGM, respectively. Although metreleptin supplementation failed to improve the hyperglycemia in this study before SGLT2 inhibitor administration, a previous study demonstrated consistent improvement in glucose levels in a patient with CCS-related diabetic dystrophy (7). Leptin

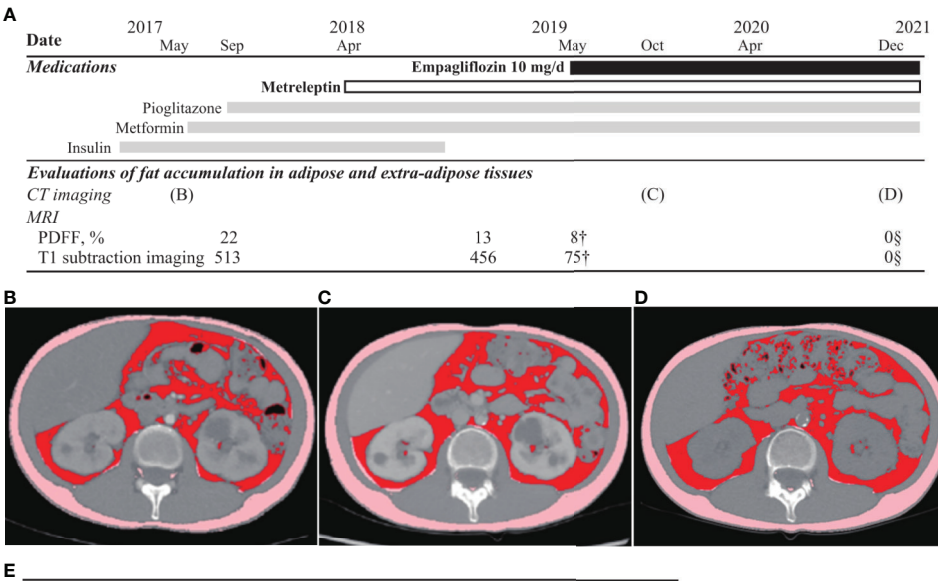

E

Parameters	May 19, 2017 pre-treatment	Oct 16, 2019 post-treatment	Dec 9, 2020 post-treatment
Body mass index, kg/m^2	15.6	14.8	14.6
Total fat area, cm^2	82.1	92.0	92.7
Visceral fat area, cm^2	42.4	45.4	48.9
Subcutaneous fat area, cm^2	39.7	46.6	43.8
Muscle area, cm^2	31.4	27.4	28.4

FIGURE 2 | Evaluations of fat accumulation in the adipose and extra-adipose tissues. Body fat accumulation has been evaluated during the clinical course. **(A)** The time of evaluation using computed tomography (CT) imaging and magnetic resonance imaging as well as clinical time course of medications are presented. Fat accumulation in liver is decreased and eventually, not detected using the proton density fat fraction (PDFF) method and T1 subtraction imaging. Areas of visceral, subcutaneous, and total fat are increased, observed in the CT imaging analysis between before **(B)** and after **(C, D)** metreleptin and empagliflozin administrations, although muscle areas are not increased **(E)**. Additionally, changes in fat volume and body mass index between before- and after-combination therapy using SGLT2 inhibitor and metreleptin administration are demonstrated. CT, computed tomography; PDFF, proton density fat fraction.

administration has been shown to improve insulin sensitivity through the activation of adenosine monophosphate-activated protein kinase (17). Furthermore, metreleptin supplementation enhances satiety through the hypothalamus (18), while SGLT2 inhibitor administration enhances appetite as an adverse effect (15). Considering these findings, sufficient leptin activity is required in patients with lipodystrophy for effective diabetes mellitus therapy using an SGLT2 inhibitor.

SGLT2 inhibitor administration under sufficient leptin function was suggested to decrease adipose accumulation in the extra-adipose tissues, and increased it in the adipose tissues. Combination therapy with SGLT2 inhibitor and metreleptin increased both subcutaneous and visceral adipose volume in our patient, who had low adiposity. Administration of an SGLT2 inhibitor may demonstrate adipose redistribution through attenuation of insulin resistance and lipolysis in the extra-adipose tissues (11). Additionally, a recent study has described a case of CCS-related acquired partial lipodystrophy with high adiposity wherein adiposity in the fat tissue was decreased after metreleptin administration. Furthermore, metreleptin supplementation activates brown adipose tissue and lipolysis in some regions, including extra-adipose tissues, through sympathetic nerve stimulation (18, 19). In this context, the combination therapy should lead to the redistribution of adipose tissues in the patients with CCS-related lipodystrophy. Notably, disturbance in both white and brown adipose tissues has been observed in CCSs with lipodystrophy, although white adipose tissue insufficiency is observed predominantly in patients with inherited complete lipodystrophy (8). Furthermore, both visceral and subcutaneous fat volumes were recovered using the combination therapy of metreleptin and SGLT2 inhibitor administration in this case. SGLT2 inhibitor with metreleptin supplementation may improve glucose metabolism impairment, compensating for the brown and white adipose tissue dysfunction and preserving skeletal muscle volume (9–11) in CCSs with diabetic lipodystrophy.

SGLT2 inhibitor could improve the prognosis of CCSs through risk reduction of their cardiovascular events. The patient in this case had multiple risk factors for cardiovascular disease, including diabetes mellitus with insulin resistance and high daily glucose fluctuation, hypertriglyceridemia, non-alcoholic fatty liver disease, and low adiponectin level. Empagliflozin has been shown to improve cardiovascular outcomes such as the all-cause mortality rate of patients with

TABLE 2 | Results of laboratory examinations pre- and post-treatment with an SGLT2-inhibitor.

Variables, unit	Value		Reference range
	Pre-treatment	Post-treatment	
Serum chemistry			
Albumin, g/dL	4.0	4.3	4.1–5.1
AST, IU/L	17	16	13–30
ALT, IU/L	21	11	7–30
γ-Glutamyl transpeptidase	26	19	9–32
Lipid profile			
LDL cholesterol, mg/dL	80	136	65.0–139.0
HDL cholesterol, mg/dL	29	32	40–103
RLP cholesterol, mg/dL	88.7	31.5	≤ 7.5
Triglyceride, mg/dL	1816	652	30–149
Apolipoprotein			
A-I, mg/dL	102	110	122–161
A-II, mg/dL	35.4	33.3	24.6–33.3
B, mg/dL	159	145	69–105
C-II, mg/dL	31.4	16.1	1.5–3.8
C-III, mg/dL	85.3	40.2	5.4–9.0
E, mg/dL	23.3	8.6	> 36
Leptin, ng/mL	10†	856‡, 240	2.5–21.8
Adiponectin, μg/mL	0.3†	1.79	> 4.0

Blood surrogate markers related to fatty liver or lipid profile are listed. The values described for before and after SGLT2 inhibitor administration are presented as pre-treatment and post-treatment, respectively. Both pre-treatment and post-treatment values are those measured with the administration of metreleptin, except for the measurement of leptin and adiponectin. †Measured before metreleptin administration. ‡Measured after metreleptin administration and before SGLT2 inhibitor administration.

T2DM (20). Furthermore, several advantages of SGLT2 inhibitor use have been reported, which includes reduction in hyperinsulinemia in patients with T2DM (21). Additionally, improvements in daily glucose fluctuation, which promote cardiovascular events (22), have been studied (11, 23). Both amelioration of insulin resistance and daily glucose fluctuation are plausible pathophysiological mechanisms of reducing the risk of a cardiovascular event. Ectopic adiposities, especially as liver and muscle steatosis, can be the targets of SGLT2 inhibitor use in non-obese patients with T2DM (11, 24). CCSs, with accumulating re-distributed ectopic fat from the adipose tissues to the liver and muscles, are good candidates to explain the pathophysiological mechanism of SGLT2 inhibitors, beyond its glucose-lowering effect.

Our case study had few limitations. Administration of the SGLT2 inhibitor alone might have improved the glucose impairment and dyslipidemia in this case. Additional observation is required to demonstrate the long-term effectiveness and safety of SGLT2 inhibitors in CCSs. We believe that further case studies or large-scale studies might confirm our conclusion.

CONCLUSION

Hyperglycemia associated with acquired diabetic lipodystrophy improved with the administration of an SGLT2 inhibitor in addition to metreleptin supplementation. This study revealed the potential benefits of combination therapy using metreleptin and an SGLT2 inhibitor for non-obese patients with diabetes, especially CCSs with lipodystrophy. SGLT2 inhibitors could improve the prognosis of CCSs through risk reduction of their cardiovascular events. Further, this study revealed the pathophysiological mechanisms of glucose metabolism in CCSs and non-healthy non-obese patients with insulin resistance.

DATA AVAILABILITY STATEMENT

The original contributions presented in the study are included in the article/**Supplementary Material**. Further inquiries can be directed to the corresponding author.

ETHICS STATEMENT

The studies involving human participants were reviewed and approved by Kurume University Hospital. The patients/participants provided their written informed consent to participate in this study. Written informed consent was obtained from the individual(s) for the publication of any potentially identifiable images or data included in this article.

AUTHOR CONTRIBUTIONS

AN collected the data and wrote the first draft of the manuscript with the support of KA and MN. KA, YK, HT, and MN reviewed the manuscript. AN, KA, MW, KM, AS, YK, HT, SY, SI, JY, NH, SO, SM, and MN discussed the case and approved the final manuscript. All authors contributed to the article and approved the submitted version.

ACKNOWLEDGMENTS

We would like to thank Editage (www.editage.com) for English language editing.

SUPPLEMENTARY MATERIAL

The Supplementary Material for this article can be found online at: https://www.frontiersin.org/articles/10.3389/fendo.2021.690996/full#supplementary-material

REFERENCES

1. Fidler MM, Reulen RC, Winter DL, Kelly J, Jenkinson HC, Skinner R, et al. Long Term Cause Specific Mortality Among 34 489 Five Year Survivors of Childhood Cancer in Great Britain: Population Based Cohort Study. *BMJ* (2016) 354:i4351. doi: 10.1136/bmj.i4351
2. Armstrong GT, Chen Y, Yasui Y, Leisenring W, Gibson TM, Mertens AC, et al. Reduction in Late Mortality Among 5-Year Survivors of

ChildhoodCancer. *N Engl J Med* (2016) 374:833–42. doi: 10.1056/NEJMoa1510795
3. Taskinen M, Saarinen-Pihkala UM, Hovi L, Lipsanen-Nyman M. Impaired Glucose Tolerance and Dyslipidaemia as Late Effects After Bone-Marrow Transplantation in Childhood. *Lancet* (2000) 356:993–7. doi: 10.1016/S0140-6736(00)02717-3
4. Araújo-Vilar D, Santini F. Diagnosis and Treatment of Lipodystrophy: A Step-by-Step Approach. *J Endocrinol Invest* (2019) 42:61–73. doi: 10.1007/s40618-018-0887-z
5. Nagayama A, Ashida K, Moritaka K, Hidaka M, Gobaru M, Tanaka S, et al. Metreleptin Supplementation for Improving Lipid and Glycemic Profiles in Acquired Diabetes Lipodystrophy: A Case Report. *J Endocr Soc* (2019) 3:2179–83. doi: 10.1210/js.2019-00251
6. Hosokawa M, Shibata H, Hosokawa T, Irie J, Ito H, Hasegawa T. Acquired Partial Lipodystrophy With Metabolic Disease in Children Following Hematopoietic Stem Cell Transplantation: A Report of Two Cases and a Review of the Literature. *J Pediatr Endocrinol Metab* (2019) 32:537–41. doi: 10.1515/jpem-2018-0356
7. Adachi M, Muroya K, Hanakawa J, Asakura Y. Metreleptin Worked in a Diabetic Woman With a History of Hematopoietic Stem Cell Transplantation (HSCT) During Infancy: Further Support for the Concept of 'HSCT-Associated Lipodystrophy'. *Endocr J* (2021) 68:399–407. doi: 10.1507/endocrj.EJ20-0325
8. Mann JP, Savage DB. What Lipodystrophies Teach Us About the Metabolic Syndrome. *J Clin Invest* (2019) 129:4009–21. doi: 10.1172/JCI129190
9. Kawana Y, Imai J, Sawada S, Yamada T, Katagiri H. Sodium-Glucose Cotransporter 2 Inhibitor Improves Complications of Lipodystrophy: A Case Report. *Ann Intern Med* (2017) 166:450–1. doi: 10.7326/L16-0372
10. Cai X, Yang W, Gao X, Chen Y, Zhou L, Zhang S, et al. The Association Between the Dosage of SGLT2 Inhibitor and Weight Reduction in Type 2 Diabetes Patients: A Meta-Analysis. *Obesity* (2018) 26:70–80. doi: 10.1002/oby.22066
11. Goto Y, Otsuka Y, Ashida K, Nagayama A, Hasuzawa N, Iwata S, et al. Improvement of Skeletal Muscle Insulin Sensitivity by 1-Week SGLT2 Inhibitor Use. *Endocr Connect* (2020) 9:599–606. doi: 10.1530/EC-20-0082
12. Vallon V, Thomson SC. Targeting Renal Glucose Reabsorption to Treat Hyperglycaemia: The Pleiotropic Effects of SGLT2 Inhibition. *Diabetologia* (2017) 60:215–25. doi: 10.1007/s00125-016-4157-3
13. Bannas P, Hernando D Motosugi U, Roldan A, Reeder SB. Emerging Quantitative MRI Biomarkers of Diffuse Liver Disease. *Clin Liver Dis (Hoboken)* (2015) 4:129–32. doi: 10.1002/cld.424
14. Yamada S, Kabeya Y, Noto H. Dietary Approaches for Japanese Patients With Diabetes: A Systematic Review. *Nutrients* (2018) 10:1080. doi: 10.3390/nu10081080
15. Devenny JJ, Godonis HE, Harvey SJ, Rooney S, Cullen MJ, Pelleymounter MA. Weight Loss Induced by Chronic Dapagliflozin Treatment is Attenuated by Compensatory Hyperphagia in Diet-Induced Obese (DIO) Rats. *Obes (Silver Spring)* (2012) 20:1645–52. doi: 10.1038/oby.2012.59
16. Perry RJ, Zhang D, Guerra MT, Brill AL, Goedeke L, Nasiri AR, et al. Glucagon Stimulates Gluconeogenesis by INSP3R1-mediated Hepatic Lipolysis. *Nature* (2020) 579:279–83. doi: 10.1038/s41586-020-2074-6
17. Stern JH, Rutkowski JM, Scherer PE. Adiponectin, Leptin, and Fatty Acids in the Maintenance of Metabolic Homeostasis Through Adipose Tissue Crosstalk. *Cell Metab* (2016) 23:770–84. doi: 10.1016/j.cmet.2016.04.011
18. Zeng W, Pirzgalska RM, Pereira MMA, Kubasova N, Barateiro A, Seixas E, et al. Sympathetic Neuro-Adipose Connections Mediate Leptin-Driven Lipolysis. *Cell* (2015) 163:84–94. doi: 10.1016/j.cell.2015.08.055
19. Pandit R, Beerens S, Adan RAH. Role of Leptin in Energy Expenditure: The Hypothalamic Perspective. *Am J Physiol Regul Integr Comp Physiol* (2017) 312:R938–47. doi: 10.1152/ajpregu.00045.2016
20. Zinman B, Wanner C, Lachin JM, Fitchett D, Bluhmki E, Hantel S, et al. Empagliflozin, Cardiovascular Outcomes, and Mortality in Type 2 Diabetes. *N Engl J Med* (2015) 373:2117–28. doi: 10.1056/NEJMoa1504720
21. Kaneto H, Obata A, Kimura T, Shimoda M, Okauchi S, Shimo N, et al. Beneficial Effects of Sodium-Glucose Cotransporter 2 Inhibitors for Preservation of Pancreatic β-Cell Function and Reduction of Insulin Resistance. *J Diabetes* (2017) 9:219–25. doi: 10.1111/1753-0407.12494
22. Torimoto K, Okada Y, Mori H, Tanaka Y. Relationship Between Fluctuations in Glucose Levels Measured by Continuous Glucose Monitoring and Vascular Endothelial Dysfunction in Type 2 Diabetes Mellitus. *Cardiovasc Diabetol* (2013) 12:1. doi: 10.1186/1475-2840-12-1
23. Henry RR, Rosenstock J, Edelman S, Mudaliar S, Chalamandaris A-G, Kasichayanula S, et al. Exploring the Potential of the SGLT2 Inhibitor Dapagliflozin in Type 1 Diabetes: A Randomized, Double-Blind, Placebo-Controlled Pilot Study. *Diabetes Care* (2015) 38:412–9. doi: 10.2337/dc13-2955
24. Sheu WHH, Chan SP, Matawaran BJ, Deerochanawong C, Mithal A, Chan J, et al. Use of SGLT-2 Inhibitors in Patients With Type 2 Diabetes Mellitus and Abdominal Obesity: An Asian Perspective and Expert Recommendations. *Diabetes Metab J* (2020) 44:11–32. doi: 10.4093/dmj.2019.0208

Conflict of Interest: The authors declare that the research was conducted in the absence of any commercial or financial relationships that could be construed as a potential conflict of interest.

Copyright © 2021 Nagayama, Ashida, Watanabe, Moritaka, Sonezaki, Kitajima, Takahashi, Yoshinobu, Iwata, Yasuda, Hasuzawa, Ozono, Motomura and Nomura. This is an open-access article distributed under the terms of the Creative Commons Attribution License (CC BY). The use, distribution or reproduction in other forums is permitted, provided the original author(s) and the copyright owner(s) are credited and that the original publication in this journal is cited, in accordance with accepted academic practice. No use, distribution or reproduction is permitted which does not comply with these terms.

frontiers in Physiology

MINI REVIEW
published: 08 June 2021
doi: 10.3389/fphys.2021.691824

Long Noncoding RNAs: Novel Important Players in Adipocyte Lipid Metabolism and Derivative Diseases

Bin Zhang†, Saijun Xu†, Jinyan Liu, Yong Xie and Sun Xiaobo**

Institute of Medicinal Plant Development, Peking Union Medical College and Chinese Academy of Medical Sciences, Beijing, China

Obesity, a global public health issue, is characterized by excessive adiposity and is strongly related to some chronic diseases including cardiovascular diseases and diabetes. Extra energy intake-induced adipogenesis involves various transcription factors and long noncoding RNAs (lncRNAs) that control lipogenic mRNA expression. Currently, lncRNAs draw much attention for their contribution to adipogenesis and adipose tissue function. Increasing evidence also manifests the pivotal role of lncRNAs in modulating white, brown, and beige adipose tissue development and affecting the progression of the diseases induced by adipose dysfunction. The aim of this review is to summarize the roles of lncRNAs in adipose tissue development and obesity-caused diseases to provide novel drug targets for the treatment of obesity and metabolic diseases.

Keywords: long noncoding RNAs, lipid metabolism, adipogenesis, brown/beige adipose, fat, insulin resistance

OPEN ACCESS

Edited by:
Tizhong Shan,
Zhejiang University, China

Reviewed by:
Weiqin Chen,
Augusta University, United States
Yan Xiong,
Southwest Minzu University, China
Tongxing Song,
Huazhong Agricultural University, China

****Correspondence:***
Yong Xie
yxie@implad.ac.cn
Sun Xiaobo
sun_xiaobo163@163.com

†These authors have contributed equally to this work

Specialty section:
This article was submitted to Lipid and Fatty Acid Research, a section of the journal Frontiers in Physiology

Received: *07 April 2021*
Accepted: *14 May 2021*
Published: *08 June 2021*

Citation:
Zhang B, Xu S, Liu J, Xie Y and Xiaobo S (2021) Long Noncoding RNAs: Novel Important Players in Adipocyte Lipid Metabolism and Derivative Diseases. Front. Physiol. 12:691824. doi: 10.3389/fphys.2021.691824

INTRODUCTION

Emerging data show that excessive body fat, particularly obesity, is a major risk factor of mortality worldwide (Peeters et al., 2003; Blüher, 2019; Chooi et al., 2019). As the main lipid storage organ, excess adipose tissue is closely related to the occurrence and development of obesity (Sun et al., 2011). When obesity occurs, pathological changes in the morphology, composition, and function of adipose tissues can lead to the occurrence of various metabolic diseases, such as insulin resistance, fatty liver, diabetes, and cardiovascular diseases (Lavie et al., 2009; Blüher, 2019; Ghaben and Scherer, 2019; Schetz et al., 2019). It is of great significance to identify new therapeutic targets for obesity and its related metabolic diseases.

Adipose tissues are physiologically classified into white adipose tissue (WAT) and brown adipose tissue (BAT). WAT is mainly responsible for unnecessary energy storage, whereas BAT functions as fuel oxidation and energy expenditure because of containing abundant mitochondria. With the drug treatments or thermogenic stimuli, WAT possesses the potential to convert into "brown-like" cells. These brite adipocytes can also dissipate energy. Thus, promoting WAT browning might be an effective strategy to prevent obesity.

Recently, many studies have focused on the roles of nonconding RNAs in regulation of adipose tissue activities. Thereinto, long noncoding RNAs (lncRNAs) are defined as long RNA transcripts (>200 bp) not encoding proteins and these lncRNAs are a class of RNA observed to play modulatory roles in many biological processes consistent with their tissue-specificity. LncRNAs are crucial to the regulatory network of adipocyte biology, generating both positive

and negative control in lipogenesis and adipogenesis. They also affect adipose tissue functions like white fat browning and brown fat thermogenesis.

This wide range in regulatory roles may make lncRNAs, a promising new therapeutic area in the fight against obesity and related metabolic diseases. However, reviews on the roles of lncRNAs in adipose tissue dysplasia, abnormal lipid metabolism, and associated diseases are very limited. Thus, it is necessary to summarize the latest research progress into the regulation of lncRNAs in lipid metabolism and adipocyte biology. The present review focuses on summarizing the potential of lncRNAs as therapeutic targets for obesity and related diseases caused by lipid metabolism disorders and adipose tissue dysfunction.

LncRNAs: THE EMERGING REGULATORS

Discovery and Definition of LncRNAs

The development of new technologies, including genome tiling arrays, Global Nuclear Run-On sequencing (GRO-Seq), and Chromatin Isolation by RNA Purification (ChIRP-Seq), helped to identify a mass of new RNAs. LncRNAs are defined as RNA molecules longer than 200 nucleotides (Core et al., 2008; Guttman et al., 2009; Chu et al., 2011). H19, reported in 1990, may be the first identified lncRNA. After transcription by RNA polymerase II, H19 is spliced and polyadenylated like an mRNA, but it encodes no almost protein (Brannan et al., 1990; Bartolomei et al., 1991).

Since the discovery of H19, advances in genome sequencing have identified many more lncRNAs. They generally possess little potential to encode protein for the lack of open reading frames, 3′ untranslated regions, and typical terminal regions (Jarroux et al., 2017), but they play critical roles in a diversity of cellular processes, such as translation, transcription, and epigenetic modification.

Structure and Function of LncRNAs

A vast number of lncRNAs have been identified, but they urgently need to be annotated to be useful in therapeutic applications. Annotation begins by dividing newly discovered lncRNAs into one of five categories based on their relative location in the genome to protein-coding genes (Mattick and Rinn, 2015): sense lncRNAs overlap the nearest protein coding gene along the sense direction; antisense lncRNAs are those whose transcription overlaps an mRNA in any portion; intronic lncRNAs are located in an intron of a protein-coding gene; intergenic lncRNAs that are found between two protein-coding genes; and bidirectional lncRNAs are those whose transcription start site is within 1,000 base pairs (bp) from the neighboring exon and is transcribed in the opposite direction (**Figure 1A**).

Long noncoding RNAs have diverse structural motifs, including pseudoknots, stem-loops, G-quadruplexes, and triplexes. They mediate gene expression by interacting with DNA and mRNA in the nucleus, or miRNA and protein in the cytoplasm (Willingham et al., 2005; Ulitsky and Bartel, 2013; Sun and Kraus, 2015; Qian et al., 2019). Some lncRNAs act as molecular signals to promote transcription in various metabolic pathways. Others play modulatory roles like decoy, blocking pathways by binding transcription factors. LncRNAs also function as guides, joining with protein complexes and directing them to specific genome sites. These regulatory RNAs can also form scaffolds that recruit modifying enzymes to integrate different signaling pathways (**Figure 1B**). These four roles are interconnected, and a single lncRNA may exhibit different functions depending on

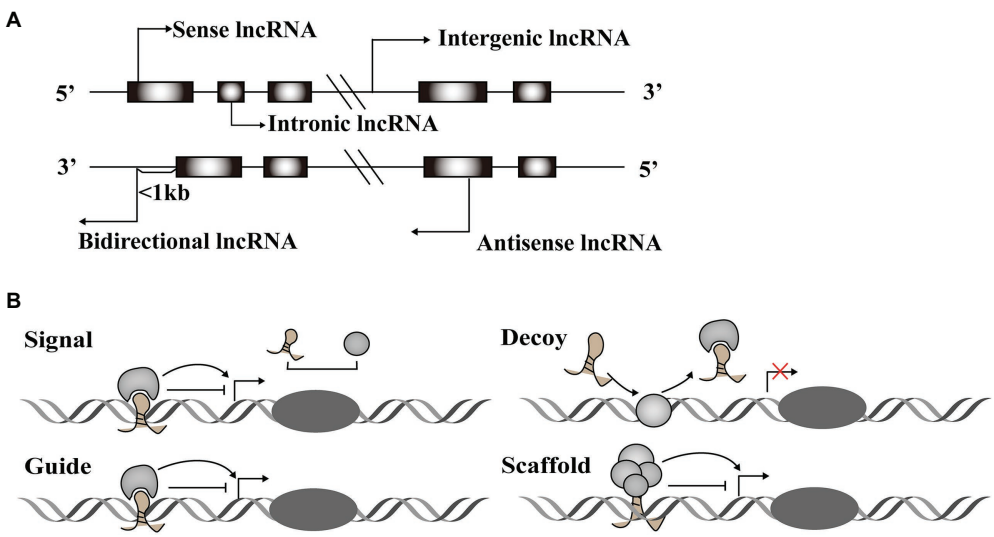

FIGURE 1 | Classification and function modes of Long noncoding RNAs (lncRNAs). **(A)** LncRNAs can be classified into five categories, including sense, antisense, intergenic, intronic, and bidirectional groups according to their relative location with the protein-coding genes. **(B)** LncRNAs function in four archetypes. Archetype I: As signals, lncRNAs can take part in signaling pathways to regulate gene expression. Archetype II: As decoys, lncRNAs combine with transcription factors to block the pathways. Archetype III: As guides, lncRNAs direct protein complexes to specific genome sites. Archetype IV: As scaffolds, lncRNAs recruit several proteins to form ribonucleoprotein complexes.

cellular conditions (Wang and Chang, 2011). Taken together, the regulatory role of lncRNAs acts across the whole process of gene expression variability.

LncRNAs and Diseases

Genome-wide association studies (GWAS) have recognized thousands of single nucleotide polymorphisms (SNPs) from noncoding regions associated with clinical phenotypes, and this intimately links lncRNAs to cardiovascular, liver, and kidney disease as well as some cancers (**Figure 2**; **Table 1**; Gao and Wei, 2017; Gong et al., 2018; Hu et al., 2019).

Long noncoding RNAs are variably expressed in the cardiovascular system under different physiological and pathological conditions. For instance, some lncRNAs regulate apoptosis of cardiomyocytes, like lncRNA Sarrah, and hypertrophy, like lncRNA cardiac-hypertrophy-associated epigenetic regulator (Chaer). Some lncRNAs can also reduce the risk of heart failure and acute myocardial infarction. For example, Mhrt prevents Brg1, a chromatin remodeling factor, from binding its DNA targets to prevent heart failure (Han et al., 2014). Another lncRNA, ZFAS1, is a marker of acute myocardial infarction in cardiac systolic function by inhibiting the activity of SERCA2a protein (Zhang Y. et al., 2018). These functions indicate that the roles of lncRNAs are critical to cardiovascular diseases.

High-throughput technologies have also characterized some lncRNAs in liver fibrosis (Bian et al., 2019). Evidence strongly support that lncRNAs are involved in regulating protein-encoding genes in liver fibrosis. For example, Zhang et al. have demonstrated that lncLFAR1 could activate TGFβ and Notch signaling pathways to promote hepatic stellate cell (HSC) activation and liver fibrosis (Zhang et al., 2017). Lnc-HSER, specifically expressed in hepatocytes (HCs), was reported to prevent the apoptosis of hepatocytes through C5AR1-Hippo-YAP pathway and alleviate hepatic fibrosis by inhibiting the HCs epithelial-mesenchymal transition mediated by Notch signaling pathway (Zhang et al., 2019).

Long noncoding RNAs also play vital roles in kidney pathogenesis (Moghaddas Sani et al., 2018). Whole transcriptome profiling analyses identified some lncRNAs associated with acute and chronic renal injury in human proximal renal tubular epithelial cells. Among them, two highlighted lncRNAs, lnc-KiAA1737-2 and lnc-MIR210HG, might participate in renal injury response (Lin et al., 2015). Furthermore, Feng et al. (2018) reported a novel lncRNA Erbb4-IR mediated by transforming growth factor/(TGFβ)/Smad3 responsible for renal fibrosis. Zhou et al. (2015) found Arid2-ir stimulated the nuclear factor kappa-B

TABLE 1 | Key roles of LncRNAs in the diseases.

Disease	LncRNA	Function	References
Cardiovascular disease	Lnc Chaer	Regulates hypertrophy	Wang et al., 2016
	LncRNA Sarrah	Suppresses cardiomyocytes' apoptosis	Trembinski et al., 2020
	Mhrt	Prevents heart failure	Han et al., 2014
Liver disease	Lnc-LFAR1	Promotes hepatic stellate cell (HSC) activation	Zhang et al., 2017
	Lnc-HSER	Prevents the apoptosis of hepatocytes	Zhang et al., 2019
Kidney disease	Linc-KiAA1737-2, lincMIR210HG	Participates in renal injury response	Lin et al., 2015
	Erbb4-IR	Responsible for renal fibrosis	Feng et al., 2018
	Arid2-IR	Activates the nuclear factor kappa-B (NF-κB) pathway	Zhou et al., 2015
Cancer	DINO	Participates in P53 signal pathway	Schmitt et al., 2016
	TUG1	Promotes the renewal of glioma stem cells (GSCs)	Katsushima et al., 2016
	TROLL-2, TROLL-3	Activates AKT pathway	Napoli et al., 2020

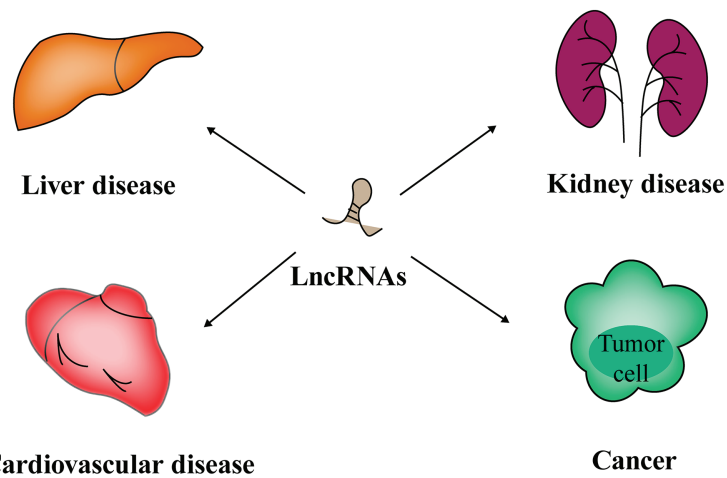

FIGURE 2 | Long noncoding RNAs play critical roles in the pathogenesis of cardiovascular, liver, and kidney disease as well as cancers.

(NF-κB)- dependent renal inflammation pathway to function in *in vitro* and *in vivo* fibrotic models.

Long noncoding RNAs also participate in the emergence and progression of cancers (Iyengar et al., 2016; Peng et al., 2017). For instance, lncRNA DINO forms a positive feed-back loop with p53 protein to amplify DNA damage signals in the nucleus (Schmitt et al., 2016). Also, activation of the Notch1 signal pathway in glioma stem cells (GSCs) specifically induced expression of the lncRNA TUG1. TUG1 functions to sponge miR-145 in cytoplasm and recruit polycomb in the nucleus to promote the renewal of GSCs (Katsushima et al., 2016). Two TAp63-regulated lncRNAs, TROLL-2, and TROLL-3, can form a trimer complex with the effector WDR26 in cytoplasm to activate AKT pathway (Napoli et al., 2020).

In summary, lncRNAs participate in different disease processes, hinting at their key roles in maintaining homeostasis of human bodies.

KEY ROLES OF LncRNAs IN CONTROLLING LIPID METABOLISM AND ADIPOCYTE DEVELOPMENT

The Roles of LncRNAs in Controlling White Adipogenesis

Adipogenesis mainly includes two stages. The first stage occurs when embryonic stem cells or mesenchymal stem cells in adipose tissue differentiate into adipose progenitor cells and then to preadipocytes. In the second stage, preadipocytes differentiate into mature adipocytes (**Figure 3**; Ali et al., 2013; Ambele et al., 2020). The whole process is accompanied by the temporal expression of many crucial adipogenesis-related genes and key transcriptional factors such as lipoprotein lipase (LPL) and sterol regulatory element binding proteins-1c (SREBP-1C). Peroxisome proliferators-activated receptor γ (PPARγ) and CCAAT/enhancer binding proteins (C/EBPs) are common markers of mature adipocytes and the major drivers of adipocyte differentiation. An increasing body of research has found that lncRNAs can regulate these pivotal genes and exert key roles in adipogenesis (Cipolletta et al., 2012; Ghaben and Scherer, 2019).

Human adipose tissue-derived stem cells (hASCs) have the ability to differentiate into both osteocytes and adipocytes. LncRNA MEG3 is upregulated in osteocyte differentiation and downregulated in adipocyte differentiation. Accordingly, MEG3 knockouts promote adipogenic differentiation but suppress osteogenic differentiation, suggesting that MEG3 may serve as a switch for hASCs' adipogenic or osteogenic differentiation (Li Z. et al., 2017).

Long noncoding RNA ADINR, transcribed from a position about 450 bp upstream of the C/EBPα gene, is induced during adipogenic differentiation. Xiao et al. (2015) revealed that ADINR increases the H3K4me3 methylation but impairs the H3K27me3 histone modification of C/EBPα during adipogenic differentiation to coordinate the transcription of C/EBPα, and this finally promoted adipogenesis in hMSCs. *Plnc1* was an lncRNA transcribed from a position 25,000 bp upstream of PPARγ2. *In vitro* studies showed that a plnc1 knockout decreases the expression of PPARγ, C/EBPα, and Fatty Acid Binding Protein 4 (AP2), which subsequently suppresses the differentiation of ST2 cells and BMSCs into mature adipocytes. However, overexpression of *Plnc1* has the opposite effect. Mechanistically, plnc1 enhances the transcriptional activity of PPARγ2 by decreasing the methylation level of CPG in PPARγ2 promoter (Zhu et al., 2019).

Long noncoding RNA MIR-140 knockout decreases the expression of key transcription factors (C/EBP and PPARγ), which directly impairs the mice's adipogenic capabilities. It suggestd that MIR-140 is a necessary regulatory factor for

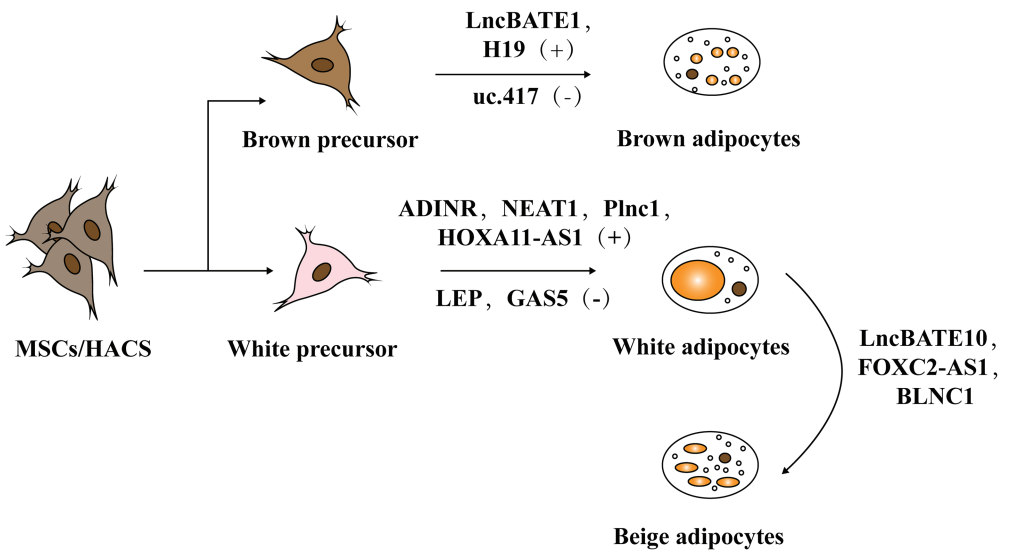

FIGURE 3 | The role of lncRNA in adipogenesis. Adipogenesis mainly includes two stages: mesenchymal stem cells (MSCs) or human adipose tissue-derived stem cells (hASCs) in adipose tissue differentiate into adipose progenitor cells and further into preadipocytes. In the second stage, preadipocytes differentiate into mature adipocytes including white adipose tissue (WAT) and brown adipose tissue (BAT).

adipocyte differentiation. Non-coding RNA qPCR array showed that NEAT1 is highly conserved between humans and mice and is upregulated in hASC differentiation. Using RNA hybrid, Gernapudi et al. (2016) identified the miR140 binding site in NEAT1 and they found that mature miR-140 can physically interact with NEAT1 in the nucleus. Further experimental data indicated that the binding of MIR-140 to NEAT1 in the nucleus increases NEAT1 stability, thus promoting adipogenesis.

Nuermaimaiti et al. (2018) found HOXA11-AS1 knockdown inhibits the transcription of adipogenesis-related genes in hASCs differentiation model, leading to the suppression of adipogenic differentiation and alleviation of lipid accumulation. Moreover, HOXA11-AS1 is highly expressed during the process of adipocyte differentiation in obese patients, indicating that it might be a potential target for the treatment of obesity.

In addition, bioinformatics analyses were used to identify a series of key mRNAs, miRNAs, and lncRNAs in hASCs adipogenesis. Several interaction axes were observed to regulate the adipogenic differentiation of hASCs, among which the leptin (LEP)-related axis was particularly important by analyzing the region upstream and downstream of leptin gene (Guo and Cao, 2019).

Some lncRNAs are reported to be potential targets that inhibit adipogenesis. The investigation based on a cDNA chip to analyze the adipogenesis regulatory genes found that the expression of lnc-U90926 was negatively correlated with the differentiation of 3 T3-L1 preadipocyte. Then, using RNA fluorescence *in situ* hybridization (FISH), researchers confirmed lnc-U90926 mainly localized to the cytoplasm of mice's preadipocytes. Gain- and loss-of-function experiments showed that the overexpression of lnc-U90926 blocked adipocyte differentiation in 3 T3-L1 as evidenced by reductions in lipid accumulation and specific protein expression, like that of PPARγ and AP2. Additionally, lnc-U90926 had lower expression levels in obese mice, which indicates it can inhibit adipogenesis by suppressing the transcriptional activity of key genes (Chen et al., 2017).

In a study on adipogenic differentiation, Li M. et al. (2018) found lncRNA GAS5 is negatively associated with adipogenesis of mesenchymal stromal cells (MSCs). Using luciferase reporter assays they further discovered that GAS5 inhibits MSCs' adipogenic differentiation by competitively sponging miR-18a. Likewise, Liu et al. (2018) determined that GAS5 has a negative role in 3 T3 cells' adipogenesis by repressing miR-21a-5p. Thus, GAS5 is an important regulator in the adipogenic differentiation.

LncHCG11 is another target for inhibiting adipogenesis. Li et al. (2020) found that the expression of lncHCG11 declines during the adipogenic differentiation in an *in vitro* hADMSCs differentiation model. Specifically, both the activity of related lipogenesis enzymes and the expressions of adipogenic proteins increase in HCG11 knockdowns, while the reverse response is observed when HCG11 is overexpressed. Bioinformatics analyses of the HCG11/miR204-5p/SIRT1 axis, in addition to experimental evidence, show that when co-transfected with a miR-204-5p mimic and pcDNA-HCG11, the miR-204-5p mimic reduced SIRT1's inhibitory effects on the expression of lipogenesis enzymes and adipogenic marker proteins to reverse pcDNA-HCG11's depression effects on adipogenesis.

The majority of lncRNAs are poorly conserved among mammals, many therapeutic applications necessitate that more attention is placed on identifying and characterizing lncRNAs in human adipose tissue. Zhang X. et al. (2018) performed RNA-seq on subcutaneous biopsy samples from healthy, lean humans and detected 1,001 adipose-enriched lncRNAs, among which lnc-ADAL is the most highly expressed. Lnc-ADAL is a non-conserved lncRNA closely tied to obesity. ShRNA-mediated knockouts suppressed the expression of lipid synthesis genes, while ASO-mediated knockouts not only impaired the expression of lipid synthesis genes in mature adipocytes but also damaged the preadipocyte differentiation. Researchers then verified that lnc-ADAL interacted with both the nuclear protein hnRNPU and cytoplasmic protein IGF2BP2 to control preadipocyte differentiation and *de novo* lipogenesis. These studies collectively support that lncRNAs emerge as important regulatory players in the process of white adipogenesis (**Table 2**).

The Roles of LncRNAs in Brown/Beige Fat Development and Their Function

Brown adipocytes (BAT) possess abundant mitochondria in the cytoplasm and high levels of uncoupling protein 1 (UCP1; Cannon et al., 1982). Accordingly, they can generate heat through uncoupling the lipid oxidative phosphorylation, facilitating the burning of fatty acid and glucose. Earlier studies supported that BAT is present and active in newborns to maintain their body temperature through non-shivering thermogenesis (Cannon and Nedergaard, 2004). Positron emission tomography (PET) detected considerable amounts of BAT in adult males, suggesting that BAT also plays an essential role in adult metabolism (Nedergaard et al., 2007). To date, a series of studies have indicated that lncRNAs are indispensable regulators in brown adipogenesis and thermogenesis (You et al., 2015).

For example, H19, a maternally inherited lncRNA, is inversely correlated with Body Mass Index (BMI) in humans. Schmidt et al. (2018) reported that H19 overexpression promotes adipogenesis and mitochondrial respiration in BAT by recruiting PEG-inactivating H19-MBD1 complexes. This study illustrated the function of H19 in regulating the BAT thermogenic gene program and metabolism.

Cui et al. (2016) identified uc.417, an ultra-conserved lncRNA that is abundant in differentiated brown adipocytes. They found that overexpression of uc.417 inhibits the differentiation of brown fat cells. They also analyzed oxygen consumption of brown adipocytes with uc.417 overexpressed and evaluated the negative roles of uc.417 overexpression in BAT's thermogenesis progress. However, knockouts of uc.417 had no significant impact on the differentiation and thermogenesis of brown adipocytes. Another lncRNA, lncBATE1, has been found to interact with hnRNP U that is necessary for brown adipogenesis and maintaining its thermogenic capacity (Alvarez-Dominguez et al., 2015). These data strongly support lncRNAs' roles in driving brown fat formation and maintaining energy balance.

Beige fat is usually stored in white fat warehouses and can be differentiated into specific beige precursor cells in WAT or derived directly from the browning of mature white fat cells under exposure to cold or other stimuli. Because they can highly express

TABLE 2 | Key roles of LncRNAs in regulating white adipogenesis.

LncRNA	Roles in adipogenesis	Proposed mechanism of action	References
MEG3	Negative	Inhibits adipogenesis *via* downregulation of miR-140-5p	Li Z. et al., 2017
ADINR	Positive	Activates C/enhancer binding proteins (EBPs) transcription	Xiao et al., 2015
Plnc1	Positive	Increases PPAR-γ2 promoter activity	Zhu et al., 2019
NEAT1	Positive	Mature miR-140 binds to NEAT1 to increase NEAT1 expression	Gernapudi et al., 2016
HOXA11-AS1	Positive	Promotes adipogenic-related genes' transcription (CEBP-α, DGAT2, etc.)	Nuermaimaiti et al., 2018
LncRNA-LEP	Positive	Activation of RP11-552F3.9- hsa-miR-130b-5p- LEP interaction axes increases leptin expression	Guo and Cao, 2019
GAS5	Negative	Suppression of miR-18a decreases CTGF expression	Li M. et al., 2018; Liu et al., 2018
Linc-ADAL	Both	Interacts with hnRNPU and IGF2BP2	Zhang X. et al., 2018

TABLE 3 | Key roles of LncRNAs in regulating brown/beige adipogenesis.

LncRNA	Roles in BAT or beige adipocytes	Proposed mechanism of action	References
H19	Positive	Recruits PEG-inactivating H19-MBD1 complexes to control brown adipocyte differentiation	Schmidt et al., 2018
uc.417	Negative	Suppresses p38MAPK's phosphorylation to impair adipogenesis	Cui et al., 2016
LncBATE1	Positive	Binds to hnRNP U to facilitate brown adipogenesis	Alvarez-Dominguez et al., 2015
FOXC2-AS1	Positive	Promote white-to-brown adipocyte conversion through autophagy activation	Wang Y. et al., 2020
LncBATE10	Positive	Elevate Pgc1α expression through decoying Celf1 from it	Bai et al., 2017
BLNC1	Positive	Form Blnc1/hnRNPU/EBF2/Zbtb7b ribonucleoprotein complexes to accelerate white adipose tissue (WAT) browning	Zhao et al., 2014; Li S. et al., 2017; Mi et al., 2017

UCP1 protein and function as BAT, induction of beige fat adipogenesis helps resist obesity and is assumed to be a promising strategy to covert unhealthy WAT into metabolically active BAT (Guerra et al., 1998; Bartelt and Heeren, 2014; Wang and Seale, 2016).

Wang Y. et al. (2020) found high expression of FOXC2-AS1 in the forskolin (Fsk)-stimulating adipocytes with high levels of UCP1 and peroxisome proliferator-activated receptorγcoactivator-1α (PGC1α). They found that FOXC2-AS1 may promote WAT browning and thermogenic program through the autophagy signaling pathway. The result showed that lncRNAs also play crucial roles in the development and functional activation of beige adipose.

In fact, some lncRNAs regulate through the co-expression network. For instance, Bai et al. (2017) found a large number of lncRNAs embedded into metabolic pathways by establishing an mRNA-lncRNA co-expression network. Through this network, they identified lncBATE10 that is rich in BAT and can decoy Celf1 from Pgc1α, activating Pgc1α expression and promoting thermogenesis and WAT browning.

Additionally, AK079912 is another BAT-enriched lncRNA. Knockdown of AK079912 decreases the expression of vital adipogenic and thermogenic genes; while overexpression upregulates the thermogenic program by increasing protein expressions of UCP1 and mitochondria electron transport chain (ETC) complexes. Moreover, Xiong et al. (2018) found expression of AK079912 in inguinal WAT could induce their browning.

Blnc1 is rich in both the brown and beige adipocytes. Overexpression of BLNC1 in brown adipocytes increases the expression of thermogenic genes through the formation of the Blnc1/hnRNPU/EBF2 ribonucleoprotein complex (Mi et al., 2017). The effects of Blnc1 on beige adipocytes were also evaluated. During brown fat whitening induced by a high-fat diet (HFD), specific deactivation of Blnc1 in the fat tissue not only accelerated the BAT to bleach, but also exacerbated the inflammation. However, fat-specific Blnc1 transgenic mice have the opposite effects. The molecular mechanism is that Blnc1, as a target of EBF2, built a feedforward regulatory loop to promote browning of WAT (Zhao et al., 2014). Additionally, Lin et al. (2015) found that BTB domain-containing 7b (Zbtb7b) could recruit the lncRNA Blnc1 through hnRNP U to increase thermogenic genes expression, and the function of Blnc1 is conserved in mice and humans (Li S. et al., 2017).

Thus, lncRNAs are important regulators for activating brown/beige adipocytes to function with the benefit of decreasing serum triglycerides and fighting against obesity (**Table 3**).

LncRNA and Lipid Homeostasis in the Liver

Besides the known roles in adipocytes, a series of studies have shown that lncRNAs regulate lipid metabolism in the liver by targeting several crucial transcription factors, such as liver X receptor (LXRs), sterol-regulatory element binding proteins (SREBPs), and peroxisome proliferation-activated receptor α (PPARα). These transcription factors are regulators of gene expression for the synthesis and uptake of cholesterol, fatty

TABLE 4 | Key roles of LncRNAs in regulating lipid homeostasis in the liver.

LncRNA	Tissue/cell type	Loss-of-Function	Gain-of-function	References
LncHR1	Hepatic cells	-	Decreases triglycerides and lipid droplets	Li D. et al., 2017
LncLSTR	Human liver	Reduces triglyceride levels	-	Li et al., 2015
Lnc19959.2	Rat liver	Lowers plasma triglyceride	-	Wang J. et al., 2020
DYN-LRB2-2	THP-1 and Raw264.7 cells	-	Upregulates cholesterol efflux	Li Y. et al., 2018
TUG1	NCTC 1469 cells	-	Slows down CE rate	Yang and Li, 2020
LncARSR	Hepatic cells	-	Promotes cholesterol biosynthesis	Huang et al., 2018
HULC	HCC cells	-	-	Cui et al., 2015
Lnc-HC	Rat liver	Increases lipid accumulation	-	Lan et al., 2019

acids, and phospholipids in the liver (Sun and Lin, 2019). Here, we summarize the regulatory mechanisms of lncRNAs in liver lipid homeostasis (**Table 4**).

LncHR1, identified in human hepatoma cells infected with HCV, negatively regulates the expression of SREBP-1c and fatty acid synthase. Overexpression of lncHR1 inhibits the accumulation of triglyceride and lipid droplets in liver cells (Li D. et al., 2017). Li et al. (2015) found liver-enriched lncLSTR could decrease the plasma triglyceride levels (TDP43/FXR/APOC2) by competitively binding with TDP-43 to regulate the expression of Cyp8b1, leading to the activation of Apoc2 *via* the nuclear receptor farnesoid-X-receptor (FXR) pathway.

Additionally, Wang J. et al. (2020) found that Lnc19959.2 was upregulated in high fat-induced hepatocytes. Mechanically, overexpressed lnc19959.2 promotes the expression of ApoA4 by interacting with nuclear protein Purb. Lnc19959.2 specifically binds to hnRNPA2B1 to negatively regulate the expression of genes related to TG metabolism. Taken together, the investigations of lncHR1 and lnc19959.2 indicate that lncRNAs specifically expressed in liver are emerging as key players in the regulation of triglycerides.

Long noncoding RNAs are also closely related to the cholesterol metabolism. Hu et al. (2019) found that ox-LDL could significantly upregulate the expression of lincRNA-DYN-LRB2-2, directly leading to an increased expression of ATP-binding cassette transporter A1 (ABCA1). Elevated expression of ABCA1 mediated cholesterol efflux (CE) in foam cells, thus reducing cholesterol levels (Li Y. et al., 2018). Another study found that lncTUG1 inhibited CE by inhibiting the expression of APOM in an miR-92a/FXR1 dependent manner (Yang and Li, 2020). Additionally, Huang et al. (2018) found overexpression of lncARSR can activate PI3K/Akt signal pathway, promoting the expression of transcription factor SREBP2. This transcription factor, in turn, increased the expression level of the rate-liming enzyme in cholesterol, HMG-CoA reductase (HMGCR), and accelerated cholesterol biosynthesis in liver.

Another group of lncRNAs can influence both the cholesterol and triglyceride level. HULC was reported to mediate abnormal lipid metabolism in hepatocellular carcinoma and elevate the levels of intracellular triglycerides and cholesterol by activating ACSL1/miR-9/PPARA signaling pathway (Cui et al., 2015). Moreover, Lan et al. (2019) identified a novel noncoding RNA lnc-HC that not only reduced cholesterol efflux by inhibiting the expression of cholesterol 7α-hydroxylase (Cyp7a1) and ABCA1, but also promoted hepatic triglyceride metabolism by negatively regulating PPARγ expression. Overall, lncRNAs play vital roles in maintaining lipid homeostasis in the liver and emerge as important targets to alleviate liver diseases caused by fat metabolic disorders, such as nonalcoholic fatty liver disease.

THE POTENTIAL OF LncRNAs AS THERAPEUTIC TARGETS OF RELATED DISEASES INDUCED BY ADIPOCYTE DYSFUNCTION

Obesity is becoming a global pandemic and usually leads to some metabolic diseases, including nonalcoholic fatty liver disease (NAFLD), diabetes, and other diabetic complications (Kusminski et al., 2009). However, therapeutic targets and methods for the treatment of obesity and related metabolic diseases remain limited in the clinic (Kakkar and Dahiya, 2015). The existing approved drugs mainly function to combat obesity by reducing intestinal fat absorption or suppressing appetite (Tsilingiris et al., 2020). Treatments to improve related metabolic disease are mainly through the use of drugs with hypoglycemic, anti-hypertensive or lipid-lowering activity. However, these agents usually have larger side effects on human body and their protective effect is limited. For examples, statins commonly cause muscular adverse reactions such as fatal rhabdomyolysis (Bouitbir et al., 2020). Chronic administration of niacin can decrease glucose tolerance and increase uric acid level, potentially induce gouty attacks and impaired liver function (Kei et al., 2011). Thus, there is an urgent need to identify novel targets and develop new effective and safe drug candidates. Functional studies of lncRNAs provide new insight for the establishment of related drugs.

The Roles of LncRNAs in Insulin Resistance

Low-grade chronic inflammation, as a marker of obesity, has been identified as a vital risk factor for the occurrence of insulin resistance (Glass and Olefsky, 2012). The increased free fatty acids in the obese can promote NF-κB signaling, which upregulates the expression of pro-inflammatory cytokines, such as TNF-α and IL-6 (Tangvarasittichai, 2015). The pro-inflammatory signals then inhibit the function of insulin in metabolic tissue, thereby mediating insulin resistance.

Because the inflammation reaction is a phenotype caused by macrophages responding to excessive lipid accumulation, researchers have focused on macrophages to reduce this inflammation. These studies have found several novel lncRNAs enriched in macrophages and differentially expressed in diet-induced mice models with obesity and early diabetes.

For example, Stapleton et al. (2020) found that MIST was associated with a macrophage anti-inflammatory phenotype during gain- and loss-of-function experiments. When transcription or interaction with RNAs of MIST was disrupted, expression of inflammatory genes heavily increased. They then discovered that MIST interacted with poly ADP-ribose polymerase (PARP1) in the nucleus. It may act as a protective lncRNA by interfering with the formation of pro-inflammatory cytokines that are closely correlated with insulin sensitivity index. In addition, Zhang et al. (2020) identified lncRNA uc.333 that improved obesity-induced insulin resistance by binding to miR-223. Moreover, Liu S. et al. (2014) reported that knocking out lncRNA SRA protected mice against high fat diet-induced obesity and improved their glucose tolerance. All the above indicate that lncRNAs are potential therapeutic targets for improving insulin resistance.

The Roles of LncRNAs in Hepatic Steatosis

Metabolic disorders often cause non-alcoholic fatty liver disease (NAFLD) and hepatic steatosis (NASH) that are characterized by the accumulation of liver lipids (Kawano and Cohen, 2013). If NAFLD is not treated in time, it can gradually develop into NASH and then into hepatocellular cancer or other malignant diseases (Kanwal et al., 2018; Lindenmeyer and McCullough, 2018). LncRNAs may be checkpoints to enable unhealthy hepatic lipogenesis and impair liver lipid homeostasis. In an animal model with NAFLD, Wang (2018) found that lncRNA-NEAT1 knockdown may alleviate the NAFLD *via* regulating the mTOR/S6K1 signaling pathway. Another lncRNA, MALAT1, is highly expressed in livers of ob/ob mice. Mechanism research demonstrated that inhibiting MALAT1 suppresses hepatic lipid accumulation and attenuates hepatic steatosis by reducing the stability of nuclear SREBP-1c protein in hepatocytes (Yan et al., 2016). Considering that hepatic expression of BLNC1 is evidently elevated in the obesity and NAFLD in mice, researchers studied the effects of BLNC1 on HFD – induced hepatic steatosis. They found that BlNC1 deficiency greatly inhibits both the plasma TAG levels and the induction of SREBP1 protein expression by LXR agonists. Additionally, liver-specific BLNC1 knockout mice exhibited resistance to HFD-induced hepatic steatosis, manifested as reduced hepatic damage and fibrosis. These responses indicated that BLNC1 may work cooperatively with LXR to control hepatic lipid metabolism, which may serve as a therapeutic target for the treatment of NAFLD patients (Zhao et al., 2018).

The Roles of LncRNAs in Atherosclerosis

The pathogenesis of atherosclerosis is complex, although current research as established that dyslipidemia (abnormal plasma cholesterol and lipoprotein levels) is one of the crucial risk factors (Gisterå and Ketelhuth, 2018). Since many studies have confirmed lncRNAs' regulatory roles in lipid homeostasis, some researchers think they may take part in the development of atherosclerosis. LncRNA KCNQ1OT1 could inhibit cholesterol efflux and promote lipid accumulation in macrophages *via* the miR-452-3p/HDAC3/ABCA1 pathway, and, thus, contribute to the development of atherosclerosis (Yu et al., 2020). A key node in atherosclerosis is when macrophages uptake lipoproteins and form foam cells (Tabas and Bornfeldt, 2020). Kanwal et al. (2018) found lncRNA E330013P06 upregulated the expression of CD36 in macrophages to promote foam cells formation (Reddy et al., 2014). Another lncRNA, AT102202, controls the expression of mRNA-3-hydroxy-3-methylglutaryl coenzyme A reductase (HMGCR) to affect the accumulation of cholesterol in macrophages (Liu et al., 2015). Although the function and mechanism of lncRNAs in atherosclerosis still need further exploration, lncRNAs are apparently vital regulatory factors implicated in the pathological process of atherosclerosis. LncRNAs have may have future clinical applications as biomarkers and potential therapeutic targets of atherosclerosis.

The Roles of LncRNAs in Diabetic Complications

Epidemiological studies have reported a large increase in the prevalence of diabetes, which mainly happens among people with long-term abdominal obesity (Ampofo and Boateng, 2020). The main harm of diabetes lies in its severe complications, such as diabetic retinopathy, nephropathy, cardiomyopathy, etc.; however, the therapeutic targets and drugs still remain limited (Harding et al., 2019). LncRNAs recently gained attention for their regulatory roles in diabetic complications (**Figure 4**).

Diabetic retinopathy is a common complication caused by hyperglycemia and dyslipidemia. At present, retinal gene expression profiles have identified more than 300 differentially expressed lncRNAs associated with diabetic retinopathy (Yan et al., 2014). One study showed that an lncRNA MALAT1 knockdown can inhibit the proliferation, migration, and tube formation of retinal endothelial cells (Liu J.-Y. et al., 2014). Radhakrishnan and Kowluru (2021) verified MALAT1 suppression attenuates oxidative damage *via* the Keap1-Nrf2 pathway to improve retinal vascular function and slow diabetic retinopathy. Additionally, Yan et al. found lncRNA MIAT can form a feedback loop with VEGF and miR-150-5p to regulate endothelial cell function and improve the microvascular dysfunction induced by diabetes (Yan et al., 2015). Thus, lncRNAs are involved in the development of diabetic retinopathy and may be potential therapeutic targets for the disease.

Chronic hyperglycemia and dyslipidemia are also the main causes of diabetic nephropathy, a microvascular complication characterized by the damage of glomerular capillaries (Opazo-Ríos et al., 2020). Accumulating evidence supports lncRNAs' involvement in the occurrence and development of this disease.

For example, LncRNA Tug1 was found to interact with PGC-1 to regulate its expression and affect the mitochondrial bioenergetics in podocytes (Long et al., 2016). Additionally, in type II diabetic patients with end-stage renal disease, lncPVT1 controlled the accumulation of the extracellular matrix and the progression of renal cells fibrosis, thereby mediating the development of diabetic kidney disease (Alvarez and DiStefano, 2011).

Diabetic cardiomyopathy is mainly caused by cardiac lipotoxicity (Nakamura and Sadoshima, 2020). LncRNA GAS5 regulates the miR-34b-3p/AHR pathway to repress the pyroptosis induced by NLRP3 inflammasome activation, making GAS5 a potential therapeutic target (Xu et al., 2020). Wang et al. (2021) found that silencing lncRNA MALAT1 could inhibit EZH2 expression *via* the EZH2/miR-22/ABCA1 signaling axis, which prevents

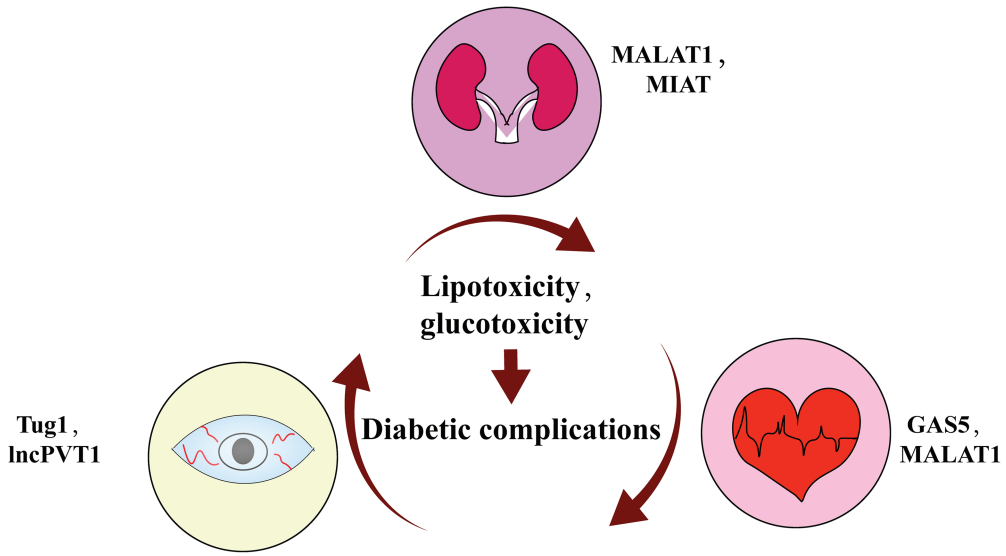

FIGURE 4 | Summary of key roles of lncRNAs in diabetic complications.

cardiomyocyte apoptosis and attenuates cardiac dysfunction. Above all, many studies have demonstrated that lncRNAs play functional roles in the pathological processes of diabetic complications and have potential therapeutic significance for the diseases.

CONCLUSION

This review mainly summarized the studies on the regulation of lncRNAs in lipid metabolism in the liver as well as the development and function of adipose tissue. Meanwhile, numerous examples have been provided of a series of lncRNAs involved in adipocyte dysfunction-induced diseases, such as insulin resistance, hepatic steatosis, and diabetic complications. Currently, most of the drugs used to fight obesity target proteins, but these drugs have side effects because of the unintended regulation of non-target protein. Thus, the development of new drugs that target nucleic acids might provide a novel therapeutic strategy for the treatment of obesity and its related diseases.

Some targeted nucleic acid therapies, such as antibacterial and anticancer therapy are gradually being applied to treat some diseases (Aradi et al., 2020; Javanmard et al., 2020). Nucleic acid targeting methods are considered the third generation of therapeutic drugs, and three main strategies have been reported thus far: (i) small interfering RNA (siRNA), targeting cytoplasmic lncRNAs, like Givlaari (Givosiran) which was approved to treat adult acute hepatic porphyria; (ii) antisense oligonucleotides (ASO), targeting nuclear lncRNAs. LNA gapmeR ASO-targeting lncRNA MALAT1 possesses anti-multiple myeloma activity (Amodio et al., 2018); (iii) CRISPR/Cas9 technology is suitable for dual-located lncRNAs, and it has been widely used in the discovery and annotation of lncRNAs but, as of yet, is not ideal for systematic drug delivery. These three therapies have been approved for clinical application, but all face off-target problems (Caffrey et al., 2011; Fu et al., 2014; Rinaldi and Wood, 2018).

Some lncRNAs positively regulate white adipogenesis and are upregulated in the obese patients, and they might be suitable ASO targets. However, no lncRNA targeting drugs have entered clinical trials, and many therapies are still in the preclinical stage. Because many lncRNAs are poorly conserved, researchers often struggle to transfer successful mouse model experiments to human treatments. Thus, more humanized lncRNAs remain to be probed and more applicable preclinical study models need to be established. On the other hand, the regulation network of lncRNAs is complex and it is not easy to achieve accurate regulation *in vivo*. Accordingly, it is necessary to establish a highly organized lncRNA research database, D-LNC platform is such an attempt to query and analyze the modification effects of drugs on the expression of lncRNAs (Jiang et al., 2019).

To sum up, the study of lncRNAs in adipose metabolism and obesity-caused diseases, as well as the therapeutic strategies presented above, may provide novel medication for the treatment of obesity and related metabolic diseases.

AUTHOR CONTRIBUTIONS

BZ, YX, and SuX contributed to the conception of the review. BZ and SaX contributed significantly to the complete manuscript preparation. SaX and JL contributed to constructive discussions. All authors contributed to the article and approved the submitted version.

FUNDING

This work was supported by Natural Sciences Foundation for Young Scientists of China (grant no. 81803803) and the CAMS Innovation Fund for Medical Sciences (CIFMS; grant no. 2019-I2M-1-005).

REFERENCES

Ali, A. T., Hochfeld, W. E., Myburgh, R., and Pepper, M. S. (2013). Adipocyte and adipogenesis. *Eur. J. Cell Biol.* 92, 229–236. doi: 10.1016/j.ejcb.2013.06.001

Alvarez, M. L., and DiStefano, J. K. (2011). Functional characterization of the plasmacytoma variant translocation 1 gene (PVT1) in diabetic nephropathy. *PLoS One* 6:e18671. doi: 10.1371/journal.pone.0018671

Alvarez-Dominguez, J. R., Bai, Z., Xu, D., Yuan, B., Lo, K. A., Yoon, M. J., et al. (2015). De novo reconstruction of adipose tissue transcriptomes reveals long non-coding RNA regulators of brown adipocyte development. *Cell Metab.* 21, 764–776. doi: 10.1016/j.cmet.2015.04.003

Ambele, M. A., Dhanraj, P., Giles, R., and Pepper, M. S. (2020). Adipogenesis: a complex interplay of multiple molecular determinants and pathways. *Int. J. Mol. Sci.* 21:4283. doi: 10.3390/ijms21124283

Amodio, N., Stamato, M. A., Juli, G., Morelli, E., Fulciniti, M., Manzoni, M., et al. (2018). Drugging the lncRNA MALAT1 via LNA gapmeR ASO inhibits gene expression of proteasome subunits and triggers anti-multiple myeloma activity. *Leukemia* 32, 1948–1957. doi: 10.1038/s41375-018-0067-3

Ampofo, A. G., and Boateng, E. B. (2020). Beyond 2020: modelling obesity and diabetes prevalence. *Diabetes Res. Clin. Pract.* 167:108362. doi: 10.1016/j.diabres.2020.108362

Aradi, K., Di Giorgio, A., and Duca, M. (2020). Aminoglycoside conjugation for RNA targeting: antimicrobials and beyond. *Chemistry* 26, 12273–12309. doi: 10.1002/chem.202002258

Bai, Z., Chai, X. R., Yoon, M. J., Kim, H. J., Lo, K. A., Zhang, Z. C., et al. (2017). Dynamic transcriptome changes during adipose tissue energy expenditure reveal critical roles for long noncoding RNA regulators. *PLoS Biol.* 15:e2002176. doi: 10.1371/journal.pbio.2002176

Bartelt, A., and Heeren, J. (2014). Adipose tissue browning and metabolic health. *Nat. Rev. Endocrinol.* 10, 24–36. doi: 10.1038/nrendo.2013.204

Bartolomei, M. S., Zemel, S., and Tilghman, S. M. (1991). Parental imprinting of the mouse H19 gene. *Nature* 351, 153–155. doi: 10.1038/351153a0

Bian, E. B., Xiong, Z. G., and Li, J. (2019). New advances of lncRNAs in liver fibrosis, with specific focus on lncRNA-miRNA interactions. *J. Cell. Physiol.* 234, 2194–2203. doi: 10.1002/jcp.27069

Blüher, M. (2019). Obesity: global epidemiology and pathogenesis. *Nat. Rev. Endocrinol.* 15, 288–298. doi: 10.1038/s41574-019-0176-8

Bouitbir, J., Sanvee, G. M., Panajatovic, M. V., Singh, F., and Krähenbühl, S. (2020). Mechanisms of statin-associated skeletal muscle-associated symptoms. *Pharmacol. Res.* 154:104201. doi: 10.1016/j.phrs.2019.03.010

Brannan, C. I., Dees, E. C., Ingram, R. S., and Tilghman, S. M. (1990). The product of the H19 gene may function as an RNA. *Mol. Cell. Biol.* 10, 28–36. doi: 10.1128/mcb.10.1.28

Caffrey, D. R., Zhao, J., Song, Z., Schaffer, M. E., Haney, S. A., Subramanian, R. R., et al. (2011). siRNA off-target effects can be reduced at concentrations that match their individual potency. *PLoS One* 6:e21503. doi: 10.1371/journal.pone.0021503

Cannon, B., Hedin, A., and Nedergaard, J. (1982). Exclusive occurrence of thermogenin antigen in brown adipose tissue. *FEBS Lett.* 150, 129–132. doi: 10.1016/0014-5793(82)81319-7

Cannon, B., and Nedergaard, J. (2004). Brown adipose tissue: function and physiological significance. *Physiol. Rev.* 84, 277–359. doi: 10.1152/physrev.00015.2003

Chen, J., Liu, Y., Lu, S., Yin, L., Zong, C., Cui, S., et al. (2017). The role and possible mechanism of lncRNA U90926 in modulating 3T3-L1 preadipocyte differentiation. *Int. J. Obes.* 41, 299–308. doi: 10.1038/ijo.2016.189

Chooi, Y. C., Ding, C., and Magkos, F. (2019). The epidemiology of obesity. *Metabolism* 92, 6–10. doi: 10.1016/j.metabol.2018.09.005

Chu, C., Qu, K., Zhong, F. L., Artandi, S. E., and Chang, H. Y. (2011). Genomic maps of long noncoding RNA occupancy reveal principles of RNA-chromatin interactions. *Mol. Cell* 44, 667–678. doi: 10.1016/j.molcel.2011.08.027

Cipolletta, D., Feuerer, M., Li, A., Kamei, N., Lee, J., Shoelson, S. E., et al. (2012). PPAR-γ is a major driver of the accumulation and phenotype of adipose tissue Treg cells. *Nature* 486, 549–553. doi: 10.1038/nature11132

Core, L. J., Waterfall, J. J., and Lis, J. T. (2008). Nascent RNA sequencing reveals widespread pausing and divergent initiation at human promoters. *Science* 322, 1845–1848. doi: 10.1126/science.1162228

Cui, M., Xiao, Z., Wang, Y., Zheng, M., Song, T., Cai, X., et al. (2015). Long noncoding RNA HULC modulates abnormal lipid metabolism in hepatoma cells through an miR-9-mediated RXRA signaling pathway. *Cancer Res.* 75, 846–857. doi: 10.1158/0008-5472.CAN-14-1192

Cui, X., You, L., Li, Y., Zhu, L., Zhang, F., Xie, K., et al. (2016). A transcribed ultraconserved noncoding RNA, uc.417, serves as a negative regulator of brown adipose tissue thermogenesis. *FASEB J.* 30, 4301–4312. doi: 10.1096/fj.201600694R

Feng, M., Tang, P. M., Huang, X. R., Sun, S. F., You, Y. K., Xiao, J., et al. (2018). TGF-β mediates renal fibrosis via the Smad3-Erbb4-IR long noncoding RNA Axis. *Mol. Ther.* 26, 148–161. doi: 10.1016/j.ymthe.2017.09.024

Fu, Y., Sander, J. D., Reyon, D., Cascio, V. M., and Joung, J. K. (2014). Improving CRISPR-Cas nuclease specificity using truncated guide RNAs. *Nat. Biotechnol.* 32, 279–284. doi: 10.1038/nbt.2808

Gao, P., and Wei, G. H. (2017). Genomic insight into the role of lncRNA in cancer susceptibility. *Int. J. Mol. Sci.* 18:1239. doi: 10.3390/ijms18061239

Gernapudi, R., Wolfson, B., Zhang, Y., Yao, Y., Yang, P., Asahara, H., et al. (2016). MicroRNA 140 promotes expression of long noncoding RNA NEAT1 in adipogenesis. *Mol. Cell. Biol.* 36, 30–38. doi: 10.1128/MCB.00702-15

Ghaben, A. L., and Scherer, P. E. (2019). Adipogenesis and metabolic health. *Nat. Rev. Mol. Cell Biol.* 20, 242–258. doi: 10.1038/s41580-018-0093-z

Gisterå, A., and Ketelhuth, D. F. J. (2018). Lipid-driven immunometabolic responses in atherosclerosis. *Curr. Opin. Lipidol.* 29, 375–380. doi: 10.1097/MOL.0000000000000540

Glass, C. K., and Olefsky, J. M. (2012). Inflammation and lipid signaling in the etiology of insulin resistance. *Cell Metab.* 15, 635–645. doi: 10.1016/j.cmet.2012.04.001

Gong, Z., Tang, J., Xiang, T., Lin, J., Deng, C., Peng, Y., et al. (2018). Genome-wide identification of long noncoding RNAs in CCl4-induced liver fibrosis via RNA sequencing. *Mol. Med. Rep.* 18, 299–307. doi: 10.3892/mmr.2018.8986

Guerra, C., Koza, R. A., Yamashita, H., Walsh, K., and Kozak, L. P. (1998). Emergence of brown adipocytes in white fat in mice is under genetic control. Effects on body weight and adiposity. *J. Clin. Invest.* 102, 412–420. doi: 10.1172/JCI3155

Guo, Z., and Cao, Y. (2019). An lncRNA-miRNA-mRNA ceRNA network for adipocyte differentiation from human adipose-derived stem cells. *Mol. Med. Rep.* 19, 4271–4287. doi: 10.3892/mmr.2019.10067

Guttman, M., Amit, I., Garber, M., French, C., Lin, M. F., Feldser, D., et al. (2009). Chromatin signature reveals over a thousand highly conserved large non-coding RNAs in mammals. *Nature* 458, 223–227. doi: 10.1038/nature07672

Han, P., Li, W., Lin, C. H., Yang, J., Shang, C., Nuernberg, S. T., et al. (2014). A long noncoding RNA protects the heart from pathological hypertrophy. *Nature* 514, 102–106. doi: 10.1038/nature13596

Harding, J. L., Pavkov, M. E., Magliano, D. J., Shaw, J. E., and Gregg, E. W. (2019). Global trends in diabetes complications: a review of current evidence. *Diabetologia* 62, 3–16. doi: 10.1007/s00125-018-4711-2

Hu, W., Ding, H., Ouyang, A., Zhang, X., Xu, Q., Han, Y., et al. (2019). LncRNA MALAT1 gene polymorphisms in coronary artery disease: a case-control study in a Chinese population. *Biosci. Rep.* 39:BSR20182213. doi: 10.1042/bsr20182213

Huang, J., Chen, S., Cai, D., Bian, D., and Wang, F. (2018). Long noncoding RNA lncARSR promotes hepatic cholesterol biosynthesis via modulating Akt/SREBP-2/HMGCR pathway. *Life Sci.* 203, 48–53. doi: 10.1016/j.lfs.2018.04.028

Iyengar, N. M., Gucalp, A., Dannenberg, A. J., and Hudis, C. A. (2016). Obesity and cancer mechanisms: tumor microenvironment and inflammation. *J. Clin. Oncol.* 34, 4270–4276. doi: 10.1200/JCO.2016.67.4283

Jarroux, J., Morillon, A., and Pinskaya, M. (2017). History, discovery, and classification of lncRNAs. *Adv. Exp. Med. Biol.* 1008, 1–46. doi: 10.1007/978-981-10-5203-3_1

Javanmard, S. H., Vaseghi, G., Ghasemi, A., Rafiee, L., Ferns, G. A., Esfahani, H. N., et al. (2020). Therapeutic inhibition of microRNA-21 (miR-21) using locked-nucleic acid (LNA)-anti-miR and its effects on the biological behaviors of melanoma cancer cells in preclinical studies. *Cancer Cell Int.* 20:384. doi: 10.1186/s12935-020-01394-6

Jiang, W., Qu, Y., Yang, Q., Ma, X., Meng, Q., Xu, J., et al. (2019). D-lnc: a comprehensive database and analytical platform to dissect the modification of drugs on lncRNA expression. *RNA Biol.* 16, 1586–1591. doi: 10.1080/15476286.2019.1649584

Kakkar, A. K., and Dahiya, N. (2015). Drug treatment of obesity: current status and future prospects. *Eur. J. Intern. Med.* 26, 89–94. doi: 10.1016/j.ejim.2015.01.005

Kanwal, F., Kramer, J. R., Mapakshi, S., Natarajan, Y., Chayanupatkul, M., Richardson, P. A., et al. (2018). Risk of hepatocellular cancer in patients with non-alcoholic fatty liver disease. *Gastroenterology* 155, 1828.e1822–1837.e1822. doi: 10.1053/j.gastro.2018.08.024

Katsushima, K., Natsume, A., Ohka, F., Shinjo, K., Hatanaka, A., Ichimura, N., et al. (2016). Targeting the notch-regulated non-coding RNA TUG1 for glioma treatment. *Nat. Commun.* 7:13616. doi: 10.1038/ncomms13616

Kawano, Y., and Cohen, D. E. (2013). Mechanisms of hepatic triglyceride accumulation in non-alcoholic fatty liver disease. *J. Gastroenterol.* 48, 434–441. doi: 10.1007/s00535-013-0758-5

Kei, A., Liberopoulos, E. N., and Elisaf, M. S. (2011). What restricts the clinical use of nicotinic acid? *Curr. Vasc. Pharmacol.* 9, 521–530. doi: 10.2174/157016111796197215

Kusminski, C. M., Shetty, S., Orci, L., Unger, R. H., and Scherer, P. E. (2009). Diabetes and apoptosis: lipotoxicity. *Apoptosis* 14, 1484–1495. doi: 10.1007/s10495-009-0352-8

Lan, X., Wu, L., Wu, N., Chen, Q., Li, Y., Du, X., et al. (2019). Long noncoding RNA lnc-HC regulates PPARγ-mediated hepatic lipid metabolism through miR-130b-3p. *Mol. Ther. Nucleic Acids* 18, 954–965. doi: 10.1016/j.omtn.2019.10.018

Lavie, C. J., Milani, R. V., and Ventura, H. O. (2009). Obesity and cardiovascular disease: risk factor, paradox, and impact of weight loss. *J. Am. Coll. Cardiol.* 53, 1925–1932. doi: 10.1016/j.jacc.2008.12.068

Li, D., Cheng, M., Niu, Y., Chi, X., Liu, X., Fan, J., et al. (2017). Identification of a novel human long non-coding RNA that regulates hepatic lipid metabolism by inhibiting SREBP-1c. *Int. J. Biol. Sci.* 13, 349–357. doi: 10.7150/ijbs.16635

Li, Z., Jin, C., Chen, S., Zheng, Y., Huang, Y., Jia, L., et al. (2017). Long non-coding RNA MEG3 inhibits adipogenesis and promotes osteogenesis of human adipose-derived mesenchymal stem cells via miR-140-5p. *Mol. Cell. Biochem.* 433, 51–60. doi: 10.1007/s11010-017-3015-z

Li, D., Liu, Y., Gao, W., Han, J., Yuan, R., Zhang, M., et al. (2020). LncRNA HCG11 inhibits adipocyte differentiation in human adipose-derived mesenchymal stem cells by sponging miR-204-5p to upregulate SIRT1. *Cell Transplant.* 29:963689720968090. doi: 10.1177/0963689720968090

Li, S., Mi, L., Yu, L., Yu, Q., Liu, T., Wang, G. X., et al. (2017). Zbtb7b engages the long noncoding RNA Blnc1 to drive brown and beige fat development and thermogenesis. *Proc. Natl. Acad. Sci. U. S. A.* 114, E7111–E7120. doi: 10.1073/pnas.1703494114

Li, P., Ruan, X., Yang, L., Kiesewetter, K., Zhao, Y., Luo, H., et al. (2015). A liver-enriched long non-coding RNA, lncLSTR, regulates systemic lipid metabolism in mice. *Cell Metab.* 21, 455–467. doi: 10.1016/j.cmet.2015.02.004

Li, Y., Shen, S., Ding, S., and Wang, L. (2018). LincRNA DYN-LRB2-2 upregulates cholesterol efflux by decreasing TLR2 expression in macrophages. *J. Cell. Biochem.* 119, 1911–1921. doi: 10.1002/jcb.26352

Li, M., Xie, Z., Wang, P., Li, J., Liu, W., Tang, S., et al. (2018). The long noncoding RNA GAS5 negatively regulates the adipogenic differentiation of MSCs by modulating the miR-18a/CTGF axis as a ceRNA. *Cell Death Dis.* 9:554. doi: 10.1038/s41419-018-0627-5

Lin, J., Zhang, X., Xue, C., Zhang, H., Shashaty, M. G., Gosai, S. J., et al. (2015). The long noncoding RNA landscape in hypoxic and inflammatory renal epithelial injury. *Am. J. Physiol. Ren. Physiol.* 309, F901–F913. doi: 10.1152/ajprenal.00290.2015

Lindenmeyer, C. C., and McCullough, A. J. (2018). The natural history of nonalcoholic fatty liver disease-an evolving view. *Clin. Liver Dis.* 22, 11–21. doi: 10.1016/j.cld.2017.08.003

Liu, H., Li, H., Jin, L., Li, G., Hu, S., Ning, C., et al. (2018). Long noncoding RNA GAS5 suppresses 3T3-L1 cells adipogenesis through miR-21a-5p/PTEN signal pathway. *DNA Cell Biol.* 37, 767–777. doi: 10.1089/dna.2018.4264

Liu, S., Sheng, L., Miao, H., Saunders, T. L., MacDougald, O. A., Koenig, R. J., et al. (2014). SRA gene knockout protects against diet-induced obesity and improves glucose tolerance. *J. Biol. Chem.* 289, 13000–13009. doi: 10.1074/jbc.M114.564658

Liu, J.-Y., Yao, J., Li, X. M., Song, Y. C., Wang, X. Q., Li, Y. J., et al. (2014). Pathogenic role of lncRNA-MALAT1 in endothelial cell dysfunction in diabetes mellitus. *Cell Death Dis.* 5:e1506. doi: 10.1038/cddis.2014.466

Liu, G., Zheng, X., Xu, Y., Lu, J., Chen, J., and Huang, X. (2015). Long non-coding RNAs expression profile in HepG2 cells reveals the potential role of long non-coding RNAs in the cholesterol metabolism. *Chin. Med. J.* 128, 91–97. doi: 10.4103/0366-6999.147824

Long, J., Badal, S. S., Ye, Z., Wang, Y., Ayanga, B. A., Galvan, D. L., et al. (2016). Long noncoding RNA Tug1 regulates mitochondrial bioenergetics in diabetic nephropathy. *J. Clin. Invest.* 126, 4205–4218. doi: 10.1172/JCI87927

Mattick, J. S., and Rinn, J. L. (2015). Discovery and annotation of long noncoding RNAs. *Nat. Struct. Mol. Biol.* 22, 5–7. doi: 10.1038/nsmb.2942

Mi, L., Zhao, X. Y., Li, S., Yang, G., and Lin, J. D. (2017). Conserved function of the long noncoding RNA Blnc1 in brown adipocyte differentiation. *Mol. Metab.* 6, 101–110. doi: 10.1016/j.molmet.2016.10.010

Moghaddas Sani, H., Hejazian, M., Hosseinian Khatibi, S. M., Ardalan, M., and Zununi Vahed, S. (2018). Long non-coding RNAs: an essential emerging field in kidney pathogenesis. *Biomed. Pharmacother.* 99, 755–765. doi: 10.1016/j.biopha.2018.01.122

Nakamura, M., and Sadoshima, J. (2020). Cardiomyopathy in obesity, insulin resistance and diabetes. *J. Physiol.* 598, 2977–2993. doi: 10.1113/JP276747

Napoli, M., Li, X., Ackerman, H. D., Deshpande, A. A., Barannikov, I., Pisegna, M. A., et al. (2020). Pan-cancer analysis reveals TAp63-regulated oncogenic lncRNAs that promote cancer progression through AKT activation. *Nat. Commun.* 11:5156. doi: 10.1038/s41467-020-18973-w

Nedergaard, J., Bengtsson, T., and Cannon, B. (2007). Unexpected evidence for active brown adipose tissue in adult humans. *Am. J. Physiol. Endocrinol. Metab.* 293, E444–E452. doi: 10.1152/ajpendo.00691.2006

Nuermaimaiti, N., Liu, J., Liang, X., Jiao, Y., Zhang, D., Liu, L., et al. (2018). Effect of lncRNA HOXA11-AS1 on adipocyte differentiation in human adipose-derived stem cells. *Biochem. Biophys. Res. Commun.* 495, 1878–1884. doi: 10.1016/j.bbrc.2017.12.006

Opazo-Ríos, L., Mas, S., Marín-Royo, G., Mezzano, S., Gómez-Guerrero, C., Moreno, J. A., et al. (2020). Lipotoxicity and diabetic nephropathy: novel mechanistic insights and therapeutic opportunities. *Int. J. Mol. Sci.* 21:2632. doi: 10.3390/ijms21072632

Peeters, A., Barendregt, J. J., Willekens, F., Mackenbach, J. P., Al Mamun, A., and Bonneux, L. (2003). Obesity in adulthood and its consequences for life expectancy: a life-table analysis. *Ann. Intern. Med.* 138, 24–32. doi: 10.7326/0003-4819-138-1-200301070-00008

Peng, W. X., Koirala, P., and Mo, Y. Y. (2017). LncRNA-mediated regulation of cell signaling in cancer. *Oncogene* 36, 5661–5667. doi: 10.1038/onc.2017.184

Qian, X., Zhao, J., Yeung, P. Y., Zhang, Q. C., and Kwok, C. K. (2019). Revealing lncRNA structures and interactions by sequencing-based approaches. *Trends Biochem. Sci.* 44, 33–52. doi: 10.1016/j.tibs.2018.09.012

Radhakrishnan, R., and Kowluru, R. A. (2021). Long noncoding RNA MALAT1 and regulation of the antioxidant defense system in diabetic retinopathy. *Diabetes* 70, 227–239. doi: 10.2337/db20-0375

Reddy, M. A., Chen, Z., Park, J. T., Wang, M., Lanting, L., Zhang, Q., et al. (2014). Regulation of inflammatory phenotype in macrophages by a diabetes-induced long noncoding RNA. *Diabetes* 63, 4249–4261. doi: 10.2337/db14-0298

Rinaldi, C., and Wood, M. J. A. (2018). Antisense oligonucleotides: the next frontier for treatment of neurological disorders. *Nat. Rev. Neurol.* 14, 9–21. doi: 10.1038/nrneurol.2017.148

Schetz, M., De Jong, A., Deane, A. M., Druml, W., Hemelaar, P., Pelosi, P., et al. (2019). Obesity in the critically ill: a narrative review. *Intensive Care Med.* 45, 757–769. doi: 10.1007/s00134-019-05594-1

Schmidt, E., Dhaouadi, I., Gaziano, I., Oliverio, M., Klemm, P., Awazawa, M., et al. (2018). LincRNA H19 protects from dietary obesity by constraining expression of monoallelic genes in brown fat. *Nat. Commun.* 9:3622. doi: 10.1038/s41467-018-05933-8

Schmitt, A. M., Garcia, J. T., Hung, T., Flynn, R. A., Shen, Y., Qu, K., et al. (2016). An inducible long noncoding RNA amplifies DNA damage signaling. *Nat. Genet.* 48, 1370–1376. doi: 10.1038/ng.3673

Stapleton, K., Das, S., Reddy, M. A., Leung, A., Amaram, V., Lanting, L., et al. (2020). Novel long noncoding RNA, macrophage inflammation-suppressing transcript (MIST), regulates macrophage activation during obesity. *Arterioscler. Thromb. Vasc. Biol.* 40, 914–928. doi: 10.1161/ATVBAHA.119.313359

Sun, M., and Kraus, W. L. (2015). From discovery to function: the expanding roles of long noncoding RNAs in physiology and disease. *Endocr. Rev.* 36, 25–64. doi: 10.1210/er.2014-1034

Sun, K., Kusminski, C. M., and Scherer, P. E. (2011). Adipose tissue remodeling and obesity. *J. Clin. Invest.* 121, 2094–2101. doi: 10.1172/JCI45887

Sun, L., and Lin, J. D. (2019). Function and mechanism of long noncoding RNAs in adipocyte biology. *Diabetes* 68, 887–896. doi: 10.2337/dbi18-0009

Tabas, I., and Bornfeldt, K. E. (2020). Intracellular and intercellular aspects of macrophage immunometabolism in atherosclerosis. *Circ. Res.* 126, 1209–1227. doi: 10.1161/CIRCRESAHA.119.315939

Tangvarasittichai, S. (2015). Oxidative stress, insulin resistance, dyslipidemia and type 2 diabetes mellitus. *World J. Diabetes* 6, 456–480. doi: 10.4239/wjd.v6.i3.456

Trembinski, D. J., Bink, D. I., Theodorou, K., Sommer, J., Fischer, A., van Bergen, A., et al. (2020). Aging-regulated anti-apoptotic long non-coding RNA Sarrah augments recovery from acute myocardial infarction. *Nat. Commun.* 11:2039. doi: 10.1038/s41467-020-15995-2

Tsilingiris, D., Liatis, S., Dalamaga, M., and Kokkinos, A. (2020). The fight against obesity escalates: new drugs on the horizon and metabolic implications. *Curr. Obes. Rep.* 9, 136–149. doi: 10.1007/s13679-020-00378-x

Ulitsky, I., and Bartel, D. P. (2013). lincRNAs: genomics, evolution, and mechanisms. *Cell* 154, 26–46. doi: 10.1016/j.cell.2013.06.020

Wang, X. (2018). Down-regulation of lncRNA-NEAT1 alleviated the non-alcoholic fatty liver disease via mTOR/S6K1 signaling pathway. *J. Cell. Biochem.* 119, 1567–1574. doi: 10.1002/jcb.26317

Wang, K. C., and Chang, H. Y. (2011). Molecular mechanisms of long noncoding RNAs. *Mol. Cell* 43, 904–914. doi: 10.1016/j.molcel.2011.08.018

Wang, Y., Hua, S., Cui, X., Cao, Y., Wen, J., Chi, X., et al. (2020). The effect of FOXC2-AS1 on white adipocyte browning and the possible regulatory mechanism. *Front. Endocrinol.* 11:565483. doi: 10.3389/fendo.2020.565483

Wang, C., Liu, G., Yang, H., Guo, S., Wang, H., Dong, Z., et al. (2021). MALAT1-mediated recruitment of the histone methyltransferase EZH2 to the microRNA-22 promoter leads to cardiomyocyte apoptosis in diabetic cardiomyopathy. *Sci. Total Environ.* 766:142191. doi: 10.1016/j.scitotenv.2020.142191

Wang, W., and Seale, P. (2016). Control of brown and beige fat development. *Nat. Rev. Mol. Cell Biol.* 17, 691–702. doi: 10.1038/nrm.2016.96

Wang, J., Xiang, D., Mei, S., Jin, Y., Sun, D., Chen, C., et al. (2020). The novel long noncoding RNA Lnc19959.2 modulates triglyceride metabolism-associated genes through the interaction with Purb and hnRNPA2B1. *Mol. Metab.* 37:100996. doi: 10.1016/j.molmet.2020.100996

Wang, K. C., Yang, Y. W., Liu, B., Sanyal, A., Corces-Zimmerman, R., Chen, Y., et al. (2011). A long noncoding RNA maintains active chromatin to coordinate homeotic gene expression. *Nature* 472, 120–124. doi: 10.1038/nature09819

Wang, Z., Zhang, X. J., Ji, Y. X., Zhang, P., Deng, K. Q., Gong, J., et al. (2016). The long noncoding RNA Chaer defines an epigenetic checkpoint in cardiac hypertrophy. *Nat. Med.* 22, 1131–1139. doi: 10.1038/nm.4179

Willingham, A. T., Orth, A. P., Batalov, S., Peters, E. C., Wen, B. G., Aza-Blanc, P., et al. (2005). A strategy for probing the function of noncoding RNAs finds a repressor of NFAT. *Science* 309, 1570–1573. doi: 10.1126/science.1115901

Xiao, T., Liu, L., Li, H., Sun, Y., Luo, H., Li, T., et al. (2015). Long noncoding RNA ADINR regulates adipogenesis by transcriptionally activating C/EBPα. *Stem Cell Rep.* 5, 856–865. doi: 10.1016/j.stemcr.2015.09.007

Xiong, Y., Yue, F., Jia, Z., Gao, Y., Jin, W., Hu, K., et al. (2018). A novel brown adipocyte-enriched long non-coding RNA that is required for brown adipocyte differentiation and sufficient to drive thermogenic gene program in white adipocytes. *Biochim. Biophys. Acta Mol. Cell Biol. Lipids* 1863, 409–419. doi: 10.1016/j.bbalip.2018.01.008

Xu, Y., Fang, H., Xu, Q., Xu, C., Yang, L., and Huang, C. (2020). LncRNA GAS5 inhibits NLRP3 inflammasome activation-mediated pyroptosis in diabetic cardiomyopathy by targeting miR-34b-3p/AHR. *Cell Cycle* 19, 3054–3065. doi: 10.1080/15384101.2020.1831245

Yan, C., Chen, J., and Chen, N. (2016). Long noncoding RNA MALAT1 promotes hepatic steatosis and insulin resistance by increasing nuclear SREBP-1c protein stability. *Sci. Rep.* 6:22640. doi: 10.1038/srep22640

Yan, B., Tao, Z. F., Li, X. M., Zhang, H., Yao, J., and Jiang, Q. (2014). Aberrant expression of long noncoding RNAs in early diabetic retinopathy. *Invest. Ophthalmol. Vis. Sci.* 55, 941–951. doi: 10.1167/iovs.13-13221

Yan, B., Yao, J., Liu, J. Y., Li, X. M., Wang, X. Q., Li, Y. J., et al. (2015). lncRNA-MIAT regulates microvascular dysfunction by functioning as a competing endogenous RNA. *Circ. Res.* 116, 1143–1156. doi: 10.1161/CIRCRESAHA.116.305510

Yang, L., and Li, T. (2020). LncRNA TUG1 regulates ApoM to promote atherosclerosis progression through miR-92a/FXR1 axis. *J. Cell. Mol. Med.* 24, 8836–8848. doi: 10.1111/jcmm.15521

You, L. H., Zhu, L. J., Yang, L., Shi, C. M., Pang, L. X., Zhang, J., et al. (2015). Transcriptome analysis reveals the potential contribution of long noncoding RNAs to brown adipocyte differentiation. *Mol. Gen. Genomics.* 290, 1659–1671. doi: 10.1007/s00438-015-1026-6

Yu, X. H., Deng, W. Y., Chen, J. J., Xu, X. D., Liu, X. X., Chen, L., et al. (2020). LncRNA kcnq1ot1 promotes lipid accumulation and accelerates atherosclerosis via functioning as a ceRNA through the miR-452-3p/HDAC3/ABCA1 axis. *Cell Death Dis.* 11:1043. doi: 10.1038/s41419-020-03263-6

Zhang, K., Han, X., Zhang, Z., Zheng, L., Hu, Z., Yao, Q., et al. (2017). The liver-enriched lnc-LFAR1 promotes liver fibrosis by activating TGFβ and notch pathways. *Nat. Commun.* 8:144. doi: 10.1038/s41467-017-00204-4

Zhang, Y., Jiao, L., Sun, L., Li, Y., Gao, Y., Xu, C., et al. (2018). LncRNA ZFAS1 as a SERCA2a inhibitor to cause intracellular Ca^{2+} overload and contractile dysfunction in a mouse model of myocardial infarction. *Circ. Res.* 122, 1354–1368. doi: 10.1161/circresaha.117.312117

Zhang, Y., Sun, J., Yao, H., Lin, Y., Wei, J., Hu, G., et al. (2020). Ultraconserved element uc.333 increases insulin sensitivity by binding to miR-223. *Aging* 12, 6667–6679. doi: 10.18632/aging.103020

Zhang, X., Xue, C., Lin, J., Ferguson, J. F., Weiner, A., Liu, W., et al. (2018). Interrogation of nonconserved human adipose lincRNAs identifies a regulatory role of linc-ADAL in adipocyte metabolism. *Sci. Transl. Med.* 10:eaar5987. doi: 10.1126/scitranslmed.aar5987

Zhang, K., Zhang, M., Yao, Q., Han, X., Zhao, Y., Zheng, L., et al. (2019). The hepatocyte-specifically expressed lnc-HSER alleviates hepatic fibrosis by inhibiting hepatocyte apoptosis and epithelial-mesenchymal transition. *Theranostics* 9, 7566–7582. doi: 10.7150/thno.36942

Zhao, X. Y., Li, S., Wang, G. X., Yu, Q., and Lin, J. D. (2014). A long noncoding RNA transcriptional regulatory circuit drives thermogenic adipocyte differentiation. *Mol. Cell* 55, 372–382. doi: 10.1016/j.molcel.2014.06.004

Zhao, X. Y., Xiong, X., Liu, T., Mi, L., Peng, X., Rui, C., et al. (2018). Long noncoding RNA licensing of obesity-linked hepatic lipogenesis and NAFLD pathogenesis. *Nat. Commun.* 9:2986. doi: 10.1038/s41467-018-05383-2

Zhou, Q., Huang, X. R., Yu, J., Yu, X., and Lan, H. Y. (2015). Long noncoding RNA Arid2-IR is a novel therapeutic target for renal inflammation. *Mol. Ther.* 23, 1034–1043. doi: 10.1038/mt.2015.31

Zhu, E., Zhang, J., Li, Y., Yuan, H., Zhou, J., and Wang, B. (2019). Long noncoding RNA Plnc1 controls adipocyte differentiation by regulating peroxisome proliferator-activated receptor γ. *FASEB J.* 33, 2396–2408. doi: 10.1096/fj.201800739RRR

Conflict of Interest: The authors declare that the research was conducted in the absence of any commercial or financial relationships that could be construed as a potential conflict of interest.

Copyright © 2021 Zhang, Xu, Liu, Xie and Xiaobo. This is an open-access article distributed under the terms of the Creative Commons Attribution License (CC BY). The use, distribution or reproduction in other forums is permitted, provided the original author(s) and the copyright owner(s) are credited and that the original publication in this journal is cited, in accordance with accepted academic practice. No use, distribution or reproduction is permitted which does not comply with these terms.

frontiers in Physiology

ORIGINAL RESEARCH
published: 19 August 2021
doi: 10.3389/fphys.2021.728208

Identification of Circular RNA Expression Profiles in White Adipocytes and Their Roles in Adipogenesis

Peng-peng Zhang[1], Qiu Han[1], Ming-xuan Sheng[1], Chun-yu Du[1], Ya-ling Wang[1], Xiao-fang Cheng[1], Hai-xia Xu[1], Cen-cen Li[1,2] and Yong-jie Xu[1,2]**

[1] Department of Biotechnology, College of Life Sciences, Xinyang Normal University, Xinyang, China, [2] Institute for Conservation and Utilization of Agro-Bioresources in Dabie Mountains, Xinyang Normal University, Xinyang, China

Obesity and its related metabolic diseases have become great public health threats worldwide. Although accumulated evidence suggests that circRNA is a new type of non-coding RNAs regulating various physiological and pathological processes, little attention has been paid to the expression profiles and functions of circRNAs in white adipose tissue. In this study, 3,771 circRNAs were detected in three stages of white adipogenesis (preadipocyte, differentiating preadipocyte, and mature adipocyte) by RNA-seq. Experimental validation suggested that the RNA-seq results are highly reliable. We found that nearly 10% of genes which expressed linear RNAs in adipocytes could also generate circRNAs. In addition, 40% of them produced multiple circRNA isoforms. We performed correlation analysis and found that a great deal of circRNAs (nearly 50%) and their parental genes were highly correlated in expression levels. A total of 41 differential expression circRNAs (DECs) were detected during adipogenesis and an extremely high ratio of them (80%) were correlated with their parental genes, indicating these circRNAs may potentially play roles in regulating the expression of their parental genes. KEGG enrichment and GO annotation of the parental genes suggesting that the DECs may participate in several adipogenesis-related pathways. Following rigorous selection, we found that many up-regulated circRNAs contain multiple miRNAs binding sites, such as miR17, miR-30c, and miR-130, indicating they may potentially facilitate their regulatory functions by acting as miRNA sponges. These results suggest that plenty of circRNAs are expressed in white adipogenesis and the DECs may serve as new candidates for future adipogenesis regulation.

Keywords: circRNA, adipocyte, adipogenesis, obesity, high-throughout RNA sequencing

OPEN ACCESS

Edited by:
Zhihao Jia,
Purdue University, United States

Reviewed by:
Xiaofeng Huang,
Cornell University Weill Cornell Medicine, United States
Renli Qi,
Chongqing Academy of Animal Science, China

****Correspondence:***
Cen-cen Li
licencen2009@126.com
Yong-jie Xu
yongjx81@126.com

Specialty section:
This article was submitted to Lipid and Fatty Acid Research, a section of the journal Frontiers in Physiology

Received: *21 June 2021*
Accepted: *02 August 2021*
Published: *19 August 2021*

Citation:
Zhang P-p, Han Q, Sheng M-x, Du C-y, Wang Y-l, Cheng X-f, Xu H-x, Li C-c and Xu Y-j (2021) Identification of Circular RNA Expression Profiles in White Adipocytes and Their Roles in Adipogenesis. Front. Physiol. 12:728208. doi: 10.3389/fphys.2021.728208

INTRODUCTION

Obesity is recognized as one of the severe threats to public health due to its strong positive association with various diseases, including diabetes, hypertension, cardiovascular diseases, and even cancers (Blüher, 2019). Obesity is characterized by the accumulation of white adipose tissue, which is dependent on an increase of adipocyte number (adipogenesis) and enlargement of

adipocytes (hypertrophy) (Stefan, 2020). One possible approach to prevent obesity is to reduce adipocyte number, but a better understanding of the regulators controlling adipogenesis is needed. In the last few decades, scientists have identified many key protein-encoding genes, such as PPARγ and C/EBP family genes, which are essential for adipogenesis (Rosen et al., 2000). Despite that, there has been a rapidly growing interest in the role of non-coding RNAs in adipogenesis. A larger number of microRNAs and long-non-coding RNAs have been reported to play vital roles in adipogenesis (Sun et al., 2013; Arner and Kulyté, 2015; Lorente-Cebrián et al., 2019). In recent years, circRNA is emerging as another type of non-coding RNA, with important functions in physiological systems and disease contexts.

CircRNA is a type of covalently closed and single-stranded RNA, which is produced by back-splicing of pre-mRNA (Li et al., 2018). It was first reported in the 1990s. However, it is considered as an abnormal splicing product with little function. Until recently, with the progress of high throughout technology, it has been revealed that circRNAs are widely expressed across all eukaryotic species and participate in regulating various biological activities (Kristensen et al., 2019; Patop et al., 2019). CircRNAs can act as miRNA sponges or protein decoys to regulate transcription, splicing, and RNA stability (Hansen et al., 2013; Conn et al., 2017; Du et al., 2017). Some circRNAs may even encode functional proteins by IRES-driven mechanisms (Fan et al., 2019). Through the above ways, circRNAs control many cellular processes such as cell proliferation, differentiation, and apoptosis, which are deeply related to correct tissue development and proper tissue functions. CircRNAs have been extensively studied in the organogenesis of various human organs, such as the central nervous system, cardiovascular system, and skeletal muscle (Khan et al., 2016; Piwecka et al., 2017; Zhang P. et al., 2019). It is also reported that abnormal expression of circRNAs leads to human disease, including cancers and Alzheimer's disease (Haque and Harries, 2017).

Unlike the central nervous system and cancers, fewer studies have aimed to define circRNA function in adipose tissue. Arcinas et al. (2019) performed global circRNA profiles in both epididymal and inguinal fat of humans and mice, they identified thousands of adipose circRNAs. Liu et al. (2020) tried to identify differentially expressed adipose circRNAs from obese and lean individuals. Otherwise, Zhang H. et al. (2019) reported that exosomal circRNAs, which were derived from a gastric tumor, could regulate white adipose browning. Liu et al. (2018) analyzed the expression patterns of circRNAs during porcine subcutaneous preadipocyte differentiation. However, the expression of circRNAs in the process of mouse white adipogenesis remains unknown.

The majority of research investigates adipogenesis molecular pathways was performed *in vitro* using cell lines, e.g., 3T3-L1 or C3H/10T1/2 (Bahmad et al., 2020). However, their ability to differentiate *in vivo* is limited. An alternative approach is the use of primary preadipocytes. Cells isolated from WAT stromal vascular fraction (SVF) can differentiate into mature adipocytes. Regardless some cells are included in SVF other than preadipocytes, such as endothelial cells, pericytes, and fibroblasts, it may more accurately represent adipose tissue function *in vivo* (Rodeheffer et al., 2008), thus WAT SVF is a widely used model to study adipogenesis *in vitro*.

The main goal of the current study was to determine the circRNA profiles during adipogenesis. We isolated SVF cells from mouse white adipose tissue and identify circRNAs by RNA-seq. We discovered a lot of novel circRNAs and characterized their expression profiles in the process of adipogenesis. Furthermore, we identified differential expression circRNAs (DECs) and determined their correlation with the corresponding parental genes. The miRNA binding sites of circRNAs were predicted, suggesting the potential roles of circRNAs in adipogenesis.

MATERIALS AND METHODS

Animals

Mice were bought from the Model Animal Research Centre of Nanjing University in a C57BL/6J background. All the experiments involving mice were guided by the Xinyang Normal University Animal Care and Use Committee.

Cell Culture

Primary white adipose SVF cells were cultured as we described previously (Shan et al., 2016). Briefly, the inguinal fat pad was collected from 6-week-old female mice and washed with PBS twice. Then, the fat pad was minced with scissors and digested with collagenase type I (1.5 mg/ml, #SCR103, Sigma-Aldrich) at 37°C for 40 min. When the digestion was finished, the growth medium contained 85% high glucose DMEM medium (#11965126, Thermo Fisher Scientific) and 15% fetal bovine serum (#10099141, Thermo Fisher Scientific) was added to dilute the collagenase. The tissue debris was removed through a 70-μm cell strainer. The medium was subjected to centrifuge to get SVF cells pellet. SVF cells were resuspended with the growth medium. When the cells reached 90% confluence, they were induced to adipogenesis, with a cocktail containing DMEM, 10% fetal bovine serum, 2.85 mM recombinant human insulin (#I8830, Solarbio), 0.3 mM dexamethasone (#D8040, Solarbio), and 0.63 mM 3-isobutyl-methylxanthine (#I7018, Sigma-Aldrich). After 4 days, the cocktail was switched to a DMEM medium supplemented with 10% fetal bovine serum, 10 nM triiodothyronine (T3, #T6397, Sigma-Aldrich), and 200 nM insulin to induce mature adipocytes.

Total RNA Preparation and RNA-Sequencing

Total RNA was purified from adipocytes using Trizol Reagent (#15596026, Thermo Fisher Scientific). To enrich circRNAs, the rRNA was removed with Ribo-zero rRNA Removal Kit (#RZH1046, Epicentre) and linear RNA was digested with RNase R (#RNR07250, Epicentre). Then, the sequencing libraries were prepared by RNA Library Prep Kit (#E7760S, NEB) and sequenced on an illumine platform. Raw datasets have been deposited at the Gene Expression Omnibus (#GSE178502).

Identification of CircRNA

The circRNA was identified as previously described (Zhang P. et al., 2018). First, the adapter reads and low-quality reads were removed using Fastp (version 0.20.1) (Chen S. et al., 2018). Then, the clean data were mapped to the reference mouse genome mm9 using BWA-MEM (version 0.7.17) (Li, 2013). Subsequently, circRNAs were identified using CIRI2 (Gao et al., 2018). The expression levels of circRNAs were measured by "circRNA counts per million circRNA reads" (circCPM) (Shao et al., 2019). Then, DECs were detected by DESeq2 (version 1.10.1) with a likelihood ratio test (Love et al., 2014). Expression patterns of the DECs were obtained by using degPatterns function from the R package DEGreport (version 1.28.0) (Pantano, 2021). The degPatterns function was run using the default parameters, except that the minimum number of circRNAs in each group was set to 1 (minc = 1).

qPCR Analysis

Random primers and Reverse Transcription Kit (#RR037A, Takara) were used to obtain cDNA according to the manufacturer's protocol. CircPrimer 2.0 software was used to annotate and obtain circRNA sequences (Zhong et al., 2018). Then, the divergent primers, which coved the back-splicing regions, were designed by Primer3[1] (Untergasser et al., 2012). The PCR products of divergent primers were sequenced to validate the corresponding back-splicing sites. The relative expression levels of selected circRNAs were detected by qRT-PCR using TB Green Premix Ex II (#RR820A, Takara) on a LightCycler 96 system (Roche, Germany) according to the instructions. 18S was used to normalize the threshold cycle (Ct) values, and gene expression was quantified using the relative quantitation method ($2^{-\Delta\Delta Ct}$). All experimental data are presented as means ± SD.

GO and KEGG Pathway Analyses

The parental genes of circRNAs were subjected to functional annotation. ClusterProfiler package in Bioconductor was used to perform GO analysis (Yu et al., 2012) and q-values < 0.05 were considered statistically significant. KEGG pathways were enriched by KOBAS online software[2] (Bu et al., 2021) and the corrected P-values < 0.05 were considered statistically significant.

Correlation Analyses Between CircRNAs and Their Parental Genes

To examine the correlation between each circRNA and the parental gene, expression levels of mRNA were extracted from our previous study (GEO accession number GSE173710). Then the average expression levels of circRNA and mRNA on D0, D4, and D8 were used to calculate the correlation by using the Pearson correlation test and the P-values < 0.05 were considered statistically significant.

[1]https://primer3.ut.ee/

[2]http://kobas.cbi.pku.edu.cn/kobas3

Construction of the CircRNA-miRNA Network

The circRNA-miRNA interactions were predicted using miRDB with a predicted score over 85 (Chen and Wang, 2020). Then, the circRNA-miRNA network was constructed using Cytoscape 3.8.2 (Shannon et al., 2003).

RESULTS

Identification of CircRNAs in Growth and Differentiation WAT Adipocytes

To identify circRNAs in adipogenesis, RNA was collected from WAT SVF on day 0 (D0), day 4 (D4), and day 8 (D8) post differentiation, corresponding to the proliferation, premature and mature stages of WAT adipocytes differentiation, with two biological replicates for each stage (**Figure 1A**). To enrich circRNA, the rRNA and linear RNA were removed. Then the RNA samples were subjected to RNA-seq. The CIRI2 was used to predict *de novo* circRNAs. As circRNAs identified between replicates are usually showed low consistency, we kept the circRNAs with a minimum of two reads identified in both two replicates. A total of 3,711 circRNAs were identified (**Supplementary Table 1**). Compared to the publicly available circBase database,[3] we found 1,324 circRNAs were novel (35.11%). As shown in **Figure 1B**, circRNAs were identified on D0, D4, and D8, respectively. It is noticed that 1,023 circRNAs (27.13%) were continually expressed in all stages of adipogenesis, while 588, 489, and 671 circRNAs were only detected on D0, D4, and D8 respectively, indicating the stage-specific expression of circRNAs.

Characteristics of the Adipocyte CircRNAs

We analyzed the chromosome distribution of the circRNAs. We noticed that chromosome 2 generated the greatest number of circRNAs, while chromosome X was the least (**Figure 1C**). Considering that chromosome X is the shortest, we calculated the relationship between circRNA number and chromosome length. The results showed that the correlation was significant (R = 0.69, P < 0.001). As circRNAs share pre-RNAs with mRNAs, we further analyzed the correlation between linear mRNA number and circRNA number in each chromosome, and a much higher correlation was found (R = 0.77, P < 0.05; **Figure 1D**), indicating that the generation of circRNAs may associate with linear mRNAs.

Upon the genomic origin of junction sites, circRNAs can be classified into exonic, intronic, and intergenic circRNA. As described in **Figure 1E**, the ratio of circRNA types was similar in all the stages. The majority of the circRNAs were derived from protein-coding exons (94.53%) of circRNAs. The other circRNAs were derived from introns or intergenic regions. Our previous study showed that 20,703 mRNAs could be detected during white adipogenesis (with a minimum of two reads in both

[3]http://www.circbase.org/

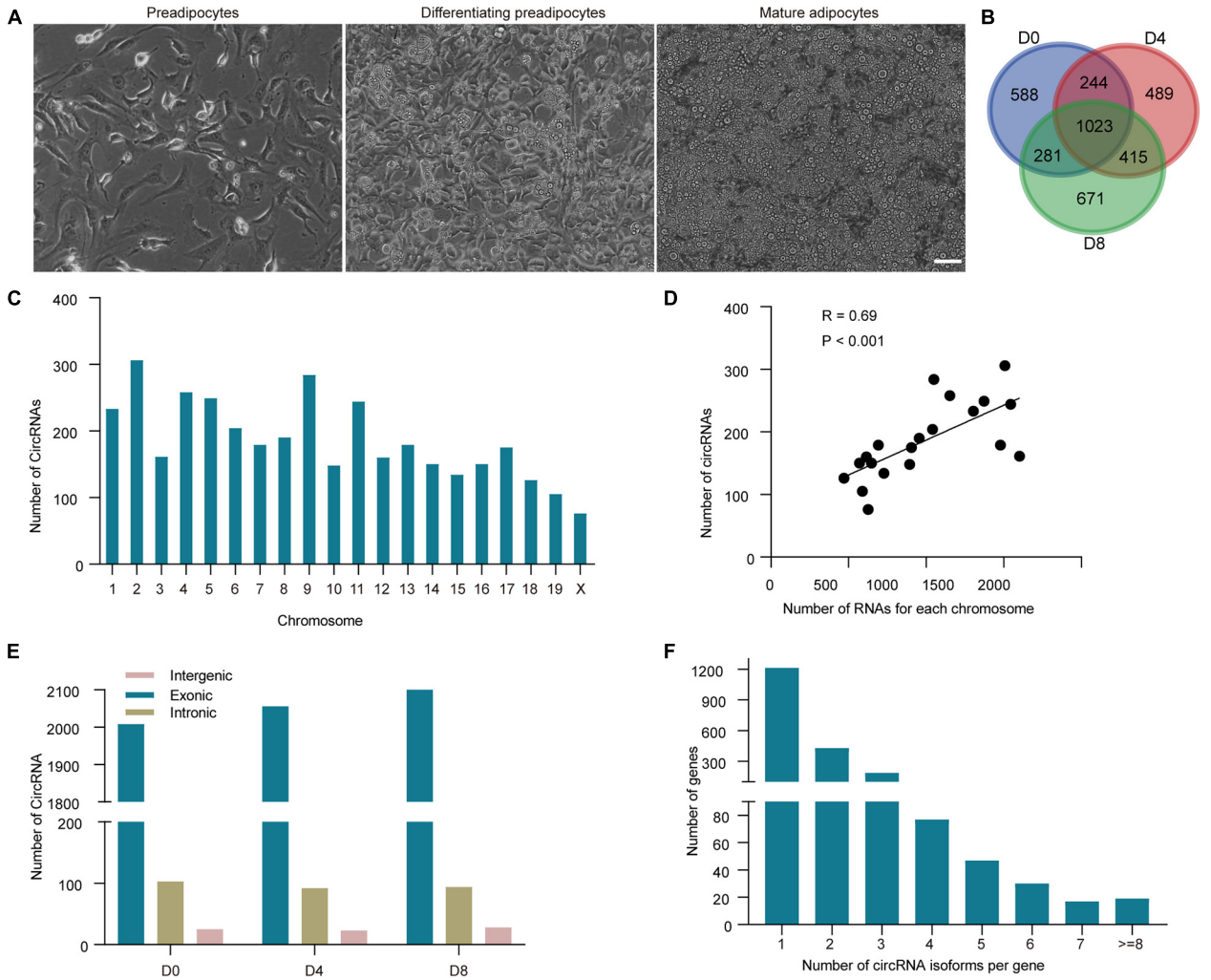

FIGURE 1 | Identification and characterization of circRNAs in white adipogenesis. **(A)** Representative pictures of WAT adipocytes during adipogenesis. Scale bar, 20 μm. **(B)** Identification of circRNAs at each adipogenesis stage. **(C)** Distribution of circRNAs on each chromosome. **(D)** Association of circRNAs and mRNA numbers from the same chromosome. **(E)** Genomic origins of the circRNA type in each adipogenesis stage. **(F)** The number of circRNAs derived from per gene.

two replicates, accession number GSE173710). We found nearly 10% (2,018 genes) of them can generate circRNAs. Further, we found that a great deal of these parental genes (about 40%) gave rise to more than one type of circRNA isoforms. Arhgap10 even produced up to 20 distinct circRNA isoforms (**Figure 1F**). The above results suggest that alternative splicing is very common in circRNA biogenesis, thus expand the diversity of circRNA expression profiles in adipogenesis.

Experimental Validation of the Predicted CircRNAs

To confirm the authenticity of the RNA-seq results, we randomly chose 12 circRNAs and designed divergent primers (primers are list in **Supplementary Table 2**). As shown in **Figure 2A**, 11 of the 12 circRNAs were successfully amplified. In some of the cases, double products were detected which may be generated by multiple rounds of RT around a circular RNA template (Danan et al., 2012). Further, Sanger sequence results detected the expected back-splicing sites (**Figure 2B**). Next, we checked circRNAs expression levels of the 11 circRNAs by qPCR (**Figure 2C**). Then the correlation between the RNA-seq results and qPCR results was examined. We found a strong correlation between them ($R = 0.800$, $P < 0.0001$; **Figure 2D**). The above results suggested that RNA-seq results are reliable.

Differential Expression of CircRNA During Adipogenesis

To compare expression levels of circRNA between different stages, we first checked the overall expression of circRNAs with the boxplot. As shown in **Figure 3A**, the average abundance of circRNAs in all the three stages of adipogenesis was comparable to each other. To explore the similarity of the samples, we performed principal component analysis. As indicated in **Figure 3B**, the distance between two biological replicates was

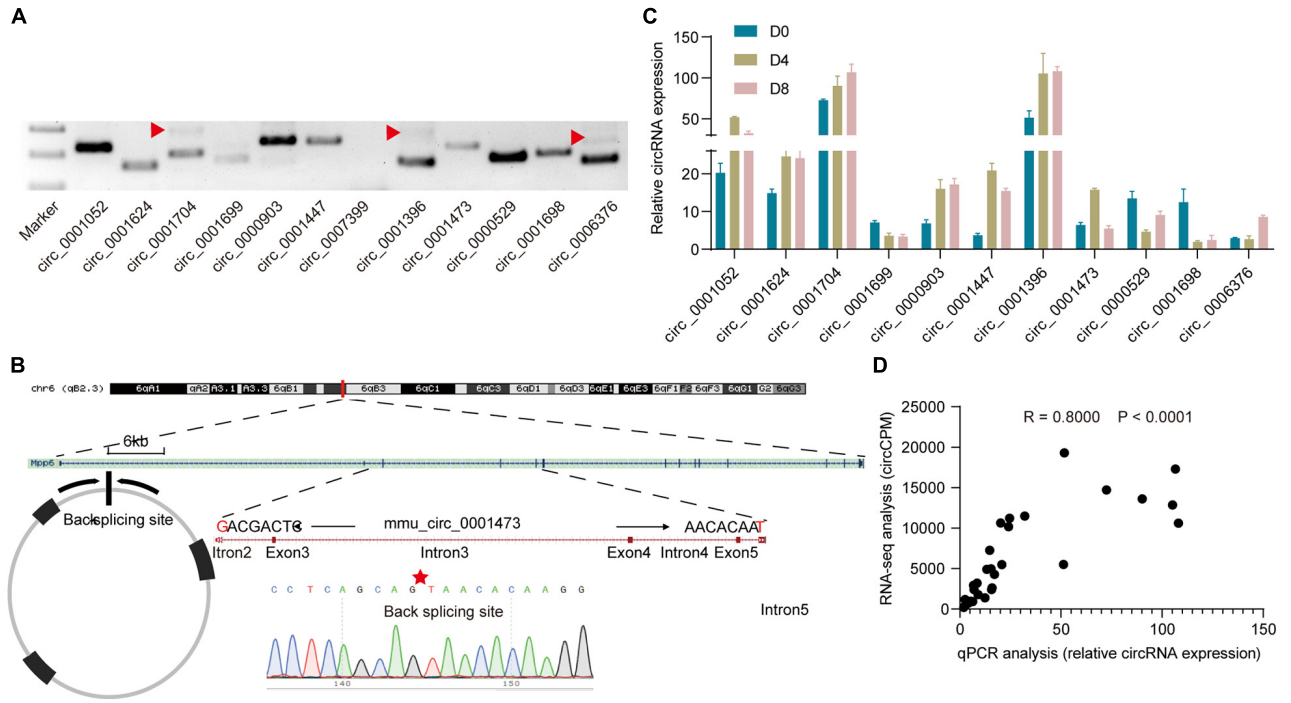

FIGURE 2 | Verification of circular RNAs. **(A)** Electrophoretic band of circRNAs. The red triangle represents double-size products. **(B)** Representative Sanger sequencing results of circRNAs. The red star represents the back-splicing site. **(C)** Relative circRNA expression levels detected by qPCR (n = 3). **(D)** Correlation analysis of qPCR results and RNA-seq results.

very close to each other, indicating high repeatability. Meanwhile, the D0 group was located far away from the other groups, suggesting a great difference in circRNA expression patterns between the proliferation and differentiation stages. Consistent with the principal component analysis, the hierarchical tree also showed biological replicates were highly correlated with each other (**Figure 3C**). Subsequently, we identified DECs across adipogenesis by DESeq2 with the Likelihood ratio test. We set the cut-off as padj $<$ 0.05. Only 41 DECs were identified. The majority of them were upregulated (28 of 41) and 13 were downregulated (**Figure 3D** and **Supplementary Table 3**). Consistent with the above results, the heatmap showed marked differences between the proliferation stage and the differentiation stages (**Figure 3E**). As many circRNAs regulate the expression of their parental genes, the roles of circRNAs may be revealed through functional analysis of their parental genes. Despite the two circRNAs fell outside the genomic regions of annotated genes, the parental genes of the other 39 DECs were used. KOBAS gene-list enrichment showed that many adipogenesis and fat metabolism pathways were significantly enriched, such as GnRH signaling pathway, MAPK signaling pathway, type II diabetes mellitus, calcium signaling pathway, and cAMP signaling pathway. GO annotations indicated that calcium channels, actinin binding, and transmembrane receptor protein kinase activity were significantly enriched (**Supplementary Table 4**).

We further examined the expression patterns of the 41 DECs using DegPatterns function of R package DEGreport. A total of four groups were identified (**Figure 3F** and **Supplementary Table 3**). The circRNA numbers ranged from 2 to 26 in the four groups. Group 1 was the largest, which contained 26 circRNAs. In group 1, the circRNAs showed increased expression levels in the differentiation stages compared to the proliferation stage. In contrast to group 1, group 4 showed an opposite trend, the circRNAs decreased in the differentiation stages. Both group 2 and group 3 contained only two circRNAs. Group 2 showed a transient increase on D4 followed by a decrease. Group 3 showed a transient decrease on D4 followed by a sharp increase. To annotate the role of the circRNAs in group 1 and group 4. We performed GO and KEGG analysis (**Supplementary Table 5**). Unfortunately, few GO terms were significantly enriched. The results showed four GO terms were enriched in group 1, they were transmembrane receptor protein kinase activity, transmembrane receptor protein serine/threonine kinase activity, activin binding, growth factor binding, and growth factor binding. In group 4, actinin binding and alpha-actinin binding were enriched. KOBAS enrichment showed no pathway was significantly enriched in group 4 and only a few pathways were enriched in group 1, such as propanoate metabolism, MAPK signaling pathway, GnRH signaling pathway, and TGF-beta signaling pathway.

Correlation of the Expression Between CircRNAs and Linear RNAs

To evaluate the change of circRNAs expression and their parental genes between different stages of adipogenesis. The

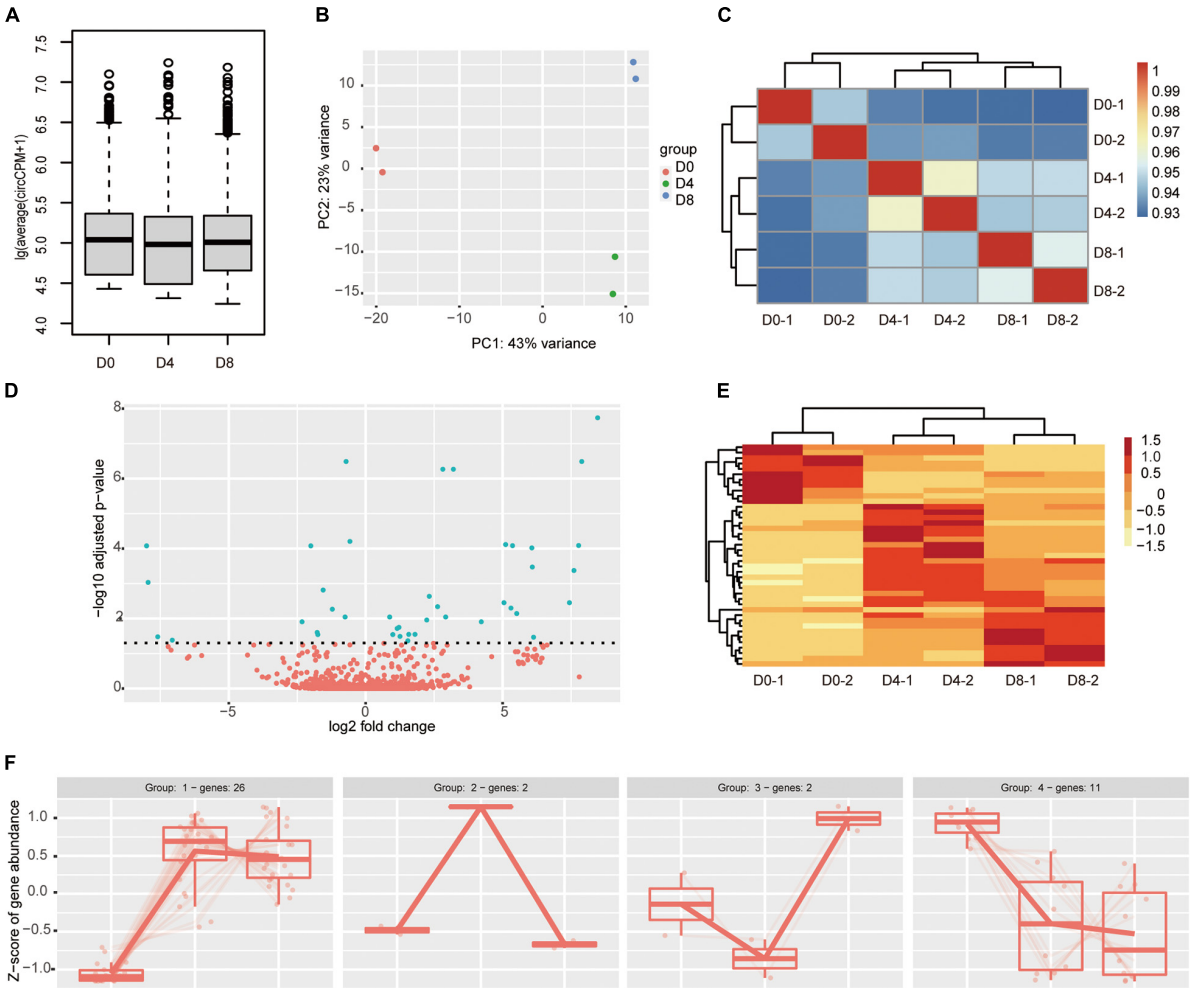

FIGURE 3 | Differential circRNAs expression during adipogenesis. **(A)** Relative expression abundance of circRNAs during adipogenesis (circCPM). **(B)** Principal component analysis (PCA) plot of RNA samples. **(C)** Hierarchical clustering analyses of samples correlation using DESeq2 rlog-normalized RNA-seq results. **(D)** Volcano plot comparing circRNAs abundance between different adipogenesis stages. The green color indicates the differentially expressed circRNAs (padj < 0.05), while the red color indicates not significant change circRNAs. **(E)** Heatmap showing differentially expressed circRNAs across different stages of adipogenesis. **(F)** Expression patterns of the differential expressed circRNAs during adipogenesis.

expression data of mRNA counterparts were collected from our previous study (GEO accession number GSE173710). We tried to calculate the overall correlation between circRNAs expression and their parental genes, but no significant correlation was found. However, when we checked the expression of individual circRNA and the parental gene in adipogenesis, we identified 1,806 circRNA-mRNA pairs (48.67%) that were significantly correlated with each other, including 1,379 (37.16%) positively correlation and 427 (11.51%) negatively correlation (**Supplementary Table 6**).

We further analyzed the correlation between the 39 DECs and their linear counterparts. We found 33 of the DECs were correlated with their linear counterparts. Interestingly, all of them showed positive correlation, ranging from 0.812 to 0.999 ($P < 0.05$, **Figure 4** showed the representative results and the other results could be found in **Supplementary Figure 1**). Notably, circRNA generated by Acvr2a showed almost the same trend as the linear counterpart ($R = 0.999$), while circRNAs generated by Fancl and Megf8 were not significantly correlated with their linear counterparts. In **Figure 4D**, the expression of Fancl linear counterpart continuously decreased in the process of adipogenesis, while the expression of circRNA showed a transient increase on D4 followed by a decrease on D8. As shown in **Figure 4A**, both two circRNA isoforms generated by Acss3 were highly correlated with the linear counterpart. But in **Figure 4C**, only one of the circRNA isoforms generated by Arhgap10 was significantly correlated with the linear counterpart. In **Figure 4L**, it seemed that the expression of the Zfx linear counterpart and the circRNA were not correlated. However, after we inspected the data, we found that the Zfx linear counterpart increased by 20% on D4, then it decreased to a similar level as D0. The corresponding circRNA showed the same expression pattern

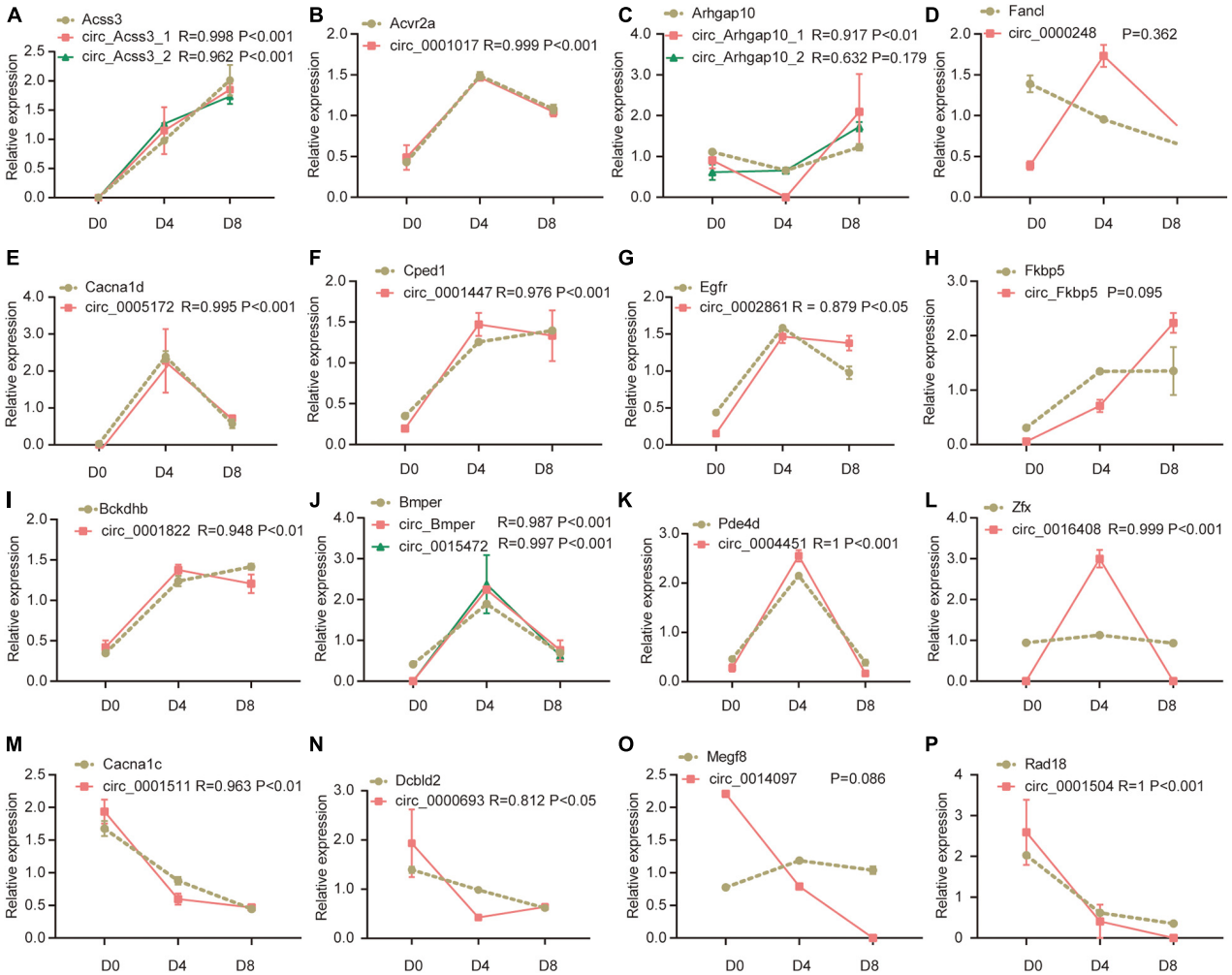

FIGURE 4 | Representative results of correlation analysis between differentially expression circRNAs and their parental genes during adipogenesis. For the convenience of drawing both circRNA and mRNA expression in the figure, the relative expression level was used (expression level at each time point was divided by its average expression level across adipogenesis). **(A–P)** The correlation between Acss3, Acvr2a, Arhgap10, Fancl, Cacna1d, Cped1, Egfr, Fkbp5, Bckdhb, Bmper, Pde4d, Zfx, Cacna1c, Dcbld2, Megf8, Rad18, and their corresponding circRNAs.

despite much more change on D4, hence they showed a high correlation. In summary, these results indicated that many of the circRNAs are highly correlated with their linear counterparts. CircRNAs may be potentially involved in the regulation of linear RNA expression in adipogenesis.

Potential CircRNA-miRNA Interaction Network

CircRNAs may affect gene expression by interacting with miRNAs (Zhong Q. et al., 2019). In the up-regulated circRNAs, we chose the top 15 highly expressed circRNAs. The potential miRNA binding sites of these circRNAs were predicted using miRDB. As some of the circRNAs may not express in adipocytes, we filtered them according to the previous data studying miRNA profiles in adipogenesis (GEO accession: GSE75697). Then, 8 of the15 circRNAs were left, which contain many miRNA binding sites. A total of 148 circRNA-miRNA interactions were identified with a predicted score over 85. Then the circRNA-miRNA interactions were used to draw an interaction network (**Figure 5** and **Supplementary Table 7**). We noticed several miRNAs which have been reported to regulate adipogenesis were included in the network, such as miR17, miR-30c, and miR-130. These results indicating that these circRNAs may potentially regulate adipogenesis by interacting with miRNAs. However, it should be noted that those results were not obtained experimentally and future work should validate the circRNA-miRNA interactions.

DISCUSSION

Prior studies have described circRNAs are abundant in white adipose tissue. Arcinas et al. (2019), for example, reported that up to 6,000 and 2,000 circRNAs were detected in human adipose tissue and mouse adipose tissue respectively.

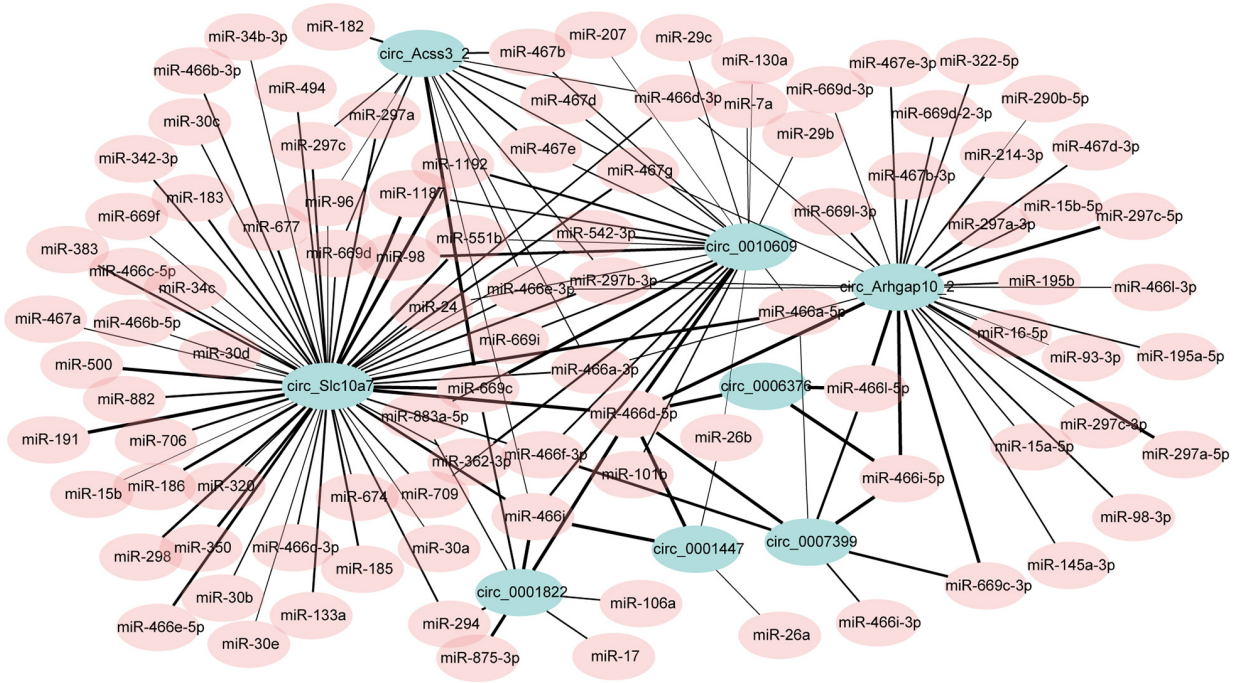

FIGURE 5 | The potential circRNA-miRNA interaction network. The width of the edge indicates the prediction score (range from 85 to 100).

Liu et al. (2020) compared the circRNA expression profiles of obese and lean individuals. They identified that circSAMD4 was highly expressed in obese individuals. However, these studies mainly focused on mature adipose tissue. Little attention has been paid to the expression profiles and functions of circRNAs in adipocytes. In the present study, we detected the expression profile of circRNAs in proliferation, pre-mature and mature stages of adipogenesis. We identified 3,711circRNAs and nearly 35% of them are novel. We noticed a dramatic change of circRNA expression profiles between the proliferation and differentiation stages. These findings confirmed that circRNAs are abundant in adipose tissue, not a by-product of splicing. In addition, we noticed the circRNA number in our study is different from the previous study, which may result from differences in cell conditions, circRNA identification methods, and sequence depth. Thus, it is essential to investigate circRNAs expression profiles in various cell lines, tissues, and developmental stages.

Several reports indicated that circRNAs can regulate the expression of their parental genes. It has been suggested that circRNAs and their linear counterparts share the same pre-RNA (Aufiero et al., 2018), thus they may compete and negatively regulate the abundance of each other. In contrast to that, other reports suggested that circRNAs can also positively regulate gene expression. Some circRNAs accumulate at promoter regions and interact with Pol II and U1 snRNP to increase transcription of their parental genes (Li et al., 2015). Another circRNA, circFECR1, can bind to its parental gene and regulate transcription by an epigenetic mechanism. CircFECR1 recruits a demethylase and induces DNA hypomethylation in CpG islands of the promoter, thus enhanced parental gene expression (Chen N. et al., 2018). We examined the correlation between individual circRNA and parental genes. We discovered that nearly 50% of circRNAs were significantly correlated with their parental genes. When we checked them in detail, we found 37% of them were positively correlated, while the other 12% were negatively correlated. The complex correlation between circRNAs and parental genes may explain why the overall correlation is very weak and not significant. Further, when we check the correlation of the DECs and their parental genes, a much higher ratio of positive correlation was found. We also noted that the circRNAs which were derived from the same parental gene show different expression trends.

The functions of circRNAs largely remained to be investigated. One clue to predict circRNA functions is their parental genes. Functional analysis showed that the parental genes of DECs were enriched in many adipogenesis and fat metabolism-related pathways, such as GnRH signaling pathway, MAPK signaling pathway, type II diabetes mellitus, and cAMP signaling pathway. We also found several parental genes of the DECs play key roles in regulating adipogenesis. Nsd2 is the parental gene of circ_0001335. Depleting Nsd2 impairs adipogenesis by increasing H3K27me3, thus preventing the induction of C/EBPα and PPARγ (Zhuang et al., 2018). The parental gene Selenbp1 is identified as an H_2S-producing enzyme. Selenbp1 silencing downregulates H_2S levels and inhibits adipogenesis (Randi et al., 2021). The Fkbp5 and Fndc3b are also circRNA parental genes that are essential for adipogenesis (Tominaga et al., 2004; Zhang L. et al., 2017). Another clue to predict circRNA functions is based on miRNAs. As circRNAs were reported to act as

sponges to titrate the levels of miRNAs, they can regulate miRNA target genes indirectly. CircSAMD4A is highly expressed in obese people and acts as a sponge for miR-138-5p to promote adipogenesis (Liu et al., 2020). The miR-138 effectively reduces lipid droplet accumulation by targeting adipogenesis genes (Yang et al., 2011). In bovine adipose tissue, circFUT10 directly interacts with let-7c/let-e to promote adipocyte proliferation and inhibit differentiation (Jiang et al., 2020). In the current study, we noticed that DECs could interact with a great number of miRNAs and many of the miRNAs have been reported to regulate adipogenesis. We predicted that circ_0010609 may act as a sponge for miR130a which was reported to inhibit adipogenesis differentiation *via* suppressing PPARγ expression (Lee et al., 2011). The miR-30 family represents 4.9% of the miRNA reads in adipocytes and positively regulates adipogenesis (Zaragosi et al., 2011; Irani and Hussain, 2015). According to our results, circSlc10a7 and circ_0010609 contained multiple binding sites for distinct miR-30 family members, indicating the potential roles of these circRNAs in regulating adipocyte activity.

CONCLUSION

In summary, we globally detected the circRNA expression profiles during adipogenesis. We concluded that circRNAs are abundant and dynamically express in adipogenesis. Nearly 50% of the circRNAs are correlated with their parental gene expression. Adipose circRNAs may be involved in adipogenesis-related pathways and act as miRNA sponges to modulate gene expression. These identified circRNAs may serve as new candidates to regulate adipogenesis and combat obesity. However, some limitations are worth noting. Although our hypotheses were supported statistically, future experimental work is needed to understand the functions of the indicated circRNAs in adipogenesis.

DATA AVAILABILITY STATEMENT

The datasets presented in this study can be found in online repositories. The names of the repository/repositories and accession number(s) can be found in the article/ **Supplementary Material**.

ETHICS STATEMENT

The animal study was reviewed and approved by the Xinyang Normal University Animal Care and Use Committee.

AUTHOR CONTRIBUTIONS

P-PZ designed the experiments and wrote the manuscript. P-PZ, Y-JX, C-CL, X-FC, and H-XX analyzed the data. P-PZ, M-XS, Y-LW, QH, and C-YD performed the experiments. All authors have read and agreed to the published version of the manuscript.

FUNDING

This research was funded by the National Natural Science Foundation of China (31601167 and 31972537), Major Science and Technology Projects of Henan Province (201300111200), Department of Education in Henan Province (21A230017), the Central Plains Technological Innovation Leading Talents Project of Henan Province (194200510022), and the Nanhu Scholars Program of XYNU.

ACKNOWLEDGMENTS

We thank Lei Wang, Feng Xing, Xudong Liu, and Yu Zhang for their comments and help in data analysis.

SUPPLEMENTARY MATERIAL

The Supplementary Material for this article can be found online at: https://www.frontiersin.org/articles/10.3389/fphys.2021.728208/full#supplementary-material

Supplementary Figure 1 | Correlation of the expression profiles of differential circRNAs and their parental genes during adipogenesis.

Supplementary Table 1 | List of circRNAs identified by RNA-seq in white adipogenesis.

Supplementary Table 2 | List of primers used to detect circRNAs.

Supplementary Table 3 | List of differentially expressed circRNAs across different stages of adipogenesis.

Supplementary Table 4 | GO terms and KEGG pathways enriched for the host genes of differentially expressed circRNAs.

Supplementary Table 5 | GO terms and KEGG pathways enriched for the host genes of group 1 and group 4 differentially expressed circRNAs.

Supplementary Table 6 | Correlation of the expression profiles of circRNAs and their parental genes during adipogenesis.

Supplementary Table 7 | Prediction of circRNA-miRNA interactions.

REFERENCES

Arcinas, C., Tan, W., Fang, W., Desai, T. P., Teh, D. C. S., Degirmenci, U., et al. (2019). Adipose circular RNAs exhibit dynamic regulation in obesity and functional role in adipogenesis. *Nat. Metab.* 1, 688–703. doi: 10.1038/s42255-019-0078-z

Arner, P., and Kulyté, A. (2015). MicroRNA regulatory networks in human adipose tissue and obesity. *Nat. Rev. Endocrinol.* 11:276. doi: 10.1038/nrendo.2015.25

Aufiero, S., van den Hoogenhof, M. M. G., Reckman, Y. J., Beqqali, A., van der Made, I., and Kluin, J. (2018). Cardiac circRNAs arise mainly from constitutive exons rather than alternatively spliced exons. *RNA* 24, 815–827. doi: 10.1261/rna.064394.117

Bahmad, H. F., Daouk, R., Azar, J., Sapudom, J., Teo, J. C. M., Abou-Kheir, W., et al. (2020). Modeling Adipogenesis: Current and Future Perspective. *Cells* 9:2326. doi: 10.3390/cells9102326

Blüher, M. (2019). Obesity: global epidemiology and pathogenesis. *Nat. Rev. Endocrinol.* 15, 288–298. doi: 10.1038/s41574-019-0176-8

Bu, D., Luo, H., Huo, P., Wang, Z., Zhang, S., He, Z., et al. (2021). KOBAS-i: intelligent prioritization and exploratory visualization of biological functions for gene enrichment analysis. *Nucleic Acids Res.* 49, W317–W325.

Chen, N., Zhao, G., Yan, X., Lv, Z., Yin, H., Zhang, S., et al. (2018). A novel FLI1 exonic circular RNA promotes metastasis in breast cancer by coordinately regulating TET1 and DNMT1. *Genome Biol.* 19:218.

Chen, S., Zhou, Y., Chen, Y., and Gu, J. (2018). fastp: an ultra-fast all-in-one FASTQ preprocessor. *Bioinformatics* 34, i884–i890.

Chen, Y., and Wang, X. (2020). miRDB: an online database for prediction of functional microRNA targets. *Nucleic Acids Res.* 48, D127–D131.

Conn, V. M., Hugouvieux, V., Nayak, A., Conos, S. A., Capovilla, G., Cildir, G., et al. (2017). A circRNA from SEPALLATA3 regulates splicing of its cognate mRNA through R-loop formation. *Nat. Plants* 3:17053.

Danan, M., Schwartz, S., Edelheit, S., and Sorek, R. (2012). Transcriptome-wide discovery of circular RNAs in Archaea. *Nucleic Acids Res.* 40, 3131–3142. doi: 10.1093/nar/gkr1009

Du, W. W., Zhang, C., Yang, W., Yong, T., Awan, F. M., and Yang, B. B. (2017). Identifying and Characterizing circRNA-Protein Interaction. *Theranostics* 7, 4183–4191. doi: 10.7150/thno.21299

Fan, X., Yang, Y., and Wang, Z. (2019). Pervasive translation of circular RNAs driven by short IRES-like elements. *bioRxiv* [preprint]. doi: 10.1101/473207

Gao, Y., Zhang, J., and Zhao, F. (2018). Circular RNA identification based on multiple seed matching. *Brief. Bioinform.* 19, 803–810. doi: 10.1093/bib/bbx014

Hansen, T. B., Jensen, T. I., Clausen, B. H., Bramsen, J. B., Finsen, B., Damgaard, C. K., et al. (2013). Natural RNA circles function as efficient microRNA sponges. *Nature* 495, 384–388. doi: 10.1038/nature11993

Haque, S., and Harries, L. W. (2017). Circular RNAs (circRNAs) in Health and Disease. *Genes* 8:353. doi: 10.3390/genes8120353

Irani, S., and Hussain, M. M. (2015). Role of microRNA-30c in lipid metabolism, adipogenesis, cardiac remodeling and cancer. *Curr. Opin. Lipidol.* 26, 139–146. doi: 10.1097/mol.0000000000000162

Jiang, R., Li, H., Yang, J., Shen, X., Song, C., Yang, Z., et al. (2020). circRNA Profiling Reveals an Abundant circFUT10 that Promotes Adipocyte Proliferation and Inhibits Adipocyte Differentiation via Sponging let-7. *Mol. Ther. Nucleic Acids* 20, 491–501. doi: 10.1016/j.omtn.2020.03.011

Khan, M. A. F., Reckman, Y. J., Aufiero, S., van den Hoogenhof, M. M. G., van der Made, I., Beqqali, A., et al. (2016). RBM20 Regulates Circular RNA Production From the Titin Gene. *Circ. Res.* 119, 996–1003.

Kristensen, L. S., Andersen, M. S., Stagsted, L. V., Ebbesen, K. K., Hansen, T. B., and Kjems, J. (2019). The biogenesis, biology and characterization of circular RNAs. *Nat. Rev. Genet.* 20, 675–691.

Lee, E. K., Lee, M. J., Abdelmohsen, K., Kim, W., Kim, M. M., Srikantan, S., et al. (2011). miR-130 suppresses adipogenesis by inhibiting peroxisome proliferator-activated receptor γ expression. *Mol. Cell. Biol.* 31, 626–638. doi: 10.1128/mcb.00894-10

Li, H. (2013). Aligning sequence reads, clone sequences and assembly contigs with BWA-MEM. *arXiv* [preprint] 1303.3997.

Li, X., Yang, L., and Chen, L.-L. (2018). The Biogenesis, Functions, and Challenges of Circular RNAs. *Mol. Cell* 71, 428–442. doi: 10.1016/j.molcel.2018.06.034

Li, Z. Y., Huang, C., Bao, C., Chen, L., Lin, M., Wang, X. L., et al. (2015). Exon-intron circular RNAs regulate transcription in the nucleus. *Nat. Struct. Mol. Biol.* 22, 256–264. doi: 10.1038/nsmb.2959

Liu, X., Liu, K., Shan, B., Wei, S., Li, D., Han, H., et al. (2018). A genome-wide landscape of mRNAs, lncRNAs, and circRNAs during subcutaneous adipogenesis in pigs. *J. Anim. Sci. Biotechnol.* 9:76.

Liu, Y., Liu, H., Li, Y., Mao, R., Yang, H., Zhang, Y., et al. (2020). Circular RNA SAMD4A controls adipogenesis in obesity through the miR-138-5p/EZH2 axis. *Theranostics* 10, 4705–4719. doi: 10.7150/thno.42417

Lorente-Cebrián, S., González-Muniesa, P., Milagro, F. I., and Martínez, J. A. (2019). MicroRNAs and other non-coding RNAs in adipose tissue and obesity: emerging roles as biomarkers and therapeutic targets. *Clin. Sci.* 133, 23–40. doi: 10.1042/cs20180890

Love, M. I., Huber, W., and Anders, S. (2014). Moderated estimation of fold change and dispersion for RNA-seq data with DESeq2. *Genome Biol.* 15, 1–21.

Pantano, L. (2021). *DEGreport: Report of DEG analysis. R package version 1.28.0.*

Patop, I. L., Wüst, S., and Kadener, S. (2019). Past, present, and future of circRNAs. *EMBO J.* 38:e100836.

Piwecka, M., Glažar, P., Hernandez-Miranda, L. R., Memczak, S., Wolf, S. A., Rybak-Wolf, A., et al. (2017). Loss of a mammalian circular RNA locus causes miRNA deregulation and affects brain function. *Science* 357:eaam8526. doi: 10.1126/science.aam8526

Randi, E. B., Casili, G., Jacquemai, S., and Szabo, C. (2021). Selenium-Binding Protein 1 (SELENBP1) Supports Hydrogen Sulfide Biosynthesis and Adipogenesis. *Antioxidants* 10:361. doi: 10.3390/antiox10030361

Rodeheffer, M. S., Birsoy, K., and Friedman, J. M. (2008). Identification of white adipocyte progenitor cells *in vivo*. *Cell* 135, 240–249. doi: 10.1016/j.cell.2008.09.036

Rosen, E. D., Walkey, C. J., Puigserver, P., and Spiegelman, B. M. (2000). Transcriptional regulation of adipogenesis. *Genes Dev.* 14, 1293–1307.

Shan, T., Zhang, P., Jiang, Q., Xiong, Y., Wang, Y., and Kuang, S. (2016). Adipocyte-specific deletion of mTOR inhibits adipose tissue development and causes insulin resistance in mice. *Diabetologia* 59, 1995–2004. doi: 10.1007/s00125-016-4006-4

Shannon, P., Markiel, A., Ozier, O., Baliga, N. S., Wang, J. T., Ramage, D., et al. (2003). Cytoscape: a software environment for integrated models of biomolecular interaction networks. *Genome Res.* 13, 2498–2504. doi: 10.1101/gr.1239303

Shao, J., Wang, L., Liu, X., Yang, M., Chen, H., Wu, B., et al. (2019). Identification and characterization of circular RNAs in Ganoderma lucidum. *Sci. Rep.* 9:16522.

Stefan, N. (2020). Causes, consequences, and treatment of metabolically unhealthy fat distribution. *Lancet Diab. Endocrinol.* 8, 616–627. doi: 10.1016/s2213-8587(20)30110-8

Sun, L., Goff, L. A., Trapnell, C., Alexander, R., Lo, K. A., Hacisuleyman, E., et al. (2013). Long noncoding RNAs regulate adipogenesis. *Proc. Natl. Acad. Sci. U. S. A.* 110, 3387–92. doi: 10.1073/pnas.1222643110

Tominaga, K., Kondo, C., Johmura, Y., Nishizuka, M., and Imagawa, M. (2004). The novel gene fad104, containing a fibronectin type III domain, has a significant role in adipogenesis. *FEBS Lett.* 577, 49–54. doi: 10.1016/j.febslet.2004.09.062

Untergasser, A., Cutcutache, I., Koressaar, T., Ye, J., Faircloth, B. C., Remm, M., et al. (2012). Primer3—new capabilities and interfaces. *Nucleic Acids Res.* 40:e115. doi: 10.1093/nar/gks596

Yang, Z., Bian, C., Zhou, H., Huang, S., Wang, S., Liao, L., et al. (2011). MicroRNA hsa-miR-138 inhibits adipogenic differentiation of human adipose tissue-derived mesenchymal stem cells through adenovirus EID-1. *Stem Cells Dev.* 20, 259–267. doi: 10.1089/scd.2010.0072

Yu, G., Wang, L.-G., Han, Y., and He, Q.-Y. (2012). clusterProfiler: an R package for comparing biological themes among gene clusters. *OMICS* 16, 284–287. doi: 10.1089/omi.2011.0118

Zaragosi, L.-E., Wdziekonski, B., Le Brigand, K., Villageois, P., Mari, B., Waldmann, R., et al. (2011). Small RNA sequencing reveals miR-642a-3p as a novel adipocyte-specific microRNA and miR-30 as a key regulator of human adipogenesis. *Genome Biol.* 12, 1–13.

Zhang, H., Zhu, L., Bai, M., Liu, Y., Zhan, Y., Deng, T., et al. (2019). Exosomal circRNA derived from gastric tumor promotes white adipose browning by targeting the miR-133/PRDM16 pathway. *Int. J. Cancer* 144, 2501–2515. doi: 10.1002/ijc.31977

Zhang, L., Qiu, B., Wang, T., Wang, J., Liu, M., Xu, Y., et al. (2017). Loss of FKBP5 impedes adipocyte differentiation under both normoxia and hypoxic stress.

Biochem. Biophys. Res. Commun. 485, 761–767. doi: 10.1016/j.bbrc.2017.02.126

Zhang, P., Chao, Z., Zhang, R., Ding, R., Wang, Y., Wu, W., et al. (2019). Circular RNA Regulation of Myogenesis. *Cells* 8:885. doi: 10.3390/cells8080885

Zhang, P., Xu, H., Li, R., Wu, W., Chao, Z., Li, C., et al. (2018). Assessment of myoblast circular RNA dynamics and its correlation with miRNA during myogenic differentiation. *Int. J. Biochem. Cell Biol.* 99, 211–218. doi: 10.1016/j.biocel.2018.04.016

Zhong, Q., Huang, J., Wei, J., and Wu, R. (2019). Circular RNA CDR1as sponges miR-7-5p to enhance E2F3 stability and promote the growth of nasopharyngeal carcinoma. *Cancer Cell Int.* 19: 252.

Zhong, S., Wang, J., Zhang, Q., Xu, H., and Feng, J. (2018). CircPrimer: a software for annotating circRNAs and determining the specificity of circRNA primers. *BMC Bioinformatics* 19: 292.

Zhuang, L., Jang, Y., Park, Y.-K., Lee, J.-E., Jain, S., Froimchuk, E., et al. (2018). Depletion of Nsd2-mediated histone H3K36 methylation impairs adipose tissue development and function. *Nat. Commun.* 9: 1796.

Conflict of Interest: The authors declare that the research was conducted in the absence of any commercial or financial relationships that could be construed as a potential conflict of interest.

Publisher's Note: All claims expressed in this article are solely those of the authors and do not necessarily represent those of their affiliated organizations, or those of the publisher, the editors and the reviewers. Any product that may be evaluated in this article, or claim that may be made by its manufacturer, is not guaranteed or endorsed by the publisher.

Copyright © 2021 Zhang, Han, Sheng, Du, Wang, Cheng, Xu, Li and Xu. This is an open-access article distributed under the terms of the Creative Commons Attribution License (CC BY). The use, distribution or reproduction in other forums is permitted, provided the original author(s) and the copyright owner(s) are credited and that the original publication in this journal is cited, in accordance with accepted academic practice. No use, distribution or reproduction is permitted which does not comply with these terms.

frontiers in Physiology

ORIGINAL RESEARCH
published: 06 October 2021
doi: 10.3389/fphys.2021.748801

Cold Exposure Affects Lipid Metabolism, Fatty Acids Composition and Transcription in Pig Skeletal Muscle

*Ziye Xu[1,2,3], Wentao Chen[1,2,3], Liyi Wang[1,2,3], Yanbing Zhou[1,2,3], Qiuyun Nong[1,2,3], Teresa G. Valencak[1], Yizhen Wang[1,2,3], Jintang Xie[4] and Tizhong Shan[1,2,3]**

[1] College of Animal Sciences, Zhejiang University, Hangzhou, China, [2] Key Laboratory of Molecular Animal Nutrition, Ministry of Education, Zhejiang University, Hangzhou, China, [3] Key Laboratory of Animal Feed and Nutrition of Zhejiang Province, Hangzhou, China, [4] Shandong Chunteng Food Co., Ltd., Zaozhuang, China

Cold exposure promotes glucose oxidation and modulates the lipid metabolism in adipose tissue, but it is still not fully clear whether cold exposure could affect meat quality and fatty acid metabolism in skeletal muscle of pig *in vivo*. Here, we kept finishing pigs under cold or room temperature overnight and determined the effects of cold exposure on meat quality, fatty acids composition and transcriptional changes in skeletal muscle of pigs. We found that cold exposure significantly reduced the meat colour$_{24\ h}$ and pH$_{24\ h}$, without affecting carcass characteristics and other meat quality traits. Considerable changes were found in the proportions of individual fatty acids and the total content of saturated fatty acid, polyunsaturated fatty acids, monounsaturated fatty acid and n3-fatty acids. RNA-seq results showed upregulated fatty acid biosynthesis genes and downregulated mitochondrial beta-oxidation genes. The lipid metabolism in cold-treated longissimus dorsi muscle might be regulated by functions of the lipoprotein particle, the extracellular matrix, and the PPAR signaling pathways. Our study revealed the potential of cold exposure to regulate the lipid metabolism and fatty acid composition in skeletal muscle of farmed animals.

Keywords: cold exposure, meat quality, fatty acid, transcriptome, pig, skeletal muscle

OPEN ACCESS

Edited by:
Naim Akhtar Khan,
Université de Bourgogne, France

Reviewed by:
Lei Zhou,
Guangxi University, China
Andrea S. Pereyra,
East Carolina University, United States

****Correspondence:***
Tizhong Shan
tzshan@zju.edu.cn

Specialty section:
This article was submitted to Lipid and Fatty Acid Research, a section of the journal Frontiers in Physiology

Received: *28 July 2021*
Accepted: *16 September 2021*
Published: *06 October 2021*

Citation:
Xu Z, Chen W, Wang L, Zhou Y, Nong Q, Valencak TG, Wang Y, Xie J and Shan T (2021) Cold Exposure Affects Lipid Metabolism, Fatty Acids Composition and Transcription in Pig Skeletal Muscle. Front. Physiol. 12:748801. doi: 10.3389/fphys.2021.748801

INTRODUCTION

Emerging evidences have indicated that cold exposure plays a crucial role in whole-body lipid metabolism, including reduced plasma triglyceride (TG) concentrations by activating brown adipose tissue (BAT)-mediated non-shivering thermogenesis (Bartelt et al., 2011), reversed cholesterol transport by high-density lipoprotein (HDL) particles (Bartelt et al., 2017) and increased conversion of cholesterol to bile acids (BAs) (Worthmann et al., 2017). Cold exposure also has multiple effects on hepatic lipid metabolism and microbiome composition, which collaborates with thermogenic BAT in maintaining whole-body metabolic homeostasis in mice (Ziętak et al., 2016; Grefhorst et al., 2018). Our previous results revealed that short-term cold exposure induces significant changes in lipid dynamics and gene expression pathways in inguinal WAT (iWAT) (Xu Z. Y. et al., 2019). These results demonstrate that cold stimulation is an effective way to modulate the systemic metabolic homeostasis, especially glucose and lipid metabolism.

Pork is the most widely consumed meat in the world accounting for over 36% of the world-wide meat intake (Dugan et al., 2015). Studies on improving pork quality and nutritive values have received wide attention over the recent 10 years, mainly in response to the stricter quality controls and increased customer awareness (Grunert et al., 2004). Pork quality generally is evaluated through water-holding capacity, meat color, pH, fat content and oxidative stability, and its nutritive value is mainly determined by fatty acid profile, especially the n-3 PUFA proportion (Rosenvold and Andersen, 2003; Hocquette et al., 2010). Intramuscular fat (IMF), also known as intramuscular triglycerides, which refers to adipose tissue located in myofibers (Liu et al., 2019). In pork production, IMF has been recognized as an important meat-quality trait of pigs owning to influencing the shearing force, tenderness and juicy flavor (Zhang et al., 2021). Moreover, IMF accumulation in muscle is related to diseases such as insulin resistance and type 2 diabetes (Buras et al., 2019). Scientists have put forward various strategies to improve pork quality and nutritive values in the past few decades, including improving the genetic background of pig breeds, optimizing nutrient supply and the production systems (Rosenvold and Andersen, 2003; Hocquette et al., 2010). However, the pork industry is challenged because many of these efforts were imperceptible to the consumer with at the same time causing increased production costs.

Improving pre-slaughtering conditions, such as housing and exercise, could be a novel and effective method to amend the sensory and nutrient quality of pork (Ngapo and Gariepy, 2008). As temperature changes are easily perceived by mammals, we hypothesized that meat quality might be improved by acute cold exposure before slaughter. Unlike rodents, pigs reportedly have no BAT and defending their body temperature depends on skeletal muscle shivering as a primary source of heat production when exposed to cold (Hou et al., 2017; Blondin and Haman, 2018). The skeletal musculature might produce heat through both shivering and non-shivering thermogenesis, both of which influence mitochondrial energetics and remodels fat content and composition (Blondin and Haman, 2018). In addition, cold exposure increases whole-body energy expenditure and improves glucose metabolism by inducing sympathetic nervous system activity and recruiting brown adipocytes as shown recently from human (Van Der Lans et al., 2013; Iwen et al., 2017). By reconstitution of the functional uncoupling protein 1 (UCP1) gene in white adipose tissue of pigs, a browning-like adipocyte of BAT was induced resulting in decreased fat deposition, increased lean percentage and altered lipid metabolism in adipose (Pan et al., 2019). In pigs, UCP3 was shown to mediate some non-shivering thermogenic activity (Lin et al., 2017). Based on these previous results, we supposed that cold exposure might influence meat quality in the skeletal muscle of pigs both directly and indirectly.

In the present study, we kept growing-finishing pigs under cold (5–7°C) or room temperature (22–25°C) overnight (14 h) and investigated the effects of acute cold exposure on carcass indicators, enzyme activity, fatty acid composition, and gene expression profiles in longissimus dorsi muscle (LDM). We revealed cold exposure plays a key role in pork lipid metabolism and fatty acid profiles. Moreover, these results were accompanied by changes in transcriptional dynamics *in vivo*, especially fatty acid oxidation and fat biosynthesis. Our results point out the importance of pre-slaughter temperature conditions for fatty acid metabolism of pork.

MATERIALS AND METHODS

Animals and Experimental Design

All procedures were approved by the University of Zhejiang Institutional Animal Care and Use Committee. The ethical committee number for the study is ZJU20170466. Duroc × Landrace × Yorkshire (DLY) boars were raised in Shandong Chunteng Food Co., Ltd., (Tengzhou city, Shangdong, China) and fed twice a day with the same diet with 67% of corn, 21% of soybean meal, 8% of wheat bran and 4% series of pig premixed feed and provided free access to water under similar environmental. At slaughter weight (120–125 kg,6.0–6.5 months), twelve finishing pigs were randomly selected and used to investigate the influence of acute cold exposure on pork meat quality and fatty acids composition.

These pigs were divided into two groups randomly and each contains six animals. These two groups experimental animals were placed at room temperature (RT, 22–25°C) and under cold conditions (COLD, 5–7°C) overnight (14 h), respectively. During the 14 h, all pigs were fasted but free access to water. These pigs were weighed and sampled immediately after short-term cold exposure.

Slaughtering, Carcass and Meat Quality Measurements

Pigs were slaughtered in a commercial abattoir by exsanguination after electric stunning (90∼100 V, 0.9–1.0 A, 50 Hz). After that, the pigs were immediately hoisted for bleeding and dehairing. Evisceration was completed about 20 min post mortem.

The carcass was split longitudinally after the head, legs, tail, and viscera were removed. Carcass traits were measured by using standard methodology for testing carcass traits in lean-type pig (Gu et al., 2019). Both the left and right hot carcass weights were recorded. Carcass yield was calculated by hot carcass weight/preslaughter weight ×100% (Gu et al., 2019). Body length was measured as the distance from the anterior edge of the first cervical vertebra to the anterior edge of the pubis (Gu et al., 2019). Skin thickness was assessed at the 6rd/7th rib of the centerline of the carcass by using a Vernier caliper (Li et al., 2020). Backfat thickness was determined by calculate the average scores of three regions of the right carcass sides (first- and last-rib, and last-lumbar) (Li et al., 2018). Simultaneously, samples of LDM from the right side of each carcass were collected and rapidly frozen in liquid nitrogen and subsequently stored at −80°C for fatty acid composition and RNA-seq analysis.

Meat quality measurements including marbling, $pH_{45\ min}$, $pH_{24\ h}$, drip loss (24 h), meat $color_{45\ min}$ and meat $color_{24\ h}$ were carried out in LDM obtained from the 3rd to 11th rib. Subjective marbling was scored from a mean of scores made by three people using the National Pork Producer Council (NPPC) standards as

previous described (Xu X. et al., 2019). The $pH_{45\ min}$ values were determined on LDM at 45 min postmortem using a portable pH meter (pH-STAR, MATTHAUS, German), previously calibrated with pH 4.6 and 7.0 buffers (Xu X. et al., 2019). The meat $color_{45\ min}$ values were measured from a mean of three random readings on LDM at 45 min postmortem using a portable chromameter (opto-STAR, MATTHAUS, German), which was calibrated with a white tile according to the manufacturer's manual (Xu X. et al., 2019). Samples were stored at 4°C for 24 h, and then $pH_{24\ h}$ and meat $color_{24\ h}$ were measured in the same way. Drip loss was measured using the hanging bag method (Honikel, 1998), 2.5 cm thick loin chops were taken from LDM at the third and fourth lumbar vertebrae after slaughter. The initial weights of these loin chops were collected, and meat samples were reweighed after stored for 24 h at 4°C to collect the terminal weights. Drip loss was calculated as the percentage of weight lost over the 24 h period. LDM samples were homogenized into freeze-dried powder and then weighed. Intramuscular fat (IMF) content was measured by determining the crude fat of LDM by using Soxhlet Extraction with petroleum ether (Tyra and Żak, 2012). Inosinic acid content was measured described by Xu X. et al. (2019). The IMF and inosinic acid contents were indicated by the weights of fat or inosinic acid, respectively, in per 100 g freeze-dried LDM (g/100 g).

Enzyme Activities

Longissimus dorsi muscle samples were lysed in phosphate buffered saline (PBS) and the supernatant was obtained by centrifugation at 2,000 rpm for 10 min and used for subsequent enzyme activities measurements. The BCA Protein Assay Kit (Thermo Fisher Scientific) was used to measure protein concentrations. The contents of triglyceride (TG) and non-esterified free fatty acids (NEFA), and the enzyme activities of lactate dehydrogenase (LDH), succinate dehydrogenase (SDH), malate dehydrogenase (MDH), malondialdehyde (MDA), lipid peroxide (LPO), total antioxidant capacity (T-AOC), glutathione peroxidase (GSH-Px), catalase (CAT) and peroxidase (POD) in COLD or RT group were measured using commercially available kits according to the manufacturer's instructions (Nanjing Jiancheng Bioengineering Institute, Nanjing, China).

Analysis of the Fatty Acid Composition

Lipids in the LDM were extracted and hydrolyzed in 2 mL KOH-methanol to obtain the free fatty acid mixture. The free fatty acid mixture was esterified in 2 mL BF3-methanol solution to obtain fatty acid methyl esters. Next, 800 μL fatty acid methyl esters were separated and analyzed with a GC-2010 plus gas chromatograph (Shimadzu, Japan). By comparing the retention times of the peaks with the known standards (Sigma, United States), fatty acids contents could be identified.

Analysis of the Amino Acid Composition

About 150 mg of the dried LDM sample were weighed and put into a glass cylinder before 15 mL of 6 molar HCl was added. After adding nitrogen and sealing, the mixture was hydrolyzed at 110°C for 22–24 h. Subsequently, the hydrolysate was transferred to a 50 mL volumetric flask and diluted into a calibration tail with ultrapure water. The solution was filtered using a 0.45 μm membrane filter into an autosampler vial before amino acid analysis with an L-8900 amino acid analyzer (HI-TACHI, Japan).

RNA Isolation, Library Construction, RNA-Seq Analysis and Quantitative Real-Time PCR

RNA extraction, library construction, RNA-seq analysis and quantitative real-time PCR (qPCR) of LDM samples from RT and cold-treated pigs were performed as previously published methods (Xu Z. et al., 2019; Xu et al., 2020). Briefly, total RNA was extracted using the Total RNA Extractor (TRIzol) Kit (B511311, Sangon, China) and the quality of the RNA samples was examined with a NanoDrop 2000 spectrophotometer (Agilent Technologies, Santa Clara, CA, United States). A total amount of 2-μg RNA per sample was used for library preparation. Subsequently, paired-end sequencing of the library was performed on HiSeq XTen sequencers (Illumina, San Diego, CA, United States). FastQC (version 0.11.2) was used to evaluate the quality of the sequenced data. Trimmomatic (version 0.36) and HISAT2 (version 2.0) were applied to filter raw reads and mapped to the reference genome, respectively. Package DESeq2 (version 1.12.4) was used to identify differentially expressed genes (DEGs) between the two groups. Genes with p value < 0.05 and $|$ Log2 (fold change) $| > 1$ were considered significant DEGs. QPCR was performed with an Applied Biosystems StepOnePlus^{TM} Real-Time PCR System using SYBR Green Master Mix (Roche, Indianapolis, IN, United States). The relative changes in gene expression were analyzed by using the $2^{-\Delta\Delta CT}$ method.

Pathway-Enrichment Assay

Gene Ontology (GO) functional analysis and KEGG pathway analysis were performed as previously published methods (Xu Z. et al., 2019; Xu et al., 2020). Briefly, DEGs are subjected to GO biological process (BP) and KEGG pathway enrichment analysis using the packages clusterProfiler and org.Ss.eg.db. P value < 0.05 was defined as statistical significance. Enriched terms and pathways were visualized by the barplot and cnetplot function.

Statistical Analysis

Data on carcass and meat characteristics, enzyme activities and fatty acid composition were presented as the mean ± SEM. Comparisons were made by unpaired two-tailed Student's t-tests. Differences between groups were considered statistically significant at $p < 0.05$.

RESULTS

Cold Exposure Induced Alterations in Meat Characteristics and Enzyme Activities

The carcass and meat characteristics from immediate post-mortem are given in **Table 1**. There were no significant differences in body weights (BW), carcass weights, body lengths,

skin thickness, and mean backfat thickness between cold-treated and RT pigs (**Table 1**). Next, we found that overnight cold exposure significantly reduced the meat colour$_{24\ h}$ ($p = 0.046$) and pH$_{24\ h}$ ($p = 0.009$), without affecting the meat colour$_{45\ min}$, pH$_{45\ min}$, marbling and drip loss of pigs (**Table 1**). Moreover, the content of IMF had an increasing tendency ($p = 0.061$) in cold-treated meat (**Table 1**). While the flavor substance and the content of inosinic acid, were not affected by cold exposure ($p > 0.05$, **Table 1**). Besides, we neither found a pH$_{24\ h}$ value above 6.0 nor a pH$_{45\ min}$ value below 5.8 in this study, indicating no dark, firm and dry (DFD) or pale, soft and exudative (PSE) meat (**Table 1**).

To further determine the effect of cold exposure on IMF content, we also measured the level of TG and NEFA in pork. Consistent with change trend of IMF content, the content of TG showed an increased trend in cold-treated LDM, while, the content of NEFA showed a decreased trend (**Figure 1A**). To explore the changes in oxidative stability and antioxidant enzymes stability in skeletal muscle from COLD pigs, we measured enzyme activities associated with oxidation-reduction, lipid oxidative, and antioxidation (**Figures 1B–D**). The activity of LDH, which is responsible for lactic acid production in glycolysis, was significantly inhibited by cold exposure. These results suggest cold exposure may inhibit glycolysis capacities in LDM. The activities of oxidative enzymes, such as SDH and MDH, showed no change (**Figure 1B**). Besides, the qPCR results indicated the mRNA level of *MYH2* was significantly downregulated, while the mRNA level of *MYH4* was significantly upregulated (**Supplementary Figure 1A**). Slightly decreased lipid peroxidation related enzymes (MDA, and LPO) were found in COLD pigs (**Figure 1C**), suggesting that cold exposure prior to slaughter might improve the quality and shelf-life of meats by lipid oxidative stability. COLD pigs also had differentially expressed antioxidant-related enzymes (T-AOC, GSH-PX, CAT, and POD) (**Figure 1D**). Taken together, cold exposure may have a positive impact on meat quality and flavor through increasing IMF content, improving oxidative capacity, inhibiting lipid peroxidation, although it did not reach statistical significance.

TABLE 1 | Effects of cold exposure on carcass characteristics, meat quality traits and flavor substances of LDM in pigs.

Variable	RT		COLD		
	Mean	SEM	Mean	SEM	*P*-value
BW (kg) [1]	121.917	2.491	124.250	5.261	0.697
Carcass weight (kg)	94.817	2.485	97.183	4.106	0.633
Carcass yield	0.777	0.007	0.784	0.021	0.777
Body length (cm)	108.333	1.498	112.167	3.027	0.283
Skin thickness (mm)	3.342	0.107	3.135	0.318	0.552
Backfat thickness (mm)	33.247	2.604	33.647	2.160	0.908
Marbling	1.000	0.000	1.167	0.167	0.341
Meat colour45 min [2]	86.361	0.983	86.589	1.333	0.893
Meat colour24 h [3]	72.778	1.593	68.400	1.083	0.046*
pH45 min [4]	6.389	0.085	6.234	0.091	0.241
pH24 h [5]	5.667	0.056	5.453	0.034	0.009**
Drip loss (%)	2.047	0.065	2.071	0.091	0.837
IMF (g/100 g) [6]	12.150	0.274	13.117	0.368	0.061
Inosinic acid (g/100 g) [7]	0.830	0.034	0.838	0.034	0.866

*Statistical effect of cold exposure on carcass and meat characteristics of pigs were analyzed by two-tailed Student's t-test (n=6). SEM, standard error of means. *P < 0.05, **P < 0.01. RT, pigs at room temperature of 22–25°C; COLD, pigs at cold temperature of 5–7°C.*

[1]BW, body weight.

[2]Meat color45 min, meat color measured 45 min after slaughter.

[3]Meat color24 h, meat color measured 24 h after slaughter.

[4]pH45 min, pH value measured 45 min after slaughter.

[5]pH24 h, pH value measured 24 h after slaughter.

[6]IMF, intramuscular fat. The IMF content was indicated by the weight of fat (g) in pre 100 g freeze-dried LDM (g/100 g).

[7]The inosinic acid content was indicated by the weights of inosinic acid (g) in pre 100 g freeze-dried LDM (g/100 g).

Cold Exposure Changed the Composition and Content of Fatty Acids

We further explored overall fatty acid composition in LDM of COLD pigs compared to RT pigs (**Figure 2**). Absolute proportions showed that cold exposure induced extensive increases in the following fatty acids: palmitic acid (C16:0), palmitoleic acid (C16:1), oleic acid (C18:1n9c), linoleic acid (C18:2n-6c), capric acid (C10:0), lauric acid (C12:0), myristic acid (C14:0), margaric acid (C17:0), arachidic acid (C20:0), eicosenic acid (C20:1), α-linolenic (C18:3n-3), eicosadienoic acid (C20:2), pentadecanoic acid (C15:0) and γ-linolenic (C18:3n6) (**Figures 2A–C**). Notably, the saturated fatty acids (SFAs), including margaric acid (C17:0), palmitic acid (C16:0), capric acid (C10:0), lauric acid (C12:0), myristic acid (C14:0), eicosadienoic acid (C20:2) and pentadecanoic acid (C15:0) were largely increased in COLD pigs (**Figures 2A–C**). In line with the increases in individual fatty acid, the total contents of saturated fatty acids (SFAs)and unsaturated fatty acids (UFAs) were significantly elevated in COLD LDM (**Figure 2D**). We further analyzed the percentages of total SFAs, monounsaturated fatty acids (MUFAs) and polyunsaturated fatty acids (PUFAs), respectively, and found no difference (**Figure 2E**). Besides, we calculated the ratio of MUFAs: PUFAs, the ratio of n6-fatty acids: n3-fatty acids (n6: n3) and the total content of n3-fatty acids (**Figures 2F–I**), all known for improving human health. Cold exposure treatment did not affect the ratio of MUFAs: PUFAs (**Figure 2F**), but significantly increased the ratio of n6: n3 in LDM (**Figure 2G**). However, the total content of n3-fatty acids was significantly increased by cold exposure (**Figure 2H**). The total content of individual fatty acids was also dramatically elevated by cold exposure treatment (**Figure 2I**). These results suggest that cold exposure induced considerable alterations in the composition and content of fatty acids in LDM.

Cold Exposure Changed the Transcriptome Profiles of Longissimus Dorsi Muscle in Pigs

To explore how the LDM transcriptome is altered upon cold exposure, we next utilized RNA-seq to map the transcriptional changes. A total of 660 DEGs were identified in the RT and COLD group using the filter criteria of | Log2 (fold change) | > 1 and *p*-value < 0.05. Of these DEGs, 452 were up-regulated

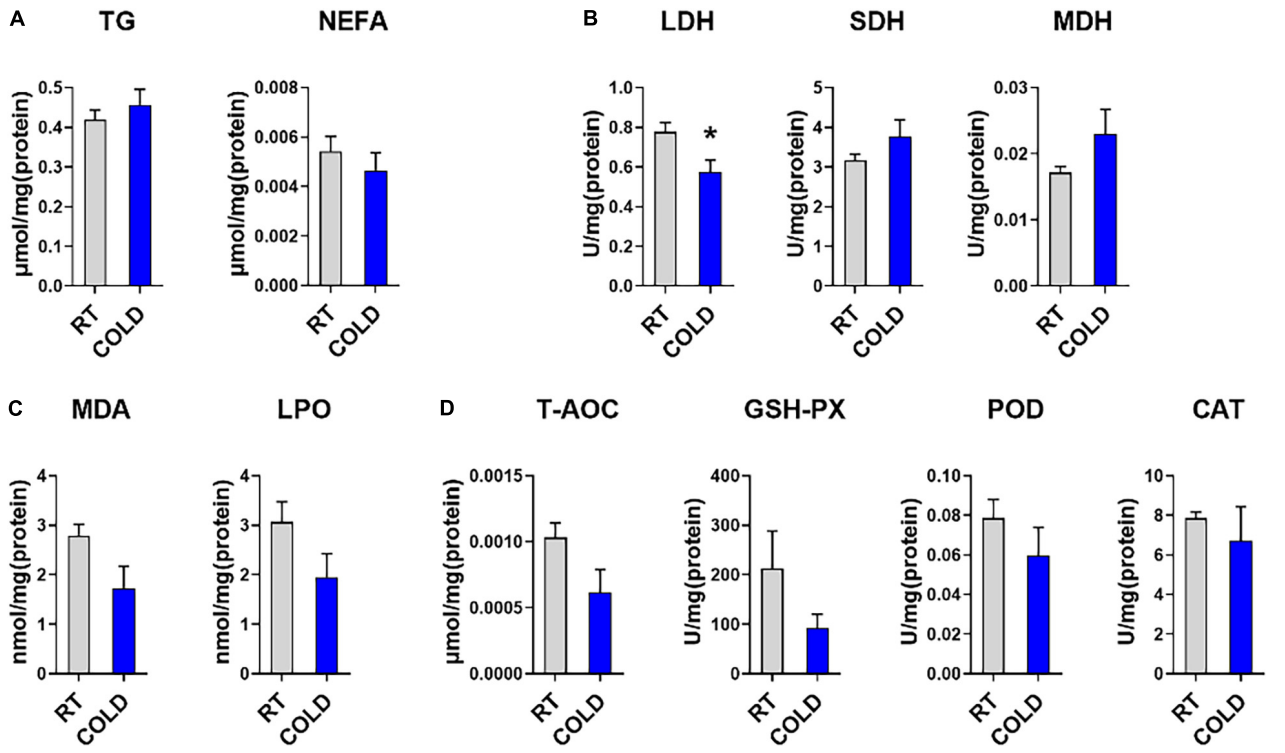

FIGURE 1 | Effects of cold exposure on lipid metabolism and various enzymes activities. **(A)** Triglyceride (TG) and non-esterified free fatty acids (NEFA) levels in LDM of pigs from room temperature (RT) or cold condition (COLD). **(B)** The activities of oxidoreductases, including Lactate dehydrogenase (LDH), succinate dehydrogenase (SDH), malate dehydrogenase (MDH). **(C)** The levels of lipid peroxide contents, including malondialdehyde (MDA), lipid peroxidation (LPO). **(D)** The levels of antioxidant non-enzymatic activity, total antioxidant capacity (T-AOC), and enzymatic activities, including glutathione peroxidase (GSH-Px), peroxidase (POD), catalase (CAT). $n = 5$. Error bars represent S.E.M. $^*P < 0.05$, two-tailed Student's *t*-test.

and 208 were down-regulated by cold exposure (**Figure 3A**). The mRNA expression levels of several genes reported previously as having altered expression upon cold exposure in skeletal muscle, including *UCP2, UCP3, PPARG, SLC2A4, NR4A3, MSTN, MFN2*, were reflected by TPM (Transcripts Per Kilobase of exon model per Million mapped read) values (**Figures 3B,C**). Interestingly, only myogenesis related genes (*MSTN, MFN2*) were decreased by cold exposure in LDM of pigs (**Figure 3B**). These genes (*UCP2, UCP3, FGF21, SLC2A4, NR4A3*) were not significantly altered in COLD groups (**Figure 3B**). We also analyzed the expression levels of lipid droplets markers (*FABP1, FABP3, FABP5, PLIN1, PLIN2, PLIN4, PLIN5*) and found that cold exposure significantly elevated the expression level of FABP3 (**Figure 3C**). Expression levels of genes involved in the main pathways associated to fatty acid metabolism are given in **Figure 3**. And include fatty acid biosynthesis (**Figure 3D**), fatty acid elongation (**Figure 3E**), biosynthesis of unsaturated fatty acids (**Figure 3F**) and fatty acid degradation (**Figure 3G**). These significantly altered genes (*CBR4, ACSL1, OXSM, TECR, ELOVL1, SCD5*, *FADS2, ELOVL7, ACADL, ACADM, ACAT1, ACASL4, ALDH3A2*) are highlighted in the heatmaps (**Figures 3D–G**). The expression levels of *CBR4*, *ACSL1* and *OXSM*, which participate in the biosynthesis of fatty acids in mitochondria (Zhang et al., 2005; Venkatesan et al., 2014), *FADS2*, which regulates the unsaturation of fatty acids, *ELOVL1*, *TECR* and *ELOVL7* which catalyze the long-chain fatty acids elongation (Moon and Horton, 2003; Naganuma et al., 2011), *SCD5*, which catalyzes the formation of monounsaturated fatty acids, was significantly altered by cold exposure. And the expression levels of mitochondrial beta-oxidation related genes (*ACADL, ACADM, ACAT1*) were significantly suppressed in COLD LDM. The RNA-seq results were further confirmed by qPCR on several key genes including *ACC*, *FABP4*, *SREBP1*, *SCD*, *ACAA1*, *PPARG*, *ELOVL6 CPT1*, *CPT2*, and *PPARGC1A* (**Figures 3H,I**). Taken together, we found extensive changes in the transcriptome of LDM in pigs in response to overnight cold compared with RT. Notably, the fatty acid anabolism related genes were activated, while fatty acid catabolism related genes were inhibited in COLD LDM.

Cold Exposure Induced Alterations in Apolipoprotein Function

Functional enrichment analysis of cold-induced DEGs were carried out using GO enrichment analysis. GO enrichment analysis for genes on biological processes (BP) revealed that cold-induced DEGs were abundant in the processes of lipid catabolism, negative regulation of coagulation and protein-lipid complex remodeling (**Figure 4A**). The cnetplot showed that these apolipoprotein encoding genes (*APOC3*, *APOA4*, *APOE*, *APOA2*, *APOC2*, *APOA5*), involved in natural lipid catabolic

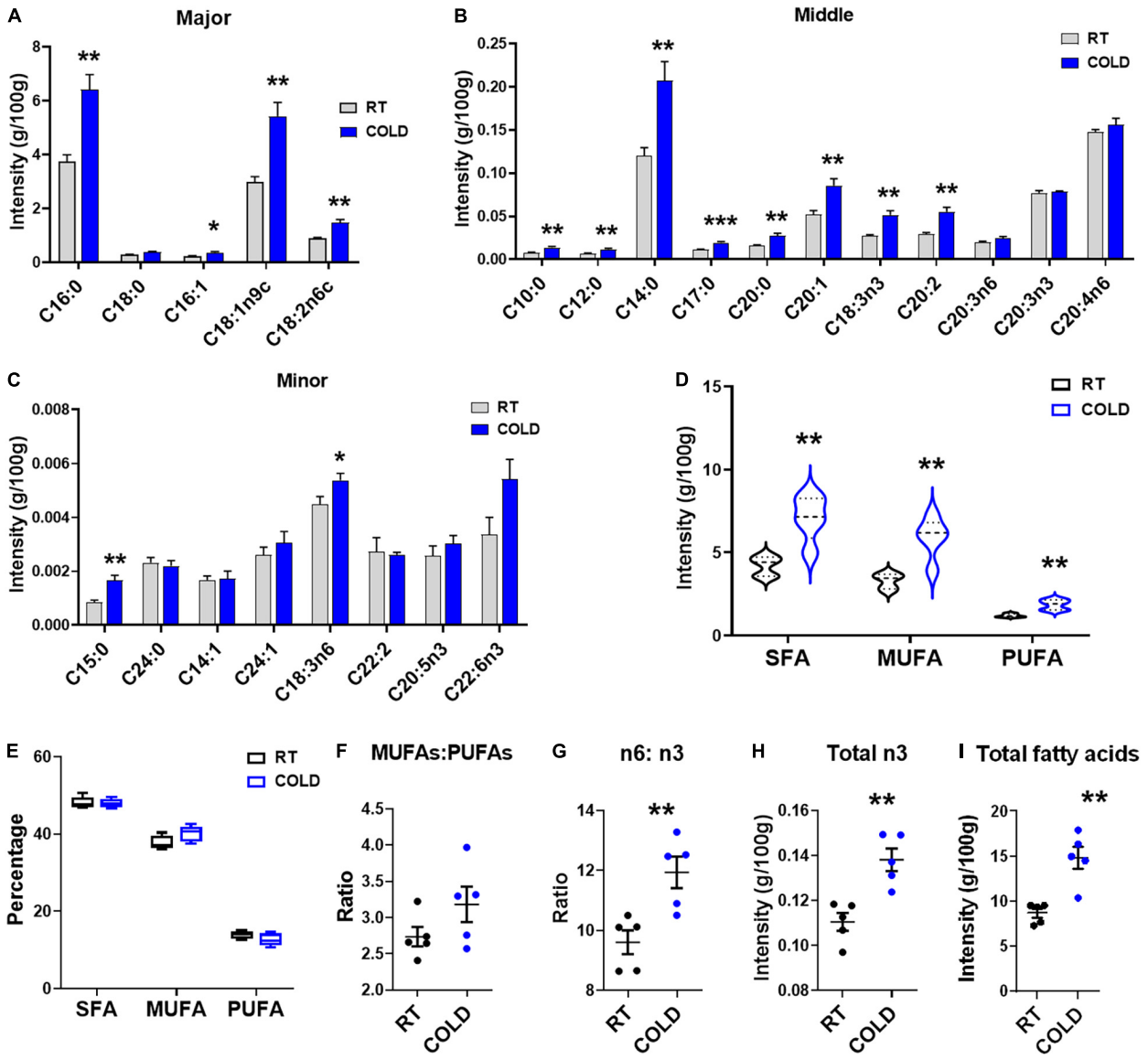

FIGURE 2 | Cold exposure changed the composition and proportions of fatty acids. Fatty acid composition analyses of LDM isolated from pigs maintained at room temperature (RT, 22–25°C) or in cold (5–7°C) for 14 h. **(A–C)** The concentration of individual fatty acids in LDM from COLD and RT pigs. Fatty acids are divided into major **(A)**, middle **(B)** and minor **(C)** species based on abundance. Fatty acids are sorted by a degree of saturation. **(D,E)** The contents **(D)** and percentages **(E)** of total SFAs, MUFAs and PUFAs in LDM from COLD and RT pigs. SFAs, saturated fatty acids; MUFAs, monounsaturated fatty acids; PUFAs, polyunsaturated fatty acids containing two or three to six double bonds. **(F,G)** The ratio of MUFAs: PUFAs **(F)** and n6-fatty acids: n3-fatty acids (n6: n3) **(G)** in LDM from COLD and RT pigs. **(H,I)** The contents of total n3-fatty acids **(H)** and total individual fatty acids **(I)**. $n = 5$. Error bars represent S.E.M. $^{*}P < 0.05$, $^{**}P < 0.01$, $^{***}P < 0.001$, two-tailed Student's *t*-test.

progress, negative regulation of coagulation, protein-lipid complex remodeling, were significantly upregulated by cold exposure (**Figure 4D**), suggesting that cold exposure might influence lipid metabolism in LDM through these processes. GO enrichment analysis for genes on molecular function (MF) revealed enrichment in lipid binding, endopeptidase inhibitor activity and extracellular matrix structural constituent (**Figure 4B**). These upregulated apolipoprotein encoding genes also participated in lipid binding (**Figure 4E**). These endopeptidase inhibitor activity related genes (*SERPIND1*, *AMBP*, *AHSG*, *SERPINA3-2*) were markedly upregulated by cold exposure (**Figure 4C**), suggesting that cold treatment induced alteration on lipid metabolism might be entangled with endopeptidase inhibitor activity, which reportedly could improve hepatic steatosis and inflammation (Jiang et al., 2020). GO enrichment analysis for genes on cellular components (CC) revealed that cold-induced DEGs were enriched in the extracellular matrix and lipoprotein particle (**Figure 4C**). The cneplot showed that lipoprotein particles were regulated by these upregulated apolipoprotein encoding genes, and extracellular

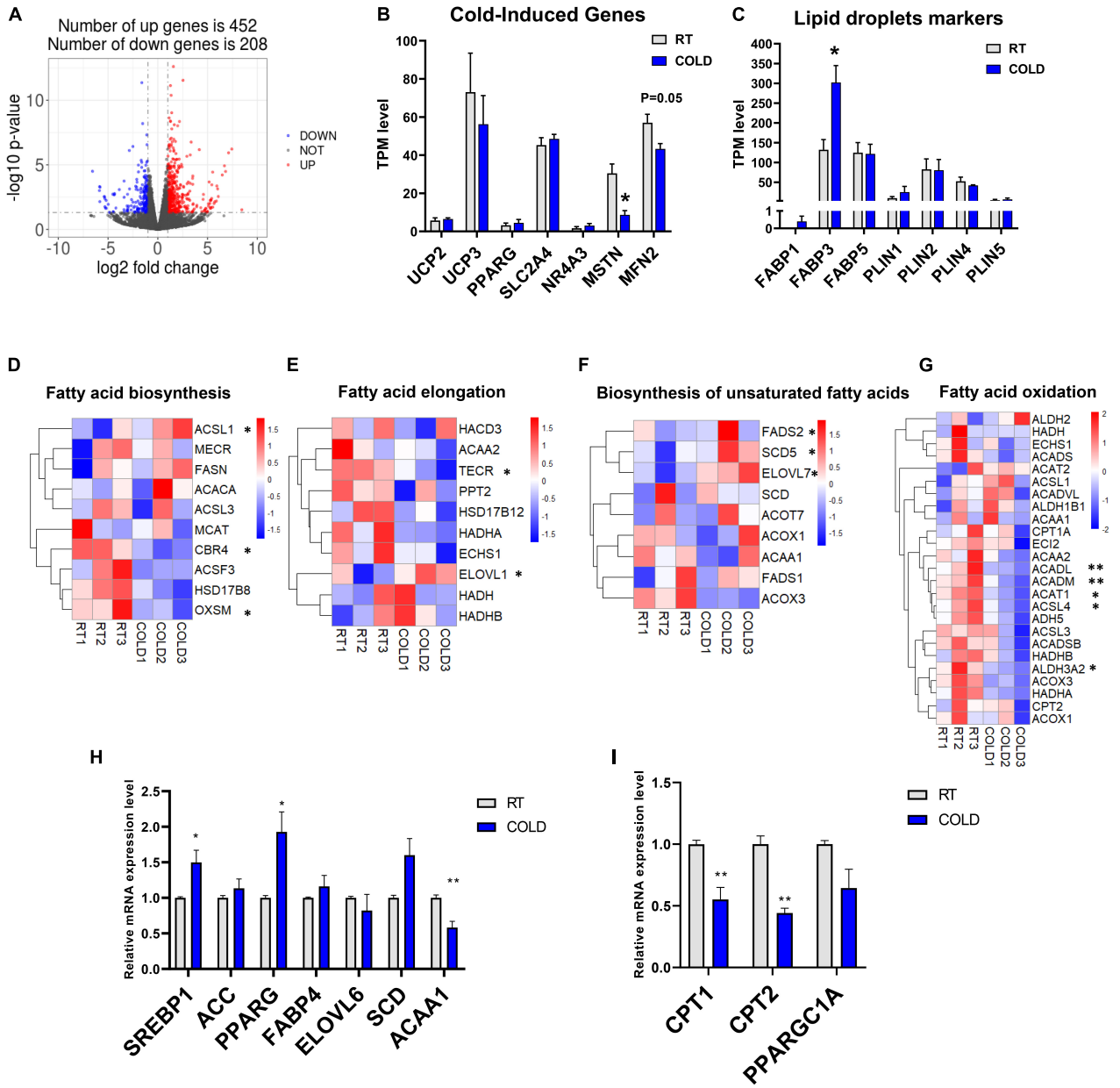

FIGURE 3 | Cold exposure changed the transcriptome profile of LDM in pigs. **(A)** Volcano plot of differently expressed genes (DEGs) expression patterns were illustrated. Red denotes upregulated genes in cold pigs; blue denotes downregulated genes in cold pigs; gray denotes genes with no significant changes. **(B,C)** Transcripts per million (TPM) expression values of cold-induced genes and lipid droplets markers LDM from cold-treated and RT pigs were shown to estimate relative gene expression abundance ($n = 3$). Error bars represent SEM. $^{*}P < 0.05$, $^{**}P < 0.01$, two-tailed Student's *t*-test. **(D–G)** Heatmaps of the TPM expression values of selected fatty acid biosynthesis, fatty acid elongation, biosynthesis of unsaturated fatty acids, fatty acid degradation regulated genes from the RNA-seq dataset. $^{*}P < 0.05$, $^{**}P < 0.01$. **(H–I)** qPCR validation of the expression of genes related to fatty acid metabolism in LDM from cold-treated and RT pigs.

matrix was mainly regulated by the matrix metalloproteinase (MMP) family (*MMP11*, *MMP8*, *MMP9*, *MMP2*), fibulin encoding genes (*FBLN5*), and fibrillin encoding gene (*FBN1*) upon cold exposure (**Figure 4F**). These results highlight the regulatory roles of lipid catabolic progress, lipoprotein complex remodeling and extracellular matrix, especially apolipoproteins, in lipid metabolism of LDM under cold exposure treatment.

Cold Exposure Induced Alterations in Metabolism and Inflammation Regulatory Pathways

KEGG pathways analysis were applied on these DEGs and revealed most enrichment in complement and coagulation cascades, ECM-receptor interaction, phenylalanine metabolism, focal adhesion, tyrosine metabolism, protein digestion and

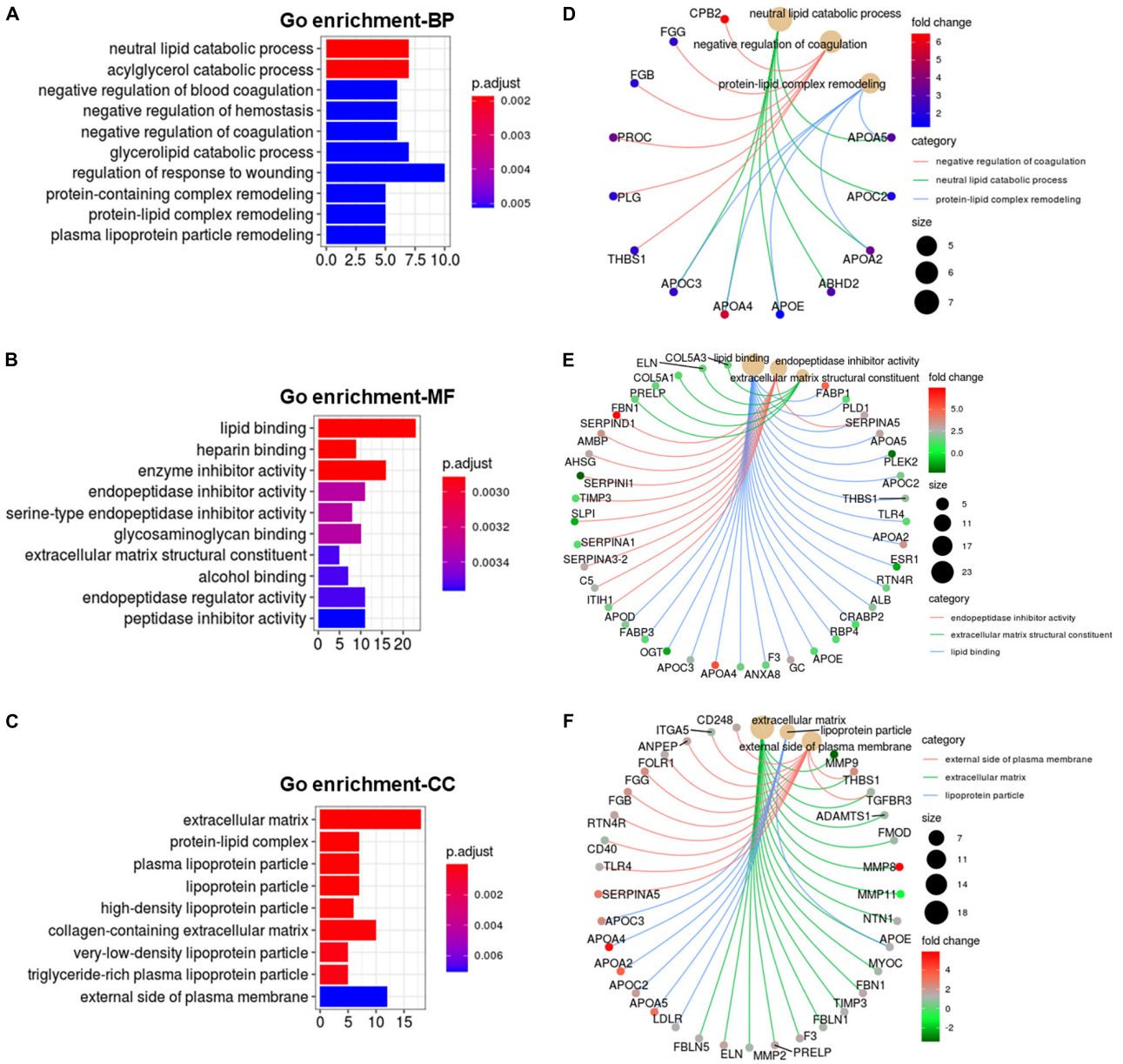

FIGURE 4 | Cold exposure induced alterations in apolipoprotein function. **(A-C)** GO annotation for DEGs in the category of biological process (BP) **(A)**, molecular function (MF) **(B)**, and cell component (CC) **(C)**. **(D–F)** The cnetplot depicts the linkages of the selected GO terms in the category of BP **(D)**, MF **(E)**, CC **(F)** and genes involved in these terms as a network.

absorption, and PPAR signaling pathways (**Figure 5A**). Heatmaps showed the expressions of genes involved in complement and coagulation cascades, ECM-receptor interaction, PPAR signaling pathways and arachidonic acid metabolism (**Figures 5B–E**). Most genes involved in complement and coagulation cascades were induced by cold exposure in LDM of pigs, especially *ACADL*, *ACADM*, *ACSL3*, *ACSL4* (**Figure 5B**). These collagen-alpha-proteins encoding genes (*COL4A2*, *COL6A2*, *COL6A3*, *COL4A1*, and *COL1A2*) involved in the ECM-receptor interaction were significantly increased in cold-treated LDM (**Figure 5C**). The expression level of hyaluronan mediated motility receptor (*HMMR*) whose function blocking reportedly promotes adipogenesis was significantly inhibited by cold exposure in LDM (**Figure 5C**), which might be partly responsible for the increased trend of IMF content. Cold exposure treatment upregulated the expression levels of fatty acid binding protein encoding genes (*FABP1*, *FABP3*) and apolipoprotein encoding genes (*APOA2*, *APOA5*, *APOC3*), and downregulated mitochondrial fatty acid beta-oxidation related genes (*ACADM*, *ACADL*), which are involved in PPAR signaling pathway (**Figure 5D**). The expression level of retinoid X receptor gamma (*RXRG*) was increased in LDM of pigs upon

cold exposure (**Figure 5D**). Notably, cold exposure significantly altered the expression of genes involved in arachidonic acid metabolism (**Figure 5E**). We found that cold exposure elevated the expression levels of *PTGIS*, *PTGS1*, *PTGS2*, *ALOX5*, *GGT5* (**Figure 5E**). These pathways enrichment results suggested that alterations in meat quality and fatty acid composition of LDM induced by cold exposure might be regulated by both metabolic and inflammatory pathways. Besides, these cold-induced DEGs were also enriched in various amino acids metabolism related pathways, including phenylalanine metabolism, tyrosine metabolism, tryptophan metabolism, alanine, aspartate and glutamate metabolism, glutathione metabolism, cysteine and methionine metabolism, which are also associated with meat nutritional values (**Figure 5A**). We further examined the amino acid contents in LDM from COLD and RT pigs, but observed no significant difference between these two groups (**Supplementary Table 1**).

DISCUSSION

Many studies have reported that cold exposure could induce various alterations on whole-body metabolism in mammals including mice, humans and birds (Chung et al., 2017; Wakabayashi et al., 2017; Nyuiadzi et al., 2020). In our experiment, we investigated the changes in meat quality and nutritional values and further discovered the regulatory mechanisms in the LDM of pigs in response to cold exposure through RNA-seq technology. Our results showed that cold exposure induced significant changes in meat $colour_{24\ h}$, $pH_{24\ h}$ and fatty acid composition, as well as lead to an increase in IMF. RNA-seq results indicated that cold exposure activated fatty acid anabolism while inhibiting fatty acid catabolism in LDM, which might be regulated by metabolic and inflammatory pathways. Our results suggest that pre-slaughter cold exposure treatment in pigs might improve the meat quality and nutritional values of skeletal muscle.

The "juiciness" and "tenderness" in pork are strongly influenced by the fat deposition and collagens proportions contained within the meat (Weston et al., 2002; Font-I-Furnols et al., 2012). In this study, we observed that the IMF content, fatty acid contents and expression levels of fatty acid metabolism related genes were altered in pigs LDM under pre-slaughter cold exposure as well as collagen synthesis enzymes encoding genes. These findings suggest that cold exposure might improve the pork eating quality through regulating the lipid metabolism and collagens synthesis toward a more beneficial direction. Besides, the water-holding capacity (WHC), the ability of meat to hold all or part of its water, is considered one of the most important trait of product yield and pork quality, and is largely influenced by meat pH. A low meat pH (below 5.8) 45 min after slaughter is often associated with low WHC and pale meat color, resulting in PSE pork. In contrast, high meat pH (above 6.0) 24 h after slaughter often causes DFD pork. The variation in meat pH, WHC and color results from the different post-mortem processes such as muscle metabolism (glycolysis) and conversion rates of glycogen into lactic acid, which are influenced by environmental factors, including breeding conditions, nutrition, transport conditions, stress, weather conditions, and the methods of slaughter (Przybylski et al., 2016). In this study, despite the stress related to a sudden lowering of temperature overnight before slaughter resulted in lower meat $colour_{24\ h}$ and $pH_{24\ h}$ while drip loss after 24 h was not affected. Also, we observed neither $pH_{24\ h}$ values above 6.0 nor $pH_{45\ min}$ below 5.8 in any of the COLD pigs or the RT controls. Thus, cold exposure treatment might prove a useful future strategy to improve meat quality.

Pork represents a rich source of lipids, which have been an important topic of discussion for consumers of meat due to the disadvantageous correlation between dietary fat intake and the incidence of various lifestyle disorders, including obesity and cardiovascular diseases (Dugan et al., 2015). Any imbalance in the ratio between PUFAs to SFAs ratio as well as omega-6 (n-6) to omega-3 (n-3) fatty acids ratio have been related to a variety of pathologies, such as cardiovascular, inflammatory diseases, diabetes and autoimmune disorders. This led to several studies suggesting to rebalance the fatty acid profiles of pork by increasing the PUFAs to SFAs ratio and n-3 fatty acids contents while decreasing its n-6: n-3 ratio (Kouba et al., 2003; Corino et al., 2014). In our study, we found that overnight cold exposure significantly increased the contents of SFAs, MUFAs, PUFAs, and n-3 fatty acids, while, the PUFAs to SFAs ratio decreased with the n-6: n-3 ratio being significantly increased. As the majority of these detected fatty acids were increased in cold-treated LDM, we conclude that the alterations in fatty acid composition in LDM were mainly the result of the increased the proportion of IMF due to cold. Previous reviews have pointed out that the fatty acid composition of pork can be regulated by reducing total fat content, due to the fairly constant proportion of PUFA-rich phospholipids in the cell membrane, with at the same time the relatively flexible proportion of SFA-rich triacylglycerol in lipid droplet (Wood et al., 2008; Huang et al., 2014). However, too low IMF content may lead to palatability issues. Thus, some strategies using dietary adjustments to ameliorate pork fatty acid profiles without changing the total fat content were used. We thus speculate that overlapping the dietary influence with pre-slaughter cold exposure treatment in pigs might become an efficient and satisfying method to improve pork quality and its nutritive value. It is useful to compare fatty acid composition in LDM from meat described in the literature. When assessing the nutritional values of pork, it is important to consider site-specific differences, because the fibrous tissue envelope, the epimysium and adipose tissue are extensive constituents of pork pieces cut from different parts, while adipose tissue always contains much more lipids than muscle fibers (Turner et al., 2014; Dugan et al., 2015). Thus, future work will have to address even precisely the effects of cold exposure on fatty acid composition of the adipose tissues on top of skeletal muscle in pigs, especially from the muscle-associated adipose tissue.

Our RNA-seq results revealed that cold exposure significantly upregulated fatty acid biosynthesis related genes (*ACSL1*, *FADS2*, *ELOVL1*, *SCD5*) and downregulated the expression of mitochondrial beta-oxidation related genes (*ACADL*, *ACADM*, *ACAT1*, *ACSL4*) in skeletal muscle, which might directly explain the increased trend of IMF content and alterations of fatty acids

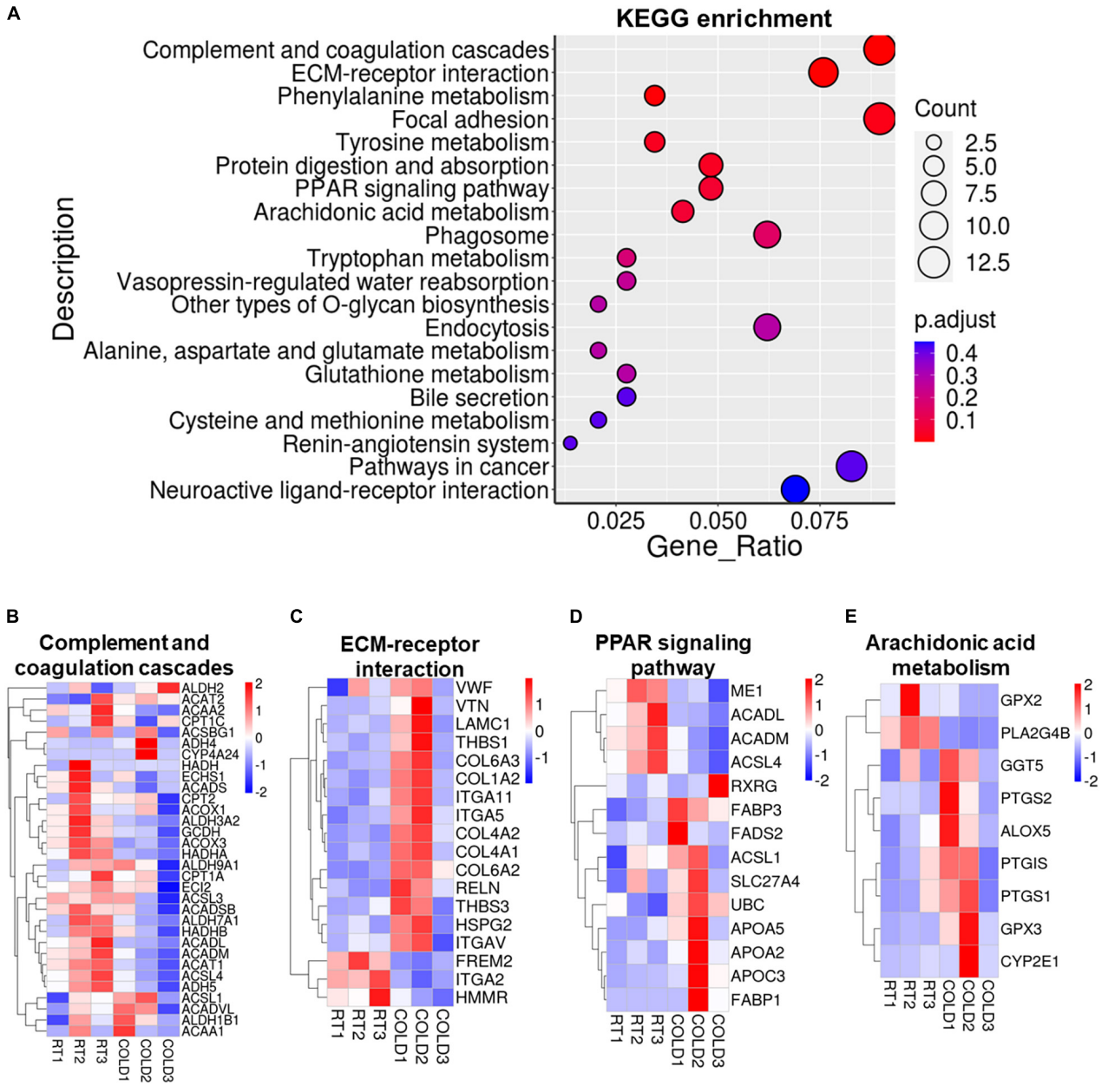

FIGURE 5 | Cold exposure induced alterations in metabolism and inflammation regulatory pathways. **(A)** Functional enrichment analyses for DEGs. **(B–E)** Heatmaps of TPM expression values of Complement and coagulation cascades **(B)**, ECM-receptor interaction **(C)**, PPAR signaling pathways **(D)** and Arachidonic acid metabolism **(E)** regulated genes from the RNA-seq dataset. Only genes with $P < 0.05$ are displayed.

in LDM of COLD pigs. In white and brown adipose tissue, cold exposure induces dynamic, heterogeneous alterations in lipid content and lipid metabolism regulatory pathways, especially the dramatically activated fatty acid beta-oxidation (Coolbaugh et al., 2019; Xu Z. et al., 2019). Both skeletal muscle and adipose tissues are considered important metabolic organs, while these two organ systems might play distinct roles in maintaining whole-body homeostasis under cold exposure treatment. The GO enrichment analysis of our RNA-seq results highlighted the alterations of apolipoprotein encoding genes (*APOA2*, *APOA5*, *APOC3*). APOC3 was reported to be among the key proteins regulating the different lipid deposition ability in skeletal muscle from Chinese native mini-type breeds' pigs and introduced western breeds (Wang et al., 2017). Thus, we concluded that lipoprotein particles might also participate in the regulation of lipid metabolism in skeletal muscle following cold exposure.

KEGG enrichment analysis of our RNA-seq results revealed that DEGs were abundant in complement and coagulation cascades, ECM-receptor interaction, phenylalanine metabolism, focal adhesion, tyrosine metabolism, protein digestion and

absorption and PPAR signaling pathway. These upregulated fatty acid binding and transport related genes (*FABP1*, *FABP3*, *SLC27A4*, and *FATP4*) might function in conjunction with fatty acid biosynthesis and oxidation related genes to adapt the lipid metabolism in skeletal muscle upon cold exposure. On the other hand, complement and coagulation are evolutionarily related proteolytic cascades in the blood, which is essential for inflammatory responses (Oikonomopoulou et al., 2012; Conway, 2018). The network of ECM-receptor interaction, focal adhesion, protein digestion and absorption play several roles including but not limited to force transmission, growth factors regulation, inflammatory responses, and muscle stem cell proliferation and differentiation (Mohassel et al., 2018; Sorensen et al., 2018; Lionello et al., 2019). Besides, previous studies demonstrated that reduced temperatures impair glutamine-induced anabolic response in human primary myotubes (Rantala and Chaillou, 2019) while cold acclimation affects L-arginine-modulated antioxidative defense in skeletal muscle (Petrovic et al., 2008). We also found an enrichment of amino acid metabolism pathways, including phenylalanine metabolism, tyrosine metabolism, tryptophan metabolism, alanine, aspartate and glutamate metabolism, glutathione metabolism, cysteine and methionine metabolism in this study. However, the content of amino acids showed no significant difference. The overnight cold exposure treatment may have been too short to cause obvious changes in the content of amino acids or amino acids are somewhat less responsive to compositional changes due to a temperature drop. Taken together, our RNA-seq results revealed various alterations in cold-treated skeletal muscle, with the specific impact and regulatory mechanisms cold exposure on skeletal muscle still unclear.

CONCLUSION

In conclusion, our study reveals significant alterations in fatty acid profile and lipid metabolism of pig skeletal muscle upon overnight cold exposure. We carefully evaluated the potential regulations for meat quality and nutritional values of pigs with our experimental test. More detailed investigations uncovering the cold exposure induced specific effects and regulatory mechanisms in skeletal muscles of economically relevant meat should be performed.

DATA AVAILABILITY STATEMENT

The datasets presented in this study can be found in NCBI under the sample ID are SRR15694341, SRR15694342, SRR15694343, SRR15694344, SRR15694345, and SRR15694346.

ETHICS STATEMENT

The animal study was reviewed and approved by the University of Zhejiang Institutional Animal Care and Use Committee.

AUTHOR CONTRIBUTIONS

ZX: investigation, methodology, formal analysis, and writing–original draft. WC and LW: investigation and writing–original draft. YZ and QN: investigation. TV: writing–review and editing. YW and JX: resources. TS: project administration, writing–review and editing, and supervision. All authors have read and approved the final manuscript.

FUNDING

This research was funded by the Zaozhuang Talent Program Funding, the Key Research and Development Program of Zhejiang Province (2021C02008), the "Hundred Talents Program" funding from Zhejiang University to TS.

ACKNOWLEDGMENTS

We would like to thank the members of the Shan laboratory for their comments.

SUPPLEMENTARY MATERIAL

The Supplementary Material for this article can be found online at: https://www.frontiersin.org/articles/10.3389/fphys.2021.748801/full#supplementary-material

REFERENCES

Bartelt, A., Bruns, O., Reimer, R., Hohenberg, H., Ittrich, H., Peldschus, K., et al. (2011). Brown adipose tissue activity controls triglyceride clearance. *Nat. Med.* 17, 200–205. doi: 10.1038/nm.2297

Bartelt, A., John, C., Schaltenberg, N., Berbée, J., Worthmann, A., Cherradi, M., et al. (2017). Thermogenic adipocytes promote HDL turnover and reverse cholesterol transport. *Nat. Commun.* 8:15010. doi: 10.1038/ncomms15010

Blondin, D. P., and Haman, F. (2018). Shivering and nonshivering thermogenesis in skeletal muscles. *Handb. Clin. Neurol.* 156, 153–173. doi: 10.1016/B978-0-444-63912-7.00010-2

Buras, E. D., Converso-Baran, K., Davis, C. S., Akama, T., Hikage, F., Michele, D. E., et al. (2019). Fibro-Adipogenic Remodeling of the Diaphragm in Obesity-Associated Respiratory Dysfunction. *Diabetes* 68, 45–56. doi: 10.2337/db18-0209

Chung, N., Park, J., and Lim, K. (2017). The effects of exercise and cold exposure on mitochondrial biogenesis in skeletal muscle and white adipose tissue. *J. Exerc. Nutrit. Biochem.* 21, 39–47. doi: 10.20463/jenb.2017.0020

Conway, E. M. (2018). Complement-coagulation connections. *Blood Coagul. Fibrinolysis* 29, 243–251. doi: 10.1097/MBC.0000000000000720

Coolbaugh, C. L., Damon, B. M., Bush, E. C., Welch, E. B., and Towse, T. F. (2019). Cold exposure induces dynamic, heterogeneous alterations in human brown adipose tissue lipid content. *Sci. Rep.* 9:13600. doi: 10.1038/s41598-019-49936-x

Corino, C., Rossi, R., Cannata, S., and Ratti, S. (2014). Effect of dietary linseed on the nutritional value and quality of pork and pork products: systematic review and meta-analysis. *Meat Sci.* 98, 679–688. doi: 10.1016/j.meatsci.2014.06.041

Dugan, M. E., Vahmani, P., Turner, T. D., Mapiye, C., Juarez, M., Prieto, N., et al. (2015). Pork as a Source of Omega-3 (n-3) Fatty Acids. *J. Clin. Med.* 4, 1999–2011. doi: 10.3390/jcm4121956

Font-I-Furnols, M., Tous, N., Esteve-Garcia, E., and Gispert, M. (2012). Do all the consumers accept marbling in the same way? The relationship between eating and visual acceptability of pork with different intramuscular fat content. *Meat Sci.* 91, 448–453. doi: 10.1016/j.meatsci.2012.02.030

Grefhorst, A., Van Den Beukel, J. C., Dijk, W., Steenbergen, J., Voortman, G. J., Leeuwenburgh, S., et al. (2018). Multiple effects of cold exposure on livers of male mice. *J. Endocrinol.* 238, 91–106. doi: 10.1530/JOE-18-0076

Grunert, K. G., Bredahl, L., and Brunsø, K. (2004). Consumer perception of meat quality and implications for product development in the meat sector-a review. *Meat Sci.* 66, 259–272 .doi: 10.1016/S0309-1740(03)00130-X

Gu, T., Shi, J., Luo, L., Li, Z., Zheng, E., Cai, G., et al. (2019). Comparison of Carcass Traits, Meat Quality, and Chemical Composition of Tissues from Progeny Derived from Cloned and Noncloned Pigs. *Cell Reprogram.* 21, 296–300. doi: 10.1089/cell.2019.0040

Hocquette, J. F., Gondret, F., Baeza, E., Medale, F., Jurie, C., and Pethick, D. W. (2010). Intramuscular fat content in meat-producing animals: development, genetic and nutritional control, and identification of putative markers. *Animal* 4, 303–319. doi: 10.1017/S1751731109991091

Honikel, K. O. (1998). Reference methods for the assessment of physical characteristics of meat. *Meat Sci.* 49, 447–457. doi: 10.1016/S0309-1740(98)00034-5

Hou, L., Shi, J., Cao, L., Xu, G., Hu, C., and Wang, C. (2017). Pig has no uncoupling protein 1. *Biochem. Biophys. Res. Commun.* 487, 795–800. doi: 10.1016/j.bbrc.2017.04.118

Huang, L., Kong, B., Zhao, J., Liu, Q., and Diao, X. (2014). Contributions of fat content and oxidation to the changes in physicochemical and sensory attributes of pork dumpling filler during frozen storage. *J. Agric. Food Chem.* 62, 6390–6399. doi: 10.1021/jf5008083

Iwen, K. A., Backhaus, J., Cassens, M., Waltl, M., Hedesan, O. C., Merkel, M., et al. (2017). Cold-Induced Brown Adipose Tissue Activity Alters Plasma Fatty Acids and Improves Glucose Metabolism in Men. *J. Clin. Endocrinol. Metab.* 102, 4226–4234. doi: 10.1210/jc.2017-01250

Jiang, D. X., Zhang, J. B., Li, M. T., Lin, S. Z., Wang, Y. Q., Chen, Y. W., et al. (2020). Prolyl endopeptidase gene disruption attenuates high fat diet-induced nonalcoholic fatty liver disease in mice by improving hepatic steatosis and inflammation. *Ann. Transl. Med.* 8:218. doi: 10.21037/atm.2020.01.14

Kouba, M., Enser, M., Whittington, F. M., Nute, G. R., and Wood, J. D. (2003). Effect of a high-linolenic acid diet on lipogenic enzyme activities, fatty acid composition, and meat quality in the growing pig. *J. Anim. Sci.* 81, 1967–1979. doi: 10.2527/2003.8181967x

Li, W., Li, R., Wei, Y., Meng, X., Wang, B., Zhang, Z., et al. (2020). Effect of MSTN Mutation on Growth and Carcass Performance in Duroc x Meishan Hybrid Population. *Animals* 10:932. doi: 10.3390/ani10060932

Li, Y., Liu, Y., Li, F., Lin, Q., Dai, Q., Sun, J., et al. (2018). Effects of dietary ramie powder at various levels on carcass traits and meat quality in finishing pigs. *Meat Sci.* 143, 52–59. doi: 10.1016/j.meatsci.2018.04.019

Lin, J., Cao, C., Tao, C., Ye, R., Dong, M., Zheng, Q., et al. (2017). Cold adaptation in pigs depends on UCP3 in beige adipocytes. *J. Mol. Cell Biol.* 9, 364–375. doi: 10.1093/jmcb/mjx018

Lionello, V. M., Nicot, A. S., Sartori, M., Kretz, C., Kessler, P., Buono, S., et al. (2019). Amphiphysin 2 modulation rescues myotubular myopathy and prevents focal adhesion defects in mice. *Sci. Transl. Med.* 11:eaav1866. doi: 10.1126/scitranslmed.aav1866

Liu, K., Yu, W., Wei, W., Zhang, X., Tian, Y., Sherif, M., et al. (2019). Melatonin reduces intramuscular fat deposition by promoting lipolysis and increasing mitochondrial function. *J. Lipid Res.* 60, 767–782. doi: 10.1194/jlr.M087619

Mohassel, P., Foley, A. R., and Bönnemann, C. G. (2018). Extracellular matrix-driven congenital muscular dystrophies. *Matrix Biol.* 71-72, 188–204. doi: 10.1016/j.matbio.2018.06.005

Moon, Y. A., and Horton, J. D. (2003). Identification of two mammalian reductases involved in the two-carbon fatty acyl elongation cascade. *J. Biol. Chem.* 278, 7335–7343. doi: 10.1074/jbc.M211684200

Naganuma, T., Sato, Y., Sassa, T., Ohno, Y., and Kihara, A. (2011). Biochemical characterization of the very long-chain fatty acid elongase ELOVL7. *FEBS Lett.* 585, 3337–3341. doi: 10.1016/j.febslet.2011.09.024

Ngapo, T. M., and Gariepy, C. (2008). Factors affecting the eating quality of pork. *Crit. Rev. Food Sci. Nutr.* 48, 599–633.

Nyuiadzi, D., Berri, C., Dusart, L., Travel, A., Meda, B., Bouvarel, I., et al. (2020). Short cold exposures during incubation and postnatal cold temperature affect performance, breast meat quality, and welfare parameters in broiler chickens. *Poult. Sci.* 99, 857–868.

Oikonomopoulou, K., Ricklin, D., Ward, P. A., and Lambris, J. D. (2012). Interactions between coagulation and complement–their role in inflammation. *Semin. Immunopathol.* 34, 151–165.

Pan, J., Tao, C., Cao, C., Zheng, Q., Lam, S. M., Shui, G., et al. (2019). Adipose lipidomics and RNA-Seq analysis revealed the enhanced mitochondrial function in UCP1 knock-in pigs. *Biochim. Biophys. Acta Mol. Cell Biol. Lipids* 1864, 1375–1383. doi: 10.1016/j.bbalip.2019.06.017

Petrovic, V., Buzadzic, B., Korac, A., Vasilijevic, A., Jankovic, A., Micunovic, K., et al. (2008). Antioxidative defence alterations in skeletal muscle during prolonged acclimation to cold: role of L-arginine/NO-producing pathway. *J. Exp. Biol.* 211, 114–120. doi: 10.1242/jeb.012674

Przybylski, W., Sionek, B., Jaworska, D., and Santé-Lhoutellier, V. (2016). The application of biosensors for drip loss analysis and glycolytic potential evaluation. *Meat Sci.* 117, 7–11. doi: 10.1016/j.meatsci.2016.02.025

Rantala, R., and Chaillou, T. (2019). Mild hypothermia affects the morphology and impairs glutamine-induced anabolic response in human primary myotubes. *Am. J. Physiol. Cell Physiol.* 317, C101–C110. doi: 10.1152/ajpcell.00008.2019

Rosenvold, K., and Andersen, H. J. (2003). Factors of significance for pork quality-a review. *Meat Sci.* 64, 219–237. doi: 10.1016/S0309-1740(02)00186-9

Sorensen, J. R., Skousen, C., Holland, A., Williams, K., and Hyldahl, R. D. (2018). Acute extracellular matrix, inflammatory and MAPK response to lengthening contractions in elderly human skeletal muscle. *Exp. Gerontol.* 106, 28–38. doi: 10.1016/j.exger.2018.02.013

Turner, T. D., Mapiye, C., Aalhus, J. L., Beaulieu, A. D., Patience, J. F., Zijlstra, R. T., et al. (2014). Flaxseed fed pork: n-3 fatty acid enrichment and contribution to dietary recommendations. *Meat Sci.* 96, 541–547. doi: 10.1016/j.meatsci.2013.08.021

Tyra, M., and Żak, G. (2012). Analysis of relationships between fattening and slaughter performance of pigs and the level of intramuscular fat (IMF) in Longissimus dorsi muscle. *Ann. Anim. Sci.* 12, 169–178. doi: 10.2478/v10220-012-0014-6

Van Der Lans, A. A., Hoeks, J., Brans, B., Vijgen, G. H., Visser, M. G., Vosselman, M. J., et al. (2013). Cold acclimation recruits human brown fat and increases nonshivering thermogenesis. *J. Clin. Invest.* 123, 3395–3403. doi: 10.1172/JCI68993

Venkatesan, R., Sah-Teli, S. K., Awoniyi, L. O., Jiang, G. Y., Prus, P., Kastaniotis, A. J., et al. (2014). Insights into mitochondrial fatty acid synthesis from the structure of heterotetrameric 3-ketoacyl-ACP reductase/3R-hydroxyacyl-CoA dehydrogenase. *Nat. Commun.* 5:4805. doi: 10.1038/ncomms5805

Wakabayashi, H., Nishimura, T., Wijayanto, T., Watanuki, S., and Tochihara, Y. (2017). Effect of repeated forearm muscle cooling on the adaptation of skeletal muscle metabolism in humans. *Int. J. Biometeorol.* 61, 1261–1267. doi: 10.1007/s00484-016-1303-z

Wang, Z., Shang, P., Li, Q., Wang, L., Chamba, Y., Zhang, B., et al. (2017). iTRAQ-based proteomic analysis reveals key proteins affecting muscle growth and lipid deposition in pigs. *Sci. Rep.* 7:46717. doi: 10.1038/srep46717

Weston, A. R., Rogers, R. W., and Althen, T. G. (2002). Review: The Role of Collagen in Meat Tenderness. *Profess. Anim. Sci.* 18, 107–111. doi: 10.15232/S1080-7446(15)31497-2

Wood, J. D., Enser, M., Fisher, A. V., Nute, G. R., Sheard, P. R., Richardson, R. I., et al. (2008). Fat deposition, fatty acid composition and meat quality: A review. *Meat Sci.* 78, 343–358. doi: 10.1016/j.meatsci.2007.07.019

Worthmann, A., John, C., Rühlemann, M., Baguhl, M., Heinsen, F.-A., Schaltenberg, N., et al. (2017). Cold-induced conversion of cholesterol to bile acids in mice shapes the gut microbiome and promotes adaptive thermogenesis. *Nat. Med.* 23, 839–849. doi: 10.1038/nm.4357

Xu, Z. Y., You, W. J., Zhou, Y. B., Chen, W. T., Wang, Y. Z., and Shan, T. Z. (2019). Cold-induced lipid dynamics and transcriptional programs in white adipose tissue. *BMC Biol.* 17:74. doi: 10.1186/s12915-019-0693-x

Xu, X., Chen, X., Chen, D., Yu, B., Yin, J., and Huang, Z. (2019). Effects of dietary apple polyphenol supplementation on carcass traits, meat quality, muscle amino acid and fatty acid composition in finishing pigs. *Food Funct.* 10, 7426–7434.

Xu, Z., You, W., Zhou, Y., Chen, W., Wang, Y., and Shan, T. (2019). Cold-induced lipid dynamics and transcriptional programs in white adipose tissue. *BMC Biol.* 17:74.

Xu, Z. Y., Zhou, Y. B., Nong, Q. Y., You, W. J., Wang, L. Y., Wang, Y. Z., et al. (2020). LKB1 Differently Regulates Adipogenesis in Intramuscular and Subcutaneous Adipocytes through Metabolic and Cytokine-Related Signaling Pathways. *Cells* 9: 2599.

Zhang, L., Joshi, A. K., Hofmann, J., Schweizer, E., and Smith, S. (2005). Cloning, expression, and characterization of the human mitochondrial beta-ketoacyl synthase. Complementation of the yeast CEM1 knock-out strain. *J. Biol. Chem.* 280, 12422–12429. doi: 10.1074/jbc.M413686200

Zhang, Z., Zhang, Z., Oyelami, F. O., Sun, H., Xu, Z., Ma, P., et al. (2021). Identification of genes related to intramuscular fat independent of backfat thickness in Duroc pigs using single-step genome-wide association. *Anim. Genet.* 52, 108–113. doi: 10.1111/age.13012

Ziêtak, M., Kovatcheva-Datchary, P., Markiewicz, L. H., Ståhlman, M., Kozak, L. P., and Bäckhed, F. (2016). Altered Microbiota Contributes to Reduced Diet-Induced Obesity upon Cold Exposure. *Cell Metab.* 23, 1216–1223. doi: 10.1016/j.cmet.2016.05.001

Conflict of Interest: JX was employed by company Shandong Chunteng Food Co., Ltd.

The remaining authors declare that the research was conducted in the absence of any commercial or financial relationships that could be construed as a potential conflict of interest.

Publisher's Note: All claims expressed in this article are solely those of the authors and do not necessarily represent those of their affiliated organizations, or those of the publisher, the editors and the reviewers. Any product that may be evaluated in this article, or claim that may be made by its manufacturer, is not guaranteed or endorsed by the publisher.

Copyright © 2021 Xu, Chen, Wang, Zhou, Nong, Valencak, Wang, Xie and Shan. This is an open-access article distributed under the terms of the Creative Commons Attribution License (CC BY). The use, distribution or reproduction in other forums is permitted, provided the original author(s) and the copyright owner(s) are credited and that the original publication in this journal is cited, in accordance with accepted academic practice. No use, distribution or reproduction is permitted which does not comply with these terms.

frontiers in Physiology

ORIGINAL RESEARCH
published: 13 October 2021
doi: 10.3389/fphys.2021.755598

LKB1 Regulates Goat Intramuscular Adipogenesis Through Focal Adhesion Pathway

Yan Xiong[1,2,3*†], *Yuxue Wang*[3†], *Qing Xu*[3,4], *An Li*[3], *Yongqi Yue*[3], *Yan Ma*[3] *and Yaqiu Lin*[1,2,3*]

[1] *Key Laboratory of Qinghai-Tibetan Plateau Animal Genetic Resource Reservation and Utilization, Ministry of Education, Southwest Minzu University, Chengdu, China,* [2] *Key Laboratory of Qinghai-Tibetan Plateau Animal Genetic Resource Reservation and Utilization, Sichuan Province, Southwest Minzu University, Chengdu, China,* [3] *College of Animal and Veterinary Sciences, Southwest Minzu University, Chengdu, China,* [4] *State Key Laboratory of Agrobiotechnology, China Agricultural University, Beijing, China*

Intramuscular fat (IMF) deposition is one of the most important factors to affect meat quality in livestock and induce insulin resistance and adverse metabolic phenotypes for humans. However, the key regulators involved in this process remain largely unknown. Although liver kinase B1 (LKB1) was reported to participate in the development of skeletal muscles and classical adipose tissues. Due to the specific autonomic location of intramuscular adipocytes, deposited between or within muscle bundles, the exact roles of LKB1 in IMF deposition need further verified. Here, we cloned the goat LKB1 coding sequence with 1,317 bp, encoding a 438 amino acid peptide. LKB1 was extensively expressed in detected tissues and displayed a trend from decline to rise during intramuscular adipogenesis. Functionally, knockdown of LKB1 by two individual siRNAs enhanced the intramuscular preadipocytes differentiation, accompanied by promoting lipid accumulation and inducing adipogenic transcriptional factors and triglyceride synthesis-related genes expression. Conversely, overexpression of LKB1 restrained these biological signatures. To further explore the mechanisms, the RNA-seq technique was performed to compare the difference between siLKB1 and the control group. There were 1,043 differential expression genes (DEGs) were screened, i.e., 425 upregulated genes and 618 downregulated genes in the siLKB1 group. The Kyoto Encyclopedia of Genes and Genomes (KEGG) analysis predicted that the DEGs were mainly enriched in the focal adhesion pathway and its classical downstream signal, the PI3K-Akt signaling pathway. Specifically, knockdown of LKB1 increased the mRNA level of focal adhesion kinase (FAK) and *vice versa* in LKB1-overexpressed cells, a key component of the activated focal adhesion pathway. Convincingly, blocking this pathway by a specific FAK inhibitor (PF573228) rescued the observed phenotypes in LKB1 knockdown adipocytes. In conclusion, LKB1 inhibited goat intramuscular adipogenesis through the focal adhesion pathway. This work expanded the genetic regulator networks of IMF deposition and provided theoretical support for improving human health and meat quality from the aspect of IMF deposition.

Keywords: IMF, intramuscular adipocyte, adipogenesis, LKB1, focal adhesion pathway, FAK, RNA-seq, RNA sequencing

OPEN ACCESS

Edited by:
Zhihao Jia,
Purdue University, United States

Reviewed by:
Weijun Pang,
Northwest A&F University, China
Wenlin Bai,
Shenyang Agricultural University, China

***Correspondence:**
Yan Xiong
xiongyan0910@126.com
Yaqiu Lin
linyq1999@163.com

† These authors have contributed equally to this work and share first authorship

Specialty section:
This article was submitted to Lipid and Fatty Acid Research, a section of the journal Frontiers in Physiology

Received: *09 August 2021*
Accepted: *10 September 2021*
Published: *13 October 2021*

Citation:
Xiong Y, Wang Y, Xu Q, Li A, Yue Y, Ma Y and Lin Y (2021) LKB1 Regulates Goat Intramuscular Adipogenesis Through Focal Adhesion Pathway. Front. Physiol. 12:755598. doi: 10.3389/fphys.2021.755598

INTRODUCTION

Intramuscular fat (IMF) was regarded as the most intramuscular adipocytes deposited between primary and secondary muscle bundles of perimysium, and a small population was also founded within muscle bundles (Li et al., 2020). The IMF accumulation was mainly determined by the hyperplasia and hypertrophy of intramuscular adipocytes, indicated by an increase in the number and size of adipocytes, respectively (Haczeyni et al., 2018). For farm animals, IMF was also referred to as marbling fat, which was highly desirable for improving the tenderness and flavor of meat quality (Hocquette et al., 2010; Hunt et al., 2016; Sun et al., 2019), while increasing IMF content in humans was associated with the occurrence of insulin resistance and adverse metabolic phenotypes, such as type 2 diabetes (Lim, 2014). Therefore, there are intensive efforts for elucidating the molecular mechanism of IMF deposition to enhance meat quality or defend against metabolic syndrome because of ectopic fat accumulation in skeletal muscle.

Liver kinase B1 (LKB1) also known as serine/threonine kinase 11 (STK11) is a serine/ threonine kinase (Berthelsen et al., 2021), which participates in the regulation of a variety of cellular physiological and pathological processes (Shan et al., 2016a,b; Xiong et al., 2017, 2018b) and phosphorylates 14 kinases of AMPK subfamily and regulates systemic glucose and energy balance (Lizcano et al., 2004). In skeletal muscle, LKB1 ablation exhibited a severe myopathy characterized by centrally nucleated myofibers, reduced mobility, growth retardation, and premature death (Shan et al., 2014), which is essential for the development and function of skeletal muscle (Shan et al., 2017). In classical adipose tissue, LKB1 gene knockout expanded the brown fat growth and increased mice energy expenditure and insulin sensitivity, associated with elevation of expression of thermogenesis-related genes (Shan et al., 2016b). Specifically, *MyoD-Cre*-derived Lkb1 deletion of muscle stem cells (satellite cells) and their descendent mature muscles increased lipid accumulation in proliferating myoblasts and myofibers (Shan et al., 2015). Intramuscular adipocyte was located within perimysium or muscle bundles, whose hyperplasia and hypertrophy were associated with reduced contractile function, insulin resistance, and type 2 diabetes (Li et al., 2020). Whether Lkb1 is involved in intramuscular adipocyte differentiation and lipid accumulation remains largely unclear. Additionally, the specific autonomic location and absence of maker genes of intramuscular adipocyte limited researchers to explore the molecular mechanism of its deposition *in vivo*.

Thus, the cultured intramuscular preadipocytes from the goat were used as the adipogenesis model to reveal the function and molecular mechanism of LKB1 regulation on IMF deposition. Here, the goat LKB1 gene-coding sequence was first cloned and further explored its function in intramuscular adipocytes by knockdown and overexpression techniques. Moreover, the RNA-seq was carried out to screen the differential transcripts affected by Lkb1 loss of function. Next, we provided sufficient evidence that LKB1 regulated adipogenesis of goat intramuscular preadipocytes through the focal adhesion pathway. Conclusively, these findings elucidated the specific molecular mechanism of LKB1 regulating the differentiation of intramuscular adipocytes and provided theoretical support for improving meat quality and human health.

MATERIALS AND METHODS

Ethical Statement

All experimental procedures were reviewed and approved by the Institutional Animal Care and Use Committee, Southwest Minzu University (Chengdu). In addition, all the experiments complied with the requirements of the directory of the Ethical Treatment of Experimental Animals of China. The 7-day-old and 1-year-old Jianzhou Daer goats were reared by standard diet and housed in a comfortable environment. The goats were purchased from Sichuan Jianyang Dageda Animal Husbandry Co., Ltd. (Sichuan, China), and humanely slaughtered in the Key Laboratory of Qinghai-Tibetan Plateau Animal Genetic Resource Reservation and Utilization, Ministry of Education, Southwest Minzu University, Chengdu, China. The experimental animal certification number was SYXK-2019-216.

Isolation and Adipogenic Differentiation of Primary Goat Intramuscular Preadipocytes

The isolation of primary goat intramuscular preadipocytes was carried out as previously reported (Xiong et al., 2018a; Huang et al., 2020). Briefly, longissimus dorsi was collected from slaughtered 7-day-old Jianzhou Daer goat after euthanatized by CO_2. The samples were washed three times in phosphate-buffered solution (PBS) supplemented with 1% penicillin/streptomycin (P/S) and then were minced into a 1 mm^3 cube. Enzymatic digestion dilution (DMEM/F12 with 2 mg/ml collagenase type II and 1% P/S) was used to isolate intramuscular preadipocytes at 37°C in the water bath for 1–1.5 h with gentle shaking and was terminated digestion by the same volume of DMEM/F12 (Hyclone, Logan, UT, USA) supplemented with 10% fetal bovine serum (FBS). The suspension was filtered through a 75-μm nylon cell strainer to remove connective tissues and undigested trunks of tissues. Cells then were centrifuged at 2,000 r/min for 5 min and re-suspended by red blood cell lysed solution for 30 min to lyse red blood cells. Next, the suspension was centrifuged at 2,000 r/min for 5 min again and the pre-adipocytes were resuspended in a growth medium (DMEM/F12 supplemented with 10% FBS and 1% P/S) and diluted to a final concentration of 10^6 cells/ml. These cells were cultured at 37°C in a humidified atmosphere containing 5% CO_2. It was previously reported that preadipocytes attached much earlier than myoblasts, the cultured cells were rinsed with PBS three times 1 h after plating to remove myoblasts, insoluble myofibrillar proteins, and other insoluble debris (Zhao et al., 2016; Sun et al., 2020). Cells were fed with fresh growth medium every 2 days until they reached 80% confluence and digested with 0.05% trypsin, then seeded at a density of 5×10^4 cells/cm in a 6-well plate. The preadipocytes with 100% confluence were induced by induction medium (IM), containing 10% FBS, 1% P/S, and 50 μM of oleic acid (Sigma) and change the IM every 2 days. The time point of cells with 100% confluence was defined

as day 0, and cell samples were collected at day 2 and day 4 post-induction.

Adenovirus Generation and Infection

The adenovirus with goat LKB1 insertion was generated using the AdMax system as reported (Zhu et al., 2018). Briefly, the Coding Sequence (CDS) of LKB1 was cloned, inserted into the pHBAd plasmid, and verified by enzyme digestion and sequencing. The positive plasmid-containing goat LKB1 was named pHBAd-LKB1. Then, HEK293A cells (50–60% confluent) in 6 cm culture dishes were co-transfected 4 μg backbone plasmid (pBHGlox(delta) E1, 3Cre) with 2 μg pHBAd-LKB1 or 2 μg pHBAd empty plasmid using Lipofectamine 3000 (Life Technologies, Carlsbad, CA, USA) according to the protocol of the manufacturer. After 2 weeks, the two strains of recombinant adenovirus were collected by three freezes–thaw–vortex cycles, named LKB1OE and NC, respectively. Two more round infected HEK293A cells were adapted to amplify the recombinant virus, and the titers were determined by the expression of red fluorescence protein. Adenovirus purification by $CsCl_2$ grade ultra-centrifuge based on described procedure (Mueller et al., 2012).

Chemical Synthesis of siRNA and Transfection

Two individual siRNAs targeted for goat LKB1 were synthesized these sequences by Thermo Fisher Scientific. siRNA-1 (5′-CCAAGCUCAUCGGAAAGUACCUGAU-3′) and siRNA-2 (5′-GACAUUGAGGACGACGUCAUCUACA-3′). Negative control (NC) was provided by Invitrogen (5′-UUCUCCGAA CGUGUCACGsUTT-3′). siRNA transfection was performed by Lipofectamine® RNAIMAX Reagent (Invitrogen, Waltham, MA, USA) at 70–80% preadipocytes confluence. Then, cells were analyzed by qPCR and oil red O staining at day 2 and day 4 after adipogenic induction.

Oil Red O Staining

The oil red O staining was carried out as previously described (Xiong et al., 2018a). In brief, goat intramuscular adipocytes were washed with PBS two times and fixed with 4% formaldehyde for 15 min at room temperature. Then the cells were incubated using the oil red O working solution containing 6 ml oil red O stock solution (5 g/L in isopropanol) and 4 ml ddH_2O for 30 min. After staining, the cells were washed with 60% isopropanol in PBS and pictured. Oil red O dye was extracted from stained adipocytes with 100% isopropanol, and the oil red O signal was quantified by measuring the optical density at 490 nm (OD 490).

Bodipy Staining

The goat intramuscular adipocytes were removed from the IM and incubated by 2 μM of BODIPY™493/503 (Thermo Fisher Scientific, D3922) diluted in IM for 1 h. Then cells were washed with PBS three times, added fresh IM, and took pictures. Fluorescent images were captured using an Olympus TH4-200 microscope (Tokyo, Japan) with the 10× objective (NA 0.70) for higher magnification views. Images for control and treatment cells were captured using identical parameters.

Total RNA Extraction and Quantitative Real-Time PCR (qPCR)

Total RNA was extracted from various tissues and intramuscular adipocytes using Trizol reagent (Takara) according to the protocol of the manufacturer. RNA was treated with RNase-free DNase I to remove genomic DNA. The purity and concentration of total RNA were measured by Nanodrop 3000 (Thermo Fisher). Ratios of absorption (260/280 nm) of all samples were between 1.8 and 2.0. Then 2 μg of total RNA were reversed transcribed using random primers and Moloney murine leukemia virus reverse transcriptase. qPCR was carried out with a Bio-Rad CFX96 PCR System using SYBR Green Master Mix (Takara) and gene-specific primers (**Table S1**). The $2^{-\Delta\Delta CT}$ method was used to analyze the relative changes of gene expression normalized against peptidylprolyl isomerase A (PPIA) as the internal control (Xiong et al., 2018a; Xu et al., 2018).

Construction of RNA-Seq Library and Sequencing

A total amount of 3 μg RNA per sample was used as input material for the RNA sample preparations. First, ribosomal RNA was removed by Epicentre Ribo-zero™ rRNA Removal Kit (Epicentre, USA), and the rRNA-free residue was cleaned up by ethanol precipitation. Subsequently, sequencing libraries were generated using the rRNA depleted RNA by NEBNext® Ultra™ Directional RNA Library Prep Kit for Illumina® (NEB, Ipswich, MA, USA) following the recommendations of the manufacturer. Briefly, fragmentation was carried out using divalent cations under elevated temperature in NEBNext First Strand Synthesis Reaction Buffer (5×). First-strand cDNA was synthesized using random hexamer primer and M-MuLV Reverse Transcriptase (RNaseH-). Second strand cDNA synthesis was subsequently performed using DNA polymerase I and RNase H. In the reaction buffer, deoxynucleotide triphosphatesd (dNTPs) with deoxythymidine triphosphate (dTTP) were replaced by deoxyuridine triphosphate (dUTP). The remaining overhangs were converted into blunt ends via exonuclease/polymerase activities. After adenylation of 3′ ends of DNA fragments, NEBNext Adaptor with hairpin loop structure was ligated to prepare for hybridization. To select cDNA fragments of preferentially 150–200 bp in length, the library fragments were purified with the AMPure XP system (Beckman Coulter, Beverly, MA, USA). Then 3 μl USER Enzyme (NEB, Ipswich, MA, USA) was used with size-selected, adaptor-ligated cDNA at 37°C for 15 min followed by 5 min at 95°C before PCR. Then PCR was performed with Phusion High-Fidelity DNA polymerase, Universal PCR primers, and Index (X) Primer. At last, products were purified (AMPure XP system) and library quality was assessed on the Agilent Bioanalyzer 2100 system.

The clustering of the index-coded samples was performed on a cBot Cluster Generation System using TruSeq PE Cluster Kit v3-cBot-HS (Illumia) according to the instructions of

the manufacturer. After cluster generation, the libraries were sequenced on an Illumina Hiseq 4000 platform and 150 bp paired-end reads were generated.

DEG and KEGG Analysis

Cuffdiff provides statistical routines for determining differential expression in digital transcript or gene expression data using a model based on the negative binomial distribution (Trapnell et al., 2010). Transcripts with a *P-adjust* < 0.05 were assigned as differentially expressed. KEGG is a database resource for understanding high-level functions and utilities of the biological system (Kanehisa et al., 2008). We used KOBAS software to test the statistical enrichment of differential expression genes (DEGs) in KEGG pathways (Mao et al., 2005).

MTT Assay

MTT (50 mg) was dissolved in 10 ml PBS (pH 7.2) to obtain a concentration of 5 mg/ml. The induced intramuscular adipocytes were seeded in 96-well plates with approximately 3,000 cells per well. Different final concentrations (0, 5, 10, 50, and 100 nM) of focal adhesion kinase (FAK) inhibitor (PF573228) were added into wells, respectively. After 24 and 48 h treated by FAK inhibitor, 10% MTT was added to wells to incubate for 4 h at 37°C. Then, the sediment was dissolved in dimethylsulfoxide (DMSO) and the absorbance was measured at 490 nm.

Statistical Analysis

All the data are presented as means ± SEM. Comparisons were made by unpaired Student's *t*-test using SPSS 17.0 software (SPSS Science, Chicago, IL, USA). Effects were considered significant at $P < 0.05$.

RESULTS

Cloning and Bioinformatics Analysis of Goat *LKB1* Gene

As the loss of validated sequence of goat *LKB1* gene in the NCBI database, its mRNA sequence was first cloned to further elucidate its function in intramuscular adipogenesis. The data showed that the full length of the LKB1 gene was 1,380 bp and was cloned by PCR using cDNA of longissimus dorsi as a template, including 1,317 bp complete open reading frame (ORF) region sequence, encoding a 438 amino acid peptide, and 63 bp 3′ untranslated region (3′UTR) sequence (**Figure 1A**). Next, the protein functional prediction showed that goat LKB1 protein had a typical (serine/threonine kinases catalytic) S-TKC domain (**Figure 1B**). Then, the amino acid sequence homology of LKB1 protein between goat and other animals was analyzed by NCBI blast (**Figure 1C**). The results showed that goat LKB1 protein was highly identical to *Bos Taurus* (98.68%). Furthermore, the phylogenetic trees of LKB1 proteins, constructed by clustalx1.83 and mega5.0, showed that goat LKB1 protein had the closest relationship with those of cattle and pig, and the farthest relationship with that of *Danio rerio* and *Drosophila* (**Figure 1D**). These results suggest that the function of the LKB1 gene was relative conservation among species.

The Expression Patterns of *LKB1* Gene in Goat Various Tissue and During Intramuscular Adipogenesis

As shown in **Figure 2A**, the expression patterns of the LKB1 gene in goat various tissues, such as the heart, liver, spleen, kidney, large intestine, rumen, subcutaneous adipose tissue, abdominal adipose tissue, longissimus dorsi muscle, biceps femoris muscle, and triceps brachii muscle, were measured by qPCR. The data showed that LKB1 mRNA was widely expressed in detected tissues of goats, and the highest expression level was found in the kidney, which was significantly higher than that in other tissues ($P < 0.01$). During intramuscular adipogenesis, the mRNA level of the LKB1 gene first displayed a declined trend, reaching the lowest point at 24 h post-induction, and then gradually increased in the late stage (**Figure 2B**). These results suggest that the *LKB1* gene might be related to IMF deposition in goats.

Knockdown of *LKB1* Promotes Intramuscular Preadipocytes Differentiation

To elucidate the role of LKB1 in regulating intramuscular lipid accumulation in goats, two individual LKB1 siRNAs were transfected into goat intramuscular preadipocytes to perform loss of function. As shown in **Figures 3A,D**, these siRNAs significantly decreased the mRNA levels of LKB1 at day 2 and day 4 post-adipogenic induction, with knockdown efficiency of ∼ 50% and ∼ 60% to that of NC, respectively ($P < 0.001$). At the morphology, bodipy staining showed that the LKB1 loss of function increased the bodipy dye in intramuscular adipocytes at day 2 adipogenic differentiation (**Figure 3B**). Consistently, oil red O staining also showed that knockdown of LKB1 promoted lipid droplet accumulation (**Figure 3B**). Statistically, LKB1 interference exhibited a dramatic increase in the signal of oil red O, indicated by the OD value at 490 nm (**Figure 3C**, $P < 0.01$). On day 4 after adipogenic induction, knockdown of LKB1 also significantly increased both signals of bodipy and oil red O in intramuscular adipocytes (**Figures 3D–F**). These data suggest that loss of LKB1 function promotes lipid accumulation in goat intramuscular adipocytes.

The lipid droplets accumulation of adipocytes is a complex biological process, which is associated with preadipocyte initial adipogenic differentiation statue, triglyceride (TG) synthesis, and decomposition, summarized as adipocyte precursor cells differentiated into mature adipocytes (Gulyaeva et al., 2019). It was well known that adipogenesis is regulated by the central cascade transcription factors (CCAAT enhancer-binding proteins/peroxisome proliferator-activated receptor γ, C/EBPs/PPARγ), TG biogenic-related genes (FASN, fatty acid synthase; ACC, acetyl-CoAcarboxyla; DGAT2, diacylglycerol acyltransferase), and TG lipolytic-related genes (HSL, hormone-sensitive lipase; LPL, lipoprotein lipase; ATGL, adipose triglyceride lipase) (Engin, 2017). The qPCR analysis was carried out to determine the LKB1 loss of function effect on intramuscular adipogenesis at the molecular level. The data showed that siRNAs treatment significantly elevated the mRNA level of *PPARγ*, *CEBPα*, and *CEBPβ*. Specifically, interference

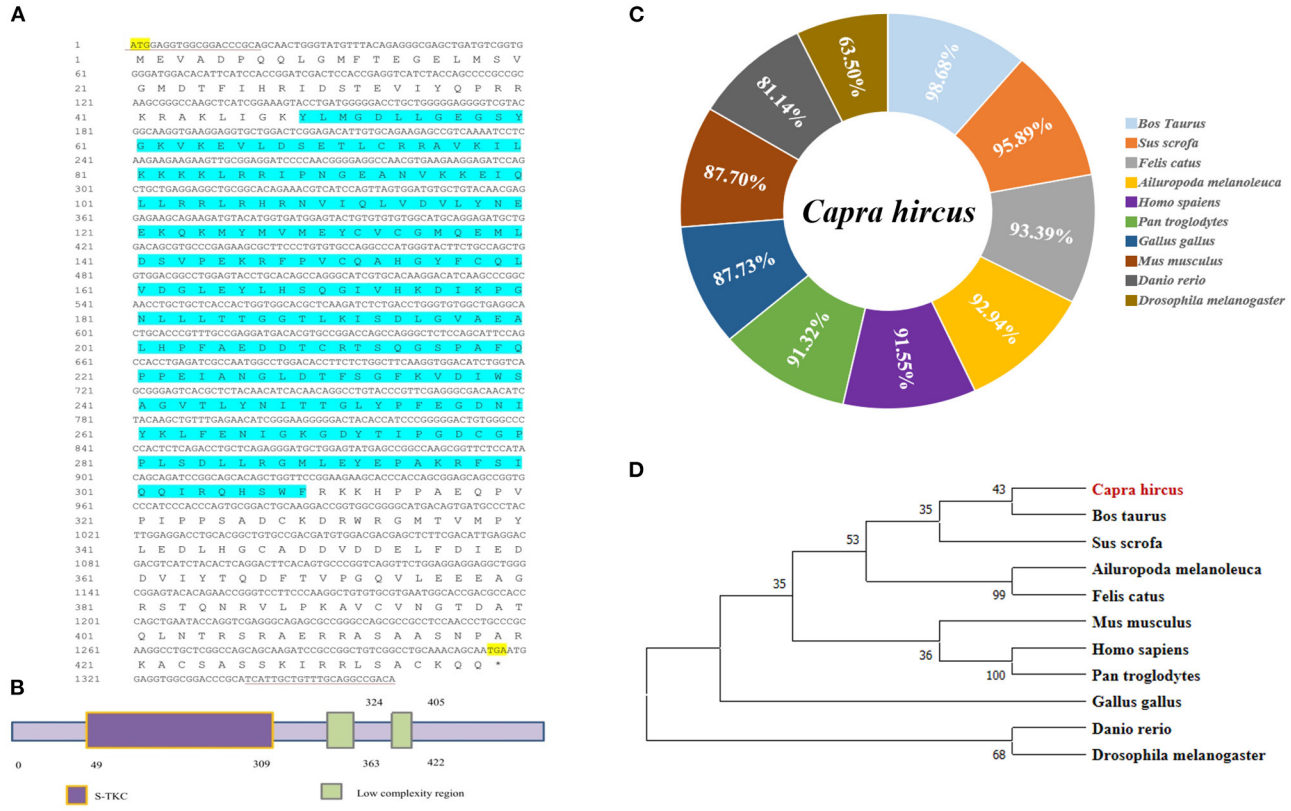

FIGURE 1 | The cloning of goat LKB1 gene and its alignment analysis among species. **(A)** The nucleotide sequence and the translated amino acid sequence of goat *LKB1* (˙ Represents the stop codon). **(B)** Prediction of the biological function of LKB1 amino acid sequence. **(C)** The amino acid sequence identity was analyzed by NCBI blast for LKB1 protein between goat and other mammalian species retrieved from GenBank. *Capra hircus* (MW664927), *Sus scrofa* (XP_020939922.1), *Ailuropoda melanoleuca* (XP_002923557.1), *Felis catus* (XP_003981653.1), *Homo sapiens* (NP_000446.1), *Pan troglodytes* (XP_024206909.1), *Gallus gallus* (NP_001039298.1), *Mus musculus* (NP_035622.1), Bos taurus (XP_024850893.1), *Danio rerio* (NP_001017839.1), and *Drosophila melanogaster* (NP_001163606.1). **(D)** LKB1 amino acid sequence phylogenetic tree was constructed by ClustalX 1.83 and MEGA7.0. LKB1, liver kinase B1.

of LKB1 respectively led to increasing by 5-fold and 4-fold changes of *CEBPβ* in siRNA1 and siRNA2 transfected cells to that of NC at day 2 post-adipogenic induction (**Figure 4A**). Conversely, knockdown of LKB1 suppressed the mRNA level of delta-like non-canonical Notch ligand 1 (*DLK1 or PREF1*), a marker gene of preadipocytes (**Figure 4A**). Furthermore, the mRNA level of *FASN* and *DGAT2* was upregulated in siRNA1 treatment, while that of *ACC* was not significant between siRNAs and NC (**Figure 4A**). In addition, inhibition of LKB1 by siRNAs promoted the expression of lipolysis genes *LPL,* but not *HSL* and *ATGL* (**Figure 4A**). Consistently, similar trends of the aforementioned genes mRNA level were also observed at day 4 post-adipogenic induction, as shown in **Figure 4B**. Thus, these data indicated that LKB1 loss of function promotes goat intramuscular adipogenesis.

Overexpression of *LKB1* Inhibits Intramuscular Adipogenesis

Our results provide evidence that LKB1 knockdown promotes intramuscular preadipocytes differentiation. Here, we generated adenovirus overexpressing LKB1 and infected goat intramuscular preadipocytes to further clarify the exact role of LKB1 by the gain of function. The images showed that the highly infected efficiency was observed in both control (NC) and LKB1 overexpression (LKB1OE) groups (**Figure 5A**). The expression of LKB1 was largely upregulated in LKB1OE cells, the elevation of ∼40-fold changes expressional level to that of NC with detail (**Figure 5B**). At the morphology, there were fewer lipid droplets labeled by bodipy dye in the LKB1OE group than that of the control, and a similar phenomenon was observed by oil red O staining (**Figure 5C**). Statically, the OD value at 490 nm showed that the oil red O signal in the overexpression group was significantly lower than that in the control group ($P < 0.05$; **Figure 5D**). In principle, the occurrence of adipogenesis depends on the efficiency of lipid accumulation of preadipocytes differentiating into adipocytes and terminal differentiation, which are regulated by adipogenic transcription factors and genes related to triglyceride synthesis and decomposition (Gulyaeva et al., 2019). Therefore, the mRNA levels of these genes were detected by qPCR. The results showed that LKB1 overexpression significantly downregulated the mRNA levels of adipogenic

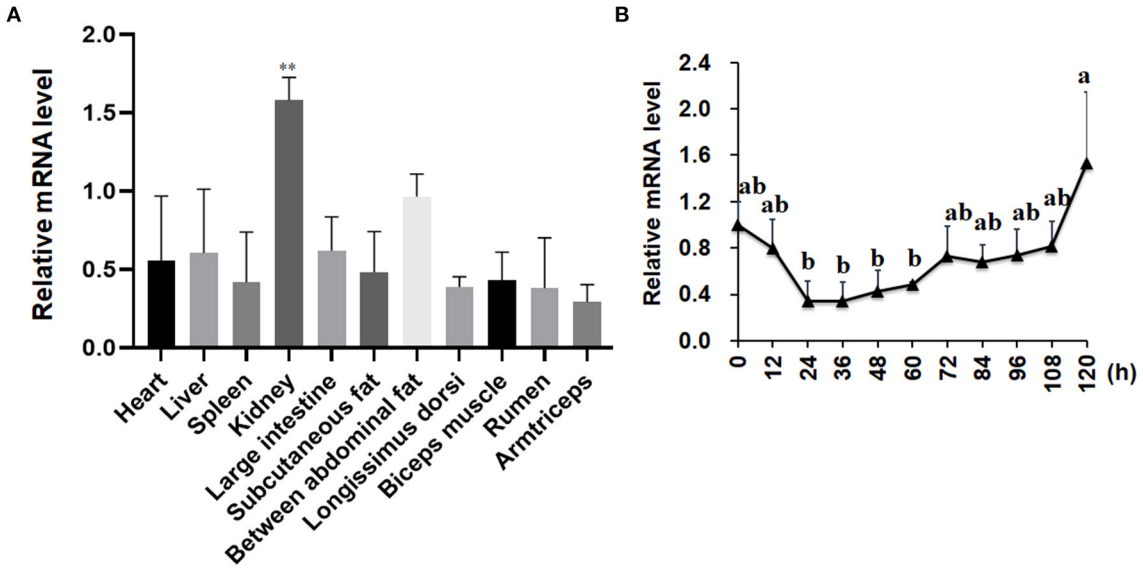

FIGURE 2 | The mRNA expression patterns of the *LKB1* gene in goat tissues and during intramuscular adipocyte differentiation. **(A)** The *LKB1* mRNA level in heart, liver, spleen, kidney, large intestine, subcutaneous fat, between abdominal fat, longissimus dorsi, biceps muscle, rumen, and arm triceps, $n = 6$. Ribosomal protein lateral stalk subunit P0 (*RPLP0*) as the internal reference gene. **(B)** The *LKB1* mRNA level at day 0, 12, 24, 36, 48, 60, 72, 84, 96, 108, and 120 h in induced differentiation intramuscular adipocyte ($n = 6$), both *UXT* and *PPIB* are as reference genes. $^{**}P < 0.01$, the *LKB1* level of kidney compared to other tissues. Different letters indicate the significant difference ($P < 0.05$), and the same lowercase indicates an insignificant difference ($P > 0.05$). LKB1, liver kinase B1.

transcription factors, including *PPARγ* ($P < 0.01$) and *SREBP1*($P < 0.01$). Moreover, LKB1 gain of function also significantly reduced the mRNA levels of TG biogenesis-related genes ($P < 0.05$), such as *FASN*, *DGAT2,* and a lipolysis gene, *LPL* (**Figure 5E**). Altogether, it is concluded that LKB1 overexpression inhibits lipid accumulation in intramuscular adipocytes.

LKB1 Loss of Function Affects the *Mrna* Transcript Profiles in Goat Intramuscular Adipocytes

To elucidate the underlying molecular mechanism of the LKB1 regulating intramuscular adipogenesis. The total RNAs from NC and LKB1 knockdown intramuscular adipocytes were performed RNA-seq analysis to identify their altered transcriptional profiles. Differentially expressed genes (DEGs) were screened based on the criteria of $p_{adj} < 0.05$ and *fold change* >2. Volcano plots showed a broad overview of changes in gene expression between NC and LKB1 knockdown groups (**Figure 6A**). Clearly, a strong transcriptional response was observed in LKB1 knockdown intramuscular adipocytes, exhibiting 1,043 genes with significantly altered expression levels, compared to those of NC. Of the 1,043 genes, 425 genes were upregulated, while 618 genes were downregulated (**Figure 6A**). Next, the DEGs of each group were analyzed by hierarchical cluster analysis in the form of a heat map to provide the visualization of the whole effect of gene expression change (**Figure 6B**). Subsequently, to further confirm the potential function of DEGs in the intramuscular adipogenesis effect by LKB1 and KEGG pathway analyses were performed. The top 20 of significant difference signaling pathways are shown in **Figure 6C**, such as arrhythmogenic right ventricular cardiomyopathy (ARVC), focal adhesion pathway, PI3K-Akt signaling pathway, fatty acid metabolism pathway, ErbB signaling pathway, regulation of actin cytoskeleton, VEGF signaling pathway, FoxO signaling pathway, and others (**Figure 6C**). Of them, PI3K-Akt signaling pathway and focal adhesion had the top 2 enrichment, with 35- and 26-DEGs enriched in these pathways, respectively (**Figure 6C**), suggesting that the two pathways may be associated with the IMF deposition effect by LKB1. Furthermore, 12 genes were randomly selected from DEGs for validation using qPCR analysis, and all genes we examined showed the same expression trend as observed by RNA-seq, with 10 of them reaching statistical significance (**Figure 6D**), which confirmed the accuracy of the sequencing data.

Elevation of Intramuscular Adipocyte Lipid Accumulation Induced by *LKB1* Partial Depends on Focal Adhesion Pathway

Our RNA-seq data showed that the DEGs were enriched in the focal adhesion pathway, and FAK is one of the main components of the focal adhesion complex to activate this pathway (Tapial Martinez et al., 2020). The expression level of *FAK* was significantly upregulated in the siRNA treatment by both RNA-seq and qPCR analysis, compared to those of control (**Figure 7A**). Comparatively, overexpression of LKB1 dramatically downregulated the expression level of FAK (**Figure 7B**). Hypothetically, the promotion of intramuscular adipogenesis mediated by LKB1 knockdown might be through enhancement of focal adhesion pathway. Previous research reported that PF-573228 was a specific inhibitor for FAK (Bai

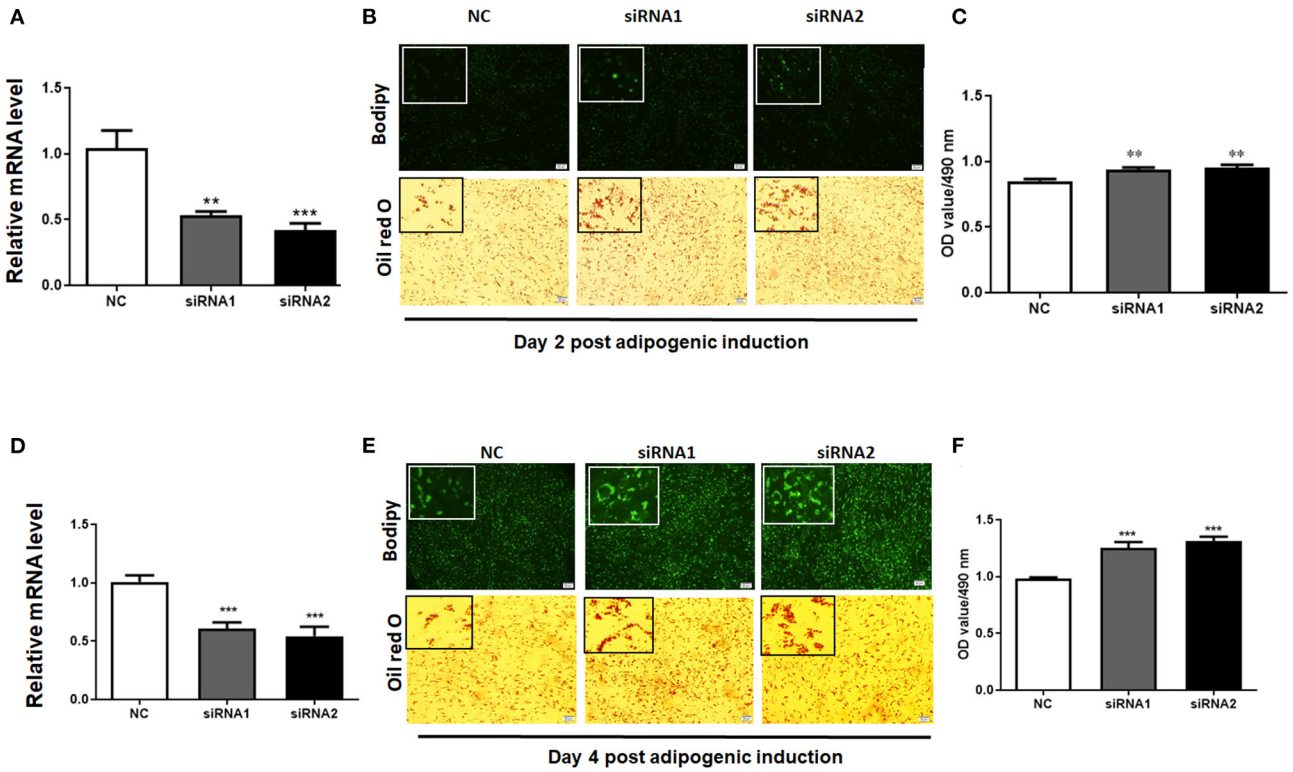

FIGURE 3 | Knockdown of LKB1 promotes goat intramuscular adipocyte lipid accumulation. **(A,D)** The knockdown efficiency of LKB1 at day 2 **(A)** and day 4 **(D)** post-adipogenic induction ($n = 6$). **(B,E)** The bodipy and oil red O staining between control and siRNAs treatment intramuscular adipocyte cells. **(C,F)** The quantitative analysis of lipid accumulation in the negative control (NC) and siRNAs transfected groups was indicated by the OD value of oil red O dye at 490 nm at day 2 **(C)** and day 4 **(F)** after adipogenic induction ($n = 6$). $^{**}P < 0.01$, $^{***}P < 0.001$, compared to that of NC. Scale bar: 100 μm. LKB1, liver kinase B1.

et al., 2021), which was used to determine whether inhibition of the FAK pathway rescues the effect of LKB1 knockdown in goat intramuscular adipocytes. Thus, different concentrations (5, 10, 50, and 100 nM) were set for the rescue experiments, and the data showed that these concentrations did not affect cell viability (**Figure S1**). The images stained by oil red O showed that siRNA combined with 5 nM FAK inhibitor treatment has less oil red O labeled lipid droplets than that of only siRNA transfected adipocytes (**Figures 7C,D**). Moreover, this reduction extent became larger and larger at a concentration of 10, 50, and 100 nM and exhibited the dose-dependent manner. In accordance with the above phenotype, the FAK inhibitor rescued all the mRNA levels of detected genes, including adipogenic transcription factor (*PPARγ* and *C/EBPβ*, **Figures 7E,F**), TG synthesis-related genes (*FASN* and *ACC*, **Figures 7G,H**), except for *LPL* (**Figure 7I**). Taken together, these data indicated that LKB1 loss of function induced enhancement of intramuscular adipocyte lipid accumulation at least partially depends on the focal adhesion pathway.

DISCUSSION

In this study, the goat LKB1 nucleotide sequence was cloned, and expression patterns in various tissues and during intramuscular adipogenesis were revealed. Functionally, we investigated the exact role of LKB1 regulation on goat IMF deposition *in vitro* by loss of and gain of function. Mechanistically, the altered transcript profiles affected by LKB1 knockdown were constructed by RNA-seq and found that knockdown of LKB1 enhanced the goat IMF deposition through the focal adhesion pathway. Overall, this work elucidates the specific molecular mechanism of LKB1 regulating the differentiation of intramuscular adipocytes and provides theoretical support for improving human health and meat quality from the aspect of IMF deposition.

The goat LKB1 gene was cloned, and its tissue expression characteristics were elucidated. It was found that the LKB1 gene was widely expressed in goat various tissues, and the highest expression level was measured in the kidney. Two pieces of evidence might account for this phenomenon. First, the kidney as one of the important and high-energy demanding organs of the body ensures normal metabolism of the organism by removing the poisons and wastes in the body (Han et al., 2016), and LKB1/AMPK pathway was regarded as the metabolic sensor in energy metabolism (Jansen et al., 2009; Han et al., 2016). Second, previous studies reported that epithelial-specific Lkb1 deletion exhibited progressive kidney disease characterized by flattened dedifferentiated tubule epithelial cells, interstitial matrix accumulation, and dilated cystic-appearing tubules (Han et al.,

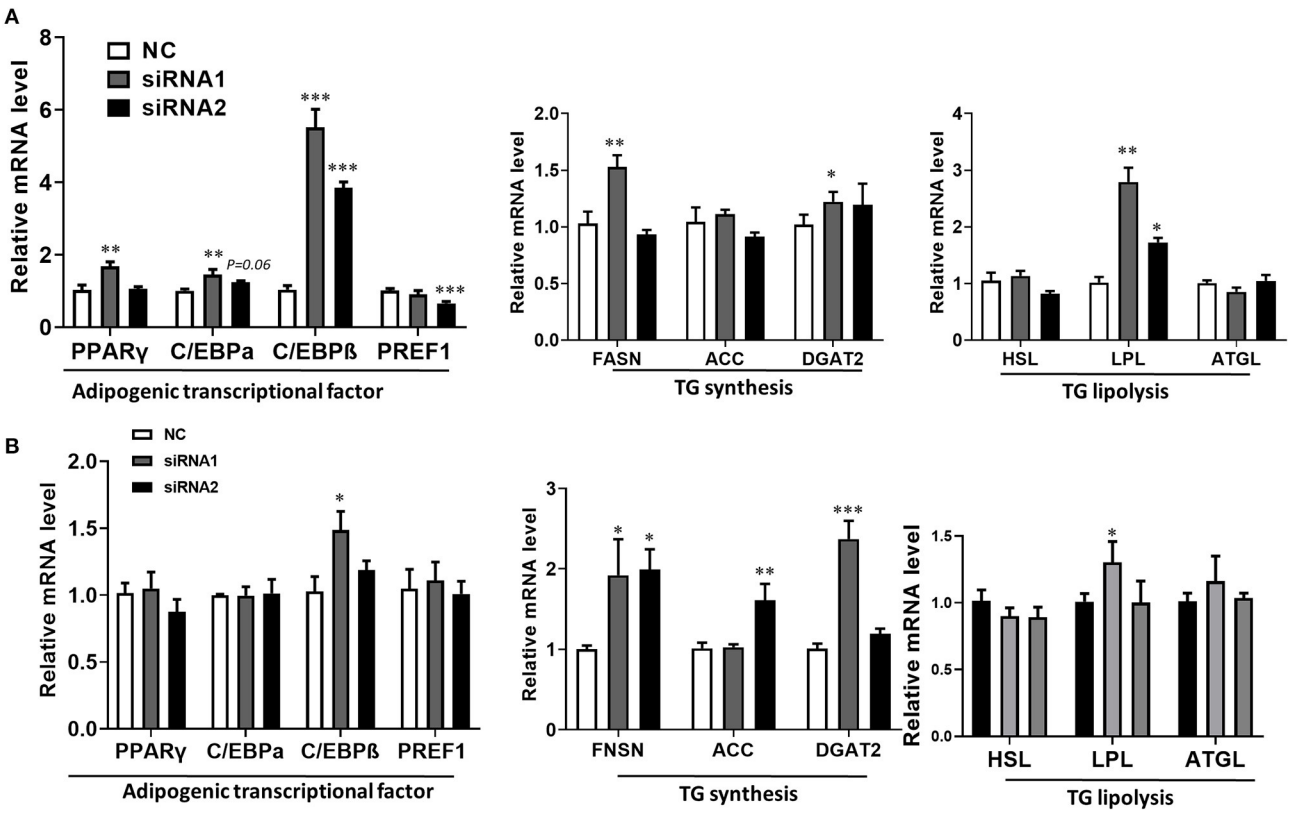

FIGURE 4 | Knockdown of LKB1 promotes adipogenic and lipid accumulation-related genes. **(A,B)** The mRNA level of adipogenic transcription factors (*PPARγ*, *C/EBPα*, *C/EBPβ*, and *PREF1*), TG synthesis genes (*FASN*, *ACC*, and *DGAT2*), and TG lipolysis genes (*HSL*, *LPL, and ATGL*) between control and siRNAs groups at day 2 **(A)** and day 4 **(B)** post-adipogenic induction. $^{*}P < 0.05$, $^{**}P < 0.01$, $^{***}P < 0.001$, compared to that of control. FASN, fatty acid synthase; ACC, acetyl-CoA carboxylase alpha; DGAT2, diacylglycerol acyltransferase, HSL, hormone-sensitive lipase; LPL, lipoprotein lipase; ATGL, adipose triglyceride lipase.

2016) and indicated that Lkb1 is essential for maintaining the normal physiological function of the kidney. Thus, the highest mRNA level in the kidney was observed among detected tissues.

In this work, we provided pieces of strong evidence that supported this conclusion LKB1 as a negative regulator for goat intramuscular preadipocytes adipogenesis. Knockdown of LKB1 promoted goat intramuscular preadipocytes differentiation, manifested by elevation of bodipy and oil red O signal, enhanced the expression levels of adipogenic transcriptional factors and TG synthesis-related genes. Moreover, overexpression of LKB1 reduced the lipid accumulation and decreased adipogenic and lipid droplets biogenic-related genes. It was known that fat deposition was mainly determined by the hyperplasia and hypertrophy of intramuscular adipocytes, the latter is associated with TG biogenesis and its lipolysis (Haczeyni et al., 2018). However, it seems contradictory observation is that promotion of lipid accumulation in LKB1 is also accompanied with upregulation of mRNA level of LPL, a key lipolytic gene, while this gene is downregulated by a gain of LKB1 function. The adipocyte lipid accumulation is a gross effect of the imbalance of TG synthesis and lipolysis (Ducharme and Bickel, 2008; Saponaro et al., 2015). Thus, this might be explained by the role of TG synthesis is greater than that of lipolysis influenced by LKB1 knockdown and the total response is exhibiting promotion of lipid accumulation in this case.

The genome-wide altered transcriptional profiles were constructed by RNA-seq, and 1,043 DEGs were screened in loss of LKB1 intramuscular adipocytes, to uncover the underlying specific molecular mechanism. Interestingly, the PI3K-Akt signaling pathway and the focal adhesion pathway were analyzed as the top two enrichment functional pathways by the KEGG analysis of DEGs. Previous extensive research reported that PI3K/Akt is the classic downstream molecules of FAK signaling (Gao et al., 2018; Zhang et al., 2019b; Wang et al., 2020) and we, therefore, focused on the Focal adhesion pathway as the direct candidate downstream of LKB1. Consistently, knockdown of LKB1 upregulated expression level of FAK, while overexpression of LKB1 downregulated its level. Similarly, it was reported that LKB1 deficiency promotes proliferation and invasion of glioblastoma through activation of focal adhesion kinase signaling pathways (Zhang et al., 2019a). In addition, Kline et al. concluded that LKB1 serves as a FAK repressor to stabilize focal adhesion sites by protein-protein interaction in tumor cells, and when LKB1 function is compromised, aberrant FAK signaling ensues, resulting in rapid FAK site maturation and poor directional

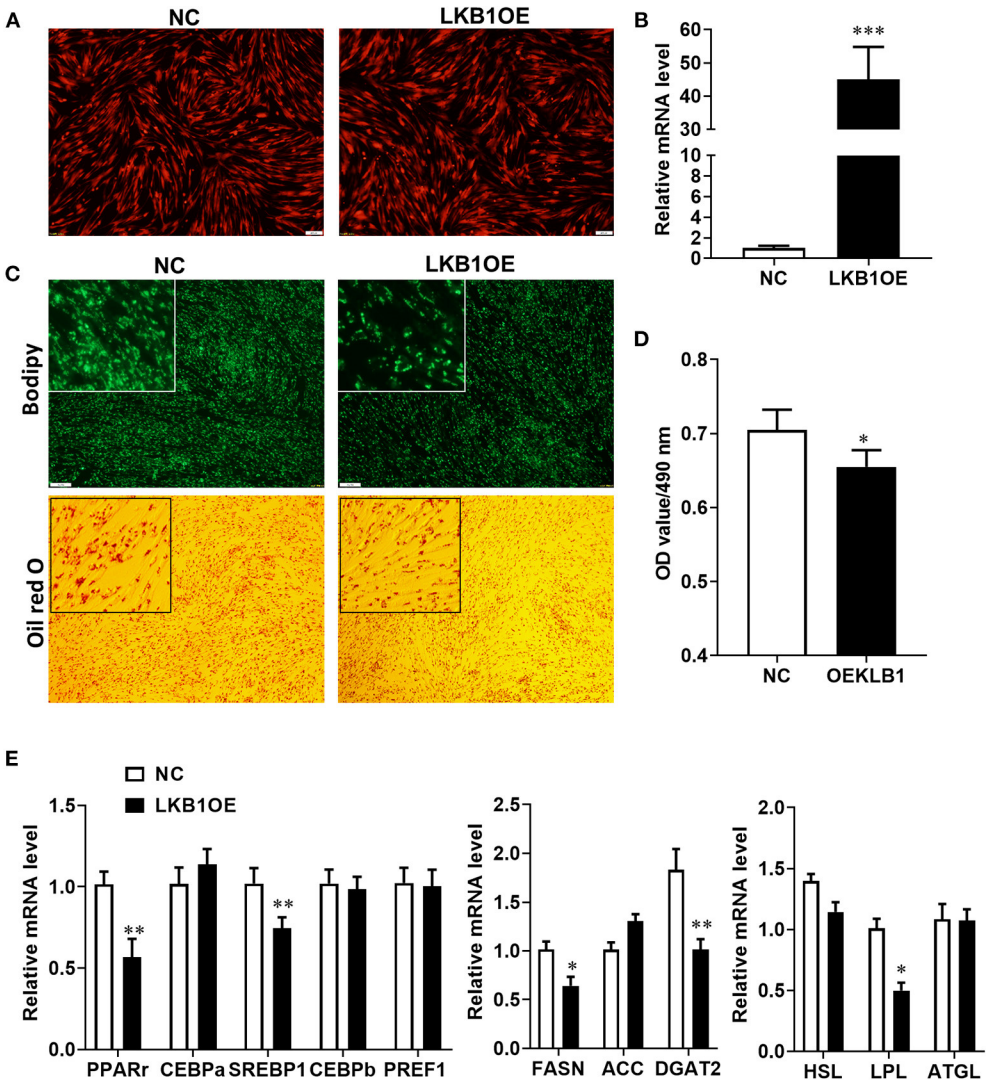

FIGURE 5 | Overexpression of LKB1 inhibits intramuscular adipocyte lipid accumulation and downregulates mRNA level of adipogenic-related genes. **(A)** The images of intramuscular preadipocytes infected by control or overexpressed LKB1 adenovirus. **(B)** The overexpression efficiency of LKB1 in intramuscular adipocyte mediated by adenovirus. **(C)** The images of mature intramuscular adipocytes stained by bodipy and oil red O dye. **(D)** Quantitative analysis of oil red O staining signal was indicated by absorbance at 490 nm. **(E)** The mRNA level of adipogenic transcription factors (*PPARγ*, *C/EBPα*, *C/EBPβ*, and *PREF1*), TG synthesis genes (*FASN*, *ACC*, and *DGAT2*), and TG lipolysis genes (*HSL*, *LPL, and ATGL*) between control and LKB1OE groups post-adipogenic induction. $^{*}P < 0.05$, $^{**}P < 0.01$, $^{***}P < 0.001$. Scale bar: 100 μm. LKB1, liver kinase B1; FASN, fatty acid synthase; ACC, acetyl-CoA carboxylase alpha; DGAT2, diacylglycerol acyltransferase, HSL, hormone-sensitive lipase; LPL, lipoprotein lipase; ATGL, adipose triglyceride lipase.

persistence (Kline et al., 2013). In intramuscular adipocyte, whether LKB1 direct associates in a complex with FAK or regulated FAK mRNA level through indirect molecules need be further explored.

In intramuscular adipocytes, interference of LKB1 activated the focal adhesion pathway and subsequently led to enhancing the intramuscular adipogenic differentiation. Intriguingly, FAK inhibitor treatment of the siRNA groups rescued the phenotype caused by the decrease of LKB1 expression in the manner of dose-dependent, manifested by debasement of oil red O signal and adipogenic-related genes expression. Thus, we concluded that loss of LKB1 function induced enhancement of intramuscular adipogenic differentiation at least partially depends on the focal adhesion pathway. Supporting our interpretation, previous studies found that FAK signaling is essential in adipocyte differentiation (Li and Xie, 2007; Yuan et al., 2018). In detail, preadipocytes differentiated into the physiological function of adipocytes are characterized by major cell morphology from fibroblastic to a rounded shape, which is closely associated with alterations in cytoskeleton and cell–ECM contacts (O'Shea Alvarez, 1991). FAK signaling pathway was proved to playing an important role in the both above biological processes (Nagamatsu et al., 2017; Zhao et al., 2018; Tapial Martinez et al., 2020). Thus, we speculated that LKB1 regulated the

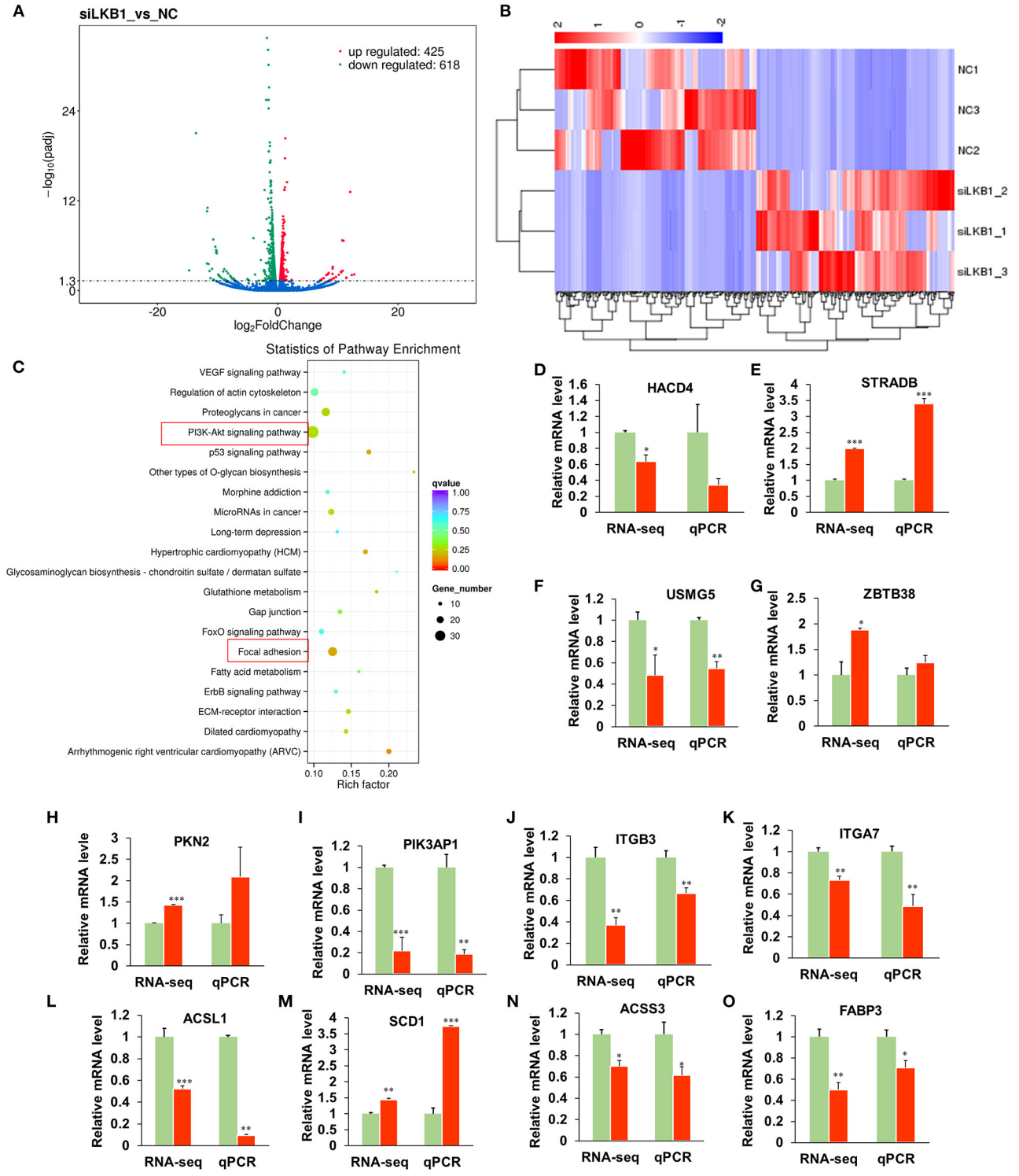

FIGURE 6 | Knockdown of LKB1 affects the mRNA transcript profiles. **(A)** RNA-seq volcano plot of significantly differential expression genes (DEGs) in siLKB1 ($n = 3$) vs. NC ($n = 3$) goat intramuscular adipocytes. Red and blue dots denote upregulated and downregulated genes, respectively. $P < 0.05$ is indicated by the gray dashed horizontal lines. **(B)** The heat map showing the relative levels (fold changes = siLKB1 signal/NC signal) of DEGs. **(C)** The KEGG pathway analysis of related DEGs. **(D–O)** Verification of representative DEGs by qPCR ($n = 3$), including 3-hydroxyacyl-CoA dehydratase 4 (HACD4), STE20-related adaptor beta (STRAD), upregulated during skeletal muscle growth protein 5 (USMG5), Zinc finger and BTB domain containing 38 (ZBTB38), protein kinase N2 (PKN2), phosphoinositide-3-kinase adaptor protein 1 (PIK3AP1), integrin subunit beta 3 (ITGB3), integrin subunit alpha 7 (ITGA7), acyl-CoA synthetase long-chain family member 1 (ACSL1), stearoyl-CoA Desaturase 1 (SCD1), acyl-CoA synthetase short-chain family member 3 (ACSS3), fatty acid-binding protein 3 (FABP3). $^*P < 0.05$, $^{**}P < 0.01$, $^{***}P < 0.001$. LKB1, liver kinase B1; NC, negative control.

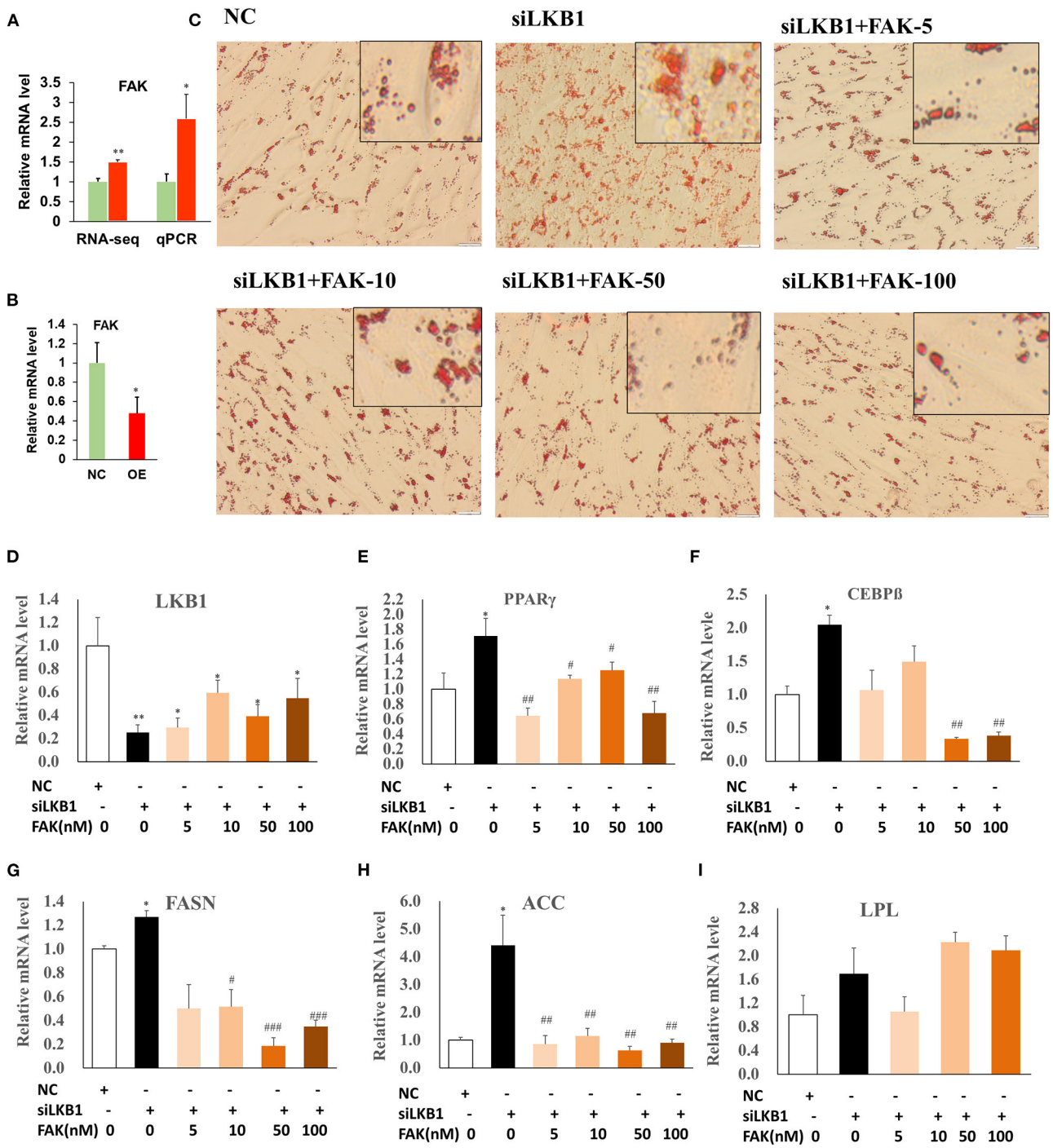

FIGURE 7 | Knockdown of LKB1 promotes intramuscular adipocyte lipid accumulation through FAK pathway. **(A,B)** The mRNA level of FAK gene in siRNA treatment **(A)** and LKB1 overexpressed **(B)** cells by qPCR analysis. **(C)** The oil red O staining images of intramuscular adipocyte cells in NC, siLKB1, and siLKB1 combined with different concentrations of FAK inhibitor (PF573228) treatment groups. **(D–I)** The mRNA level of LKB1 **(D)**, PPAR γ **(E)**, C/EBPβ **(F)**, FASN **(G)**, ACC **(H)**, LPL **(I)** cells in NC, siLKB1, and siLKB1 combined with different concentrations of FAK inhibitor (PF573228) treatment intramuscular adipocyte cells. N = 6. $^{*}P < 0.05$, $^{**}P < 0.01$, compared to those of NC group; $\#P < 0.05$, $\#\#P < 0.01$, $\#\#\#P < 0.001$, compared to those of siLKB1 group. LKB1, liver kinase B1; FAK, focal adhesion kinase; NC, negative control. FASN, fatty acid synthase; ACC, acetyl-CoA carboxylase alpha; LPL, lipoprotein lipase.

focal adhesion pathway and subsequently at least partially affect preadipocyte differentiation through altering the morphology of cells.

In conclusion, our studies validate LKB1 as the key negative factor for goat intramuscular preadipocytes differentiation and reveal LKB1 regulation on intramuscular adipogenesis through

the focal adhesion pathway. These findings contribute to expand the molecular regulation network on IMF deposition and provide theoretical support for improving human health and meat quality from this aspect.

DATA AVAILABILITY STATEMENT

The datasets presented in this study can be found in online repositories. The names of the repository/repositories and accession number(s) can be found below: NCBI Sequence Read Archive and Bioproject number PRJNA761512.

ETHICS STATEMENT

The animal study was reviewed and approved by Institutional Animal Care and Use Committee, Southwest Minzu University.

AUTHOR CONTRIBUTIONS

YX and YL conceived the project and designed the research. YX, YW, and QX performed all the experiments and analyzed the data. AL, QY, and YM cultured the cells. YX and YW wrote the manuscript. All authors contributed to the article and approved the submitted version.

FUNDING

This work was funded by the National Natural Sciences Foundation of China under Grants (Numbers 31902154 and 32072723); the Applied Basic Research Program of Sichuan Province under Grant (Number 2019JY0258); and Fundamental Research Funds for the Central Universities, Southwest Minzu University under Grant (Number 2021112).

SUPPLEMENTARY MATERIAL

The Supplementary Material for this article can be found online at: https://www.frontiersin.org/articles/10.3389/fphys.2021.755598/full#supplementary-material

REFERENCES

Bai, X., Yang, W., Luan, X., Li, H., Li, H., Tian, D., et al. (2021). Induction of cyclophilin A by influenza A virus infection facilitates group A Streptococcus coinfection. *Cell Rep*. 35:109159. doi: 10.1016/j.celrep.2021.109159

Berthelsen, M. F., Leknes, S. L., Riedel, M., Pedersen, M. A., Joseph, J. V., Hager, H., et al. (2021). Comparative analysis of Stk11/Lkb1 versus Pten deficiency in lung adenocarcinoma induced by CRISPR/Cas9. *Cancers* 13:974. doi: 10.3390/cancers13050974

Ducharme, N. A., and Bickel, P. E. (2008). Lipid droplets in lipogenesis and lipolysis. *Endocrinology* 149, 942–949. doi: 10.1210/en.2007-1713

Engin, A. (2017). Fat cell and fatty acid turnover in obesity. *Adv. Exp. Med. Biol.* 960, 135–160. doi: 10.1007/978-3-319-48382-5_6

Gao, Y. Y., Zhang, Z. H., Zhuang, Z., Lu, Y., Wu, L. Y., Ye, Z. N., et al. (2018). Recombinant milk fat globule-EGF factor-8 reduces apoptosis via integrin beta3/FAK/PI3K/AKT signaling pathway in rats after traumatic brain injury. *Cell Death Dis*. 9:845. doi: 10.1038/s41419-018-0939-5

Gulyaeva, O., Dempersmier, J., and Sul, H. S. (2019). Genetic and epigenetic control of adipose development. *Biochim. Biophys. Acta-Mol. Cell Biol. Lipids*. 1864, 3–12. doi: 10.1016/j.bbalip.2018.04.016

Haczeyni, F., Bell-Anderson, K. S., and Farrell, G. C. (2018). Causes and mechanisms of adipocyte enlargement and adipose expansion. *Obes. Rev.* 19, 406–420. doi: 10.1111/obr.12646

Han, S. H., Malaga-Dieguez, L., Chinga, F., Kang, H. M., Tao, J., Reidy, K., et al. (2016). Deletion of Lkb1 in renal tubular epithelial cells leads to CKD by altering metabolism. *J. Am. Soc. Nephrol.* 27, 439–453. doi: 10.1681/ASN.2014121181

Hocquette, J. F., Gondret, F., Baeza, E., Medale, F., Jurie, C., and Pethick, D. W. (2010). Intramuscular fat content in meat-producing animals: development, genetic and nutritional control, and identification of putative markers. *Animal* 4, 303–319. doi: 10.1017/S1751731109991091

Huang, K., Liang, J. J., Lin, Y. Q., Zhu, J. J., Ma, J. Q., and Wang, Y. (2020). Molecular characterization of fibroblast growth factor-16 and its role in promoting the differentiation of intramuscular preadipocytes in goat. *Animal* 14, 2351–2362. doi: 10.175173112000116010

Hunt, M. R., Legako, J. F., Dinh, T. T., Garmyn, A. J., O'quinn, T. G., Corbin, C. H., et al. (2016). Assessment of volatile compounds, neutral and polar lipid fatty acids of four beef muscles from USDA Choice and Select graded carcasses and their relationships with consumer palatability scores and intramuscular fat content. *Meat Sci*. 116, 91–101. doi: 10.1016/j.meatsci.2016.02.010

Jansen, M., Ten Klooster, J. P., Offerhaus, G. J., and Clevers, H. (2009). LKB1 and AMPK family signaling: the intimate link between cell polarity and energy metabolism. *Physiol. Rev.* 89, 777–798. doi: 10.1152/physrev.00026.2008

Kanehisa, M., Araki, M., Goto, S., Hattori, M., Hirakawa, M., Itoh, M., et al. (2008). KEGG for linking genomes to life and the environment. *Nucleic Acids Res*. 36, D480–D484. doi: 10.1093/nar/gkm882

Kline, E. R., Shupe, J., Gilbert-Ross, M., Zhou, W., and Marcus, A. I. (2013). LKB1 represses focal adhesion kinase (FAK) signaling via a FAK-LKB1 complex to regulate FAK site maturation and directional persistence. *J. Biol. Chem.* 288, 17663–17674. doi: 10.1074/jbc.M112.444620

Li, J. J., and Xie, D. (2007). Cleavage of focal adhesion kinase (FAK) is essential in adipocyte differentiation. *Biochem. Biophys. Res. Commun.* 357, 648–654. doi: 10.1016/j.bbrc.2007.03.184

Li, X., Fu, X., Yang, G., and Du, M. (2020). Review: Enhancing intramuscular fat development via targeting fibro-adipogenic progenitor cells in meat animals. *Animal* 14, 312–321. doi: 10.1017/S175173111900209X

Lim, S. (2014). Ectopic fat assessment focusing on cardiometabolic and renal risk. *Endocrinol. Metab*. 29, 1–4. doi: 10.3803/EnM.2014.29.1.1

Lizcano, J. M., Goransson, O., Toth, R., Deak, M., Morrice, N. A., Boudeau, J., et al. (2004). LKB1 is a master kinase that activates 13 kinases of the AMPK subfamily, including MARK/PAR-1. *EMBO J.* 23, 833–843. doi: 10.1038/sj.emboj.7600110

Mao, X., Cai, T., Olyarchuk, J. G., and Wei, L. (2005). Automated genome annotation and pathway identification using the KEGG Orthology (KO) as a controlled vocabulary. *Bioinformatics* 21, 3787–3793. doi: 10.1093/bioinformatics/bti43

Mueller, C., Ratner, D., Zhong, L., Esteves-Sena, M., and Gao, G. (2012). Production and discovery of novel recombinant adeno-associated viral vectors. *Curr. Protoc. Microbiol.*14, 14D−1. doi: 10.1002/9780471729259.mc14d01s26

Nagamatsu, T., Yoneda, S., Isogaki, H., and Mizuno, T. (2017). Acidic environment causes altered the focal adhesions and the actin cytoskeleton in mesangial cells. *J. Pharmacol. Sci.* 133, S110–S110.

O'Shea Alvarez, M. S. (1991). 3T3 cells in adipocytic conversion. *Arch. Invest. Med.* 22, 235–244.

Saponaro, C., Gaggini, M., Carli, F., and Gastaldelli, A. (2015). The subtle balance between lipolysis and lipogenesis: a critical point in metabolic homeostasis. *Nutrients* 7, 9453–9474. doi: 10.3390/nu7115475

Shan, T., Xu, Z., Liu, J., Wu, W., and Wang, Y. (2017). Lkb1 regulation of skeletal muscle development, metabolism and muscle progenitor cell homeostasis. *J. Cell. Physiol.* 232, 2653–2656. doi: 10.1002/jcp.25786

Shan, T., Zhang, P., Bi, P., and Kuang, S. (2015). Lkb1 deletion promotes ectopic lipid accumulation in muscle progenitor cells and mature muscles. *J. Cell. Physiol.* 230, 1033–1041. doi: 10.1002/jcp.24831

Shan, T., Zhang, P., Liang, X., Bi, P., Yue, F., and Kuang, S. (2014). Lkb1 is indispensable for skeletal muscle development, regeneration, and satellite cell homeostasis. *Stem Cells*. 32, 2893–2907. doi: 10.1002/stem.1788

Shan, T. Z., Xiong, Y., and Kuang, S. H. (2016a). Deletion of Lkb1 in adult mice results in body weight reduction and lethality. *Sci. Rep*. 6, 1–9. doi: 10.1038/srep36561

Shan, T. Z., Xiong, Y., Zhang, P. P., Li, Z. G., Jiang, Q. Y., Bi, P. P., et al. (2016b). Lkb1 controls brown adipose tissue growth and thermogenesis by regulating the intracellular localization of CRTC3. *Nat. Commun*. 7, 1–11. doi: 10.1038/ncomms12205

Sun, G. R., Zhang, M., Sun, J. W., Li, F., Ma, X. F., Li, W. T., et al. (2019). Kruppel-like factor KLF9 inhibits chicken intramuscular preadipocyte differentiation. *Br. Poult. Sci.* 60, 790–797. doi: 10.1080/00071668.2019.1657229

Sun, Y., Cai, R., Wang, Y., Zhao, R., Qin, J., and Pang, W. (2020). A newly identified LncRNA LncIMF4 controls adipogenesis of porcine intramuscular preadipocyte through attenuating autophagy to inhibit lipolysis. *Animals* 10:926. doi: 10.3390/ani10060926

Tapial Martinez, P., Lopez Navajas, P., and Lietha, D. (2020). FAK structure and regulation by membrane interactions and force in focal adhesions. *Biomolecules*. 10, doi: 10.3390/biom10020179

Trapnell, C., Williams, B. A., Pertea, G., Mortazavi, A., Kwan, G., Van Baren, M. J., et al. (2010). Transcript assembly and quantification by RNA-Seq reveals unannotated transcripts and isoform switching during cell differentiation. *Nat Biotechnol*. 28, 511–515. doi: 10.1038/nbt.1621

Wang, R., Liu, W., Wang, Q., Li, G., Wan, B., Sun, Y., et al. (2020). Anti-osteosarcoma effect of hydroxyapatite nanoparticles both in vitro and in vivo by downregulating the FAK/PI3K/Akt signaling pathway. *Biomater Sci*. 8, 4426–4437. doi: 10.1039/d0bm00898b

Xiong, Y., Page, J. C., Narayanan, N., Wang, C., Jia, Z. H., Yue, F., et al. (2017). Peripheral neuropathy and hindlimb paralysis in a mouse model of adipocyte-specific knockout of Lkb1. *Ebiomedicine* 24, 127–136. doi: 10.1016/j.ebiom.2017.09.017

Xiong, Y., Xu, Q., Lin, S., Wang, Y., Lin, Y. Q., and Zhu, J. J. (2018a). Knockdown of LXR alpha inhibits goat intramuscular preadipocyte differentiation. *Int. J. Mol. Sci.* 19, doi: 10.3390/ijms19103037

Xiong, Y., Xu, Z. Y., Wang, Y. Z., Kuang, S. H., and Shan, T. Z. (2018b). Adipocyte-specific DKO of Lkb1 and mTOR protects mice against HFD-induced obesity, but results in insulin resistance. *J. Lipid Res.* 59, 974–981. doi: 10.1194/jlr.M081463

Xu, Q., Lin, S., Zhu, J. J., Wang, Y., and Lin, Y. Q. (2018). The expression stability analysis of reference genes in the process of goat intramuscular preadipocytes differentiation in goat. *Acta Vet. Zootech. Sin*. 49 42–53. doi: 10.11843/j.issn.0366-6964.2018.05.005

Yuan, C., Gou, X., Deng, J., Dong, Z., Ye, P., and Hu, Z. (2018). FAK and BMP-9 synergistically trigger osteogenic differentiation and bone formation of adipose derived stem cells through enhancing Wnt-beta-catenin signaling. *Biomed. Pharmacother.* 105, 753–757. doi: 10.1016/j.biopha.2018.04.185

Zhang, K., Wang, J., Wang, J., Luh, F., Liu, X., Yang, L., et al. (2019a). LKB1 deficiency promotes proliferation and invasion of glioblastoma through activation of mTOR and focal adhesion kinase signaling pathways. *Am. J. Cancer Res.* 9, 1650–1663.

Zhang, S. L., Ma, L., Zhao, J., You, S. P., Ma, X. T., Ye, X. Y., et al. (2019b). The phenylethanol glycoside liposome inhibits PDGF-induced HSC activation via regulation of the FAK/PI3K/Akt signaling pathway. *Molecules*. 24:3282. doi: 10.3390/molecules24183282

Zhao, C., Chen, X., Wu, W., Wang, W., Pang, W., and Yang, G. (2016). MAT2B promotes adipogenesis by modulating SAMe levels and activating AKT/ERK pathway during porcine intramuscular preadipocyte differentiation. *Exp. Cell Res.* 344, 11–21. doi: 10.1016/j.yexcr.2016.02.019

Zhao, T., Li, R., Tan, X., Zhang, J., Fan, C. H., Zhao, Q., et al. (2018). Simulated microgravity reduces focal adhesions and alters cytoskeleton and nuclear positioning leading to enhanced apoptosis via suppressing FAK/RhoA-mediated mTORC1/NF-kappa B and ERK1/2 pathways. *Int. J. Mol. Sci.* 19:1994. doi: 10.3390/ijms19071994

Zhu, H. H., Wang, X. T., Sun, Y. H., He, W. K., Liang, J. B., Mo, B. H., et al. (2018). Pim1 overexpression prevents apoptosis in cardiomyocytes after exposure to hypoxia and oxidative stress via upregulating cell autophagy. *Cell. Physiol. Biochem.* 49, 2138–2150. doi: 10.1159/000493817

Conflict of Interest: The authors declare that the research was conducted in the absence of any commercial or financial relationships that could be construed as a potential conflict of interest.

Publisher's Note: All claims expressed in this article are solely those of the authors and do not necessarily represent those of their affiliated organizations, or those of the publisher, the editors and the reviewers. Any product that may be evaluated in this article, or claim that may be made by its manufacturer, is not guaranteed or endorsed by the publisher.

Copyright © 2021 Xiong, Wang, Xu, Li, Yue, Ma and Lin. This is an open-access article distributed under the terms of the Creative Commons Attribution License (CC BY). The use, distribution or reproduction in other forums is permitted, provided the original author(s) and the copyright owner(s) are credited and that the original publication in this journal is cited, in accordance with accepted academic practice. No use, distribution or reproduction is permitted which does not comply with these terms.

frontiers in Physiology

ORIGINAL RESEARCH
published: 10 February 2022
doi: 10.3389/fphys.2022.809845

Visceral Adiposity, Inflammation, and Testosterone Predict Skeletal Muscle Mitochondrial Mass and Activity in Chronic Spinal Cord Injury

Jacob A. Goldsmith[1†], Raymond E. Lai[1,2], Ryan S. Garten[3], Qun Chen[4], Edward J. Lesnefsky[4,5], Robert A. Perera[6] and Ashraf S. Gorgey[1,2†]*

[1] Spinal Cord Injury and Disorders, Hunter Holmes McGuire Veterans Affairs Medical Center (VAMC), Richmond, VA, United States, [2] Department of Physical Medicine and Rehabilitation, Virginia Commonwealth University, Richmond, VA, United States, [3] Department of Kinesiology and Health Sciences, Virginia Commonwealth University, Richmond, VA, United States, [4] Medical Service, Hunter Holmes McGuire VA Medical Center, Richmond, VA, United States, [5] Division of Cardiology, Department of Medicine, Pauley Heart Center, Virginia Commonwealth University, Richmond, VA, United States, [6] Department of Biostatistics, Virginia Commonwealth University, Richmond, VA, United States

OPEN ACCESS

Edited by:
Tizhong Shan,
Zhejiang University, China

Reviewed by:
Gregory C. Henderson,
Purdue University, United States
J. A. Taylor,
Harvard Medical School,
United States

***Correspondence:**
Ashraf S. Gorgey
ashraf.gorgey@va.gov

†ORCID:
Jacob A. Goldsmith
orcid.org/0000-0002-1699-4092
Ashraf S. Gorgey
orcid.org/0000-0002-9157-6034

Specialty section:
This article was submitted to Lipid and Fatty Acid Research, a section of the journal Frontiers in Physiology

Received: 05 November 2021
Accepted: 10 January 2022
Published: 10 February 2022

Citation:
Goldsmith JA, Lai RE, Garten RS, Chen Q, Lesnefsky EJ, Perera RA and Gorgey AS (2022) Visceral Adiposity, Inflammation, and Testosterone Predict Skeletal Muscle Mitochondrial Mass and Activity in Chronic Spinal Cord Injury. Front. Physiol. 13:809845. doi: 10.3389/fphys.2022.809845

Background: Mitochondrial health is an important predictor of several health-related comorbidities including obesity, type 2 diabetes mellitus, and cardiovascular disease. In persons with spinal cord injury (SCI), mitochondrial health has been linked to several important body composition and metabolic parameters. However, the complex interplay of how mitochondrial health is affected has yet to be determined in this population.

Objective: In this study, we examined the contribution of visceral adiposity, inflammatory biomarkers, testosterone and circulating serum growth factors as predictors of mitochondrial health in persons with chronic SCI.

Participants: Thirty-three individuals with chronic SCI (n = 27 Males, n = 6 Females, age: 40 ± 13.26 years, level of injury: C4-L1, BMI: 23 ± 5.57) participated in this cross-sectional study.

Methods: Visceral adipose tissue (VAT) was measured via magnetic resonance imaging (MRI). After an overnight fast, serum testosterone, inflammatory biomarkers [interleukin 6 (IL-6), tumor necrosis factor alpha (TNF-α), c-reactive protein (CRP)], and anabolic growth factors [insulin-like growth factor 1 (IGF-1), insulin-like growth factor binding protein 3 (IGFBP-3)] were measured. Skeletal muscle biopsies were obtained from the vastus lateralis muscle to measure citrate synthase (CS) and Complex III activity. Regression analyses were used to examine predictors of mitochondrial mass and activity.

Results: CS activity was negatively associated with VAT (r^2 = 0.360, p < 0.001), CRP (r^2 = 0.168, p = 0.047), and positively associated with testosterone (r^2 = 0.145,

$p = 0.042$). Complex III activity was negatively associated with VAT relative to total lean mass (VAT:TLM) ($r^2 = 0.169$, $p = 0.033$), trended for CRP ($r^2 = 0.142$, $p = 0.069$), and positively associated with testosterone ($r^2 = 0.224$, $p = 0.010$). Multiple regression showed CS activity was significantly associated with VAT + CRP ($r^2 = 0.412$, $p = 0.008$) and VAT + Testosterone ($r^2 = 0.433$, $p = 0.001$). Complex III activity was significantly associated with VAT relative to total trunk cross-sectional area (CSA) + CRP (VAT:total trunk CSA + CRP; $r^2 = 0.286$, $p = 0.048$) and VAT + Testosterone ($r^2 = 0.277$, $p = 0.024$).

Conclusion: Increased visceral adiposity and associated inflammatory signaling (CRP) along with reduced testosterone levels predict mitochondrial dysfunction following SCI. Specifically, lower VAT_{CSA} and higher testosterone levels or lower VAT_{CSA} and lower CRP levels positively predict mitochondrial mass and enzyme activity in persons with chronic SCI. Future research should investigate the efficacy of diet, exercise, and potentially testosterone replacement therapy on enhancing mitochondrial health in chronic SCI.

Clinical Trial Registration: [www.ClinicalTrials.gov], identifier: [NCT02660073].

Keywords: spinal cord injury, visceral adipose tissue, mitochondria, inflammation, growth factors, testosterone

INTRODUCTION

Cardiometabolic disorders are a leading cause of mortality among persons with spinal cord injury (SCI) (Schladen and Groah, 2014). Recent guidelines have emerged to highlight the magnitude of the problem and provide assessment tools for researchers and clinicians to distinguish those at risk (Nash and Gater, 2020). Cardiometabolic syndrome presents as a cluster of disorders, including impaired glucose tolerance, insulin resistance, dyslipidemia, central obesity, and elevated blood pressure (Després and Lamarche, 1993; Després et al., 2001; Grundy et al., 2004). Cardiometabolic syndrome impacts more than 50% of persons with SCI (LaVela et al., 2006; Dopier Nelson et al., 2007). Today, the root of the problem remains unresolved and likely to continue without appropriate intervention.

Recent emerging cross-sectional studies have clearly associated central obesity with cardiometabolic disorder after SCI. Earlier studies indicated the link between waist circumference and cardiometabolic diseases in persons with SCI (Buchholz and Bugaresti, 2005; Gill et al., 2020). It appears that waist circumference reflects increased visceral adiposity. Gorgey and Gater (2011) were among the first to show that with increasing visceral adipose tissue (VAT), persons with SCI may suffer from impaired glucose intolerance, insulin resistance, and dyslipidemia. Another study showed that people with SCI had 58% greater VAT than waist circumference matched controls (Edwards et al., 2008). Using a simple linear regression model, Sumrell et al. (2018) showed that a waist circumference greater than 86.5 cm is equivalent to VAT equal to or greater than 100 cm^2. The same work demonstrated that VAT > 100 cm^2 was associated with decreased insulin sensitivity, increased inflammatory biomarkers, and reduced oxygen uptake. In a follow-up trial, the same research group showed that a waist circumference of 86.5 cm distinguishes those at risk of developing cardiometabolic disorders in persons with SCI (Gill et al., 2020). A recent review summarized potential mechanisms for increasing VAT to contribute to the prevalence of cardiometabolic diseases after SCI (Goldsmith et al., 2021).

Previous work has alluded to several potential mechanisms that likely trigger VAT-associated cardiometabolic disorders (Seidell et al., 1990; Nicklas et al., 2003; Fox et al., 2007; Katzmarzyk et al., 2013; Lee et al., 2018; Gorgey et al., 2021). Although most studies have not demonstrated causality, these studies established potential mechanisms that warrant further investigation. Farkas et al. (2018) and Farkas and Gater (2018) noted that with increasing VAT, there is a potential increase in inflammatory biomarkers, mainly tumor necrosis factor-alpha (TNF-α) and interleukin-6 (IL-6). Abilmona et al. (2019) noted that, in persons with SCI, hypogonadal individuals (<300 ng/dL) are likely to have greater VAT than persons with normal testosterone levels. Finally, O'Brien et al. (2017b) described an association between increasing VAT and mitochondrial dysfunction in persons with SCI.

Mitochondrial health is an important predictor of several health-related comorbidities, including obesity, type 2 diabetes mellitus and cardiovascular disease (Poznyak et al., 2020). Mitochondrial function is linked to several important body composition and metabolic parameters in persons with SCI. Specifically, mitochondrial mass (citrate synthase activity) and Complex III activity have been negatively associated with increased body fat and reduced cardiometabolic health (O'Brien et al., 2017a,b, 2018). Based on the above evidence, it appears

Abbreviations: SCI, spinal cord injury; LOI, level of injury; MRI, magnetic resonance imaging; SAT, subcutaneous adipose tissue; VAT, visceral adipose tissue; VAT:SAT, ratio of VAT to SAT; LM, Lean mass; TLM, total lean mass; IL-6, interleukin-6; IGF-1, insulin-like growth factor 1; IGFBP-3, insulin-like growth factor binding protein 3; CRP, c-reactive protein; CS, citrate synthase; TNF-α, tumor necrosis factor alpha.

that VAT exerts deleterious cardiometabolic effects in persons with SCI, by increasing systemic inflammation and diminishing testosterone levels that lead to mitochondrial dysfunction. This cross-sectional study aimed to examine the contribution of visceral adiposity, inflammatory biomarkers, testosterone, and circulating serum growth factors as predictors of mitochondrial health in persons with chronic SCI.

MATERIALS AND METHODS

Participants

Thirty-three individuals with chronic SCI (age: 40 ± 13.26 years, level of injury: C5-L1, BMI: 23 ± 5.57) participated in this cross-sectional study (registered at clinicaltrials.gov: NCT02660073). Only cross-sectional baseline data are presented in this manuscript. All procedures were in accordance with the ethical standards of the Helsinki Declaration of 1,964 and its later amendments. The McGuire Veteran Affairs Investigation Research Board and the Virginia Commonwealth University (VCU) Office of Research and Innovation approved the current study. A neurological examination was performed per the International Standards for Neurological Classification of SCI (ISNCSCI) to determine the American Spinal Injury Association (ASIA) Impairment Scale (AIS) for each participant. Participants provided written, informed consent before the study commenced. Participants with the following pre-existing medical conditions were excluded: active urinary tract infection, those using insulin, hematocrit > 50%, stage 3 pressure sore or above, uncontrolled hypertension, cardiovascular disease or uncontrolled type 2 diabetes mellitus, and individuals with neck of femur or total body osteoporosis (T-score ≤ −2.5 according to the World health organization guidelines) (Reginster and Burlet, 2006; Gorgey et al., 2019a). All participants were instructed to abstain from exercise, alcohol, and caffeine consumption 24 h before the examination. Participants underwent a general physical examination to rule out any preexisting cardiac problems that included measuring vital signs and a resting 12-lead electrocardiogram. After a 10–12 h fast, a cannula was inserted into an antecubital vein of one arm for blood sampling. Fasting whole-blood samples were drawn into serum separator and potassium oxalate/sodium fluoride tubes and centrifuged to collect serum and plasma samples, respectively. The majority of blood samples were sent to the Chemistry Pathology Laboratory for analysis; however, a subset was sent to a research lab at VCU for further analysis using the same protocol and assay kits. Inflammatory biomarkers (Tumor necrosis factor-alpha; TNF-α, Interleukin-6; IL-6, and c-reactive protein; CRP) were also analyzed in serum samples by enzyme-linked immunosorbent assays (ELISA) (ALPACO; Salem, NH). Total serum testosterone was measured by liquid chromatography with isotope dilution mass spectrometry detection after supported liquid extraction (Esoterix, Inc.). Testosterone levels in each sample were calculated from a linear plot generated by purified testosterone standards ranging from 2.5 to 5,000 ng/dL. Serum insulin-like growth factor-1 (IGF-I) and insulin-like growth factor-binding protein 3 (IGFBP-3) concentrations were measured with immunoassays (Quantikine R&D Systems, Inc., Minneapolis, MN, United States).

Magnetic Resonance Imaging

Abdominal MRI scans were imaged using a 1.5- or 3 Tesla magnet (General Electric, Waukesha, WI) whole-body scanner, using a fast spin-echo sequence described previously (Gorgey et al., 2019b). Transverse images (slice thickness of 0.8 cm, inter-slice space of 1.2 cm) were captured from the xiphoid process to the femoral heads. Depending on the individual's torso length, approximately 20 ± 30 images were obtained. Participants were asked to remain as still as possible during the entirety of the scan. In addition, participants were instructed to hold their breath for approximately 20 s to prevent respiratory artifacts from altering image quality. Images were sequenced anatomically using Image-J software (National Institute of Health, Bethesda, Maryland) and analyzed using Win Vessel software (Win Vessel 2.0, Ronald Meyer, Michigan State University, East Lansing, MI, United States). Each image was automatically segmented into fat and muscle, with bone and background tissue identified based on its signal intensity. Abdominal adipose tissue was separated into subcutaneous adipose tissue (SAT) and VAT depots. An experienced technician manually identified regions of interest guided by anatomical landmarks. The cross-sectional areas (CSA) of these different compartments were used to derive the VAT:SAT ratio to control for regional adiposity. The total area within the outer border of the trunk represented the total trunk CSA, which was used to normalize VAT_{CSA} to Total trunk CSA (VAT:total trunk CSA ratio) (Abilmona and Gorgey, 2018). All values were averaged across images to reflect the whole torso.

Dual-Energy X-Ray Absorptiometry

Total body and regional DXA scans were performed using a GE Lunar iDXA (Lunar Inc., Madison, WI, United States) bone densitometer at the Hunter Holmes VA Medical Center. All scans were performed and analyzed using Lunar software version 10.5. After scanning, total and regional % fat mass and fat-free mass were determined using DXA software. The longitudinal precision of total and regional body composition using DXA has been determined in persons with SCI (Lester et al., 2019). As previously described, VAT mass was made relative to SAT mass to account for differences in SAT mass between individuals. Additionally, VAT was made relative to total lean mass (TLM) and trunk CSA to account for differences between individuals, as previous research has demonstrated a relationship between VAT mass, total trunk mass, and LM (O'Brien et al., 2017b; Abilmona et al., 2019).

Enzyme Activities

Muscle biopsies from the vastus lateralis of the right leg were collected using a 14-gauge Tru Cut™ needle under local anesthesia (2% lidocaine). Samples were snap-frozen in liquid nitrogen and stored at −70°C. Connective and adipose tissue was removed from a portion of the sample (∼10–25 mg), then homogenized in ice-cold buffer containing 220 mM mannitol, 70 mM sucrose, 5 mM MOPS, 2 mM EDTA, with cOmplete™ protease inhibitor cocktail, pH 7.4 (Sigma-Aldrich).

The homogenate was centrifuged at 2,000 rpm (371 g) for 5 min at 4°C and the supernatant was used for analysis. Protein concentration was quantified, and samples were solubilized in 1% potassium cholate. Homogenization and assays were completed on the same day. CS and Complex III activity were measured spectrophotometrically in duplicate or triplicate as previously described (Brass et al., 2001; O'Brien et al., 2017a). CS activity, a measure of mitochondrial mass, was measured as the formation of thionitrobenzoate at 412 nm after the addition of 5, 5-dithiobis-(2, 4-nitrobenzoic acid), acetyl-CoA, and oxaloacetate (n = 32). Complex III activity was reflected by the rate of cytochrome c reduction in absorbance at 550 nm (n = 32) (Brass et al., 2001; Spinazzi et al., 2012). Antimycin A was used to inhibit Complex III. The activity of Complex III was expressed as the antimycin A-sensitive rate. Absorbance was measured before and after the addition of oxaloacetate, and background absorbance was subtracted from the final reading. Data were converted from arbitrary units per minute to nmol/min by using the extinction coefficients of 13.6 mM^{-1} cm^{-1} for CS and 19.1 mM^{-1} cm^{-1} for Complex III. Data were normalized to mg of protein added.

Statistical Analysis

All data were analyzed for normality of distribution. Data that were not normally distributed were log-transformed to permit the use of parametric statistics. Single and multiple linear regression models were used to examine the relationships between measures of mitochondrial mass (citrate synthase activity) and activity (Complex III), visceral adiposity, serum inflammatory biomarkers, anabolic growth factors, and testosterone. We used a maximum of two predictors in each regression to avoid multicollinearity issues due to the relatively low sample size. Instead of adding variables including time since injury (TSI), level of injury (LOI), and age as predictors in these models, we controlled these variables using weighted least squares regressions. We continued with multiple regression models only if a predictor was independently significant with either CS or Complex III activity. Statistical analyses were performed using SPSS (SPSS Statistics version 24, IBM Corp., Armonk, United States). Statistical significance was accepted at *a priori* of $\alpha \leq 0.05$.

RESULTS

Participant Characteristics

Participant demographics and injury characteristics are presented in **Table 1**. Twenty-two were paraplegic (T1-L1) and 11 were tetraplegic (C4-C8). Participants ranged in age from 20 to 61 and BMI ranged from 14.2 to 35.3 kg/m^2. Age, height, weight, BMI, and TSI were not significantly different between tetraplegics and paraplegics or Caucasians and African Americans. Inflammatory biomarkers, anabolic growth factors, serum testosterone levels, mitochondrial enzyme activity, and MRI outcomes are presented in **Table 2**. Values were not significantly different between paraplegics and tetraplegics or Caucasians and African Americans. Central adiposity was apparent in 21 and 32% of the participants using cutoffs of $\geq$ 100 cm^2 MRI VAT_{CSA}, and $\geq$ 0.66 VAT:SAT ratio, respectively (Gorgey et al., 2011, 2014). Importantly, a fraction of the samples (eight samples used for IL-6, TNF-α, IGF-1, and IGFBP-3) sent to VCU for further analysis experienced degradation that resulted

TABLE 1 | Baseline demographics and spinal cord injury characteristics for 33 participants.

Ethnicity	Caucasian: n = 18
	African American: n = 15
Sex	Male: n = 27
	Female: n = 6
Age (year)	40 ± 13.00
Weight (kg)	70 ± 15.18
Height (cm)	175 ± 8.99
BMI (kg/m^2)	23 ± 5.25
Level of injury (range)	C5–L1
Time since injury (yr)	11 ± 10.59
AIS (score)	A: n = 19
	B: n = 9
	C: n = 5
SCI classification	Paraplegia: n = 22
	Tetraplegia: n = 11

BMI, body mass index; AIS, American Spinal Injury Association Impairment Scale; AIS-A, complete motor and sensory loss below the level of injury; AIS-B, complete motor loss and incomplete sensory loss below the level of injury; AIS-C, incomplete motor and sensory loss with less than half of the muscles tested below the LOI graded ≥ 3. Mean ± SD unless otherwise noted.

TABLE 2 | Citrate synthase activity, inflammatory biomarkers, anabolic growth factors, and serum testosterone levels.

Anabolic growth factors	Mean ± SD	Range	Sample size
IGF-1 (ng/mL)	143.99 ± 58.73	72.90–267.85	25
IGFBP-3 (ng/mL)	1851.40 ± 368.57	1320.50–2598.55	25
MRI and DXA measures			
Total $trunk_{CSA}$ (cm^2)	571.44 ± 174.17	323.16–940.64	28
SAT_{CSA} (cm^2)	136.43 ± 100.30	22.97–369.89	28
VAT_{CSA} (cm^2)	71.73 ± 64.97	4.06–220.01	28
VAT:SAT ratio	0.64 ± 0.47	0.10–2.22	28
VAT:total trunk CSA	0.11 ± 0.08	0.01–0.30	28
VAT:TLM	0.0015 ± 0.0013	0.0001–0.0043	28
VAT:Leg LM	0.0054 ± 0.0049	0.0004–0.02	28
TLM (kg)	448.48 ± 77.57	288.83–616.34	32
Leg LM (kg)	131.69 ± 28.58	64.55–188.77	32
Inflammatory biomarkers			
CRP (ng/mL)	14580.81 ± 19705.45	185.0–73530.25	25
IL-6 (pg/mL)	3.18 ± 2.49	0.68–9.27	22
TNF-α (pg/mL)	22.50 ± 3.96	15.24–30.63	25
Serum testosterone levels			
Testosterone (ng/dL)	346.72 ± 223.71	8.30–751.00	30
Enzyme activity			
CS (nmol/mg/min)	101.22 ± 59.83	24.00–303.00	32
Complex III (nmol/mg/min)	190.00 ± 125.51	47.10–679.00	32

MRI, magnetic resonance imaging; DXA, Dual energy x-ray absorptiometry; SAT, subcutaneous adipose tissue; VAT, visceral adipose tissue; ng/dL, IGF-1, insulin-like growth factor 1; IGFBP-3, insulin-like growth factor binding protein 3; CRP, c-reactive protein; IL-6, interleukin 6; CS, citrate synthase; TNF-α, tumor necrosis factor alpha; nanograms per deciliter; CSA, cross sectional area; Kg, kilograms. Mean ± SD unless otherwise noted.

in erroneous values. Therefore, we excluded these samples from analyses, which resulted in an uneven sample size depending on the marker be analyzed (**Table 2**). **Figure 1** shows the hypothesized factors predicting mitochondrial health following SCI. This hypothesized model shows that, after SCI, visceral adiposity increases and releases inflammatory cytokines that negatively affect testosterone levels and mitochondrial health. While it is clear that visceral adiposity, inflammation, and testosterone are involved in this deleterious process, there are still factors that remain unidentified.

Independent Predictors of Citrate Synthase Activity

Figure 2 shows the significant relationships predicting Citrate Synthase (CS) activity. CS activity was negatively associated with VAT ($r^2 = 0.360$, $p < 0.001$), CRP ($r^2 = 0.168$, $p = 0.047$), VAT:total trunk CSA ($r^2 = 0.372$, $p < 0.001$), and VAT:TLM ($r^2 = 0.434$, $p < 0.001$), and positively associated with testosterone ($r^2 = 0.145$, $p = 0.042$) (**Table 3**). CS activity was not independently associated with VAT:SAT, IL-6, TNF-α, IGF-1, or IGFBP-3 (data not shown). The relationships between CS activity and VAT, VAT:total trunk CSA, and VAT:TLM remained significant when controlling for TSI, age, and LOI (**Table 4**). However, testosterone ($r^2 = 0.087$, $p = 0.119$) and CRP ($r^2 = 0.081$, $p = 0.176$) were no longer significant when controlling for TSI. When controlling for age or LOI (paraplegic vs. tetraplegic), CRP ($r^2 = 0.249$, $p = 0.013$) and testosterone ($r^2 = 0.170$, $p = 0.026$) were negatively and positively significant, respectively. Moreover, IL-6 showed a significant negative association with CS activity when controlling for age ($r^2 = 0.237$, $p = 0.019$). IL-6 was only a significant predictor of CS activity in participants over 40 ($r^2 = 0.466$, $p = 0.014$) but not participants under 40 ($r^2 = 0.068$, $p = 0.437$).

Multiple Regressions to Predict Citrate Synthase Activity

CS activity was significantly associated with VAT + CRP ($r^2 = 0.412$, $p = 0.008$) and VAT + testosterone ($r^2 = 0.433$, $p = 0.001$). Within this model, individuals with lower VAT_{CSA} and lower CRP levels had higher CS activity. Furthermore, individuals with lower VAT_{CSA} and higher testosterone levels had higher CS activity. These relationships remained significant when VAT was made relative to total trunk CSA (CRP: $r^2 = 0.454$, $p = 0.004$, testosterone: $r^2 = 0.467$, $p < 0.001$), and TLM (CRP: $r^2 = 0.444$, $p = 0.005$; testosterone: $r^2 = 0.473$, $p < 0.001$) (**Table 3**). These relationships also remained significant when controlling for age [VAT + CRP ($r^2 = 0.365$, $p = 0.017$), VAT + testosterone ($r^2 = 0.382$, $p = 0.004$)]. As previously stated, IL-6 became significantly negatively associated with CS activity when controlling for age, and VAT + IL-6 ($r^2 = 0.412$, $p = 0.011$) was also significantly negatively associated when controlling for age. Specifically, VAT + IL-6 was a significant predictor of CS activity in participants over 40 ($r^2 = 0.511$, $p = 0.041$) but not in individuals under 40 ($r^2 = 0.293$, $p = 0.353$). Multiple regressions (VAT + CRP, VAT:total trunk CSA + CRP, VAT:TLM + CRP, VAT:total trunk CSA + testosterone, and VAT:TLM + testosterone), remained significant when controlling for TSI, while VAT + testosterone trended toward significance ($p = 0.053$) (**Table 4**). When controlling for LOI, VAT + CRP ($r^2 = 0.503$, $p = 0.002$), VAT + testosterone ($r^2 = 0.508$, $p < 0.001$), VAT:total trunk CSA + CRP ($r^2 = 0.537$, $p = 0.001$), VAT:total trunk CSA + testosterone ($r^2 = 0.534$, $p = < 0.001$), VAT:TLM + CRP ($r^2 = 0.531$, $p = 0.001$), and VAT:TLM + testosterone ($r^2 = 0.548$, $p < 0.001$) remained significant (**Table 4**). All other possible models to predict CS activity were tested and not significant.

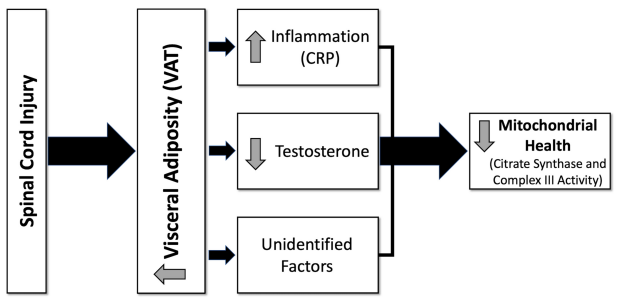

FIGURE 1 | Hypothesized diagram of factors predicting mitochondrial health following spinal cord injury (SCI). After SCI, visceral adiposity increases and releases inflammatory cytokines that negatively affect testosterone levels and mitochondrial health. Visceral adiposity, inflammation, and testosterone are involved in this deleterious process; however, there are still factors that remain unidentified. CRP, c-reactive protein; VAT, visceral adipose tissue.

Independent Predictors of Complex III Activity

Figure 3 shows the significant relationships predicting Complex III activity. Complex III activity was negatively associated with VAT:TLM ($r^2 = 0.169$, $p = 0.033$) but positively associated with testosterone ($r^2 = 0.224$, $p = 0.010$). Complex III trended toward significance and was negatively associated with VAT ($r^2 = 0.134$, $p = 0.061$), CRP ($r^2 = 0.142$, $p = 0.069$), and VAT:total trunk CSA ($r^2 = 0.140$, $p = 0.055$) (**Table 5**). Complex III activity was not independently associated with VAT:SAT, IL-6, TNF-α, IGF-1, or IGFBP-3 (data not shown). Testosterone ($r^2 = 0.177$, $p = 0.023$) and VAT:TLM ($r^2 = 0.210$, $p = 0.016$) remained significant when controlling for TSI, but CRP became insignificant. Testosterone ($r^2 = 0.269$, $p = 0.004$), IL-6 ($r^2 = 0.195$, $p = 0.035$), and VAT:TLM ($r^2 = 0.148$, $p = 0.047$) were significant when controlling for age, while VAT and VAT:total trunk CSA were no longer significantly associated with Complex III activity ($p > 0.05$; **Table 6**). All predictors remained significantly associated with Complex III activity when controlling for LOI, while VAT ($r^2 = 0.245$, $p = 0.009$), CRP ($r^2 = 0.204$, $p = 0.027$), and VAT:total trunk CSA ($r^2 = 0.239$, $p = 0.010$) became significant when controlling for LOI (**Table 6**).

Multiple Regressions to Predict Complex III Activity

Complex III was negatively associated with VAT:total trunk CSA + CRP ($r^2 = 0.286$, $p = 0.048$) and trended toward significance for VAT + CRP ($r^2 = 0.270$, $p = 0.059$) and

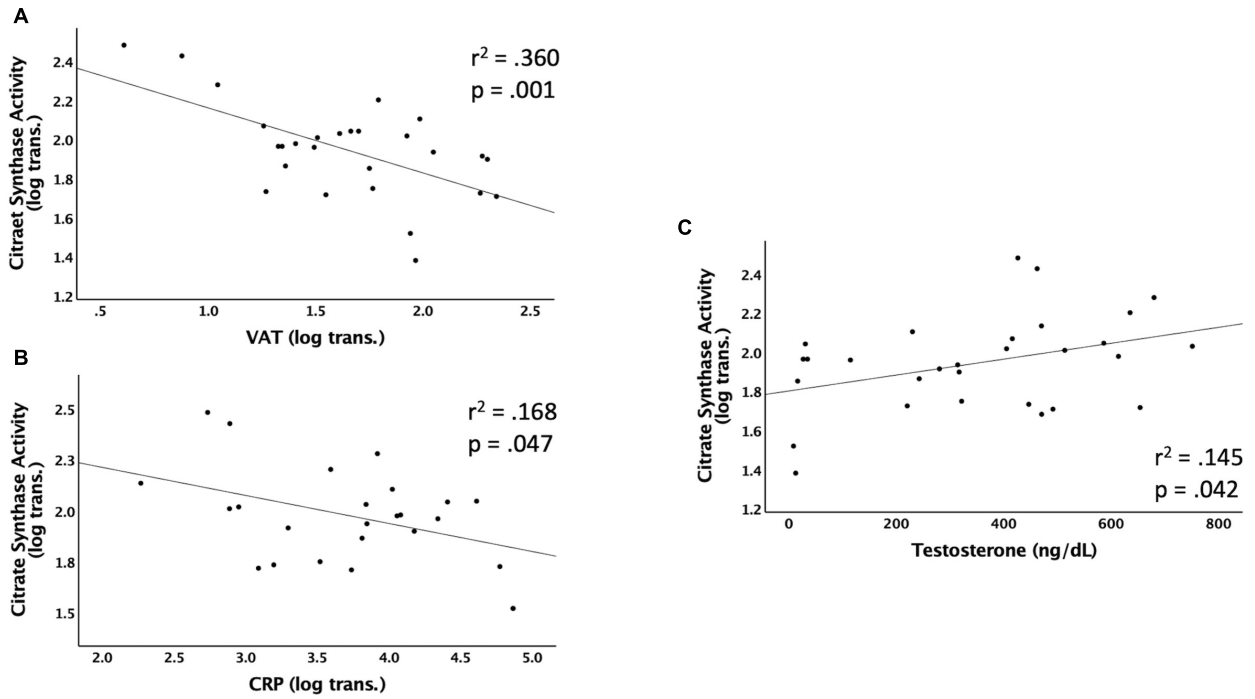

FIGURE 2 | Linear regressions predicting Citrate Synthase (CS) activity. Data that were not normally distributed were log-transformed to permit the use of parametric statistics. The log transformed values of CS enzyme activity are plotted on the Y axis against the predicted values for each variable on the X axis. **(A)** VAT (log transformed) as a predictor of CS activity, **(B)** CRP (log transformed) as a predictor of CS activity, **(C)** testosterone (ng/dL) as a predictor of CS activity. VAT, visceral adipose tissue; CRP, c-reactive protein; ng/dL, nanograms per deciliter.

VAT:TLM + CRP (r^2 = 0.275, p = 0.055). Within this model, individuals with lower VAT_{CSA} and lower CRP levels had higher Complex III activity. Complex III was also significantly associated with VAT + testosterone (r^2 = 0.277, p = 0.024), even when VAT was made relative to total trunk CSA (r^2 = 0.303, p = 0.016) and TLM (r^2 = 0.286, p = 0.021) (**Table 5**). Within this model, individuals with lower VAT_{CSA} and higher testosterone levels had higher Complex III activity. VAT + testosterone (r^2 = 0.264, p = 0.029) and VAT + CRP (r^2 = 0.286, p = 0.048) remained significant when controlling for TSI, even when VAT was made relative to total trunk CSA and TLM (**Table 6**). These relationships remained significant when controlling for age, with the exception of VAT + CRP (r^2 = 0.264, p = 0.063) and VAT:TLM + CRP (r^2 = 0.279, p = 0.053) which trended toward significance (**Table 6**). When controlling for LOI, VAT + CRP (r^2 = 0.371, p = 0.015) remained significant even when VAT was made relative to total trunk CSA (r^2 = 0.379, p = 0.014) and TLM (r^2 = 0.372, p = 0.015). VAT + testosterone (r^2 = 0.392, p = 0.003) also remained significant when controlling for LOI, even when VAT was made relative to total trunk CSA (r^2 = 0.412, p = 0.002) and TLM (r^2 = 0.397, p = 0.003) (**Table 6**). Again, individuals with lower VAT_{CSA} and higher testosterone levels had higher Complex III activity within this model. All other possible models to predict Complex III activity were tested and insignificant.

TABLE 3 | Single and multiple regressions predicting citrate synthase activity.

Predictor variables	β	r^2	*p*-value
VAT	−0.600	0.360	<0.001
Testosterone	0.380	0.145	0.042
CRP	−0.410	0.168	0.047
VAT:total trunk CSA	−0.610	0.372	<0.001
VAT:TLM	−0.659	0.434	<0.001
VAT + CRP	−0.530, −0.194	0.412	0.008
VAT + Testosterone	−0.540, 0.272	0.433	0.001
VAT:total trunk CSA + CRP	−0.561, −0.211	0.454	0.004
VAT:total trunk CSA + Testosterone	−0.562, 0.315	0.467	<0.001
VAT:TLM + CRP	−0.579, −0.151	0.444	0.005
VAT:TLM + Testosterone	−0.592, 0.210	0.473	<0.001

Single and multiple regressions predicting Citrate Synthase activity. Non-significant r^2 are not shown (non-significant = ns), but non-significant yet trending r^2 are included. Standardized Beta weights are presented to demonstrate directionality of associations.
TSI, time since injury; LOI, level of injury; VAT, visceral adipose tissue; TEST, testosterone; CRP, c-reactive protein; IL-6, interleukin 6; LM, lean mass; TLM, total lean mass; CSA, cross sectional area.

DISCUSSION

Major Findings

This study determined mitochondrial health by CS and Complex III activity, surrogate markers for mitochondrial mass, and electron transport chain activity, respectively

TABLE 4 | Single and multiple regressions predicting Citrate Synthase activity after controlling for TSI, LOI, or age.

	Citrate synthase activity r^2 (*p*-value)					
Marker	**TSI**	**β (TSI)**	**LOI**	**β (LOI)**	**Age**	**β (Age)**
VAT	0.174 (0.030)	−0.418	0.432 (<0.001)	−0.657	0.277 (0.005)	−0.526
Testosterone	ns	0.296	0.170 (0.026)	0.412	0.176 (0.023)	0.420
CRP	ns	−0.285	0.249 (0.013)	−0.499	0.184 (0.036)	−0.429
VAT:total trunk CSA	0.162 (0.038)	−0.402	0.435 (0.001)	−0.660	0.285 (0.004)	−0.534
VAT:TLM	0.264 (0.006)	−0.514	0.507 (0.001)	−0.712	0.376 (0.001)	−0.613
VAT + CRP	0.294 (0.044)	−0.479, −0.216	0.503 (0.002)	−0.546, −0.251	0.365 (0.017)	−0.449, −0.273
VAT + Testosterone	0.226 (0.053)	−0.370, 0.238	0.508 (0.001)	−0.592, 0.279	0.382 (0.004)	−0.456, 0.334
VAT:total trunk CSA + CRP	0.245 (0.022)	−0.529, −0.287	0.537 (0.001)	−0.571, −0.263	0.415 (0.008)	−0.494, −0.298
VAT:total trunk CSA + Testosterone	0.250 (0.037)	−0.396, 0.306	0.534 (0.001)	−0.606, 0.322	0.414 (0.002)	−0.483, 0.374
VAT:TLM + CRP	0.343 (0.023)	−0.533, −0.171	0.531 (0.001)	−0.599, −0.200	0.410 (0.009)	−0.515, −0.222
VAT:TLM + Testosterone	0.288 (0.020)	−0.460, 0.176	0.548 (0.001)	−0.642, 0.216	0.432 (0.001)	−0.525, 0.265
IL-6	ns	−0.382	ns	−0.389	0.237 (0.019)	−0.486
VAT + IL-6	ns	−0.479, −0.399	ns	−0.492, −0.326	0.412 (0.011)	−0.419, −0.457

Weighted least squares regressions predicting Citrate Synthase activity when controlling for TSI, LOI, or age. Non-significant r^2 are not shown (non-significant = ns), but non-significant yet trending r^2 are included. Standardized Beta weights are presented to demonstrate directionality of associations.
TSI, time since injury; LOI, level of injury; VAT, visceral adipose tissue; CRP, c-reactive protein; IL-6, interleukin 6; LM, lean mass; TLM, total lean mass; CSA, cross sectional area.

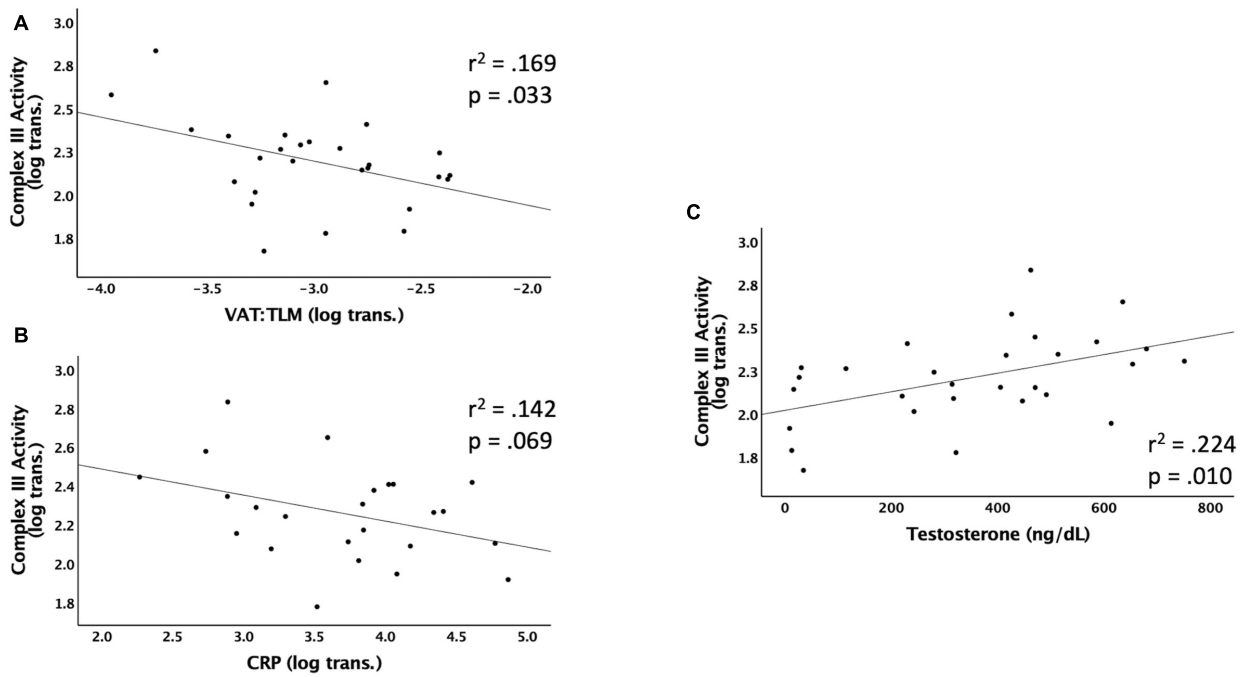

FIGURE 3 | Linear regressions predicting Complex III activity. Data that were not normally distributed were log-transformed to permit the use of parametric statistics. The log transformed values of Complex III enzyme activity are plotted on the Y axis against the predicted values for each variable on the X axis. **(A)** VAT (log transformed) relative to TLM as a predictor of Complex III activity, **(B)** CRP (log transformed) as a predictor of Complex III activity, **(C)** testosterone (ng/dL) as a predictor of Complex III activity. VAT, visceral adipose tissue; CRP, c-reactive protein; TLM, total lean mass; ng/dL, nanograms per deciliter.

(O'Brien et al., 2017b). The current findings suggest that reduced mitochondrial mass and enzyme activity can be predicted by increased visceral adiposity, inflammatory signaling, and reduced testosterone levels. Research has demonstrated that inflammation, markers of anabolism, and visceral adiposity are independently associated with mitochondria dysfunction, yet how these factors interact to predict mitochondrial function in chronic SCI is unclear. The results of the current study suggest that, in individuals with chronic SCI, lower VAT_{CSA} and higher testosterone levels or lower VAT_{CSA} and lower CRP

TABLE 5 | Single and multiple regressions predicting Complex III activity.

Predictor variables	β	r^2	*p*-value
VAT	−0.366	0.134	0.061
Testosterone	0.473	0.224	0.010
CRP	−0.377	0.142	0.069
VAT:total trunk CSA	−0.374	0.140	0.055
VAT:TLM	−0.411	0.169	0.033
VAT + CRP	−0.315, −0.294	0.270	0.059
VAT + Testosterone	−0.275, 0.390	0.277	0.024
VAT:total trunk CSA + CRP	−0.335, −0.304	0.286	0.048
VAT:total trunk CSA + Testosterone	−0.316, 0.408	0.303	0.016
VAT:TLM + CRP	−0.332, −0.275	0.275	0.055
VAT:TLM + Testosterone	−0.299, 0.359	0.286	0.021

Single and multiple regressions predicting Complex III activity. Non-significant r^2 are not reported, but non-significant yet trending r^2 are included. Standardized Beta weights are presented to demonstrate directionality of associations.
TSI, time since injury; LOI, level of injury; VAT, visceral adipose tissue; CRP, c-reactive protein; IL-6, interleukin 6; LM, lean mass; TLM, total lean mass; CSA, cross sectional area.

levels positively predict mitochondrial function. The goal of the current study was to elucidate these relationships further to inform future longitudinal intervention programs aimed at enhancing mitochondrial function. The hypothesis that a combination of increased VAT and inflammation along with reduced testosterone levels are associated with the mitochondrial dysfunction seen in chronic SCI was confirmed. To our knowledge, this is the first report to examine the combination of these variables on mitochondrial dysfunction in chronic SCI. Based on the current results, an intervention that reduces visceral adiposity, inflammatory signaling, and optimizes testosterone levels may improve mitochondrial health. Prior work demonstrated that neuromuscular electrical stimulation resistance exercise decreases VAT and inflammatory biomarkers while enhancing citrate synthase and succinate dehydrogenase activities in persons with SCI (Gorgey et al., 2019b, 2020). Future work may examine the effects of exercise or pharmaceutical interventions on the VAT-inflammation-mitochondria axis.

Mitochondrial Function and Visceral Adipose Tissue

VAT mass was negatively related to both CS and Complex III activity, which agrees with previous results (O'Brien et al., 2017b). The relationships between VAT and CS activity remained significant when controlling for TSI, age, and LOI. VAT was also negatively associated with Complex III activity when VAT was made relative to LM. VAT and VAT:total trunk CSA trended toward significance with Complex III and became significant when controlling for LOI, which may be due to VAT volume being associated with LOI (Farkas et al., 2018). Unlike previous results, VAT:SAT ratio was not independently associated with either CS or Complex III activity (O'Brien et al., 2017b). However, unlike the current study, these previous results were found only in men with motor complete SCI. Overall, there was a clear relationship between visceral adiposity and mitochondrial health. Individuals with lower VAT had higher mitochondrial mass and enzyme activity, which is in agreement with previous research (O'Brien et al., 2017b). Previous research has clearly shown that excess accumulation of VAT appears to play a significant detrimental role in cardiometabolic health (Freedland, 2004; Emmons et al., 2011; Gorgey and Gater, 2011). Indeed, O'Brien et al. (2017) demonstrated that lipid and metabolic profiles are related to mitochondrial mass and activity in individuals with SCI. Similar to the current results, O'Brien et al. (2017b) showed that many body composition measures remained related to CS and Complex III activity when

TABLE 6 | Single and multiple regressions predicting Complex III Activity after controlling for TSI, LOI, or age.

	Complex III Activity r^2 (*p*-value)					
Marker	**TSI**	**β (TSI)**	**LOI**	**β (LOI)**	**Age**	**β (Age)**
VAT	0.142 (0.053)	−0.377	0.245 (0.009)	−0.495	ns	−0.315
Testosterone	0.177 (0.023)	0.421	0.254 (0.005)	0.504	0.269 (0.004)	0.519
CRP	ns	−0.262	0.204 (0.027)	−0.451	0.159 (0.053)	−0.399
VAT:total trunk CSA	0.120 (0.077)	−0.346	0.239 (0.010)	−0.488	ns	−0.321
VAT:TLM	0.210 (0.016)	−0.459	0.283 (0.004)	−0.532	0.148 (0.047)	−0.385
VAT + CRP	0.286 (0.048)	−0.459, −0.238	0.371 (0.015)	−0.390, −0.308	0.264 (0.063)	−0.289, −0.334
VAT + Testosterone	0.264 (0.029)	−0.313, 0.355	0.392 (0.003)	−0.401, 0.394	0.300 (0.016)	−0.220, 0.458
VAT:total trunk CSA + CRP	0.317 (0.032)	−0.491, −0.305	0.379 (0.014)	−0.392, −0.324	0.290 (0.046)	−0.326, −0.347
VAT:total trunk CSA + Testosterone	0.291 (0.019)	−0.348, 0.412	0.412 (0.002)	−0.421, 0.422	0.326 (0.011)	−0.270, 0.474
VAT:TLM + CRP	0.316 (0.033)	−0.496, −0.198	0.372 (0.015)	−0.405, −0.284	0.279 (0.053)	−0.323, −0.304
VAT:TLM + Testosterone	0.299 (0.017)	−0.375, 0.307	0.397 (0.003)	−0.418, 0.357	0.313 (0.013)	−0.255, 0.425
IL−6	ns	−0.396	ns	−0.269	0.195 (0.035)	−0.422
VAT + IL−6	ns	−0.468, −398	ns	−0.423, −0.211	0.290 (0.054)	−0.312, −0.418

Weighted least squares regressions predicting Complex III activity when controlling for TSI, LOI, or age. Non-significant r^2 are not shown (non-significant = ns), but non-significant yet trending r^2 are included. Standardized Beta weights are presented to demonstrate directionality of associations.
TSI, time since injury; LOI, level of injury; VAT, visceral adipose tissue; CRP, c-reactive protein; IL-6, interleukin 6; LM, lean mass; TLM, total lean mass; CSA, cross sectional area.

normalized to thigh muscle CSA. Together, these results suggest that increased visceral adiposity results in decreased skeletal muscle mitochondrial mass and activity in individuals with chronic SCI. Future interventions targeting both reductions in VAT mass and improved mitochondrial function may enhance cardiometabolic health in individuals with chronic SCI.

Mitochondrial Function and Testosterone

Testosterone was independently associated with Complex III and CS activity even when controlling for age and LOI. VAT + testosterone was also significantly associated with both Complex III and CS activity. Individuals with lower VAT_{CSA} and higher testosterone levels had higher CS and Complex III activity within these models. These relationships were robust and remained significant when VAT was made relative to total trunk CSA or LM. The levels in the current study were 346.72 ± 223.7 ng/dL, which included six females. When excluding the females, the levels were 428.08 ± 168.93 ng/dL. Six males (25%) in the current study were hypogonadal (<300 ng/dL), 11 males (46%) were in the low normal range (i.e., 301–500 ng/dL), and seven males (29%) were in the upper range of normal (>500 ng/dL). Therefore, the majority of the males in the current study were either hypogonadal or in the low normal range and could potentially benefit from therapeutic replacement. Men with SCI have reduced testosterone levels (Clark et al., 2008; Durga et al., 2011; Bauman et al., 2014; Sullivan et al., 2018), and reduced testosterone levels are associated with greater VAT mass in men with SCI (Abilmona et al., 2019). In persons with SCI, the decline in testosterone levels is 50% greater than in able-bodied individuals (Gray et al., 1991). VAT is inversely related to plasma total and free testosterone levels in healthy men (Seidell et al., 1990). Deficient testosterone levels increase cardiometabolic risk in young men with chronic SCI. Men with SCI that have total testosterone in the low normal range (i.e., 301–500 ng/dL) have increased risk compared to men with levels in the upper range of normal (>500 ng/dL) (Sullivan et al., 2018). Indeed, low serum testosterone in men with SCI is associated with a poorer cardiometabolic prognosis than men with high serum testosterone (Abilmona et al., 2019). Previous research showed that testosterone replacement therapy can reduce VAT (Gorgey et al., 2019b) and increase peroxisome proliferator-activated receptor-γ coactivator-1α (PGC-1α), the master regulator of mitochondrial biogenesis (Gorgey et al., 2020). Future interventions targeting both reductions in VAT mass and optimization of testosterone levels may improve cardiometabolic health in individuals with chronic SCI.

Mitochondrial Function and Inflammation

CRP was significantly negatively associated with CS activity and trended toward a significant association with Complex III. VAT + CRP was also significantly negatively associated with CS activity. VAT + CRP trended toward a significant association with Complex III and became significant when VAT was made relative to total trunk CSA. Within these models, individuals with lower VAT_{CSA} and CRP levels had higher CS and Complex III activity. CRP is elevated in persons with chronic SCI (Gibson et al., 2008), is an important predictor of cardiovascular health, and can predict myocardial infarction and stroke (Ridker, 2003). In previous reports, CRP has been associated with VAT mass in various populations (Saijo et al., 2004; Pou et al., 2007; Faber et al., 2010). VAT surrounds the internal organs of the abdominal cavity (Després et al., 2001) and synthesizes and releases proinflammatory cytokines (Yudkin et al., 2005; Farkas and Gater, 2018). VAT secretes higher levels of IL-6, plasminogen activator inhibitor-1, and TNF-α compared to SAT (Farkas and Gater, 2018). While IL-6 and TNF-α were not independently associated with CS or Complex III activity in the current study, CRP is elevated in chronic SCI and is reportedly stimulated by both IL-6 and TNF-α (Edwards et al., 2008; Sam et al., 2009; Farkas and Gater, 2018). However, it is unknown if VAT directly contributes to elevated CRP levels in chronic SCI. Interestingly, IL-6 predicted mitochondrial health, but only in individuals over 40. IL-6 levels have been shown to increase with aging and are associated with increased cardiovascular disease risk (Rea et al., 2018). Future interventions targeting both reductions in VAT mass and inflammation may improve cardiometabolic health in individuals with chronic SCI.

LIMITATIONS

It should be noted that this study does not precisely identify the complex causal relationships between inflammation, testosterone, anabolic markers, visceral adiposity, and mitochondrial health among those with chronic SCI. This is a correlative analysis based on baseline cross-sectional data. A small number of females ($n = 6$ out of 33, ∼18%) were included in these analyses; however, this may serve as an added benefit to the generalizability of the results of this study because this closely mirrors the actual proportion of males and females living with SCI (NSCISC Annual Report, 2020). This study used a small sample of healthy individuals (i.e., no cardiovascular disease, type 2 diabetes, pressure ulcers, or common medical and psychiatric comorbidities), limiting the generalizability of findings beyond individuals with similar levels of function. Another concern is that conducting simultaneous multiple regressions may result in a multicollinearity problem, especially with a small sample size.

It has been suggested that for a multiple regression with six or more predictors, a sample size of at least 100 is necessary (Green, 1991). In this study, constraints such as access to this specific population and the cost of MRI and DXA limited the sample size. We attempted to limit this multicollinearity problem by including a maximum of two predictors per model. Another limitation is that high variability within the sample resulted in non-normal distributions for several variables. Since we believe it is essential to capture the true variability within the chronic SCI population, we log transformed these variables rather than eliminating statistical outliers, which would have reduced our sample size. For example, removing outliers for VAT alone would have decreased our sample by ∼17% ($n = 5$). The results of this study are exploratory, evaluating potential predictors of mitochondrial function in chronic SCI. Considering these

limitations, the current findings identify potential predictors of mitochondrial dysfunction following SCI. A large multi-center trial is highly warranted to address the aforementioned limitations effectively.

CONCLUSION

Increased visceral adiposity, associated inflammatory signaling (CRP), and reduced testosterone levels predict mitochondrial dysfunction following SCI. Specifically, lower VAT_{CSA} and higher testosterone levels or lower VAT_{CSA} and lower CRP levels positively predict mitochondrial mass and enzyme activity in persons with chronic SCI (**Figure 1**). TNF-α, IGF-1, and IGFBP-3 were not related to mitochondrial function in this study. IL-6 predicted mitochondrial health, but only in individuals over 40. Future research should further investigate the causal relationships between visceral adiposity, inflammation, testosterone, and mitochondrial health in persons with chronic SCI. Furthermore, interventional studies should be designed to examine the efficacy of diet, exercise, and potentially testosterone replacement therapy on enhancing mitochondrial health in chronic SCI.

DATA AVAILABILITY STATEMENT

The raw data supporting the conclusions of this article will be made available by the authors, without undue reservation.

ETHICS STATEMENT

The studies involving human participants were reviewed and approved by the McGuire Veteran Affairs Investigation Research Board and the Virginia Commonwealth University (VCU) Office of Research and Innovation approved the current study. The patients/participants provided their written informed consent to participate in this study.

AUTHOR CONTRIBUTIONS

RL, EL, and QC conducted the experiments. RG analyzed blood markers. JG analyzed the data, interpreted the experimental results, designed the figures and tables, and drafted the manuscript. AG, EL, and QC designed the study and interpreted the experimental results. RP assisted with the statistical modeling. AG established funding support. All authors reviewed, revised, and approved the final version of the manuscript.

FUNDING

This study was supported by the DoD-CDMRP (W81XWH-14-SCIRP-CTA). The funding agents have nothing to do with the study design, data collection, analysis, interpretation, or manuscript writing.

ACKNOWLEDGMENTS

We would like to acknowledge all our study participants, AG, for establishing funding support (DoD-CDMRP, W81XWH-14-SCIRP-CTA), the assistance of Refka Khalil, D.C. for research coordination and participant recruitment, Timothy Lavis, M.D., Lance Goetz, M.D., and Teodoro Castillo, M.D. for their help with screenings and physical examinations, technical assistance, and the Hunter Holmes McGuire Medical Center for the opportunity to conduct clinical research.

REFERENCES

Abilmona, S. M., and Gorgey, A. S. (2018). Associations of the trunk skeletal musculature and dietary intake to biomarkers of cardiometabolic health after spinal cord injury. *Clin. Physiol. Funct. Imaging* 38, 949–958. doi: 10.1111/cpf.12505

Abilmona, S. M., Sumrell, R. M., Gill, R. S., Adler, R. A., and Gorgey, A. S. (2019). Serum testosterone levels may influence body composition and cardiometabolic health in men with spinal cord injury. *Spinal Cord* 57, 229–239. doi: 10.1038/s41393-018-0207-7

Bauman, W. A., La Fountaine, M. F., and Spungen, A. M. (2014). Age-related prevalence of low testosterone in men with spinal cord injury. *J. Spinal Cord Med.* 37, 32–39. doi: 10.1179/2045772313Y.0000000122

Brass, E. P., Hiatt, W. R., Gardner, A. W., and Hoppel, C. L. (2001). Decreased NADH dehydrogenase and ubiquinol-cytochrome c oxidoreductase in peripheral arterial disease. *Am. J. Physiol. Heart Circ. Physiol.* 280, H603–9. doi: 10.1152/ajpheart.2001.280.2.H603

Buchholz, A., and Bugaresti, J. (2005). A review of body mass index and waist circumference as markers of obesity and coronary heart disease risk in persons with chronic spinal cord injury. *Spinal Cord* 43, 513–518. doi: 10.1038/sj.sc.3101744

Clark, M. J., Schopp, L. H., Mazurek, M. O., Zaniletti, I., Lammy, A. B., Martin, T. A., et al. (2008). Testosterone levels among men with spinal cord injury: relationship between time since injury and laboratory values. *Am. J. Phys. Med. Rehabil.* 87, 758–767. doi: 10.1097/phm.0b013e3181837f4f

Després, J.-P., and Lamarche, B. (1993). Effects of diet and physical activity on adiposity and body fat distribution: implications for the prevention of cardiovascular disease. *Nutr. Res. Rev.* 6, 37–159. doi: 10.1079/NRR19930010

Després, J.-P., Lemieux, I., and Prud'Homme, D. (2001). Treatment of obesity: need to focus on high risk abdominally obese patients. *BMJ* 322, 716–720. doi: 10.1136/bmj.322.7288.716

Dopier Nelson, M., Widman, L. M., Ted Abresch, R., Stanhope, K., Havel, P. J., Styne, D. M., et al. (2007). Metabolic syndrome in adolescents with spinal cord dysfunction. *J. Spinal Cord Med.* 30, S127–S139. doi: 10.1080/10790268.2007.11754591

Durga, A., Sepahpanah, F., Regozzi, M., Hastings, J., and Crane, D. A. (2011). Prevalence of testosterone deficiency after spinal cord injury. *PM R* 3, 929–932. doi: 10.1016/j.pmrj.2011.07.008

Edwards, L. A., Bugaresti, J. M., and Buchholz, A. C. (2008). Visceral adipose tissue and the ratio of visceral to subcutaneous adipose tissue are greater in adults with than in those without spinal cord injury, despite matching waist circumferences. *Am. J. Clin. Nutr.* 87, 600–607. doi: 10.1093/ajcn/87.3.600

Emmons, R. R., Garber, C. E., Cirnigliaro, C. M., Kirshblum, S. C., Spungen, A. M., and Bauman, W. A. (2011). Assessment of measures for abdominal adiposity in persons with spinal cord injury. *Ultrasound Med. Biol.* 37, 734–741. doi: 10.1016/j.ultrasmedbio.2011.02.002

Faber, D. R., van der Graaf, Y., Westerink, J., and Visseren, F. L. (2010). Increased visceral adipose tissue mass is associated with increased C-reactive protein in patients with manifest vascular diseases. *Atherosclerosis* 212, 274–280. doi: 10.1016/j.atherosclerosis.2010.04.029

Farkas, G. J., and Gater, D. R. (2018). Neurogenic obesity and systemic inflammation following spinal cord injury: a review. *J. Spinal Cord Med.* 41, 378–387. doi: 10.1080/10790268.2017.1357104

Farkas, G. J., Gorgey, A. S., Dolbow, D. R., Berg, A. S., and Gater, D. R. (2018). The influence of level of spinal cord injury on adipose tissue and its relationship to inflammatory adipokines and cardiometabolic profiles. *J. Spinal Cord Med.* 41, 407–415. doi: 10.1080/10790268.2017.1357918

Fox, C., Massaro, J., Hoffmann, U., Pou, K., Maurovich-Horvat, P., Liu, C., et al. (2007). Abdominal visceral and subcutaneous adipose tissue compartments: association with metabolic risk factors in the Framingham Heart Study. *Circulation* 116, 39–48. doi: 10.1161/CIRCULATIONAHA.106.675355

Freedland, E. S. (2004). Role of a critical visceral adipose tissue threshold (CVATT) in metabolic syndrome: implications for controlling dietary carbohydrates: a review. *Nutr. Metab.* 1:12. doi: 10.1186/1743-7075-1-12

Gibson, A., Buchholz, A., and Ginis, K. M. (2008). C-Reactive protein in adults with chronic spinal cord injury: increased chronic inflammation in tetraplegia vs paraplegia. *Spinal Cord* 46, 616–621. doi: 10.1038/sc.2008.32

Gill, S., Sumrell, R. M., Sima, A., Cifu, D. X., and Gorgey, A. S. (2020). Waist circumference cutoff identifying risks of obesity, metabolic syndrome, and cardiovascular disease in men with spinal cord injury. *PLoS One* 15:e0236752. doi: 10.1371/journal.pone.0236752

Goldsmith, J. A., Ennasr, A. N., Farkas, G. J., Gater, D. R., and Gorgey, A. S. (2021). Role of exercise on visceral adiposity after spinal cord injury: a cardiometabolic risk factor. *Eur. J. Appl. Physiol.* 121, 2143–2163. doi: 10.1007/s00421-021-04688-3

Gorgey, A. S., Dolbow, D. R., Dolbow, J. D., Khalil, R. K., Castillo, C., and Gater, D. R. (2014). Effects of spinal cord injury on body composition and metabolic profile–Part I. *J. Spinal Cord Med.* 37, 693–702. doi: 10.1179/2045772314Y.0000000245

Gorgey, A. S., Ennasr, A. N., Farkas, G. J., and Gater, D. R. Jr. (2021). Anthropometric Prediction of Visceral Adiposity in Persons With Spinal Cord Injury. *Top. Spinal Cord Inj. Rehabil.* 27, 23–35. doi: 10.46292/sci20-00055

Gorgey, A. S., and Gater, D. R. (2011). Regional and relative adiposity patterns in relation to carbohydrate and lipid metabolism in men with spinal cord injury. *Appl. Physiol. Nutr. Metab.* 36, 107–114. doi: 10.1139/H10-091

Gorgey, A. S., Graham, Z. A., Chen, Q., Rivers, J., Adler, R. A., Lesnefsky, E. J., et al. (2020). Sixteen weeks of testosterone with or without evoked resistance training on protein expression, fiber hypertrophy and mitochondrial health after spinal cord injury. *J. Appl. Physiol.* 128, 1487–1496. doi: 10.1152/japplphysiol.00865.2019

Gorgey, A. S., Khalil, R. E., Davis, J. C., Carter, W., Gill, R., Rivers, J., et al. (2019a). Skeletal muscle hypertrophy and attenuation of cardio-metabolic risk factors (SHARC) using functional electrical stimulation-lower extremity cycling in persons with spinal cord injury: study protocol for a randomized clinical trial. *Trials* 20:526. doi: 10.1186/s13063-019-3560-8

Gorgey, A. S., Khalil, R. E., Gill, R., Gater, D. R., Lavis, T. D., Cardozo, C. P., et al. (2019b). Low-dose testosterone and evoked resistance exercise after spinal cord injury on cardio-metabolic risk factors: an open-label randomized clinical trial. *J. Neurotrauma* 36, 2631–2645. doi: 10.1089/neu.2018.6136

Gorgey, A. S., Mather, K. J., and Gater, D. R. (2011). Central adiposity associations to carbohydrate and lipid metabolism in individuals with complete motor spinal cord injury. *Metabolism* 60, 843–851. doi: 10.1016/j.metabol.2010.08.002

Gray, A., Feldman, H. A., McKinlay, J. B., and Longcope, C. (1991). Age, disease, and changing sex hormone levels in middle-aged men: results of the Massachusetts Male Aging Study. *J. Clin. Endocrinol. Metab.* 73, 1016–1025. doi: 10.1210/jcem-73-5-1016

Green, S. B. (1991). How many subjects does it take to do a regression analysis. *Multivariate Behav. Res.* 26, 499–510. doi: 10.1207/s15327906mbr2603_7

Grundy, S. M., Brewer, H. B Jr., Cleeman, J. I., Smith, S. C Jr., Lenfant, C. (2004). Definition of metabolic syndrome: report of the National Heart. *Circulation* 109, 433–438. doi: 10.1161/01.cir.0000111245.75752.c6

Katzmarzyk, P. T., Heymsfield, S. B., and Bouchard, C. (2013). Clinical utility of visceral adipose tissue for the identification of cardiometabolic risk in white and African American adults. *Am. J. Clin. Nutr.* 97, 480–486. doi: 10.3945/ajcn.112.047787

LaVela, S. L., Weaver, F. M., Goldstein, B., Chen, K., Miskevics, S., Rajan, S., et al. (2006). Diabetes mellitus in individuals with spinal cord injury or disorder. *J. Spinal Cord Med.* 29, 387–395. doi: 10.1080/10790268.2006.11753887

Lee, J. J., Pedley, A., Hoffmann, U., Massaro, J. M., Levy, D., and Long, M. T. (2018). Visceral and intrahepatic fat are associated with cardiometabolic risk factors above other ectopic fat depots: the Framingham Heart Study. *Am. J. Med.* 131, 684–692. doi: 10.1016/j.amjmed.2018.02.002

Lester, R. M., Ghatas, M. P., Khan, R. M., and Gorgey, A. S. (2019). Prediction of thigh skeletal muscle mass using dual energy x-ray absorptiometry compared to magnetic resonance imaging after spinal cord injury. *J. Spinal Cord Med.* 42, 622–630. doi: 10.1080/10790268.2019.1570438

Nash, M. S., and Gater, D. R. (2020). Cardiometabolic disease and dysfunction following spinal cord injury: origins and guideline-based countermeasures. *Phys. Med. Rehabil. Clin.* 31, 415–436. doi: 10.1016/j.pmr.2020.04.005

Nicklas, B. J., Penninx, B. W., Ryan, A. S., Berman, D. M., Lynch, N. A., and Dennis, K. E. (2003). Visceral adipose tissue cutoffs associated with metabolic risk factors for coronary heart disease in women. *Diabetes Care* 26, 1413–1420. doi: 10.2337/diacare.26.5.1413

NSCISC Annual Report (2020). *National Spinal Cord Injury Statistical Center. 2020 Annual Statistical Report for the Spinal Cord Injury Model Systems*. Birmingham: University of Alabama at Birmingham.

O'Brien, L. C., Chen, Q., Savas, J., Lesnefsky, E. J., and Gorgey, A. S. (2017). Skeletal muscle mitochondrial mass is linked to lipid and metabolic profile in individuals with spinal cord injury. *Eur. J. Appl. Physiol.* 117, 2137–2147.

O'Brien, L. C., Wade, R. C., Segal, L., Chen, Q., Savas, J., Lesnefsky, E. J., et al. (2017b). Mitochondrial mass and activity as a function of body composition in individuals with spinal cord injury. *Physiol. Rep.* 5:e13080. doi: 10.14814/phy2.13080

O'Brien, L. C., Chen, Q., Savas, J., Lesnefsky, E. J., and Gorgey, A. S. (2017a). Skeletal muscle mitochondrial mass is linked to lipid and metabolic profile in individuals with spinal cord injury. *Eur. J. Appl. Physiol.* 117, 2137–2147. doi: 10.1007/s00421-017-3687-9

O'Brien, L. C., Graham, Z. A., Chen, Q., Lesnefsky, E. J., Cardozo, C., and Gorgey, A. S. (2018). Plasma adiponectin levels are correlated with body composition, metabolic profiles, and mitochondrial markers in individuals with chronic spinal cord injury. *Spinal Cord* 56, 863–872. doi: 10.1038/s41393-018-0089-8

Pou, K. M., Massaro, J. M., Hoffmann, U., Vasan, R. S., Maurovich-Horvat, P., Larson, M. G., et al. (2007). Visceral and subcutaneous adipose tissue volumes are cross-sectionally related to markers of inflammation and oxidative stress: the Framingham Heart Study. *Circulation* 116, 1234–1241. doi: 10.1161/CIRCULATIONAHA.107.710509

Poznyak, A. V., Ivanova, E. A., Sobenin, I. A., Yet, S.-F., and Orekhov, A. N. (2020). The role of mitochondria in cardiovascular diseases. *Biology* 9:137.

Rea, I. M., Gibson, D. S., McGilligan, V., McNerlan, S. E., Alexander, H. D., and Ross, O. A. (2018). Age and age-related diseases: role of inflammation triggers and cytokines. *Front. Immunol.* 9:586. doi: 10.3389/fimmu.2018.00586

Reginster, J.-Y., and Burlet, N. (2006). Osteoporosis: a still increasing prevalence. *Bone* 38, 4–9. doi: 10.1016/j.bone.2005.11.024

Ridker, P. M. (2003). C-reactive protein: a simple test to help predict risk of heart attack and stroke. *Circulation* 108, e81–5. doi: 10.1161/01.CIR.0000093381.57779.67

Saijo, Y., Kiyota, N., Kawasaki, Y., Miyazaki, Y., Kashimura, J., Fukuda, M., et al. (2004). Relationship between C-reactive protein and visceral adipose tissue in healthy Japanese subjects. *Diabetes Obes. Metab.* 6, 249–258. doi: 10.1111/j.1462-8902.2003.0342.x

Sam, S., Haffner, S., Davidson, M. H., D'Agostino, R. B., Feinstein, S., Kondos, G., et al. (2009). Relation of abdominal fat depots to systemic markers of inflammation in type 2 diabetes. *Diabetes Care* 32, 932–937. doi: 10.2337/dc08-1856

Schladen, M., and Groah, S. (2014). State of the science on cardiometabolic risk after spinal cord injury: recap of the 2013 ASIA pre-conference on cardiometabolic disease. *Top. Spinal Cord INJ. Rehabil.* 20, 105–112. doi: 10.1310/sci2002-105

Seidell, J. C., Björntorp, P., Sjöström, L., Kvist, H., and Sannerstedt, R. (1990). Visceral fat accumulation in men is positively associated with insulin, glucose,

and C-peptide levels, but negatively with testosterone levels. *Metabolism* 39, 897–901. doi: 10.1016/0026-0495(90)90297-p

Spinazzi, M., Casarin, A., Pertegato, V., Salviati, L., and Angelini, C. (2012). Assessment of mitochondrial respiratory chain enzymatic activities on tissues and cultured cells. *Nature protocols* 7, 1235–1246. doi: 10.1038/nprot.2012.058

Sullivan, S. D., Nash, M. S., Tefara, E., Tinsley, E., and Groah, S. (2018). Relationship between gonadal function and cardiometabolic risk in young men with chronic spinal cord injury. *PMR* 10, 373–381. doi: 10.1016/j.pmrj.2017.08.404

Sumrell, R. M., Nightingale, T. E., McCauley, L. S., and Gorgey, A. S. (2018). Anthropometric cutoffs and associations with visceral adiposity and metabolic biomarkers after spinal cord injury. *PLoS One* 13:e0203049. doi: 10.1371/journal.pone.0203049

Yudkin, J. S., Eringa, E., and Stehouwer, C. D. (2005). "Vasocrine" signalling from perivascular fat: a mechanism linking insulin resistance to vascular disease. *Lancet* 365, 1817–1820. doi: 10.1016/S0140-6736(05)66585-3

Conflict of Interest: The authors declare that the research was conducted in the absence of any commercial or financial relationships that could be construed as a potential conflict of interest.

Publisher's Note: All claims expressed in this article are solely those of the authors and do not necessarily represent those of their affiliated organizations, or those of the publisher, the editors and the reviewers. Any product that may be evaluated in this article, or claim that may be made by its manufacturer, is not guaranteed or endorsed by the publisher.

Copyright © 2022 Goldsmith, Lai, Garten, Chen, Lesnefsky, Perera and Gorgey. This is an open-access article distributed under the terms of the Creative Commons Attribution License (CC BY). The use, distribution or reproduction in other forums is permitted, provided the original author(s) and the copyright owner(s) are credited and that the original publication in this journal is cited, in accordance with accepted academic practice. No use, distribution or reproduction is permitted which does not comply with these terms.

frontiers in Endocrinology

MINI REVIEW
published: 17 February 2022
doi: 10.3389/fendo.2022.849877

Global Adipose Tissue Remodeling During the First Month of Postnatal Life in Mice

Johanna Bruder[1,2] *and Tobias Fromme*[2]*

[1] Else Kröner-Fresenius Center for Nutritional Medicine (EKFZ), Technical University of Munich, Freising, Germany, [2] Chair of Molecular Nutritional Medicine, TUM School of Life Sciences, Technical University of Munich, Freising, Germany

During the first month of postnatal life, adipose tissue depots of mice go through a drastic, but transient, remodeling process. Between postnatal days 10 and 20, several white fat depots display a strong and sudden surge in beige adipocyte emergence that reverts until day 30. At the same time, brown fat depots appear to undergo an opposite phenomenon. We comprehensively describe these events, their depot specificity and known environmental and genetic interactions, such as maternal diet, housing temperature and mouse strain. We further discuss potential mechanisms and plausible purposes, including the tempting hypothesis that postnatal transient remodeling creates a lasting adaptive capacity still detectable in adult animals. Finally, we propose postnatal adipose tissue remodeling as a model process to investigate mechanisms of beige adipocyte recruitment advantageous to cold exposure or adrenergic stimulation in its entirely endogenous sequence of events without external manipulation.

Keywords: white adipose tissue (WAT), white adipose tissue (WAT) browning, brown adipose tissue (BAT), beige adipocyte, postnatal, organ development

OPEN ACCESS

Edited by:
Seung-Hyun Ro, University of Nebraska-Lincoln, United States

Reviewed by:
Alexander Bartelt, Ludwig Maximilian University of Munich, Germany

***Correspondence:**
Tobias Fromme
fromme@tum.de

Specialty section:
This article was submitted to Obesity, a section of the journal Frontiers in Endocrinology

Received: *06 January 2022*
Accepted: *21 January 2022*
Published: *17 February 2022*

Citation:
Bruder J and Fromme T (2022) Global Adipose Tissue Remodeling During the First Month of Postnatal Life in Mice. Front. Endocrinol. 13:849877. doi: 10.3389/fendo.2022.849877

INTRODUCTION

Mammalian adipose tissue is a plastic organ with the capacity to dramatically alter size and composition. White adipose tissue (WAT) represents the classical, fat-storing adipose tissue composed of large cells with a single lipid droplet. It also acts as an endocrine organ secreting hormones, such as adiponectin and leptin. Brown adipose tissue (BAT), on the other hand, provides a means of non-shivering thermogenesis in many mammals including adult humans (1–3). It consists of multilocular cells equipped with many mitochondria featuring uncoupling protein 1 (UCP1), the functional core of heat generation. By uncoupling respiration from ATP synthesis, energy of proton motive force is dissipated as heat [reviewed in (4)]. Beyond BAT, UCP1 expressing multilocular cells with high thermogenic capacity are also found interspersed within WAT depots, a cell population called beige or brite adipocytes (5–7).

Mechanisms governing the considerable variability and plasticity of beige cell number are subject to intense research for their potential targeting in humans. Beige and brown adipocyte overall thermogenic capacity is a bottleneck in the efficacy of brown fat targeting drugs in development for the treatment of metabolic disease (8–10).

Well investigated models include cold exposure and application of β-adrenergic agonists in rodents (6, 11). Less studied is a phenomenon that occurs even in the absence of external intervention, i.e. the global remodeling of adipose tissues early in mouse postnatal life.

TRANSIENT, POSTNATAL ADIPOSE TISSUE REMODELING

During the first three weeks of postnatal life, murine adipose tissues undergo a drastic, if transient, remodeling. This phenomenon was first observed in retroperitoneal WAT (rWAT) of male A/J and C57BL6/J mice (12). Here, UCP1 transcript and protein expression sharply increases between postnatal day 10 and 20, only to decrease again towards day 30. A similar transient browning of WAT was again reported for rWAT and inguinal WAT (iWAT) of 1296sv/ev and C57BL6/N mice (13). Thus, a surge in WAT browning takes place around day 20 in multiple fat depots and all studied mouse strains, while in BAT and epididymal WAT (eWAT), UCP1 expression remained unchanged during this period. The extent of this transient remodeling is different by mouse strain and ambient temperature, as comprehensively reviewed below. Our understanding of its exact temporal sequence is limited by the choice of time points studied with low resolution in the past: peak browning has been varyingly detected at day 20 (12–15), several days earlier (16) or later (17, 18).

Interestingly, inguinal and retroperitoneal – but not BAT - depots display arrested growth during browning between postnatal day 10 and 20, indicating a profound, depot-level remodeling event (13). Indeed, visualized by phase contrast computed tomography, virtually all mouse fat depots undergo a significant transient period of remodeling around day 20 (14). The evaluated electron density is a combined (alas inseparable) measure of fat content and mitochondrial density and clearly portrays the strong browning surge in rWAT, iWAT and other white depots. Surprisingly, a concomitant, but reverse, remodeling appears to occur in BAT depots. Since this 'whitening' surge in BAT does not include altered UCP1 expression (12), it is likely explained by altered fat, not mitochondrial, content. To date it remains unclear whether concurrent 'whitening of BAT' and 'browning of WAT' are separate events or aspects of the same epi-phenomenon.

ADIPOSE TISSUE DEVELOPMENT AND PLASTICITY

White and brown fat differ in extent and direction of postnatal remodeling as well as in their preceding development. BAT fully develops before birth, as determined by mass, UCP1 transcript and protein expression (12, 19). Immediately at birth, pups have to be able to defend body temperature. After birth, brown adipose tissue still grows, mainly due to proliferation until postnatal day 14 and thereafter by storing more lipid (20), a transition suggestively synchronous to the observed whitening (14).

Compared to BAT, development of WAT is less advanced at birth. The iWAT and rWAT depots are still very small, although development has started in the embryo already (21, 22) and existing adipocytes are essentially functional (22, 23). In the first days, these depots expand quickly (23–25). More delayed, functional gonadal WAT (gWAT) is absent at birth (21–23). The first fully differentiated cells do not appear until day 7 (23). The depot specificity of this developmental timeline matches the pattern of depot specific postnatal remodeling with transient browning in fully differentiated WAT depots, but not in still immature eWAT. Intriguingly, and plausibly a repercussion, adult mouse eWAT is considered the whitest depot of all, containing the least fraction of beige adipocytes.

In the adult mouse, adipose tissue remains an organ with extraordinary plasticity that constantly adapts to environmental challenges. Its most obvious flexibility is the huge expandability by combined hyperplasia and hypertrophy, i.e. by adding more adipocytes and by increasing their triglyceride stores (26). Fat mass increase in response to positive energy balance is predominantly attributable to the largest subcutaneous depot, iWAT. The largest visceral adipose tissue depot, gWAT, also has the capability to store an enormous amount of lipids, but in contrast to iWAT it decreases expansion speed after several weeks of high fat diet feeding (27, 28). In comparison to postnatal remodeling, however, the pattern of expansion potential (high in both gWAT and iWAT, low in rWAT) does not seem to match the proneness to transient browning (high in iWAT and rWAT, low in gWAT).

Another plastic characteristic of WAT in adult mice is the flexible number of interspersed beige adipocytes. The interconversion from white to beige adipocytes is a reversible, adaptive process (29), conferring varying degrees of non-shivering thermogenic capacity (30, 31). Accordingly, beige adipocyte recruitment is intensely studied as putative pharmacological target process in the field of metabolic disease [reviewed in (32)]. In iWAT, cold stimulation leads to a strong increase in the number of beige adipocytes (11). On the contrary, thermoneutrality decreases thermogenic beige cell number in mice (33). Being fully reversible, the process can repeatedly be re-activated anytime by another bout of cold stimulation (34), although to a lesser extent with increasing age (31). Intriguingly, adaptive browning in response to cold in the adult mouse displays a similar pattern as postnatal, transient browning, both on the level of depot specificity and in the proneness of different mouse strains. Either both the postnatal, transient process and its adult, adaptive counterpart are subject to the same underlying preconditions or the former establishes the capacity of the latter. Indeed, ablation of postnatally recruited beige cells impairs cold-induced beige adipocyte formation in the adult animal (18).

POTENTIAL MECHANISMS OF ADIPOSE TISSUE REMODELING

Postnatal remodeling of mouse fat depots is characterized by parallel changes in the abundance of UCP1 transcript,

mitochondrial density, fat content, and histological appearance (12–14). Categorically, these changes can be driven by differentiation of new cells with different characteristics or, alternatively or additionally, by the transdifferentiation of existing mature adipocytes. These same two options apply for the second, reverting phase of remodeling and not necessarily to the same extent.

Both mechanisms, stem cell differentiation and transdifferentiation, in principle exist and have been described to contribute to adipose tissue plasticity. The existence of the former is non-controversial as every mature adipocyte necessarily descends from a precursor, i.e. a committed preadipocyte and that in turn from a pluripotent, mesenchymal stem cell (35–37). During maintenance, cellular turnover in adipose tissues is regarded to be low, ~10%/year (38). At the same time, the vast expandability of adipose tissue mass in response to prolonged, positive energy balance showcases the massive capacity to generate new adipocytes when hypertrophy of existing ones is exceeded [reviewed in (39)]. In addition, the quick expansion of certain virtually absent adipose tissue depots directly after birth provides ample support for the possibility of rapid hyperplasia being behind the observed remodeling.

The second option, transdifferentiation of preexisting mature adipocytes, has long been suspected and recently proved to constitute a relevant *in vivo* mechanism of white/beige fat cell conversions (29, 40). During this process, formerly white adipocytes acquire the characteristics of beige adipocytes and vice versa. As of today, it is unknown whether all or most white adipocytes inherently possess this ability or only a subset of 'camouflaged', white-appearing beige precursors. In any case, the sudden appearance and disappearance of white versus beige adipocytes during postnatal adipose tissue remodeling would be well in line with a transdifferentiation process and importantly, would as such not require massive proliferation and later apoptosis (41). These two latter processes thereby represent indicators to differentiate between the underlying processes at work, but have not been studied exhaustively in this context. At least as far as proliferation is concerned, virtually all adipocytes present at postnatal day 28 (late in the remodeling phase) seem to have already been present at day 10 (early in the remodeling phase), in murine subcutaneous fat that is prone to browning (21), arguing against progenitor proliferation and differentiation as a significant source of beige adipocytes.

Further available evidence to distinguish differentiation from transdifferentiation is limited to depot mass and volume changes concomitant to postnatal browning/whitening. While admittedly crude proxies, these clearly correlate with adipose tissue remodeling, i.e. depots arrest growth during browning and do not during whitening, both on the level of individual fat depots (13) and as a general trend across all depots (14). Specifically in white fat and far from a final assessment, these observations are in line with predominant transdifferentiation of existing cells during both the browning of white fat and its reversion, possibly accompanied by a diluting effect of newly differentiating cells during the latter phase.

POTENTIAL PHYSIOLOGICAL PURPOSES OF POSTNATAL ADIPOSE TISSUE REMODELING

Apart from the exact mechanisms at work bringing about postnatal, transient fat browning or whitening, the overarching question certainly pertains to the 'why' of this adipose organ-wide phenomenon. Two alternative, principal scenarios are possible: first, adipose tissues are transiently remodeled to serve an acute functional purpose specific during this short period in postnatal development, or second, postnatal adipose tissue remodeling is a preparative phenomenon creating a cellular complexity to be adaptively utilized during adult life. The crucial difference between these is whether those adipocytes that underwent a transient change revert to their original state after fulfilling a transient role or whether they become a new type of cell with perpetually altered adaptive potential.

At three weeks of age, mice are typically weaned and forced to replace a diet of mother's milk with solid food, a transition with plausible profound effects on metabolism and adipose tissues. Left with the dam, pups still undergo adipose tissue remodeling (13), but must be expected to start nibbling solid food around the same age. How and why this dietary transition would lead to a massive bout of WAT browning seems questionable. More intuitively, the thermoregulatory requirements of small, fur-less mouse pups support a functional role of transient browning in non-shivering thermogenesis. Birth marks a radical transition from the controlled, thermoneutral environment of the womb into a cool world. This plausibly requires a transient extra-capacity of non-shivering thermogenesis that is later alleviated by a rapidly decreasing surface-to-volume ratio and fur growth. Indeed, brown adipose tissue is already fully developed at birth, while non-thermogenic white adipose tissue development occurs mostly postnatally (42, 43).

As plausible as this interpretation sounds, it fails to explain a simultaneous whitening of brown adipose tissues, if these two transitions are in fact causally connected. Both types of adipose tissue undergo postnatal developmental stages possibly accounting for the observed remodeling events: although functional at birth, BAT continues growth by an initial postnatal phase of rapid precursor proliferation and subsequent terminal differentiation including triglyceride loading (20). At the turning point, these events may be misinterpreted as whitening of existing brown adipocytes. In comparison with the adult version of BAT whitening during extended periods of thermoneutrality, postnatal whitening appears to be limited to fat content, not UCP1 abundance, and thus to serve a different purpose (14). Possibly, increased fat content is the consequence of a developmental bout of increased *de novo* lipogenesis, a powerful, cold-stimulated process in mature BAT (44, 45). Similarly, white adipose tissue experiences a distinct postnatal phase of strong sympathetic neurite innervation independent of ambient temperature (16, 17). This may be accompanied by a transient increase in sympathetic tone during the establishment of ligand-receptor connections, in turn underlying an apparent browning.

Importantly, none of these options are mutually exclusive and the causal reason may be distinct from the final one. Browning caused by developmental innervation may at the same time serve the acute purpose of additional thermogenic capacity or create a subset of adipocytes pre-programmed to serve as future beige adipocytes in the adult animal. The existence of the latter, the creation of a separate pool of cells with adaptive potential in the adult animal, is clearly evidenced by reduced, cold-induced browning of adult WAT after ablation of postnatal beige cells (18). Their functional role can be probed by comprehensive mapping of the adult, phenotypic response to a variety of metabolic and environmental challenges after manipulating postnatal browning/whitening surge intensity, as outlined in the following.

FACTORS MODULATING POSTNATAL ADIPOSE TISSUE REMODELING

Genetic background plays an important role in postnatal adipose tissue remodeling. Several studies established a different susceptibility to transient WAT browning, e.g. lower in C67BL6/J and /N compared to A/J or 129SvEv mice (12, 13, 15). This pattern matches well with the known propensity to adult, adaptive browning (30, 46–48). Phenotypic strain differences offer the chance to identify genetic factors (48), but efforts to identify adult consequences of postnatal adipose tissue remodeling will be superimposed by unrelated differences in genetic outfit. Ideally, postnatal events could be gradually manipulated in genetically identical animals followed by comprehensive mapping of the adult response to metabolic challenges.

The ontogenetic earliness of postnatal adipose tissue remodeling limits the experimental options to manipulate these events to the first days in life or to maternal effects (maternal programming). Luckily, there is evidence for the efficacy of both. The most obvious environmental parameter interacting with the abundance of thermogenic cells is ambient temperature. Indeed, the peak of postnatal browning in iWAT occurs earlier (day 21) and is more pronounced when offspring and dam are housed at 30°C as compared to 22°C (day 28) (17). Furthermore, offspring of dams housed at 17°C during lactation showed higher UCP1 expression in iWAT at postnatal day 21 than of dams at thermoneutrality (15). When exposed to cold as adults, however, temperature early in life did not impact later browning capacity in fat depots in this study. Since ablation of postnatally recruited beige cells did lead to an adult limitation of browning capacity (18), it will be interesting to investigate the extent at which a postnatal manipulation robustly manifests in adult, metabolic consequences in future studies.

An alternative condition to manipulate postnatal adipose tissue remodeling in pups is maternal diet quality and quantity during gestation or lactation. Indeed, undernutrition of pups leads to reduced postnatal browning at postnatal day 21 in iWAT, while overfeeding does not (49). Interestingly, neither affects susceptibility to diet induced obesity later in life or the extent of browning in response to cold exposure. Adult UCP1 expression and thermogenic capacity of BAT, however, is clearly altered in response to manipulated maternal lactation, either by high fat diet feeding or as a function of litter size (50–52). Possibly, a direct effect of these regimes on postnatal BAT remodeling programs this tissue to different states of adult adaptability. And indeed, altered milk quality acutely impacts postnatal adipose tissue remodeling, as demonstrated by supplementation of n-3 polyunsaturated fatty acids to lactating dams (53). This dietary challenge leads to increased BAT UCP1 transcript and protein expression in 21 day old pups. It remains to be tested whether these direct, postnatal effects of lactation are a causal step along the causal route of maternal programming of adult BAT adaptability.

A further approach is based on the development of adipose tissue sympathetic innervation. In adult mice, sympathetic norepinephrine recruits and activates beige/brown adipocytes (54). Sympathetic innervation development and postnatal browning of white adipose tissue have recently been debated to be causally linked (55) or not (17). In any case, from postnatal day 6 onwards, sympathetic innervation and number of beige cells concomitantly increase in iWAT of C57BL6/J mice, until a peak around day 12-16 (16). Importantly, the hormone leptin constitutes the key driver of sympathetic innervation, potentially offering an experimental route to influence postnatal browning in iWAT. Experiments with ob/ob mice, devoid of leptin, revealed less beige adipocytes as well as less dense sympathetic innervation in iWAT, while daily leptin injections between postnatal days 8 and 16 rescued this phenotype (55).

Taken together, ambient temperature and maternal diet are efficient means to manipulate both postnatal adipose tissue remodeling and adult cold response. Initial such experiments report conflicting evidence on a possible causal link between the two.

DISCUSSION AND OUTLOOK

During the past decade, many studies have corroborated postnatal adipose tissue remodeling (12–14, 17, 19, 21, 55) and addressed putative functional aspects [reviewed in (56)] (**Figure 1**). It is now clear that virtually all fat depots, white and brown, simultaneously undergo transient remodeling during the first weeks of postnatal life (14). It is unknown whether 'whitening in brown' and 'browning in white' fat are independent or linked.

The key question is why these changes occur and whether they serve an acute physiological purpose or are a developmental step in the preparation of later, adult capabilities. Both scenarios can be addressed by similar experimental models, i.e. the targeted manipulation of postnatal events and measurement of acute and delayed impairment of metabolic flexibility. A first step in this direction has already been undertaken by the targeted ablation of postnatally recruited beige cells. This intervention does indeed impair browning capacity later in life (18). Less drastic regimes employing ambient temperature, litter size and maternal diet quality and quantity did, however, not yield unequivocal results so far (15, 17, 50–53, 55). Manipulations of leptin levels

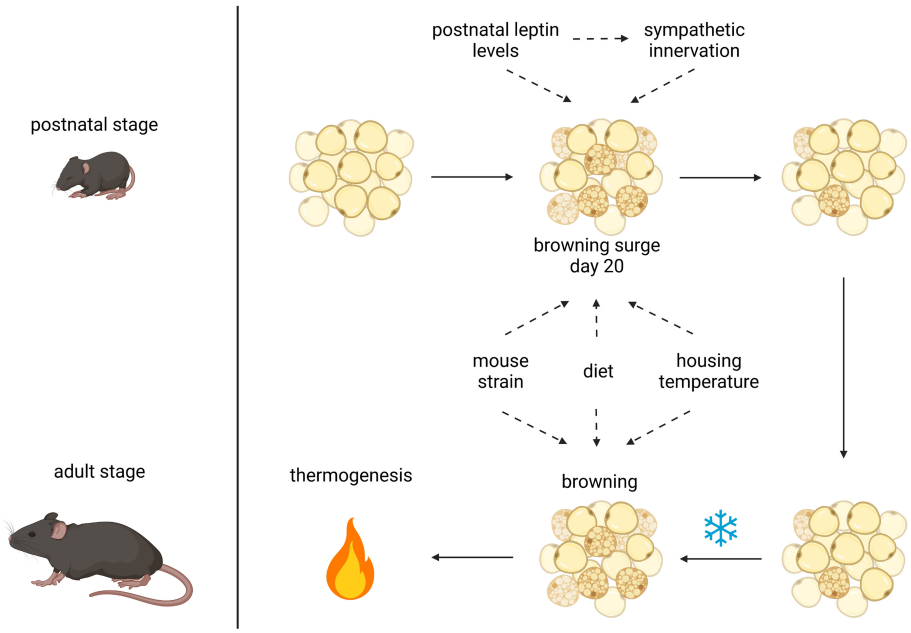

FIGURE 1 | Postnatal and adult adipose tissue remodeling and its possible influencing factors. Browning of white adipose tissue after birth may be affected by leptin levels, sympathetic innervation, mouse strain, maternal diet and housing temperature. The latter 3 factors also have an impact on browning of WAT in the adult animal upon cold stimulation to induce thermogenesis, possibly in concert with postnatally acquired capabilities; created with BioRender.com.

constitute additional, experimental opportunities *via* its role during developmental adipose tissue innervation.

Beyond acute thermogenic activation, modulating the capacity and number of brown and beige adipocytes has long been identified a key challenge in their pharmacological exploitation in human metabolic disease. While cold-induced and adrenergic recruitment in rodent models have been intensely studied to identify putative target mechanisms, postnatal adipose tissue remodeling has attracted much less attention - an undeserved neglect in the light of its endogenous occurrence without external intervention, offering an unbiased mechanistic discovery potential.

AUTHOR CONTRIBUTIONS

Both authors jointly and equally conceived, wrote and approved the manuscript.

FUNDING

JB is supported by the Else Kröner-Fresenius Stiftung (EKFS). TF is supported by the German Research Foundation (DFG; FR 3628/2-1 and TRR333/1 - 450149205).

REFERENCES

1. Saito M, Okamatsu-Ogura Y, Matsushita M, Watanabe K, Yoneshiro T, Nio-Kobayashi J, et al. High Incidence of Metabolically Active Brown Adipose Tissue in Healthy Adult Humans: Effects of Cold Exposure and Adiposity. *Diabetes* (2009) 58(7):1526–31. doi: 10.2337/db09-0530
2. Van Marken Lichtenbelt WD, Vanhommerig JW, Smulders NM, Drossaerts JMAFL, Kemerink GJ, Bouvy ND, et al. Cold-Activated Brown Adipose Tissue in Healthy Men. *N Engl J Med* (2009) 360(15):1500–8. doi: 10.1056/NEJMoa0808718
3. Cypess AM, Lehman S, Williams G, Tal I, Rodman D, Goldfine AB, et al. Identification and Importance of Brown Adipose Tissue in Adult Humans. *N Engl J Med* (2009) 360(15):1509–17. doi: 10.1056/NEJMoa0810780
4. Klingenspor M, Bast A, Bolze F, Li Y, Maurer S, Schweizer S, et al. Chapter 4 Brown Adipose Tissue. In: ME Symonds, editor. *Adipose Tissue Biology*, *2nd*. New York: Springer International Publishing (2017). p. 91–147.
5. Wu J, Boström P, Sparks LM, Ye L, Choi JH, Giang AH, et al. Beige Adipocytes Are a Distinct Type of Thermogenic Fat Cell in Mouse and Human. *Cell* (2012) 150(2):366–76. doi: 10.1016/j.cell.2012.05.016
6. Okamatsu-Ogura Y, Fukano K, Tsubota A, Uozumi A, Terao A, Kimura K, et al. Thermogenic Ability of Uncoupling Protein 1 in Beige Adipocytes in Mice. *PloS One* (2013) 8(12):1–10. doi: 10.1371/journal.pone.0084229
7. Klingenspor M, Herzig S, Pfeifer A. Brown Fat Develops a Brite Future. *Obes Facts* (2012) 5:890–6. doi: 10.1159/000346337
8. Gerngroß C, Schretter J, Klingenspor M, Schwaiger M, Fromme T. Active Brown Fat During 18F-FDG PET/CT Imaging Defines a Patient Group With Characteristic Traits and an Increased Probability of Brown Fat Redetection. *J Nucl Med* (2017) 58(7):1104–10. doi: 10.2967/jnumed.116.183988
9. Lidell ME, Betz MJ, Enerbäck S. Brown Adipose Tissue and Its Therapeutic Potential. *J Intern Med* (2014) 276(4):364–77. doi: 10.1111/joim.12255
10. Singh AM, Dalton S. What Can "Brown-Ing" Do for You? *Trends Endocrinol Metab* (2018) 29(5):349–59. doi: 10.1016/j.tem.2018.03.002
11. Lee YH, Petkova AP, Konkar AA, Granneman JG. Cellular Origins of Cold-Induced Brown Adipocytes in Adult Mice. *FASEB J* (2015) 29(1):286–99. doi: 10.1096/fj.14-263038
12. Xue B, Rim JS, Hogan JC, Coulter AA, Koza RA, Kozak LP. Genetic Variability Affects the Development of Brown Adipocytes in White Fat But

Not in Interscapular Brown Fat. *J Lipid Res* (2007) 48(1):41–51. doi: 10.1194/jlr.M600287-JLR200
13. Lasar D, Julius A, Fromme T, Klingenspor M. Browning Attenuates Murine White Adipose Tissue Expansion During Postnatal Development. *Biochim Biophys Acta* (2013) 1831(5):960–8. doi: 10.1016/j.bbalip.2013.01.016
14. Birnbacher L, Maurer S, Scheidt K, Herzen J, Pfeiffer F, Fromme T. Electron Density of Adipose Tissues Determined by Phase-Contrast Computed Tomography Provides a Measure for Mitochondrial Density and Fat Content. *Front Physiol* (2018) 9(707):1–8. doi: 10.3389/fphys.2018.00707
15. Chabowska-Kita A, Trabczynska A, Korytko A, Kaczmarek MM, Kozak LP. Low Ambient Temperature During Early Postnatal Development Fails to Cause a Permanent Induction of Brown Adipocytes. *FASEB J* (2015) 29 (8):3238–52. doi: 10.1096/fj.15-271395
16. Chi J, Lin Z, Barr W, Crane A, Ge ZX, Cohen P. Early Postnatal Interactions Between Beige Adipocytes and Sympathetic Neurites Regulate Innervation of Subcutaneous Fat. *Elife* (2021) 10:1–21. doi: 10.7554/eLife.64693
17. Wu Y, Kinnebrew MA, Kutyavin VI, Chawla A. Distinct Signaling and Transcriptional Pathways Regulate Peri-Weaning Development and Cold-Induced Recruitment of Beige Adipocytes. *Proc Natl Acad Sci USA* (2020) 117 (12):6883–9. doi: 10.1073/pnas.1920419117
18. Wang Y, Paulo E, Wu D, Wu Y, Huang W, Chawla A, et al. Adipocyte Liver Kinase B1 Suppresses Beige Adipocyte Renaissance Through Class IIa Histone Deacetylase 4. *Diabetes* (2017) 66(12):2952–63. doi: 10.2337/db17-0296
19. Giralt M, Martin I, Iglesias R, Vinas O, Villarroya F, Mampel T. Ontogeny and Perinatal Modulation of Gene Expression in Rat Brown Adipose Tissue: Unaltered Iodothyronine 5′-Deiodinase Activity Is Necessary for the Response to Environmental Temperature at Birth. *Eur J Biochem* (1990) 193(1):297–302. doi: 10.1111/j.1432-1033.1990.tb19336.x
20. Negron SG, Ercan-Sencicek AG, Freed J, Walters M, Lin Z. Both Proliferation and Lipogenesis of Brown Adipocytes Contribute to Postnatal Brown Adipose Tissue Growth in Mice. *Sci Rep* (2020) 10(1):1–11. doi: 10.1038/s41598-020-77362-x
21. Wang QA, Tao C, Gupta RK, Scherer PE. Tracking Adipogenesis During White Adipose Tissue Development, Expansion and Regeneration. *Nat Med* (2013) 19(10):1338–44. doi: 10.1038/nm.3324
22. Hudak CS, Gulyaeva O, Wang Y, Park S, Lee L, Kang C, et al. Pref-1 Marks Very Early Mesenchymal Precursors Required for Adipose Tissue Development and Expansion. *Cell Rep* (2014) 8(3):678–87. doi: 10.1016/j.celrep.2014.06.060
23. Han J, Lee JE, Jin J, Lim JS, Oh N, Kim K, et al. The Spatiotemporal Development of Adipose Tissue. *Development* (2011) 138(22):5027–37. doi: 10.1242/dev.067686
24. Kozak LP, Newman S, Chao PM, Mendoza T, Koza RA. The Early Nutritional Environment of Mice Determines the Capacity for Adipose Tissue Expansion by Modulating Genes of Caveolae Structure. *PloS One* (2010) 5(6):e11015. doi: 10.1371/journal.pone.0011015
25. Birsoy K, Berry R, Wang T, Ceyhan O, Tavazoie S, Friedman JM, et al. Analysis of Gene Networks in White Adipose Tissue Development Reveals a Role for ETS2 in Adipogenesis. *Development* (2011) 138(21):4709–19. doi: 10.1242/dev.067710
26. Chen HC, Farese RV. Determination of Adipocyte Size by Computer Image Analysis. *J Lipid Res* (2002) 43(6):986–9. doi: 10.1016/S0022-2275(20)30474-0
27. van Beek L, van Klinken JB, Pronk ACM, van Dam AD, Dirven E, Rensen PCN, et al. The Limited Storage Capacity of Gonadal Adipose Tissue Directs the Development of Metabolic Disorders in Male C57Bl/6J Mice. *Diabetologia* (2015) 58(7):1601–9. doi: 10.1007/s00125-015-3594-8
28. Gawronska-Kozak B, Staszkiewicz J, Gimble JM, Kirk-Ballard H. Recruitment of Fat Cell Precursors During Long-Term High Fat Diet in C57BL/6J Mice Is Fat Depot Specific. *Obesity* (2014) 22(4):1091–102. doi: 10.1002/oby.20671
29. Rosenwald M, Perdikari A, Rülicke T, Wolfrum C. Bi-Directional Interconversion of Brite and White Adipocytes. *Nat Cell Biol* (2013) 15 (6):659–67. doi: 10.1038/ncb2740
30. Vitali A, Murano I, Zingaretti MC, Frontini A, Ricquier D, Cinti S. The Adipose Organ of Obesity-Prone C57BL/6J Mice Is Composed of Mixed White and Brown Adipocytes. *J Lipid Res* (2012) 53(4):619–29. doi: 10.1194/jlr.M018846
31. Kodde A, Engels E, Oosting A, van Limpt K, van der Beek EM, Keijer J. Maturation of White Adipose Tissue Function in C57BL/6j Mice From Weaning to Young Adulthood. *Front Physiol* (2019) 10(836):1–14. doi: 10.3389/fphys.2019.00836
32. Roth CL, Molica F, Kwak BR. Browning of White Adipose Tissue as a Therapeutic Tool in the Fight Against Atherosclerosis. *Metabolites* (2021) 11(319):1–20. doi: 10.3390/metabo11050319
33. Cui X, Nguyen NLT, Zarebidaki E, Cao Q, Li F, Zha L, et al. Thermoneutrality Decreases Thermogenic Program and Promotes Adiposity in High-Fat Diet-Fed Mice. *Physiol Rep* (2016) 4(10):1–14. doi: 10.14814/phy2.12799
34. Moser C, Straub LG, Rachamin Y, Dapito DH, Kulenkampff E, Ding L, et al. Quantification of Adipocyte Numbers Following Adipose Tissue Remodeling. *Cell Rep* (2021) 35(4):1–11. doi: 10.1016/j.celrep.2021.109023
35. Rosen ED, MacDougald OA. Adipocyte Differentiation From the Inside Out. *Nat Rev Mol Cell Biol* (2006) 7(12):885–96. doi: 10.1038/nrm2066
36. Pittenger MF, Mackay AM, Beck SC, Jaiswal RK, Douglas R, Mosca JD, et al. Multilineage Potential of Adult Human Mesenchymal Stem Cells. *Science (80)* (1999) 284:143–7. doi: 10.1126/science.284.5411.143
37. Rangwala SM, Lazar MA. Transcriptional Control of Adipogenesis. *Annu Rev Nutr* (2000) 20:535–59. doi: 10.1146/annurev.nutr.20.1.535
38. Arner E, Westermark PO, Spalding KL, Britton T, Rydén M, Frisén J, et al. Adipocyte Turnover: Relevance to Human Adipose Tissue Morphology. *Diabetes* (2010) 59(1):105–9. doi: 10.2337/db09-0942
39. White U, Ravussin E. Dynamics of Adipose Tissue Turnover in Human Metabolic Health and Disease HHS Public Access. *Diabetologia* (2019) 62 (1):17–23. doi: 10.1007/s00125-018-4732-x
40. Guerra C, Koza RA, Yamashita H, Walsh K, Kozak LP. Emergence of Brown Adipocytes in White Fat in Mice Is Under Genetic Control Effects on Body Weight and Adiposity. *J Clin Invest* (1998) 102(2):412–20. doi: 10.1172/JCI3155
41. Himms-Hagen J, Melnyk A, Zingaretti MC, Ceresi E, Barbatelli G, Cinti S. Multilocular Fat Cells in WAT of CL-316243-Treated Rats Derive Directly From White Adipocytes. *Am J Physiol Cell Physiol* (2000) 279:670–81. doi: 10.1152/ajpcell.2000.279.3.C670
42. Ailhaud G, Hauner H. Development of White Adipose Tissue. In: M Dekker, editor. *Handbook of Obesity: Etiology and Pathophysiology*, *2nd ed*. New York: (2003). p. 481–514.
43. Skála J, Barnard T, Lindberg O. Changes in Interscapular Brown Adipose Tissue of the Rat During Perinatal and Early Postnatal Development and After Cold Acclimation - II. Mitochondrial Changes. *Comp Biochem Physiol* (1970) 33:509–28. doi: 10.1016/0010-406x(70)90368-3
44. Schlein C, Fischer AW, Sass F, Worthmann A, Tödter K, Jaeckstein MY, et al. Endogenous Fatty Acid Synthesis Drives Brown Adipose Tissue Involution. *Cell Rep* (2021) 34(2):1–12. doi: 10.1016/j.celrep.2020.108624
45. Mottillo EP, Balasubramanian P, Lee YH, Weng C, Kershaw EE, Granneman JG. Coupling of Lipolysis and *De Novo* Lipogenesis in Brown, Beige, and White Adipose Tissues During Chronic β3-Adrenergic Receptor Activation. *J Lipid Res* (2014) 55(11):2276–86. doi: 10.1194/jlr.M050005
46. Almind K, Manieri M, Sivitz WI, Cinti S, Kahn CR. Ectopic Brown Adipose Tissue in Muscle Provides a Mechanism for Differences in Risk of Metabolic Syndrome in Mice. *Proc Natl Acad Sci USA* (2007) 104(7):2366–71. doi: 10.1073/pnas.0610416104
47. Collins S, Daniel KW, Petro AE, Surwit RS. Strain-Specific Response to β3-Adrenergic Receptor Agonist Treatment of Diet-Induced Obesity in Mice. *Endocrinology* (1997) 138(1):405–13. doi: 10.1210/endo.138.1.4829
48. Li Y, Bolze F, Fromme T, Klingenspor M. Intrinsic Differences in BRITE Adipogenesis of Primary Adipocytes From Two Different Mouse Strains. *Biochim Biophys Acta Mol Cell Biol Lipids* (2014) 1841(9):1345–52. doi: 10.1016/j.bbalip.2014.06.003
49. Kozak LP, Koza RA, Anunciado-Koza R, Mendoza T, Newman S. Inherent Plasticity of Brown Adipogenesis in White Fat of Mice Allows for Recovery From Effects of Post-Natal Malnutrition. *PloS One* (2012) 7(2):1–13. doi: 10.1371/journal.pone.0030392
50. Liang X, Yang Q, Zhang L, Maricelli JW, Rodgers BD, Zhu MJ, et al. Maternal High-Fat Diet During Lactation Impairs Thermogenic Function of Brown Adipose Tissue in Offspring Mice. *Sci Rep* (2016) 6(34345):1–12. doi: 10.1038/srep34345
51. De Almeida DL, Fabrício GS, Trombini AB, Pavanello A, Tófolo LP, Da Silva Ribeiro TA, et al. Early Overfeed-Induced Obesity Leads to Brown Adipose Tissue Hypoactivity in Rats. *Cell Physiol Biochem* (2013) 32(6):1621–30. doi: 10.1159/000356598

52. Xiao QX, Williams SM, Grayson BE, Glavas MM, Cowley MA, Smith MS, et al. Excess Weight Gain During the Early Postnatal Period Is Associated With Permanent Reprogramming of Brown Adipose Tissue Adaptive Thermogenesis. *Endocrinology* (2007) 148(9):4150–9. doi: 10.1210/en.2007-0373
53. Fan R, Toney AM, Jang Y. Maternal N-3 PUFA Supplementation Promotes Fetal Brown Adipose Tissue Development Through Epigenetic Modifications in C57BL/6 Mice. *Biochim Biophys Acta Mol Cell Biol Lipids* (2018) 1863 (12):1488–97. doi: 10.1016/j.bbalip.2018.09.008
54. Cao Q, Jing J, Cui X, Shi H, Xue B. Sympathetic Nerve Innervation Is Required for Beigeing in White Fat. *Physiol Rep* (2019) 7(6):1–7. doi: 10.14814/phy2.14031
55. Wu R, Yu W, Fu L, Li F, Jing J, Cui X, et al. Postnatal Leptin Surge Is Critical for the Transient Induction of the Developmental Beige Adipocytes in Mice. *Am J Physiol Endocrinol Metab* (2020) 318(4):E453–61. doi: 10.1152/ajpendo.00292.2019
56. Chabowska-Kita A, Kozak LP. The Critical Period for Brown Adipocyte Development: Genetic and Environmental Influences. *Obesity* (2016) 24 (2):283–90. doi: 10.1002/oby.21376

Conflict of Interest: The authors declare that the research was conducted in the absence of any commercial or financial relationships that could be construed as a potential conflict of interest.

Publisher's Note: All claims expressed in this article are solely those of the authors and do not necessarily represent those of their affiliated organizations, or those of the publisher, the editors and the reviewers. Any product that may be evaluated in this article, or claim that may be made by its manufacturer, is not guaranteed or endorsed by the publisher.

Copyright © 2022 Bruder and Fromme. This is an open-access article distributed under the terms of the Creative Commons Attribution License (CC BY). The use, distribution or reproduction in other forums is permitted, provided the original author(s) and the copyright owner(s) are credited and that the original publication in this journal is cited, in accordance with accepted academic practice. No use, distribution or reproduction is permitted which does not comply with these terms.

frontiers in Physiology

MINI REVIEW
published: 02 March 2022
doi: 10.3389/fphys.2022.856298

Adipokine Retinol Binding Protein 4 and Cardiovascular Diseases

*Yanjing Ji†, Jinyou Song†, Tianhong Su and Xiaosong Gu**

Department of Cardiology, The Second Affiliated Hospital of Soochow University, Suzhou, China

The morbidity and mortality of cardiovascular diseases (CVDs) have been increasing year by year all over the world and expanding greatly to the younger population, which becomes the leading causes of death globally that threatens human life safety. Prediction of the occurrence of diseases by using risk related adverse events is crucial for screening and early detection of CVDs. Thus, the discovery of new biomarkers that related to risks of CVDs are of urgent in the field. Retinol-binding protein 4 (RBP4) is a 21-kDa adipokine, mainly secreted by adipocytes. Besides its well-established function in the induction of insulin resistance, it has also been found in recent years to be closely associated with CVDs and other risk factors, such as hypertension, coronary heart disease, heart failure, obesity, and hyperlipidemia. In this review, we mainly focus on the progress of research that establishes the correlation between RBP4 and CVDs and the corresponding major risk factors in recent years.

Keywords: retinol-binding protein 4, cardiovascular disease, lipids metabolism, vascular injury, adipokine

OPEN ACCESS

Edited by:
Zhihao Jia,
Purdue University, United States

Reviewed by:
Y. An Xiong,
Southwest Minzu University, China
Kuilong Huang,
Chongqing University of Technology, China

****Correspondence:***
Xiaosong Gu
xiaosonggu@Hotmail.com

† These authors have contributed equally to this work

Specialty section:
This article was submitted to Lipid and Fatty Acid Research, a section of the journal Frontiers in Physiology

Received: *17 January 2022*
Accepted: *31 January 2022*
Published: *02 March 2022*

Citation:
Ji Y, Song J, Su T and Gu X (2022) Adipokine Retinol Binding Protein 4 and Cardiovascular Diseases. Front. Physiol. 13:856298. doi: 10.3389/fphys.2022.856298

INTRODUCTION

Retinol-binding protein 4 (RBP4), whose gene is located near chromosome 10 (10q23-q24), is a 21-kDa protein secreted by hepatocytes and adipocytes. RBP4, as the sole carrier of retinol in the blood, increases the hydrophilicity of retinol upon binding and completes the transport of retinol from the liver to target tissues. Retinol-bound RBP4 (HoloRBP) further complexes with the tetrameric structure of transthyretin protein (TTR) to form a retinol transport complex, which prevents glomerular filtration of HoloRBP (Hamilton and Benson, 2001) and effectively increases and maintains the circulating concentration of RBP4. Initially, RBP4 was found to be involved in the pathogenesis of insulin resistance in type 2 diabetic patients (Yang et al., 2005). In recent years, more studies have suggested that RBP4 is also closely associated with lipid parameters and cardiovascular disease (Broch et al., 2010).

Multiple factors have now been found to influence circulating RBP4 concentrations. Adipose tissue is not only an energy-preserving tissue but can also release numerous substances known as "adipokines" or "adipocytokines." Adipocytes are the main source of RBP4 secretion, Atrial natriuretic peptide (ANP) directly regulates the secretory activity of adipocytes in adipose tissue (Moro et al., 2007) and reduces the production of RBP4. RBP4 is excreted mainly from the kidneys. In patients with type 2 diabetes, microalbuminuria and glomerular filtration rate (GFR) are independent determinants of elevated serum RBP4 levels (Akbay et al., 2010). But it was shown that RBP4 is already diagnostically elevated before their appearance (Abbasi et al., 2020).

There are other factors regulate the serum RPB4. The effect of exercise on RBP4 levels depends on the intensity of exercise (Yu et al., 2009), with high levels of physical activity significantly reducing circulating RBP4 concentrations, but moderate and lower intensity activities have no

significant effect on RBP4 concentrations. Resistance exercise reduces circulating RBP4 levels without altering intramuscular adipocytes or insulin resistance (Ku et al., 2010), whereas neither anaerobic exercise nor controls reduce RBP4. One mechanism for the effect of exercise on RBP4 may be an elevation of ANP (Niessner et al., 2003). The effect of diet on the magnitude of the decrease in circulating RBP4 depends on the amount of weight loss and the nature of the food, with carbohydrate-restricted diets leading to a greater decrease in serum RBP4 levels compared to low-fat diets (Volek et al., 2009). Statins do not seem to produce a significant effect on RBP4 (Szendroedi et al., 2009). The effect of glucose-lowering drugs on RBP4 concentrations in diabetic or non-diabetic patients has not been consistently concluded (Yao-Borengasser et al., 2007; Lin et al., 2008; Pfützner et al., 2009).

In recent years RBP4 have achieved significant efficacy coronary heart disease, hypertension, heart failure (Zhang et al., 2021). In this review, we will focus on RBP4 and their implication in cardiovascular disorder. The purpose of this review is to summarize current information on the RBP4 and risk factors of CVD.

Retinol-Binding Protein 4 and Lipids Metabolism

Abnormal lipid metabolism is the most important risk factor for atherosclerosis, and hyperlipidemia, which includes hypercholesterolemia, hypertriglyceridemia, or both, requires binding to apolipoprotein plasm in plasma in the form of lipoproteins due to its lipid-soluble physical properties. The expression of RBP4 is negatively correlated with blood cholesterol (TC) levels (Jugnam-Ang et al., 2015). and the underlying mechanism may be that hypercholesterolemia causes adipocyte cholesterol overload, which interferes with adipocyte differentiation and maturation, causing adipocyte hypertrophy, adipose tissue inflammation (Mohapatra et al., 2011; Aguilar and Fernandez, 2014), and endocrine dysfunction, and adipose inflammation can lead to the release of pro-inflammatory factors (for example, TNF-α, IL-1β), and the accumulation of pro-inflammatory factors further inhibits the release of RBP4 from adipocytes into the blood (Zoccali et al., 2003).

Usui et al. (2009) found that RBP4 was positively associated with small and dense low-density lipoprotein (sdLDL) levels in young women and RBP4 was one of major factors affecting sdLDL-cholesterol levels. Similarly, sdLDL was found to be an independent predictor of oxidized low-density lipoprotein (ox-LDL) in patients with dyslipidemia, and sdLDL may be an important link between RBP4 and ox-LDL (Wu et al., 2012). It is now known that sdLDL and ox-LDL are components of atherogenic lipoproteins, and RBP4 may be involved in atherogenesis by directly or indirectly upregulating sdLDL levels. SdLDL was found to be an independent predictor of RBP4 in patients with dyslipidemia (Wu et al., 2012). Also, blood RBP4 levels were found to be negatively associated with indirect VLDL-apoB100 FCR and not significantly associated with direct VLDL-apoB100 FCR, suggesting that RBP4 is associated with more with VLDL dilapidation compared to direct uptake (Vergès et al., 2012), which may also explain the relationship between RBP4 and blood triglycerides in patients with type 2 diabetes. Wessel et al. (2019) found that RBP4 levels were positively correlated with large very low-density lipoproteins (VLDL) versus small LDL, but no physical interaction was found between them. In patients with type 2 diabetes, RBP4 has a strong positive correlation with blood triglyceride (TG) levels (Vergès et al., 2012; Wessel et al., 2019; **Table 1**), The same correlation with blood triglycerides and HDL was found in RBP4 single nucleotide polymorphisms (Codoñer-Franch et al., 2016). All these results suggest that RBP4 may be involved in the pathophysiological process of atherosclerosis by altering the distribution of proatherosclerotic plasma lipoproteins.

Obesity, one of the risk factors for atherosclerosis, can lead to increased blood triglyceride and cholesterol levels. The close correlation between visceral adiposity and cardiovascular disease has been previously demonstrated (Després and Lemieux, 2006). Won et al. (2012) found that RBP4 levels increased with the accumulation of visceral adiposity and were associated with risk factors for cardiovascular diseases (CVDs). RBP4 was more frequently expressed in visceral adipose tissue than in subcutaneous adipose tissue and was not affected by adiposity size, fat distribution, body fat percentage and other factors (Klöting et al., 2007). Serum RBP4 levels decreased by 25.5% in non-diabetic subjects after completing a 16-week weight loss program, and changes of RBP4 levels were significantly and positively associated with abdominal visceral fat loss, but not with total body fat loss or abdominal subcutaneous fat loss (Lee et al., 2008). In studies of genetic variants, different types of RBP4 single nucleotide polymorphisms (SNPs) were found to affect circulating RBP4 levels and were strongly associated with obesity, with the association of SNPrs3758538 with obesity being noteworthy, suggesting a possible predictive role of RBP4 gene variants on obesity risk (Tsutsumi et al., 1992). These studies suggest that RBP4 has a predictive value for visceral fat accumulation and that adipose tissue, as the main source of RBP4 secretion by the body (White and Kelly, 2001), suggests that RBP4 may be a key mediator of the increased risk of cardiovascular disease in obese patients.

Retinol-Binding Protein 4 and Cardiovascular Diseases

Retinol-Binding Protein 4 and Vascular Injury

Oxidative stress-mediated changes promoted the development of cardiovascular disease (Massaeli and Pierce, 1995). It was found that RBP4 induces mitochondrial dysfunction and apoptosis, which in turn promotes vascular oxidative stress. RBP4 impaired mitochondrial number and integrity and reduced membrane potential by inducing reactive oxygen species (ROS) in mitochondria, and increased ROS and decreased ATP production affected normal endothelial cell. Increased cytochrome C release from mitochondria, increased Bax (pro-apoptotic protein) and decreased Bcl-2 were observed in arteries from RBP4 overexpressing (RBP4-Tg) mice, suggesting that RBP4 increased apoptosis of endothelial cell (Wang et al., 2015).

Chronic vascular inflammation plays an important role in the development of atherosclerosis, and vascular dysfunction

TABLE 1 | Associated factors and diseases correlated with RBP4 levels.

	Involved diseases	Correlation with blood RBP4 levels	References
ANP	Heart failure	Negative	Moro et al., 2007
GFR	Chronic kidney disease	Negative	Akbay et al., 2010; Abbasi et al., 2020
High-intensity exercise	—	Negative	Yu et al., 2009
Blood cholesterol	Abnormal lipid metabolism,T2DM	Negative	Jugnam-Ang et al., 2015
Blood triglyceride		Positive	Vergès et al., 2012
Indirect VLDL-apoB100 FCR		Negative	Vergès et al., 2012
sdLDL	Atherosclerosis	Positive	Usui et al., 2009
SNPrs3758538	Obesity	Negative	Codoñer-Franch et al., 2016
ROS	Vascular injury,atherosclerosis	Positive	Wang et al., 2015
LVEF	Heart failure	Negative	Li et al., 2020
LVMI and LAD		Positive	von Jeinsen et al., 2018
TLR4 and MyD88		Positive	Gao et al., 2016
Carotid intima and plaque echogenicity	Coronary heart disease	Negative	Stakhneva et al., 2020
TTR	Amyloidosis	Positive	Suhr et al., 2015; Santos et al., 2016; Chan et al., 2017

ANP, Atrial natriuretic peptide; GFR, glomerular filtration rate; VLDL, very low-density lipoproteins; sdLDL, small and dense low-density lipoprotein; ROS, reactive oxygen species; LVEF, left ventricular ejection fraction; LVMI, left ventricular mass index; LAD, left atrial internal diameter; TLR4, Toll-like receptor 4; MyD88, myeloid differentiation primary response gene 88; TTR, transthyretin protein.

promotes plaque initiation and progression (Endemann and Schiffrin, 2004). RBP4 may be involved in the development of cardiovascular disease by inducing an inflammatory response. Norseen et al. (2012) found that RBP4 induced macrophage pro-inflammatory cytokine secretion and expression through activation of C-Jun N-terminal protein kinase (JNK) and Toll-like receptor 4 (TLR4)-dependent signaling pathways (**Figure 1**). Similarly, RBP4 was found to mediate vascular endothelial cell inflammatory responses *via* NADPH oxidase and NF-κB-dependent pathways (Farjo et al., 2012). In addition to endothelial cells, RBP4 also increases the proliferation of vascular smooth muscle cells through MAPK pathway and increases the risk of cardiovascular diseases (Li et al., 2015). the receptor and signaling pathways by which RBP4 acts with endothelial cells and VSMCs deserve to be explored in further studies, which may contribute to the understanding of the RBP4 and cardiovascular disease linkage.

Retinol-Binding Protein 4 and Hypertension

Hypertension is primarily a disease that results from genetic and environmental interactions, and its prevalence in the population is increasing year by year. It was found that blood RBP4 levels were significantly elevated in patients with untreated essential hypertension (Solini et al., 2009; Zachariah et al., 2016; Li et al., 2019) and significantly correlated with left ventricular diastolic function (Porcar-Almela et al., 2015; Li et al., 2019). RBP4 may be related to the left ventricular hypertrophy, and carotid intra-medial membrane thickness (IMT), suggesting that RBP4 may serve as a marker of vascular injury in hypertensive patients at early stage (Mansouri et al., 2012; Kraus et al., 2015). Significantly elevated levels of RBP4 were also found in patients with prehypertension, and RBP4 was independently associated with elevated diastolic and systolic blood pressure (Zhang et al., 2017). Insulin resistance (IR) has recently been suggested as a common pathophysiological basis for the development of type 2 diabetes and hypertension. Sasaki et al. (2020) found that the prevalence of hypertension increased with the degree of impaired glucose metabolism and elevated RBP4 may be involved in the development of hypertension by inducing IR. The mechanism of RBP4 in hypertension has not been clearly elucidated. Chiba et al. (2010) found that the binding of RBP4 to retinol activated inflammatory response that induced atherosclerosis, decreased vascular compliance and thus raised blood pressure. The correlation between RBP4 and arterial stiffness was also confirmed (Chondrou et al., 2020). It was found that blood pressure was reduced in RBP4 knockout (RBP-KO) mice and increased in RBP4 overexpressing (RBP-Tg) mice, while RBP-KO mice were protected from Ang-II-induced hypertension, confirming the presence of RBP4 as a risk factor in the development of hypertension (Kraus et al., 2015). The effect of RBP4 on blood pressure may be partly attributed to its effect on vascular endothelial function, as elevated RBP4 attenuates eNOS Ser1177 phosphorylation, which in turn attenuates the endothelium-dependent vasodilatory effect mediated by nitric oxide (Kraus et al., 2015; **Figure 1**).

Although the underlying mechanisms need to be further explored, more and more studies are now showing the close correlation between RBP4 and hypertension, and the monitoring of RBP4 may be a valuable indicator in determining early ventricular diastolic insufficiency and changes in vascular compliance in hypertensive patients. RBP4 may be a potential targeted molecule for preventing the progression of prehypertension and delaying ventricular remodeling.

Retinol-Binding Protein 4 and Heart Failure

Terminal B-type natriuretic peptide (NT-proBNP) is now known to be widely used as a diagnostic indicator of heart failure. Previous studies in elderly patients hospitalized with heart

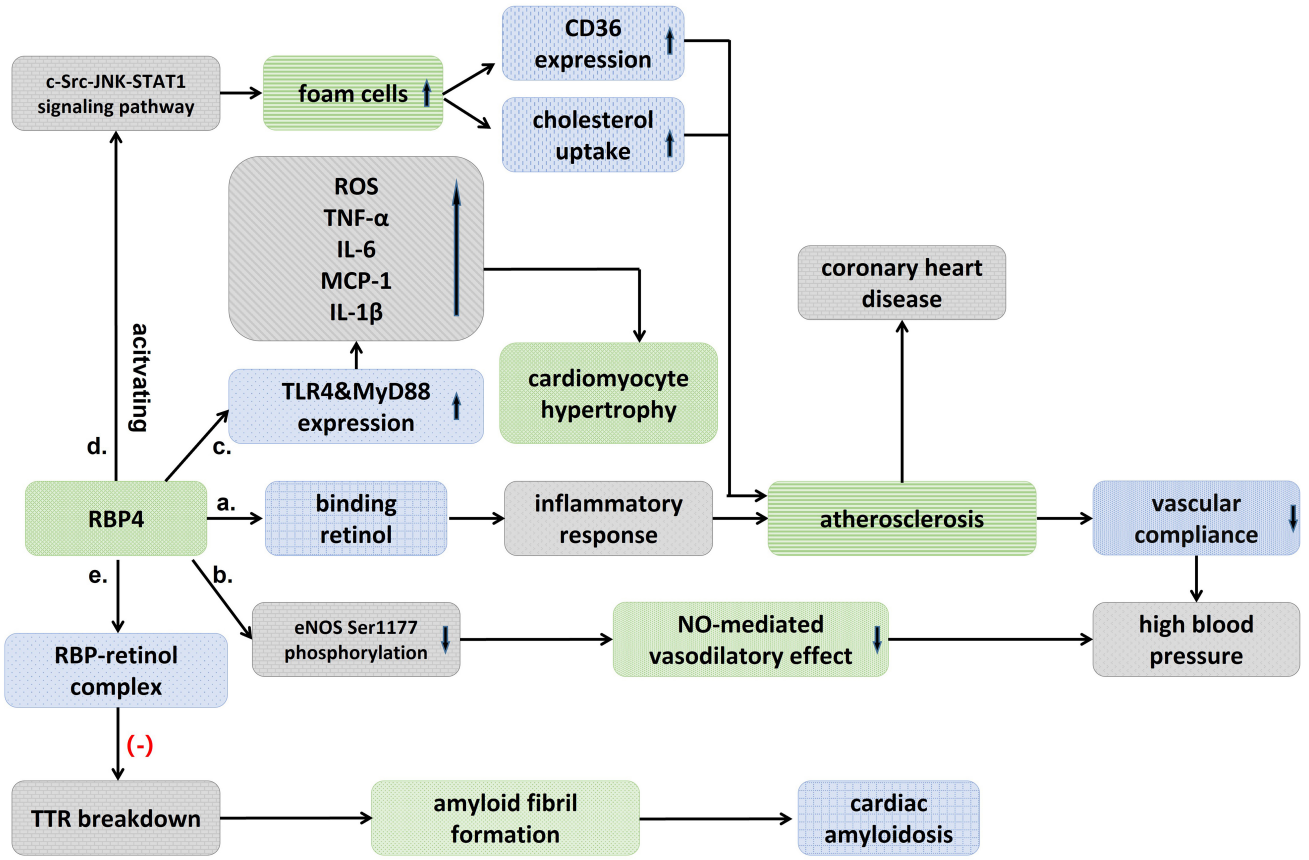

FIGURE 1 | Schematic diagram showing an association between RBP4 and cardiovascular diseases. (a) Binding to retinol, RBP4 activates an inflammatory response that induces atherosclerosis and decreased vascular compliance, and thus raises blood pressure. (b) RBP4 could also result in high blood pressure by attenuating eNOS Ser1177 phosphorylation and then the nitric-oxide (NO)-mediated vasodilatory effect. (c) RBP4 stimulates TLR4 and MyD88 experssion, which significantly promotes the pro-inflammatory response and increases ROS, and then cause cardiomyocyte hypertrophy. (d) RBP4 promotes the formation of foam cells, which upregulates CD36 expression and cholesterol uptake, and atherosclerosis, thereby leading to coronary heart disease. (e) RBP-retinol complex could reduce TTR breakdown and then inhibit the formation of amyloid fibril and avoid cardiac amyloidosis.

failure have shown that RBP4 did not correlate with NT-proBNP, and that changes of blood RBP4 levels are more likely attributable to the deterioration of renal function in patients with advanced heart failure, resulting in the accumulation of circulating adipokines (Majerczyk et al., 2018). It was found that alterations in RBP4 in patients with type 2 diabetes were also attributed to the changes of renal function (Henze et al., 2008). It seems to be no relationship between RBP4 and diagnosing of heart failure. But a subsequent prospective cohort study showed that in elderly patients with chronic heart failure, blood RBP4 levels were negatively correlated with left ventricular ejection fraction (LVEF) and positively correlated with NT-proBNP, and that serum RBP4 levels increased with decreasing cardiac function (Li et al., 2020; **Table 1**), In addition, the results of a 60-month follow-up suggested that blood RBP4 levels were positively correlated with adverse events in patients with chronic heart failure. The finding that RBP4 levels were positively correlated with left ventricular mass index (LVMI) and left atrial internal diameter (LAD) also suggests that RBP4 plays a role in the process of cardiac remodeling (von Jeinsen et al., 2018). The blood RBP4 levels in patients with advanced heart failure can be improved by implantation of a ventricular assist device (Chavarria et al., 2012). So RBP4 is a valuable diagnostic indicator of heart failure, and may be involved in the pathogenesis and development of heart failure.

Retinol-binding protein 4 is involved in the pathological process of heart failure through a variety of mechanisms. The elevation of RBP4 in patients with advanced heart failure may result from upregulation of RBP4 mRNA expression by IL-8 (Bobbert et al., 2009). In addition, RBP4 was found to cause cardiomyocyte hypertrophy, which may mediate a vicious cycle between insulin resistance and heart failure (Gao et al., 2016; von Jeinsen et al., 2018). RBP4 increased cell size, enhanced protein synthesis, and elevated the expression of hypertrophic markers including Anp, Bnp, and Myh7 in primary cardiomyocytes, but inhibition or knockdown of the TLR4/MyD88 pathway attenuated inflammatory and hypertrophic responses to RBP4 stimulation (Gao et al., 2016; **Figure 1**). Angiotensin II (Ang-II) also increases the expression of RBP4 in adipocytes, and the

use of Ang-II receptor antagonists may eliminate this effect, which may explain another mechanism of the renin-angiotensin-aldosterone system (RASS) in exacerbating the deterioration of cardiac function (Gao et al., 2016). This needs to be explored in more clinical studies in the future.

Retinol-Binding Protein 4 and Coronary Heart Disease

Retinol-binding protein 4 levels in patients with coronary artery disease were found to be significantly higher than in the non-coronary artery disease (CAD) group (Ingelsson and Lind, 2009; Li et al., 2014; Liu et al., 2019) and positively correlated with the number of diseased vessels (Cubedo et al., 2014; Liu et al., 2015; Wessel et al., 2019), some clinical results have shown that serum RBP4 levels are reduced in patients with acute myocardial infarction, in male patients with familial hypercholesterolemia, a reduction in RBP4 has shown predictive significance for the possibility of ischemic events in the next 2 years, suggesting that RBP4 may be involved in the AMI (Cubedo et al., 2014). Similarly, Liu et al. (2015) found that patients with CAD with higher RBP4 had a concomitant increase in acute coronary syndrome (ACS) events in a 3-year follow-up (**Table 1**).

Previously, Mallat found that RBP did not provide additional predictive value compared to traditional risk factors in normal subjects (Mallat et al., 2009). But in a 16-year prospective case-control study (Sun et al., 2013), both full-length and total RBP4 levels were found to be strongly associated with the risk of coronary heart disease in women, with this association diminishing over time. Full-length RBP4 may exist as the most biologically active isoform of RBP4. In addition, increased values of both RBP4 and lipoprotein conjugate index (LCI) were found to be independent risk factors for ACS, and the combined test results of LCI and RBP4 values may serve as a potential indicator for the diagnosis of ACS (Wessel et al., 2019). RBP4 gene polymorphism was also found to be closely associated with coronary artery disease (Wan et al., 2014). Liu et al. (2017) found that RBP4 was localized in macrophage-rich foam cells, that RBP4 promotes the formation of macrophage-derived foam cells by activating the c-Src-JNK-STAT1 signaling pathway, which in turn upregulates CD36 expression and cholesterol uptake, and that RBP4 concentration is negatively correlated with carotid intima and plaque echogenicity (Stakhneva et al., 2020; **Figure 1** and **Table 1**). The results suggested that RBP4 was involved in the progression of atherosclerosis. In conclusion, RBP4 involved in the pathophysiological process of coronary heart disease, as a risk factor, has shown valuable in predictor of coronary complexity and the occurrence of adverse cardiovascular events in patients with CAD. RBP4 is expected to be a new biological indicator of coronary heart disease, and a clinical risk factor of coronary heart disease.

Retinol-Binding Protein 4 and Cardiac Amyloidosis

Cardiac amyloidosis (CA) is an accumulation of insoluble fibrous deposits composed of abnormally folded protein molecules in the myocardial interstitial, which mainly manifests clinically as cardiac insufficiency, various arrhythmias, and angina pectoris, among which the transthyretin amyloidosis (ATTR) type is more common in clinical work. It was found that blood RBP4 levels in patients with transthyretin amyloidosis were significantly lower than in controls (Arvanitis et al., 2017a,b). Chan et al. (2017) further found that RBP4 was significantly decreased in mutant myocardial amyloidosis (ATTRm) compared to controls, but not in wild-type myocardial amyloidosis (ATTRwt) by using blood proteomics analysis. The reduced level of serum TTR was closely correlated with the reduced level of RBP4 (Suhr et al., 2015). The lower levels of RBP4 paralleled to serum TTR levels, which may be related to the fact that TTR acts as a transporter protein to bind the RBP4-retinol complex and thus reduces renal excretion of RBP4 (Hamilton and Benson, 2001; **Table 1**).

Retinol-binding protein 4 has been found to have anti-amyloidogenic properties, and the decrease of RBP4 alleviate the formation of the RBP4-retinol complex and attenuates its role in stabilizing the TTR tetrameric structure (White and Kelly, 2001; Santos et al., 2016). *In vitro* assays have shown that the RBP-retinol complex (holoRBP) inhibits the rate of amyloid fibril formation in a concentration-dependent manner (White and Kelly, 2001). holoRBP at physiological concentrations slowed down the rate of TTR breakdown approximately sixfold compared to TTR breakdown alone (Hyung et al., 2010). RBP4 concentrations higher than or equal to 50 μg/mL were found to be up to 100% sensitive for the diagnosis of ATTRV122I amyloidosis, although its specificity decreased to 38%, suggesting that RBP4 could provide 100% negative predictive value when used to rule out ATTRV122I amyloidosis (Arvanitis et al., 2017a; **Table 1**). The diagnostic and predictive value of RBP4 in ATTR amyloidosis needs to be confirmed in larger and more pathologically diverse cohort studies.

SUMMARY

As an adipokine, RBP4 has shown a close association with dyslipidemia, obesity, and vascular impairment. RBP4 also derives exclusively from hepatocytes, but liver-secreted RBP4 does not impair glucose homeostasis (Fedders et al., 2018). In addition, RBP4 has shown promising value for cardiovascular disease diagnosis and treatment, such as predicting the risk of hypertension and coronary heart disease in the general population, and assessing the prognosis of patients with coronary heart disease and heart failure, etc. RBP4 is expected to be a new biomarker for cardiovascular disease in the future. The study of RBP4 antagonists may also be a new therapeutic agent for cardiovascular diseases.

AUTHOR CONTRIBUTIONS

XG conceived the study and designed the study protocol. YJ and JS conducted the literature review and drafted the manuscript. TS reviewed the manuscript for intellectual content, made revisions as needed. All authors contributed to the article and approved the submitted version.

FUNDING

This work was supported by the National Natural Science Foundation of China (Grant Number 82170831), Science and Technology Development Plan of Suzhou City, China (Grant Numbers SYS2019061 and SYSD2018097), MSD cholesterol Fund of China Heart House – China Cardiovascular Association (Grant Number 2017-CCA-Msdlipid-014), and Young Investigator Pre-Research Foundation of the Second Affiliated Hospital of Soochow University (Grant Number SDFEYQN1717).

REFERENCES

Abbasi, F., Moosaie, F., Khaloo, P., Dehghani Firouzabadi, F., Fatemi Abhari, S. M., Atainia, B., et al. (2020). Neutrophil gelatinase-associated lipocalin and retinol-binding protein-4 as biomarkers for diabetic kidney disease. *Kid. Blood Press Res.* 45, 222–232. doi: 10.1159/000505155

Aguilar, D., and Fernandez, M. L. (2014). Hypercholesterolemia induces adipose dysfunction in conditions of obesity and nonobesity. *Adv. Nutr.* 5, 497–502. doi: 10.3945/an.114.005934

Akbay, E., Muslu, N., Nayir, E., Ozhan, O., and Kiykim, A. (2010). Serum retinol binding protein 4 level is related with renal functions in Type 2 diabetes. *J. Endocrinol. Invest.* 33, 725–729. doi: 10.1007/BF03346678

Arvanitis, M., Koch, C. M., Chan, G. G., Torres-Arancivia, C., LaValley, M. P., Jacobson, D. R., et al. (2017a). Identification of transthyretin cardiac amyloidosis using serum retinol-binding protein 4 and a clinical prediction model. *JAMA Cardiol.* 2, 305–313. doi: 10.1001/jamacardio.2016.5864

Arvanitis, M., Simon, S., Chan, G., Fine, D., Beardsley, P., LaValley, M., et al. (2017b). Retinol binding protein 4 (RBP4) concentration identifies V122I transthyretin cardiac amyloidosis. *Amyloid* 24(Suppl. 1), 120–121. doi: 10.1080/13506129.2017.1295371

Bobbert, P., Weithäuser, A., Andres, J., Bobbert, T., Kühl, U., Schultheiss, H. P., et al. (2009). Increased plasma retinol binding protein 4 levels in patients with inflammatory cardiomyopathy. *Eur. J. Heart Fail.* 11, 1163–1168. doi: 10.1093/eurjhf/hfp153

Broch, M., Gómez, J. M., Auguet, M. T., Vilarrasa, N., Pastor, R., Elio, I., et al. (2010). Association of retinol-binding protein-4 (RBP4) with lipid parameters in obese women. *Obesity Surg.* 20, 1258–1264. doi: 10.1007/s11695-010-0200-5

Chan, G. G., Koch, C. M., and Connors, L. H. (2017). Blood proteomic profiling in inherited (ATTRm) and acquired (ATTRwt) forms of transthyretin-associated cardiac amyloidosis. *J. Proteome Res.* 16, 1659–1668. doi: 10.1021/acs.jproteome.6b00998

Chavarria, N., Kato, T. S., Khan, R., Chokshi, A., Collado, E., Akashi, H., et al. (2012). Increased levels of retinol binding protein 4 in patients with advanced heart failure correct after hemodynamic improvement through ventricular assist device placement. *Circ. J.* 76, 2148–2152. doi: 10.1253/circj.cj-12-0350

Chiba, M., Saitoh, S., Ohnishi, H., Akasaka, H., Mitsumata, K., Furukawa, T., et al. (2010). Associations of metabolic factors, especially serum retinol-binding protein 4 (RBP4), with blood pressure in Japanese–the Tanno and Sobetsu study. *Endocr. J.* 57, 811–817. doi: 10.1507/endocrj.k10e-054

Chondrou, A., Nigdelis, M. P., Armeni, E., Augoulea, A., Rizos, D., Kaparos, G., et al. (2020). Retinol-binding protein 4 is associated with arterial stiffness in early postmenopausal women. *Menopause* 27, 906–912. doi: 10.1097/GME.0000000000001598

Codoñer-Franch, P., Carrasco-Luna, J., Allepuz, P., Codoñer-Alejos, A., and Guillem, V. (2016). Association of RBP4 genetic variants with childhood obesity and cardiovascular risk factors. *Pediatr. Diabetes* 17, 576–583. doi: 10.1111/pedi.12339

Cubedo, J., Padró, T., Cinca, J., Mata, P., Alonso, R., and Badimon, L. (2014). Retinol-binding protein 4 levels and susceptibility to ischaemic events in men. *Eur. J. Clin. Invest.* 44, 266–275. doi: 10.1111/eci.12229

Després, J. P., and Lemieux, I. (2006). Abdominal obesity and metabolic syndrome. *Nature* 444, 881–887. doi: 10.1038/nature05488

Endemann, D. H., and Schiffrin, E. L. (2004). Endothelial dysfunction. *J. Am. Soc. Nephrol.* 15, 1983–1992. doi: 10.1097/01.ASN.0000132474.50966.DA

Farjo, K. M., Farjo, R. A., Halsey, S., Moiseyev, G., and Ma, J. X. (2012). Retinol-binding protein 4 induces inflammation in human endothelial cells by an NADPH oxidase- and nuclear factor kappa B-dependent and retinol-independent mechanism. *Mol. Cell Biol.* 32, 5103–5115. doi: 10.1128/MCB.00820-12

Fedders, R., Muenzner, M., Weber, P., Sommerfeld, M., Knauer, M., Kedziora, S., et al. (2018). Liver-secreted RBP4 does not impair glucose homeostasis in mice. *J. Biol. Chem.* 293, 15269–15276. doi: 10.1074/jbc.RA118.004294

Gao, W., Wang, H., Zhang, L., Cao, Y., Bao, J. Z., Liu, Z. X., et al. (2016). Retinol-binding protein 4 induces cardiomyocyte hypertrophy by activating TLR4/MyD88 pathway. *Endocrinology* 157, 2282–2293. doi: 10.1210/en.2015-2022

Hamilton, J. A., and Benson, M. D. (2001). Transthyretin: a review from a structural perspective. *Cell. Mol. Life Sci. CMLS* 58, 1491–1521. doi: 10.1007/PL00000791

Henze, A., Frey, S. K., Raila, J., Tepel, M., Scholze, A., Pfeiffer, A. F., et al. (2008). Evidence that kidney function but not type 2 diabetes determines retinol-binding protein 4 serum levels. *Diabetes* 57, 3323–3326. doi: 10.2337/db08-0866

Hyung, S. J., Deroo, S., and Robinson, C. V. (2010). Retinol and retinol-binding protein stabilize transthyretin via formation of retinol transport complex. *ACS Chem. Biol.* 5, 1137–1146. doi: 10.1021/cb100144v

Ingelsson, E., and Lind, L. (2009). Circulating retinol-binding protein 4 and subclinical cardiovascular disease in the elderly. *Diabetes Care* 32, 733–735. doi: 10.2337/dc08-1656

Jugnam-Ang, W., Pannengpetch, S., Isarankura-Na-Ayudhya, P., Thippakorn, C., Isarankura-Na-Ayudhya, C., Lawung, R., et al. (2015). Retinol-binding protein 4 and its potential roles in hypercholesterolemia revealed by proteomics. *Excli J.* 14, 999–1013. doi: 10.17179/excli2015-478

Klöting, N., Graham, T. E., Berndt, J., Kralisch, S., Kovacs, P., Wason, C. J., et al. (2007). Serum retinol-binding protein is more highly expressed in visceral than in subcutaneous adipose tissue and is a marker of intra-abdominal fat mass. *Cell Metab.* 6, 79–87. doi: 10.1016/j.cmet.2007.06.002

Kraus, B. J., Sartoretto, J. L., Polak, P., Hosooka, T., Shiroto, T., Eskurza, I., et al. (2015). Novel role for retinol-binding protein 4 in the regulation of blood pressure. *Faseb. J.* 29, 3133–3140. doi: 10.1096/fj.14-266064

Ku, Y. H., Han, K. A., Ahn, H., Kwon, H., Koo, B. K., Kim, H. C., et al. (2010). Resistance exercise did not alter intramuscular adipose tissue but reduced retinol-binding protein-4 concentration in individuals with type 2 diabetes mellitus. *J. Int. Med. Res.* 38, 782–791. doi: 10.1177/147323001003800305

Lee, J. W., Lee, H. R., Shim, J. Y., Im, J. A., and Lee, D. C. (2008). Abdominal visceral fat reduction is associated with favorable changes of serum retinol binding protein-4 in nondiabetic subjects. *Endocr. J.* 55, 811–818. doi: 10.1507/endocrj.k08e-030

Li, F., Xia, K., Li, C., and Yang, T. (2014). Retinol-binding protein 4 as a novel risk factor for cardiovascular disease in patients with coronary artery disease and hyperinsulinemia. *Am. J. Med. Sci.* 348, 474–479. doi: 10.1097/MAJ.0000000000000347

Li, F., Xia, K., Sheikh, S. A., Cheng, J., Li, C., and Yang, T. (2015). Involvement of RBP4 in hyperinsulinism-induced vascular smooth muscle cell proliferation. *Endocrine* 48, 472–482. doi: 10.1007/s12020-014-0304-0

Li, X. Z., Zhang, K. Z., Yan, J. J., Wang, L., Wang, Y., Shen, X. Y., et al. (2020). Serum retinol-binding protein 4 as a predictor of cardiovascular events in elderly patients with chronic heart failure. *ESC Heart Fail.* 7, 542–550. doi: 10.1002/ehf2.12591

Li, X., Zhu, S., Song, G., Zhang, K., Gao, W., Huang, J., et al. (2019). Retinol-binding protein 4 is closely correlated to blood pressure level and E/A in untreated essential hypertension patients. *Ann. Palliat. Med.* 8, 645–650. doi: 10.21037/apm.2019.11.07

Lin, K. D., Chang, Y. H., Wang, C. L., Yang, Y. H., Hsiao, P. J., Li, T. H., et al. (2008). Thiazolidinedione addition reduces the serum retinol-binding protein 4 in type 2 diabetic patients treated with metformin and sulfonylurea. *Trans. Res. J. Lab. Clin. Med.* 151, 309–314. doi: 10.1016/j.trsl.2008.04.003

Liu, T., Han, C., Sun, L., Ding, Z., Shi, F., Wang, R., et al. (2019). Association between new circulating proinflammatory and anti-inflammatory

adipocytokines with coronary artery disease. *Coron Artery Dis.* 30, 528–535. doi: 10.1097/MCA.0000000000000778

Liu, Y., Wang, D., Chen, H., and Xia, M. (2015). Circulating retinol binding protein 4 is associated with coronary lesion severity of patients with coronary artery disease. *Atherosclerosis* 238, 45–51. doi: 10.1016/j.atherosclerosis.2014.11.016

Liu, Y., Zhong, Y., Chen, H., Wang, D., Wang, M., Ou, J. S., et al. (2017). Retinol-binding protein-dependent cholesterol uptake regulates macrophage foam cell formation and promotes atherosclerosis. *Circulation* 135, 1339–1354. doi: 10.1161/CIRCULATIONAHA.116.024503

Majerczyk, M., Chorêza, P., Mizia-Stec, K., Bożentowicz-Wikarek, M., Brzozowska, A., Arabzada, H., et al. (2018). Plasma level of retinol-binding protein 4, N-terminal proBNP and renal function in older patients hospitalized for heart failure. *Cardior. Med.* 8, 237–248. doi: 10.1159/000489403

Mallat, Z., Simon, T., Benessiano, J., Clément, K., Taleb, S., Wareham, N. J., et al. (2009). Retinol-binding protein 4 and prediction of incident coronary events in healthy men and women. *J. Clin. Endocrinol. Metab.* 94, 255–260. doi: 10.1210/jc.2008-0253

Mansouri, M., Heshmat, R., Tabatabaei-Malazy, O., Sharifi, F., Badamchizadeh, Z., Alatab, S., et al. (2012). The association of carotid intima media thickness with retinol binding protein-4 and total and high molecular weight adiponectin in type 2 diabetic patients. *J. Diab. Metab. Disord.* 11:2. doi: 10.1186/2251-6581-11-2

Massaeli, H., and Pierce, G. N. (1995). Involvement of lipoproteins, free radicals, and calcium in cardiovascular disease processes. *Cardiovas. Res.* 29, 597–603.

Mohapatra, J., Sharma, M., Acharya, A., Pandya, G., Chatterjee, A., Balaraman, R., et al. (2011). Retinol-binding protein 4: a possible role in cardiovascular complications. *Br. J. Pharmacol.* 164, 1939–1948. doi: 10.1111/j.1476-5381.2011.01492.x

Moro, C., Klimcakova, E., Lolmède, K., Berlan, M., Lafontan, M., Stich, V., et al. (2007). Atrial natriuretic peptide inhibits the production of adipokines and cytokines linked to inflammation and insulin resistance in human subcutaneous adipose tissue. *Diabetologia* 50, 1038–1047. doi: 10.1007/s00125-007-0614-3

Niessner, A., Ziegler, S., Slany, J., Billensteiner, E., Woloszczuk, W., and Geyer, G. (2003). Increases in plasma levels of atrial and brain natriuretic peptides after running a marathon: are their effects partly counterbalanced by adrenocortical steroids? *Eur. J. Endocrinol.* 149, 555–559. doi: 10.1530/eje.0.1490555

Norseen, J., Hosooka, T., Hammarstedt, A., Yore, M. M., Kant, S., Aryal, P., et al. (2012). Retinol-binding protein 4 inhibits insulin signaling in adipocytes by inducing proinflammatory cytokines in macrophages through a c-Jun N-terminal kinase- and toll-like receptor 4-dependent and retinol-independent mechanism. *Mol. Cell Biol.* 32, 2010–2019. doi: 10.1128/MCB.06193-11

Pfützner, A., Schöndorf, T., Hanefeld, M., Lübben, G., Kann, P. H., Karagiannis, E., et al. (2009). Changes in insulin resistance and cardiovascular risk induced by PPARgamma activation have no impact on RBP4 plasma concentrations in nondiabetic patients. *Horm. Metab. Res.* 41, 202–206. doi: 10.1055/s-0028-1104592

Porcar-Almela, M., Codoñer-Franch, P., Tuzón, M., Navarro-Solera, M., Carrasco-Luna, J., and Ferrando, J. (2015). Left ventricular diastolic function and cardiometabolic factors in obese normotensive children. *Nutr. Metab. Cardiovasc. Dis.* 25, 108–115. doi: 10.1016/j.numecd.2014.08.013

Santos, D., Coelho, T., Alves-Ferreira, M., Sequeiros, J., Mendonça, D., Alonso, I., et al. (2016). Variants in RBP4 and AR genes modulate age at onset in familial amyloid polyneuropathy (FAP ATTRV30M). *Eur. J. Hum. Genet.* 24, 756–760. doi: 10.1038/ejhg.2015.180

Sasaki, N., Ozono, R., Higashi, Y., Maeda, R., and Kihara, Y. (2020). Association of insulin resistance, plasma glucose level, and serum insulin level with hypertension in a population with different stages of impaired glucose metabolism. *J. Am. Heart Assoc.* 9:e015546. doi: 10.1161/JAHA.119.015546

Solini, A., Santini, E., Madec, S., Rossi, C., and Muscelli, E. (2009). Retinol-binding protein-4 in women with untreated essential hypertension. *Am. J. Hypertens* 22, 1001–1006. doi: 10.1038/ajh.2009.116

Stakhneva, E. M., Meshcheryakova, I. A., Demidov, E. A., Starostin, K. V., Peltek, S. E., Voevoda, M. I., et al. (2020). Changes in the proteomic profile of blood serum in coronary atherosclerosis. *J. Med. Biochem.* 39, 208–214. doi: 10.2478/jomb-2019-0022

Suhr, O. B., Coelho, T., Buades, J., Pouget, J., Conceicao, I., Berk, J., et al. (2015). Efficacy and safety of patisiran for familial amyloidotic polyneuropathy: a phase II multi-dose study. *Orphanet. J. Rare Dis.* 10:109. doi: 10.1186/s13023-015-0326-6

Sun, Q., Kiernan, U. A., Shi, L., Phillips, D. A., Kahn, B. B., Hu, F. B., et al. (2013). Plasma retinol-binding protein 4 (RBP4) levels and risk of coronary heart disease: a prospective analysis among women in the nurses' health study. *Circulation* 127, 1938–1947. doi: 10.1161/CIRCULATIONAHA.113.002073

Szendroedi, J., Anderwald, C., Krssak, M., Bayerle-Eder, M., Esterbauer, H., Pfeiler, G., et al. (2009). Effects of high-dose simvastatin therapy on glucose metabolism and ectopic lipid deposition in nonobese type 2 diabetic patients. *Diabetes Care* 32, 209–214. doi: 10.2337/dc08-1123

Tsutsumi, C., Okuno, M., Tannous, L., Piantedosi, R., Allan, M., Goodman, D. S., et al. (1992). Retinoids and retinoid-binding protein expression in rat adipocytes. *J. Biol. Chem.* 267, 1805–1810.

Usui, S., Ichimura, M., Ikeda, S., and Okamoto, M. (2009). Association between serum retinol-binding protein 4 and small dense low-density lipoprotein cholesterol levels in young adult women. *Clin. Chim. Acta* 399, 45–48. doi: 10.1016/j.cca.2008.08.017

Vergès, B., Guiu, B., Cercueil, J. P., Duvillard, L., Robin, I., Buffier, P., et al. (2012). Retinol-binding protein 4 is an independent factor associated with triglycerides and a determinant of very low-density lipoprotein-apolipoprotein B100 catabolism in type 2 diabetes mellitus. *Arterioscler. Thromb. Vasc. Biol.* 32, 3050–3057. doi: 10.1161/ATVBAHA.112.255190

Volek, J. S., Phinney, S. D., Forsythe, C. E., Quann, E. E., Wood, R. J., Puglisi, M. J., et al. (2009). Carbohydrate restriction has a more favorable impact on the metabolic syndrome than a low fat diet. *Lipids* 44, 297–309. doi: 10.1007/s11745-008-3274-2

von Jeinsen, B., Short, M. I., Xanthakis, V., Carneiro, H., Cheng, S., Mitchell, G. F., et al. (2018). Association of circulating adipokines with echocardiographic measures of cardiac structure and function in a community-based cohort. *J. Am. Heart Assoc.* 7:97. doi: 10.1161/JAHA.118.008997

Wan, K., Zhao, J., Deng, Y., Chen, X., Zhang, Q., Zeng, Z., et al. (2014). A genetic polymorphism in RBP4 is associated with coronary artery disease. *Int. J. Mol. Sci.* 15, 22309–22319. doi: 10.3390/ijms151222309

Wang, J., Chen, H., Liu, Y., Zhou, W., Sun, R., and Xia, M. (2015). Retinol binding protein 4 induces mitochondrial dysfunction and vascular oxidative damage. *Atherosclerosis* 240, 335–344. doi: 10.1016/j.atherosclerosis.2015.03.036

Wessel, H., Saeed, A., Heegsma, J., Connelly, M. A., Faber, K. N., and Dullaart, R. P. F. (2019). Plasma levels of retinol binding protein 4 relate to large VLDL and small LDL particles in subjects with and without type 2 diabetes. *J. Clin. Med.* 8:792. doi: 10.3390/jcm8111792

White, J. T., and Kelly, J. W. (2001). Support for the multigenic hypothesis of amyloidosis: the binding stoichiometry of retinol-binding protein, vitamin A, and thyroid hormone influences transthyretin amyloidogenicity in vitro. *Proc. Natl. Acad. Sci. U.S.A.* 98, 13019–13024. doi: 10.1073/pnas.241406698

Won, J. C., Park, C. Y., Oh, S. W., and Park, S. W. (2012). Increased plasma levels of retinol-binding protein 4 with visceral obesity is associated with cardiovascular risk factors. *J. Diabetes Investig.* 3, 457–463. doi: 10.1111/j.2040-1124.2012.00213.x

Wu, J., Shi, Y. H., Niu, D. M., Li, H. Q., Zhang, C. N., and Wang, J. J. (2012). Association among retinol-binding protein 4, small dense LDL cholesterol and oxidized LDL levels in dyslipidemia subjects. *Clin. Biochem.* 45, 619–622. doi: 10.1016/j.clinbiochem.2012.02.022

Yang, Q., Graham, T. E., Mody, N., Preitner, F., Peroni, O. D., Zabolotny, J. M., et al. (2005). Serum retinol binding protein 4 contributes to insulin resistance in obesity and type 2 diabetes. *Nature* 436, 356–362. doi: 10.1038/nature03711

Yao-Borengasser, A., Varma, V., Bodles, A. M., Rasouli, N., Phanavanh, B., Lee, M. J., et al. (2007). Retinol binding protein 4 expression in humans: relationship to insulin resistance, inflammation, and response to pioglitazone. *J. Clin. Endocrinol. Metab.* 92, 2590–2597. doi: 10.1210/jc.2006-0816

Yu, Z., Ye, X., Wang, J., Qi, Q., Franco, O. H., Rennie, K. L., et al. (2009). Associations of physical activity with inflammatory factors, adipocytokines, and metabolic syndrome in middle-aged and older chinese people. *Circulation* 119, 2969–2977. doi: 10.1161/CIRCULATIONAHA.108.833574

Zachariah, J. P., Hwang, S., Hamburg, N. M., Benjamin, E. J., Larson, M. G., Levy, D., et al. (2016). Circulating adipokines and vascular function: cross-sectional associations in a community-based cohort. *Hypertension* 67, 294–300. doi: 10.1161/HYPERTENSIONAHA.115.05949

Zhang, J. X., Zhu, G. P., Zhang, B. L., and Cheng, Y. Y. (2017). Elevated serum retinol-binding protein 4 levels are correlated with blood pressure in prehypertensive Chinese. *J. Hum. Hypertens.* 31, 611–615. doi: 10.1038/jhh.2017.44

Zhang, K. Z., Shen, X. Y., Wang, M., Wang, L., Sun, H. X., Li, X. Z., et al. (2021). Retinol-binding protein 4 promotes cardiac injury after myocardial infarction via inducing cardiomyocyte pyroptosis through an interaction with NLRP3. *J. Am. Heart Assoc.* 10:e022011. doi: 10.1161/JAHA.121.022011

Zoccali, C., Mallamaci, F., and Tripepi, G. (2003). Adipose tissue as a source of inflammatory cytokines in health and disease: focus on end-stage renal disease. *Kid. Int. Suppl.* 84, S65–S68. doi: 10.1046/j.1523-1755.63.s84.50.x

Conflict of Interest: The authors declare that the research was conducted in the absence of any commercial or financial relationships that could be construed as a potential conflict of interest.

Publisher's Note: All claims expressed in this article are solely those of the authors and do not necessarily represent those of their affiliated organizations, or those of the publisher, the editors and the reviewers. Any product that may be evaluated in this article, or claim that may be made by its manufacturer, is not guaranteed or endorsed by the publisher.

Copyright © 2022 Ji, Song, Su and Gu. This is an open-access article distributed under the terms of the Creative Commons Attribution License (CC BY). The use, distribution or reproduction in other forums is permitted, provided the original author(s) and the copyright owner(s) are credited and that the original publication in this journal is cited, in accordance with accepted academic practice. No use, distribution or reproduction is permitted which does not comply with these terms.

frontiers in Physiology

ORIGINAL RESEARCH
published: 29 March 2022
doi: 10.3389/fphys.2022.859671

Role of Endothelial Cell Lipoprotein Lipase for Brown Adipose Tissue Lipid and Glucose Handling

*Ellen Thiemann[1], Gerburg K. Schwaerzer[2], Ioannis Evangelakos[1], Marceline M. Fuh[1], Michelle Y. Jaeckstein[1], Janina Behrens[1], Stefan K. Nilsson[3], Manju Kumari[1,4], Ludger Scheja[1], Alexander Pfeifer[2], Joerg Heeren[1] and Markus Heine[1]**

[1]Department of Biochemistry and Molecular Cell Biology, University Medical Center Hamburg-Eppendorf, Hamburg, Germany, [2]Institute of Pharmacology and Toxicology, University Hospital, University of Bonn, Bonn, Germany, [3]Department of Medical Biosciences/Physiological Chemistry, Umeå University, Umeå, Sweden, [4]Department of Internal Medicine III, Heidelberg University, Heidelberg, Germany

Cold-induced activation of brown adipose tissue (BAT) has an important impact on systemic lipoprotein metabolism by accelerating the processing of circulating triglyceride-rich lipoproteins (TRL). Lipoprotein lipase (LPL) expressed by adipocytes is translocated via endothelial to the capillary lumen, where LPL acts as the central enzyme for the vascular lipoprotein processing. Based on preliminary data showing that LPL is not only expressed in adipocytes but also in endothelial cells of cold-activated BAT, we aimed to dissect the relevance of endothelial versus adipocyte LPL for lipid and energy metabolism in the context of adaptive thermogenesis. By metabolic studies we found that cold-induced triglyceride uptake into BAT, lipoprotein disposal, glucose uptake and adaptive thermogenesis were not impaired in mice lacking *Lpl* exclusively in endothelial cells. This finding may be explained by a compensatory upregulation in the expression of adipocyte-derived *Lpl and endothelial lipase (Lipg)*.

Keywords: lipoprotein lipase, triglycerides, endothelial cells, adipocytes, lipoproteins, adipose tissue, thermogenesis, de novo lipogenesis

OPEN ACCESS

Edited by:
Seung-Hyun Ro, University of Nebraska-Lincoln, United States

Reviewed by:
William T. Festuccia, University of São Paulo, Brazil
Debapriya Basu, NYU Grossman School of Medicine, United States

****Correspondence:***
Markus Heine
ma.heine@uke.de

Specialty section:
This article was submitted to Lipid and Fatty Acid Research, a section of the journal Frontiers in Physiology

Received: *21 January 2022*
Accepted: *16 March 2022*
Published: *29 March 2022*

Citation:
Thiemann E, Schwaerzer GK, Evangelakos I, Fuh MM, Jaeckstein MY, Behrens J, Nilsson SK, Kumari M, Scheja L, Pfeifer A, Heeren J and Heine M (2022) Role of Endothelial Cell Lipoprotein Lipase for Brown Adipose Tissue Lipid and Glucose Handling. Front. Physiol. 13:859671. doi: 10.3389/fphys.2022.859671

INTRODUCTION

Brown adipose tissue (BAT) is a thermogenically active organ of mammals that supports adaptation to cold environments through non-shivering thermogenesis. Heat is generated in active brown adipocytes through disconnection of the respiratory chain from oxidative phosphorylation by the proton transporter uncoupling protein-1 (UCP1) at the inner mitochondrial membrane (Cannon and Nedergaard, 2004). This process is highly connected with ß-oxidation of fatty acids that are released from intracellular lipid droplets. Lipolysis of stored triglycerides is initiated by sympathetic stimulation of ß-adrenergic receptors on brown adipocytes which initiates cyclic AMP (cAMP) signaling, resulting in activation of adipose triglyceride lipase and hormone-sensitive lipase (Young and Zechner, 2013). In rodents, BAT thermogenesis is mainly mediated by ß3-adrenergic receptor stimulation (Cannon and Nedergaard, 2004), whereas for human BAT evidence has been provided for both ß2-and ß3-adrenergic receptor signaling (Blondin et al., 2020; Cero et al., 2021). As activated BAT utilizes large amounts of fatty acids, efficient mechanisms are needed to replenish intracellular lipid stores. BAT is a highly vascularized tissue, and upon cold exposure, glucose (Bartelt et al., 2011; Stanford et al., 2013; Heine et al., 2018; Fischer et al., 2019) and fatty acids (Furler et al., 2000; Heine et al., 2018) are taken up in large quantities into brown adipocytes via the endothelium. Glucose handling by activated brown adipocytes is quite complex and a

recent elegant *in vivo* study employing ^{13}C-labeleled glucose showed that under acute cold exposure, glucose is primarily used as fuel for thermogenesis and for the pentose phosphate pathway (Jung et al., 2021). In response to sustained cold adaptation, ^{13}C is also enriched in lactate and glycerol 3-phosphate (Jung et al., 2021). Moreover, under this condition glucose is also used for *de novo* lipogenesis (DNL), which confirms previous studies demonstrating DNL to be a highly active pathway in BAT (Mottillo et al., 2014; Weir et al., 2018). Non-esterified fatty acids (NEFA) are taken up via transporters such as CD36 and are either directly channeled into ß-oxidation or stored in the form of triglycerides in lipid droplets. These fatty acids are mostly derived from triglyceride-rich lipoproteins (TRL) which are processed by lipoprotein lipase (LPL) in the capillary lumen (Bartelt et al., 2011). LPL is the key enzyme for TRL degradation and is highly expressed in organs that consume or store fatty acids in large amounts such as heart, skeletal muscle, white adipose tissue (WAT), and BAT (Merkel et al., 2002; Bartelt et al., 2011; Kersten, 2014; Khedoe et al., 2015). In BAT, LPL is known to be predominantly expressed by brown adipocytes and is translocated to the luminal site of the vascular endothelium by glycosylphosphatidylinositol anchored high density lipoprotein binding protein 1 (GPIHBP1) (Beigneux et al., 2007; Davies et al., 2010; Davies et al., 2012; Olivecrona, 2016). The expression and activity of LPL is regulated in a tissue-specific manner and controlled by different stimuli to provide the optimal supply of organs with fatty acids (Olivecrona et al., 1997; Kersten, 2014). LPL in BAT is mainly stimulated by cold-induction but also refeeding and insulin administration can stimulate enzyme activity (Mitchell et al., 1992; Deshaies et al., 1993; Klingenspor et al., 1996; Kuusela et al., 1997). On the transcriptional level, adipocyte LPL expression is regulated by several transcription factors including among others the peroxisome proliferator-activated receptor gamma (Kersten, 2014). The importance of LPL for systemic lipid metabolism is demonstrated by the observation that LPL deficiency in humans and mice leads to massive hypertriglyceridemia (Coleman et al., 1995; Weinstock et al., 1995). In line, *Gpihbp1*$^{-/-}$ mice are characterized by highly increased plasma triglyceride levels due to the missing translocation of LPL. In the present study, we show that LPL is not only expressed in adipocytes but surprisingly also in endothelial cells of cold-activated BAT. Hence, we investigated the role of LPL expression in these cells by studying transgenic mice lacking LpL exclusively in endothelial cells (EndoLPLko). We observed that LPL expressed by endothelial cells is dispensable for lipoprotein handling and adaptive thermogenesis in both fasted and postprandial state. Furthermore, we provide evidence that the lack of effect on lipoprotein processing in EndoLPLko mice may be explained by a compensatory, higher expression of LPL in brown adipocytes and of LIPG in endothelial cells.

MATERIALS AND METHODS

Animals

All experiments were performed with permission of the Animal Welfare Officers at University Medical Center Hamburg-Eppendorf and Behörde für Gesundheit und Verbraucherschutz Hamburg. To induce Cre-loxP recombination, Cdh5-Cre/ERT2 x *Lpl*$^{flox/flox}$ (EndoLPLko) mice received three consecutive doses of 0.2 mg tamoxifen (Sigma-Aldrich. St. Louis, Missouri, USA) dissolved in 100 µl sunflower oil via gavage 1 week before the experiments. All mice had ad libitum access to food and water and were kept in a temperature-controlled room at given temperatures with a 12 h light: 12 h dark cycle. The mice were fed a chow diet (P1324, Altromin, Germany) or western type diet, ssniff Spezialdiäten GmbH, Germany, duration: 2 weeks before necropsy), as indicated in the text. For the experiments, age- and weight-matched male mice were used. For the combined oral glucose and fat tolerance test (OGFT), turnover study and indirect calorimetry, mice were first fed chow diet and then received western-type diet for 2 weeks. For OGFT and lipoprotein turnover studies body composition (fat and lean mass) was analyzed using a magnetic whole-body composition analyzer (EchoMRI™, Zinsser Analytic GmbH, Eschborn, Germany) 1 day prior to the experiments. For all terminal procedures, mice received 180 mg/kg ketamine and 24 mg/kg xylazine before necropsy.

Metabolic Tracer Studies

For OGFT, mice were fasted for 2 h before receiving an oral gavage of 200 µl of a glucose-lipid emulsion containing 47 mg triglycerides/kg body weight and glucose (2 g/kg body weight). The gavage solution was labelled with ^{14}C-triolein (0.15 MBq/kg body weight, Perkin Elmer, Waltham, MA, USA) and ^{3}H-deoxyglucose (^{3}H-DOG; 0.72 MBq/kg body weight, Hartmann Analytic, Braunschweig, Germany). Organs were harvested 2 h after gavage. For lipoprotein turnover studies, mice were fasted for 4 h and were subsequently tail vein-injected with 100 µl radiolabeled TRLs. Radiolabeled TRLs were prepared by extraction of rat chylomicrons (Skottova et al., 1995) using the method of Folch, addition of radiolabelled ^{14}C-triolein and subsequent sonication. Solvents were evaporated, and labelled TRL were formed by addition of PBS and ^{14}C-triolein (MBq/kg body weight) and subsequent sonication. ^{3}H-DOG (MBq/kg body weight) was added to the emulsion to follow glucose uptake from the circulation without triggering glucose-stimulated insulin secretion. Organs were harvested 15 min after injection. For all experiments, organs from anesthetized mice were harvested after systemic perfusion with PBS-heparin (10 U/mL; Rotexmedica) via the left heart ventricle. Organs were homogenized using Solvable™ (Perkin Elmer) or frozen immediately in liquid nitrogen and stored at −80°C for further analysis. Radioactive counts were determined by scintillation counting using a Tricarb scintillation counter (Liquid Scintillation Analyzer Tri-Carb® 2810TR, Perkin Elmer).

For imaging of TRL disposal in BAT by confocal fluorescence microscopy, an immunofluorescence-based method was used. Briefly, BODIPY™ FL C 16 labeled TRL (BODIPY-TRL) were prepared using a similar approach to radiolabeled TRL. Briefly, 0.2 mg BODIPY™ FL C 16 (D3821, Thermofischer) dissolved in 1 ml Intralipid® (CLINOLEIC 20%, Baxter S.A.) was applied

intragastrically in rats and chylomicrons were obtained from cannulated lymphatic vessels. Lipids were extracted to obtain TRL particles as described above.

TRAP RNA Isolation

TRAP was performed as previously described (Long et al., 2014) with modifications. In brief, small pieces (50–100 mg) of frozen BAT were Dounce-homogenized in 4 ml homogenization buffer (50 mM Tris [pH 7.5], 12 mM MgCl2, 100 mM KCl, 1% NP-40, 100 µg/ml Cycloheximide, 1 mg/ml sodium heparin, 2 mM DTT, 0.2 U/µL RNasin, and 1x Complete EDTA-free protease inhibitor; Roche). After centrifugation at 13,000 rpm for 10 min, the lipid layer was removed and the supernatant was collected and incubated with anti-GFP antibody (5 µg/ml; Abcam, ab290) for 1 h at 4°C. Protein G dynabeads were washed twice in low-salt wash buffer (50 mM Tris [pH 7.5], 12 mM MgCl2, 100 mM KCl, 1% NP-40, 100 µg/ml cycloheximide, and 2 mM DTT), added to the homogenates with antibody, and subsequently incubated for 30 min. Dynabeads with immunoprecipitates were washed three times in high-salt wash buffer (50 mM Tris [pH 7.5], 12 mM MgCl2, 300 mM KCl, 1% NP-40, 100 µg/ml cycloheximide, and 2 mM DTT). Following the last wash, RLT buffer with β-mercaptoethanol was added to dynabeads, and RNA was extracted using a QIAGEN Micro RNeasy kit according to the manufacturer's instructions. For input RNA, 5% of homogenates were mixed with TRIzol and processed according to the manufacturer's instructions to extract total RNA. Isolated RNA was quantified by Qubit.

Gene Expression Analysis

To obtain SVF, interscapular BAT was minced and then digested with 1 mg/ml type II collagenase for 30 min at 37°C (Sigma Aldrich). The dissociated cells were passed through a 100 µm sieve to remove undigested particles. Centrifugation at 700 *g* for 10 min was then performed to separate the SVF pellet from the floating adipocytes. The resulting SVF pellet was dissolved in PBS and passed through a 40 µm sieve to achieve higher purity. For isolation of endothelial cells and brown adipocytes, the filtrate was centrifuged at 600 x g for 5 min, the cell pellet was resuspended and incubated with CD11b MicroBeads for depletion of the macrophage fraction (Miltenyi; 10 µl beads/ 107 cells). CD11b + cells were captured from the lysate using magnetic columns (Miltenyi). The flow through was centrifuged, the pellet was resuspended and incubated with CD31 MicroBeads (Miltenyi; 10 µl beads/107 cells) to isolate endothelial cells. The flow through, containing predominantly adipocytes, was collected. RNA was isolated from cells, tissue samples and SVF using TRIzol Reagent (ThermoFischer Scientific, Waltham, MA, USA) and NucleoSpin RNA/Protein kit (Macherey & Nagel, Düren, Germany) and used for cDNA preparation using the High Capacity cDNA Reverse Transcription kit with RNase Inhibitor (ThermoFischer Scientific) according to the manufacturer's instructions. Real-time PCR using TaqMan Assay-on-Demand primer sets was performed on a QuantStudio 5 Real-Time-PCR System (ThermoFischer Scientific) and relative expression was normalized to the housekeeper Tbp. Taqman® assays used in this study (assay IDs in brackets): *Acaca* (Mm01304285_m1), *Angptl4* (Mm00480431_m1), *Cd36* (Mm00432403_m1), *Chrebpß* (AIVI4CH), *Dio2* (Mm00515664_m1), *Elovl3* (Mm00468164_m1), *Elovl6* (Mm00851223_s1), *Fasn* (Mm00662319_m1), *Glut4* (Mm01245502_m1), *Lipg* (Mm00495368_m1), *Ppargc1a* (Mm00447183_m1), *Scd1* (Mm00772290_m1), *Srebp1c* (AI89KJW), *Tbp* (Mm00446973_m1), U*cp1* (Mm00494069_m1).

Plasma and Lipid Parameters

Plasma triglyceride (Triglyceride FS Kit, DiaSys, Holzheim, Germany), cholesterol (Cholesterin FS Kit, DiaSys), and NEFA levels (NEFA-HR (2)-Kit, FUJIFILM Wako Chemicals, Neuss, Germany) were determined using commercial kits according to the manufacturer's instructions. Blood glucose was determined by conventional test stripes (Accu-Chek, Roche).

Histology and Adipocyte Diameter Determination

A 5 µm thick hematoxylin and eosin-stained section were used for microscopy and size determination. The adipocyte diameter estimates were calculated by NIS-Elements from BAT of 5 independent mice per group.

Indirect Calorimetry and Body Core Temperature

Indirect calorimetry was performed in a TSE phenomaster (TSE Systems) in a temperature- and humidity-controlled chamber as described before (Heine et al., 2018). During the experiment, all mice were housed in single cages at a 12 h light: 12 h dark cycle and had ad libitum access to food and water. EndoLPLko and control mice were kept in the system at 22°C for 6d and for the analysis of energy expenditure, the temperature was decreased to 6°C for 7d. Oxygen consumption and carbon dioxide production were measured every 15 min. Body core temperature was continuously determined using an implantable mouse telemetry system based on G2 E- Mitter (Minimitter System by Starr Life Science) in the TSE phenomaster.

Transwell System

Murine brown adipocytes were seeded and differentiated in the lower chamber of a transwell system. On day seven of the brown adipocyte differentiation protocol (Haas et al., 2009), murine microvascular endothelial cells (InSCREENex GmbH) seeded in a 0.4 µM pore size TC-insert (Sarstedt) were added on the top of the adipocytes. Both brown adipocytes and endothelial cells were (co-)cultured for 4 hours in a media containing 50% differentiation media (DMEM Glutamax (ThermoFisher Scientific) supplemented with 10% FBS, 100 IU/ml penicillin, 100 µg/ml streptomycin, 20 nM insulin, 1 nM triiodothyronine) and 50% endothelial cell media (InSCREENex GmbH) with or without 10 µM CL316,243. RNA was isolated from brown adipocytes and endothelial cells separately.

Statistical Analyses

Data are presented as mean ± SEM. Two groups were compared by unpaired two-tailed Student's t test, more than two groups by one-way or two-way ANOVA, as indicated in the figure legends.

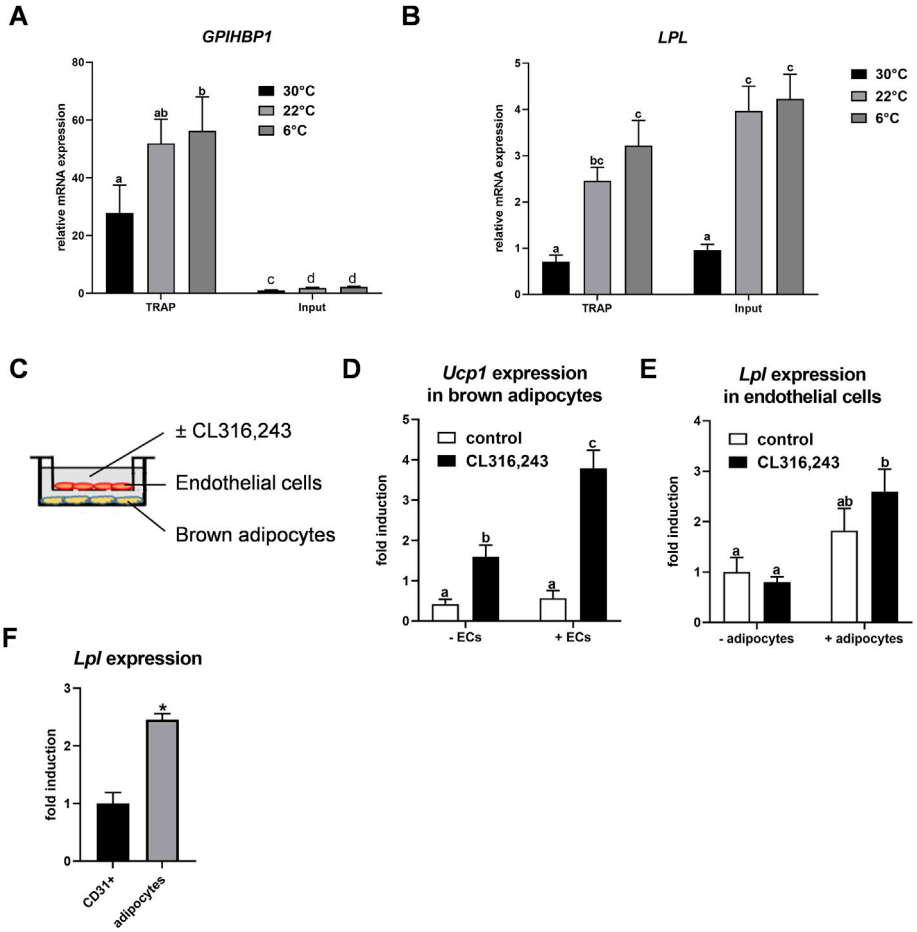

FIGURE 1 | Endothelial expression of LPL in BAT. **(A–B)** EndoNuTRAP mice were housed at 22°C, at 6°C or at 30°C for 3d. Expression of *Gpihbp1* **(A)** and *Lpl* **(B)** in endothelial cells (TRAP) and total tissue (input) of BAT were analyzed by qPCR (n = 4–5). **(C)** Transwell system for co-culturing of murine brown adipocytes with murine microvascular endothelial cells. Endothelial cells were cultured in the presence or absence of differentiated brown adipocytes and were incubated without or with the β3-adrenergic agonist CL316,243 at the same time to thermogenically activate the brown adipocytes. **(D)** *Ucp1* expression in brown adipocytes co-cultured without and with endothelial cells (ECs) (n = 4). **(E)** *Lpl* expression in endothelial cells co-cultured with brown adipocytes (+adipocytes) or without (-adipocytes), stimulated with CL316,243 or with vehicle (none) (n = 4). (F) Wild type mice were housed at 6°C for 3 days and expression of *Lpl* was determined in CD31-positive endothelial cells and thermogenic adipocytes of BAT that were isolated by MACS® (n = 3)Results are presented as mean values ±SEM. Statistical significance for **(A,B)** was determined by one-way ANOVA and for **(D,E)** by two-way ANOVA. Same letter denotes groups that are not significantly different from each other ($p \geq 0.05$). Statistical significance for **(F)** was determined by Student's t test; *$p < 0.05$.

No method was used to determine whether the data met assumptions of either Student's t test or ANOVA. The statistical parameters (i.e., p values, numbers of biological repeats) can be found in the figure legends. No exclusion or inclusion criteria were used for data analyses. Statistical analyses were conducted using Graph Pad software; $p < 0.05$ was considered significant.

RESULTS

Endothelial Cells in Murine Brown Adipose Tissue Express LPL

Previously we described that *Lpl* is expressed in CD31-positive endothelial cells of BAT (Fischer et al., 2021). To confirm this finding, we employed NUTRAP mice, a Cre recombinase-dependent transgenic model that allows cell type-specific gene expression analysis by translating ribosome affinity purification (TRAP). This method employs pulldown of polyribosomes and thus does not require tissue disintegration (Roh et al., 2017). Endothelium-specific NuTRAP (EndoNuTRAP) mice were generated by crossing NuTRAP with VE-cadherin (Cdh5)-Cre mice. To analyze the temperature-dependence of *Lpl* expression, EndoNuTRAP mice were kept at room temperature (22 °C), or exposed to either cold (6°C) or 30°C for 3 days. Efficient enrichment of mRNA from endothelial cells in the BAT lysates was confirmed by high expression of the endothelial marker *Gpihbp1* in the pulldown (TRAP) fraction as compared to whole tissue lysate (input) at all temperatures (**Figure 1A**). Of note, we observed substantial expression of

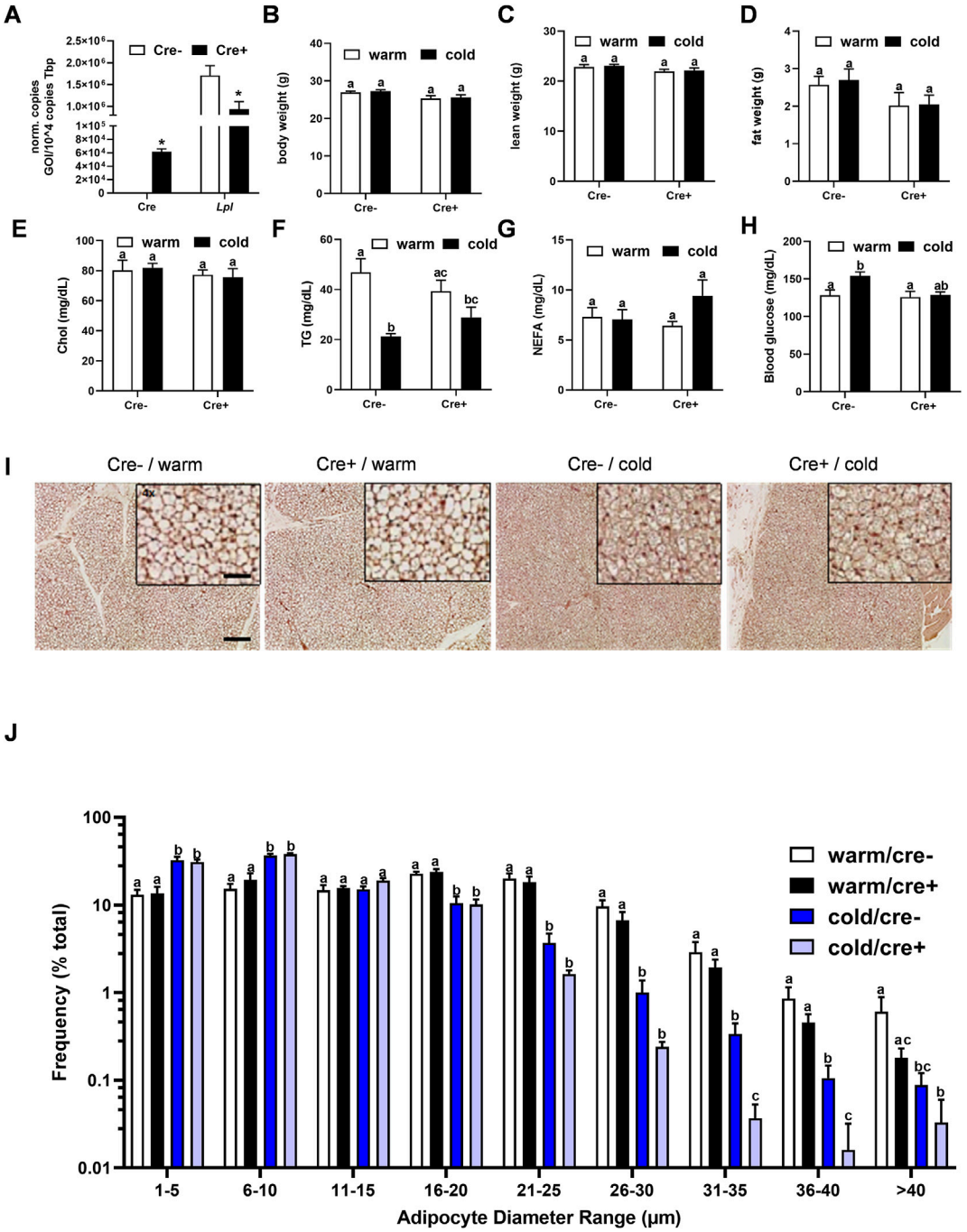

FIGURE 2 | Body composition and BAT lipid content in endothelial cell specific LPL knockout mice. **(A)** Control and EndoLPLko mice received a tamoxifen dosage to generate mice lacking LPL in endothelial cells (Cre+) and controls (Cre-). Mice were exposed to 6°C for 1 day before SVF was isolated from BAT and analyzed for Cre and Lpl expression by qPCR (n = 4). **(B–E)** EndoLPLko mice and litter mates (n = 6) were fed a western-type diet for 2 weeks, and housed at 6°C (cold) or 30°C (warm) in the second week. **(B)** Body weight, **(C)** lean weight and **(D)** fat weight determined by EchoMRI, **(E)** plasma cholesterol (chol), **(F)** triglycerides (TG), **(G)** non-esterified fatty acids (NEFA) and **(H)** blood glucose. **(I)** Hematoxylin eosin staining of BAT. Bars indicate 200 and 50 µm for lower and higher magnification, respectively. **(J)** Ranges of adipocyte diameters calculated from **(I)** using NIS-Elements (Nikon®). Results are presented as mean values ±SEM. Statistical significance was determined by Student's *t* test **(A)** or by two-way ANOVA **(B–D)**. Same letter denotes groups that are not significantly different from each other ($p \geq 0.05$).

Lpl in the endothelial cell fraction that increased with decreasing housing temperatures of the EndoNuTRAP mice (**Figure 1B**). To further investigate the expression of *Lpl* in endothelial cells, we established a transwell system for co-culturing murine microvascular endothelial cells with murine brown adipocytes (**Figure 1C**). To evaluate the potential mutual effects on gene

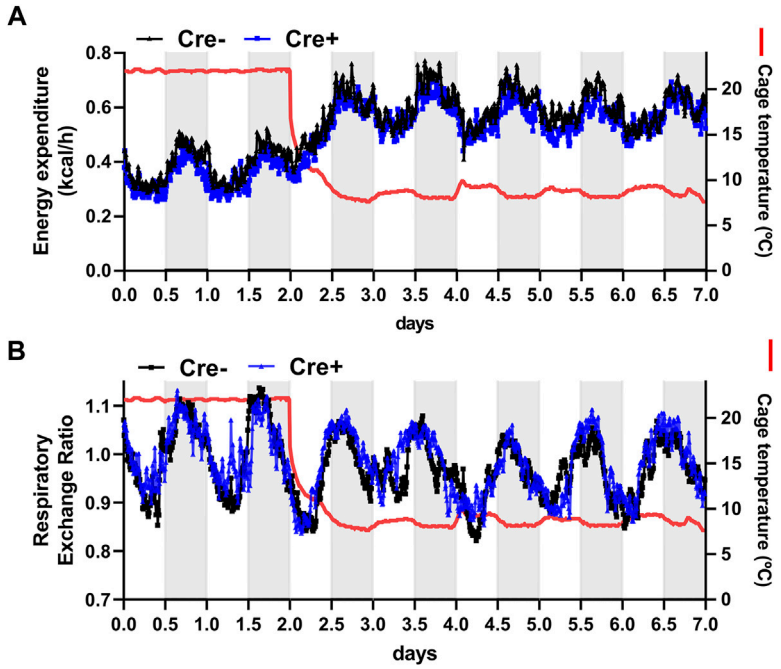

FIGURE 3 | Energy expenditure of endothelial cell-specific LPL knockout mice. For indirect calorimetry analysis EndoLPLko (Cre+) and control (Cre-) mice fed a western-type diet were placed in a TSE phenomaster system. **(A)** Energy expenditure and **(B)** respiratory exchange ratio were determined by indirect calorimetry (n = 3–4). Results are presented as mean values.

expression, we cultured cells alone or in combination that were treated without or with the β3-adrenergic agonist CL316,243. *Ucp1* expression was induced in CL316,243-treated brown adipocytes (**Figure 1D**), which confirms their thermogenic activation. Endothelial cells co-cultured with quiescent brown adipocytes showed a trend for increased *Lpl* expression in comparison to controls without adipocytes (**Figure 1E**). This effect was significant after additional incubation with the ß3-adrenergic receptor agonist CL316,243 (**Figure 1E**). These results suggested that activated brown adipocytes produce paracrine signals that lead to increased *Lpl* expression in endothelial cells. To estimate *Lpl* expression in endothelial cells versus adipocytes from BAT of cold-exposed mice, we employed antibody-based magnetic-activated cell sorting (Fischer et al., 2021). In this setup, *Lpl* mRNA levels were approximately 2.5-fold higher in thermogenic adipocytes compared endothelial cells (**Figure 1F**). Taken together, *Lpl* is expressed at appreciable levels in endothelial cells of cold-activated BAT and endothelial *Lpl* expression is stimulated by brown adipocytes.

Effect of Endothelial Cell Specific LPL Knockout on Energy Homeostasis

To analyze the relevance of endothelial LPL for BAT energy metabolism, endothelial specific LPL knockout mice were created by crossing mice expressing a tamoxifen-inducible Cre recombinase under the control of the VE-cadherin (Cdh5) promoter with floxed *Lpl* mice to generate mice lacking LPL in endothelial cells (EndoLPLko) and control littermates. Cre recombinase expression was detected in stromal vascular fraction (SVF) isolated from BAT of EndoLPLko but not in control mice (**Figure 2A**). Moreover, significant reduced expression of *Lpl* in the SVF confirmed efficient knockdown (**Figure 2A**). Next, we assessed the effect of the endothelial cell-specific knockout on energy balance and metabolism. To create nutritional conditions typical for humans that go along with elevated lipoprotein turnover in adipose tissues (Worthmann et al., 2017), the study was performed with mice that were fed western type diet for 2 weeks. Mice were then housed at thermoneutrality (30°C), a state of thermogenic inactivity (Fischer et al., 2018), or at 6°C (cold) to strongly activate BAT. Under these conditions, body weight (**Figure 2B**), lean weight (**Figure 2C**), fat weight (**Figure 2D**), plasma cholesterol (**Figure 2E**), triglycerides (**Figure 2F**), non-esterified fatty acids (**Figure 2G**) and blood glucose (**Figure 2H**) were not different in EndoLPLko mice compared to control littermates. Except for plasma triglycerides, no significant effects of housing temperature on these parameters was observed. Furthermore, lack of LPL in endothelial cells had no effect on histological BAT appearance studied by hematoxylin and eosin staining (**Figure 2I**). As expected, the diameter of brown adipocytes was smaller in cold-exposed compared to thermoneutral-housed mice but we did not observe a major effect by the genotype (**Figure 2J**).

To further address the role of endothelial cell-specific LPL expression for whole body energy balance in adaptation to cold ambient temperature, EndoLPLko and control mice were subjected to indirect calorimetry. Energy expenditure increased in both genotypes when the mice were exposed to cold

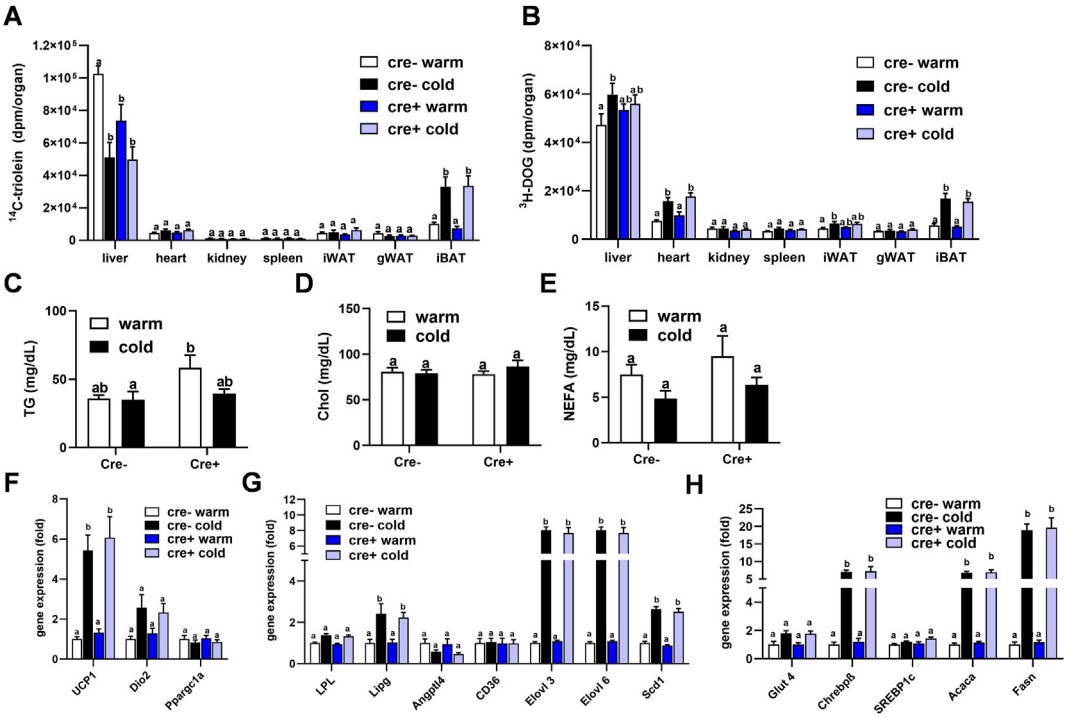

FIGURE 4 | Organ lipid and glucose uptake and BAT gene expression in the postprandial state. EndoLPLko (Cre+) mice and Cre-litter mates (n = 6) were fed a western-type diet for 2 weeks, and housed at 6°C (cold) or 30°C (warm) in the second week. Organ and plasma harvest was performed 2 h after a combined oral glucose and fat gavage. **(A)** Organ uptake of ^{14}C-Triolein and **(B)** ^{3}H-deoxyglucose (^{3}H-DOG). Plasma levels of **(C)** triglycerides, **(D)** cholesterol and **(E)** Non-esterified fatty acids (NEFA). Expression of **(F)** thermogenic, **(G)** lipoprotein and lipid-handling, and **(H)** glucose-handling genes in BAT of EndoLPLko mice. Results are presented as mean values ±SEM. Statistical significance was determined by two-way ANOVA ($p < 0.05$). Same letter denotes groups that are not significantly different from each other ($p \geq 0.05$).

temperature (**Figure 3A**). Furthermore, respiratory exchange rate was slightly lower under these conditions, indicating higher lipid compared to glucose oxidation (**Figure 3B**). However, the EndoLPLko mice exhibited no significant difference in energy expenditure or respiratory exchange rate compared to the Cre-controls, indicating preserved systemic energy homeostasis in the absence of endothelial LPL.

Organ Energy Uptake, Plasma Lipids and BAT Gene Expression in the Postprandial State

To study whether lack of endothelial LPL affects organ-specific energy handling in the postprandial state, EndoLPLko and control mice kept on a western-type diet received a combined fat and glucose gavage containing ^{3}H-deoxyglucose (^{3}H-DOG) and ^{14}C-triolein as radiolabeled tracers. In line with previous data (Bartelt et al., 2011), uptake of ^{14}C-triolein into BAT was increased in cold-exposed mice whereas lipid uptake into the liver was diminished (**Figure 4A**). No significant differences were detected in the other organs investigated. Of note, no effect of endothelial-specific LPL knockdown on ^{14}C-triolein uptake in any organ could be detected, except for a significantly lower hepatic lipid uptake in warm-housed mice (**Figure 4A**). As expected, ^{3}H-DOG uptake into BAT was higher in cold-exposed mice, and this was additionally observed for heart, inguinal WAT and liver (**Figure 4B**). Again, no effect of the different genotypes was observed. Plasma analysis demonstrated that the concentrations of triglycerides (**Figure 4C**), cholesterol (**Figure 4D**) and non-esterified fatty acids (**Figure 4E**) in these mice were not different between the experimental groups.

These data indicate that TRL and glucose disposal in BAT is independent of endothelial LPL expression in the postprandial state. Next, we tested whether this, and the lacking effect of endothelial LPL knockout on energy homeostasis (**Figure 3**), might be due to compensation by altered BAT expression of genes critical for thermogenesis (**Figure 4F**), lipoprotein and lipid processing (**Figure 4G**) or glucose handling (**Figure 4H**). As predicted, cold exposure led to the induction of *Ucp1* (**Figure 4F**) (Cannon and Nedergaard, 2004), endothelial lipase (*Lipg*) (Schaltenberg et al., 2021) and fatty acid elongase 3 (*Elovl3*) (Jakobsson et al., 2005) (**Figure 4G**). Also in line with previous work (Sanchez-Gurmaches et al., 2018), glucose-regulated DNL genes including carbohydrate response element-binding protein-β (*Chrebpβ*), *Elovl6*, acetyl-CoA carboxylase-α (*Acaca*) and fatty acid synthase (*Fasn*) were induced by cold (**Figures 4G,H**). However, at a given housing temperature expression of these genes was not different in EndoLPLko mice compared to

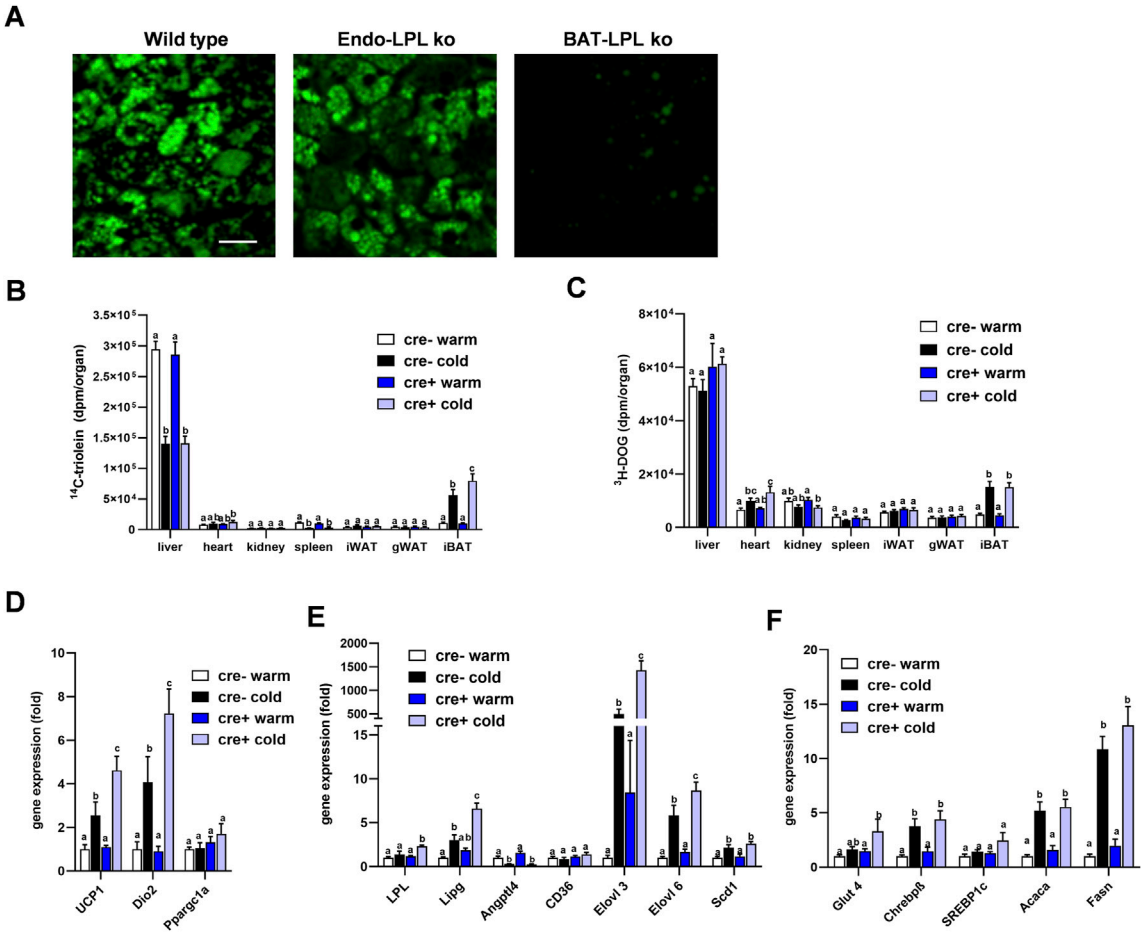

FIGURE 5 | Lipoprotein disposal and BAT gene expression in the fasted state. **(A)** EndoLPLko, mice lacking LPL in brown adipocytes (BATLPLko), and wild type control mice fed a chow diet were housed at 22°C followed by cold exposure (6°C) for 24 h. To analyze TRL uptake, BODIPY-labeled TRL were injected intravenously into animals fasted for 4 h. BAT was harvested for *ex vivo* confocal fluorescence microscopy 15 min after injection. The figure shows representative images of TRL uptake. Bar indicates 20 µm. **(B–F)** EndoLPLko and control mice (n = 5–6) were fed a western-type diet for 2 weeks and housed at 30°C (warm) or 6°C (cold) in the second week. ^{14}C-Triolein labeled TRLs were injected intravenously together with tracer amounts of ^{3}H-DOG. Organs were harvested 15 min after injection. **(B)** Organ uptake of ^{14}C-triolein, and **(C)** ^{3}H-DOG in EndoLPLko (Cre+) and control (Cre-) mice. Gene expression of **(D)** thermogenic, **(E)** lipoprotein and lipid-handling, and **(F)** glucose-handling genes in BAT of EndoLPLko and Cre-control mice. Values are shown relative to Cre-warm. Results are presented as mean values ±SEM. Statistical significance was determined by two-way ANOVA. Same letter denotes groups that are not significantly different from each other ($p \geq 0.05$).

littermates, suggesting that endothelial LPL does not influence postprandial BAT energy and lipid homeostasis.

Lipoprotein Disposal and BAT Gene Expression in the Fasted State

Insulin action on brown adipocytes has been shown to increase LPL-dependent lipoprotein disposal in BAT (Heine et al., 2018), and thus high insulin levels in the postprandial state may mask potential effects of LPL produced in endothelial cells. To investigate the role of endothelial cell LPL in BAT lipid disposal under low insulin conditions, we intravenously injected fluorescently-labeled TRL into mice fasted for 4 h. Interscapular BAT was studied *ex vivo* by confocal microscopy 15 min after the injection. Brown adipocytes from control animals (wild type) showed a strong accumulation of BODIPY-labelled fatty acids within their lipid droplets and the same was observed for EndoLPLko mice (**Figure 5A**). In contrast, mice lacking LPL selectively in brown adipocyte (BAT-LPLko) showed little accumulation of BODIPY fatty acids in BAT. Thus, LPL in endothelial cells, unlike that in brown adipocytes, is not essential for uptake of TRL-derived fatty acids in the fasted state. To further address this notion in a more quantitative fashion, we intravenously injected TRL labeled with ^{14}C-triolein together with ^{3}H-DOG in tracer amounts into fasted mice that were kept on a western type diet and either housed at 30°C (warm) or at 6°C (cold). Notably, we observed that the cold-dependent increase in BAT ^{14}C-triolein uptake was moderately but significantly higher in EndoLPLko mice compared to controls (**Figure 5B**). In contrast, other organs exhibited no genotype effect. In contrast to lipid uptake, ^{3}H-DOG uptake into BAT was not influenced by the absence of LPL in endothelial cells (**Figure 5C**). Of note, further BAT analysis revealed that cold-exposed EndoLPLko mice compared to controls exhibited

increased expression of the thermogenic markers *Ucp1* and deiodinase-2 (*Dio2*) (**Figure 5D**), and of the lipases *Lpl*, *Lipg* as well as the fatty acid elongases *Elovl3* and *Elovl6* (**Figure 5E**). In line with the lack of genotype effect on glucose handling, no effect was observed for glucose-handling genes including DNL enzymes in cold-exposed EndoLPLko versus control mice (**Figure 5F**). Altogether, the lack of endothelial LPL resulted in higher lipid disposal by activated BAT, which may be explained by the compensatory induction in the expression of adipocyte LPL and endothelial LIPG.

DISCUSSION

Activated BAT is characterized by efficient, LPL-dependent disposal of TRL, a metabolic action that is pronounced enough to reverse pathological hypertriglyceridemia (Bartelt et al., 2011). While it was originally assumed that expression of the enzyme in adipose tissue occurs mainly in adipocytes and macrophages, in the present study we detected substantial expression of LPL in endothelial cells of cold-activated BAT. To address the functional role of LPL produced by these cells, we generated and analyzed endothelium-specific LPL knockout (EndoLPLko) mice. Notably, we observed that uptake of fatty acids from TRL is not diminished in either the postprandial or the fasted state. This indicates that LPL produced in endothelial cells is not rate-limiting for TRL triglyceride hydrolysis, despite its close proximity to the site of lipoprotein processing on the vascular face of the endothelium (Goulbourne et al., 2014). Previous work showed that lack of TRL processing in BAT and WAT results in induction of glucose uptake and compensatory *de novo* synthesis of fatty acids (Weinstock et al., 1997; Ullrich et al., 2001; Bartelt et al., 2013). In the present study, we found no effect on BAT glucose uptake and unaltered, glucose-dependent DNL enzyme expression in EndoLPLko mice, indirectly supporting the notion, that influx of lipids into the organ is not altered in a meaningful manner. The underlying reason may be that endothelial LPL is quantitatively irrelevant compared to LPL produced by brown adipocytes that represent the majority of metabolic activity in BAT. LPL produced by activated brown adipocytes controls BAT TRL disposal, as shown in the present study using brown adipocyte-specific knockout, and previously using adipocyte-specific knockouts (Bartelt et al., 2013). Another reason might be, that LPL secretion is less efficient in endothelial cells than in adipocytes, which has been shown to be sensitive to intracellular disturbances requiring specific chaperones and tight redox regulation (Kristensen et al., 2021).

Apart from the lack of direct contribution to TRL hydrolysis, we provide clear evidence that endothelial LPL has a regulatory function in BAT TRL disposal. This is demonstrated by the significant induction of *Lpl* and *Lipg* in BAT of fasted EndoLPLko mice. This unexpected finding suggests that, normally, endothelial LPL generates specific autocrine and paracrine signals to suppress the lipases LIPG and LPL. Consistent with such mechanisms, induction of *Lipg* has previously been observed in mice lacking *Lpl* in whole adipose tissues (Kratky et al., 2005) but not in mice lacking *Lpl* only in adipocytes (Bartelt et al., 2013). Thus, endothelial LPL appears to have specific regulatory functions. This notion is underlined by our observation that not only lipases but also *Ucp1*, *Dio2*, *Elovl3* and *Elovl6* are upregulated in BAT of the fasted EndoLPLko mice, indicating that the genes of these thermogenic and fatty acid-processing markers are under control of endothelial LPL. The mechanisms underlying this regulation remain elusive but it is tempting to speculate that LPL, which has no known function as gene regulator, may affect gene expression via a fatty acid-related transcriptional mechanism. Supporting that view, it was recently shown that intracellular lipolysis mediated by lysosomal acid lipase and subsequent fatty acid oxidation in capillary endothelial cells of BAT is required for activation of the angiogenic transcription hypoxia induced factor (Fischer et al., 2021). This process is important for proper endothelial proliferation, vascularization and thermogenic function of BAT and WAT in response to cold exposure (Fischer et al., 2021; Fischer et al., 2022).

In conclusion, we found that LPL is expressed by endothelial cells of cold-activated BAT. Interestingly, endothelial LPL activity seems not to be involved in lipoprotein clearance needed for energy replenishment but appears to fine-tune the metabolic balance by generating fatty acid-dependent signals that modulate transcriptional pathways in BAT in response to cold exposure.

DATA AVAILABILITY STATEMENT

The original contributions presented in the study are included in the article/Supplementary Material, further inquiries can be directed to the corresponding author.

ETHICS STATEMENT

The animal study was reviewed and approved by University Medical Center Hamburg-Eppendorf and Behörde für Gesundheit und Verbraucherschutz Hamburg.

AUTHOR CONTRIBUTIONS

AP, LS, JH, and MH contributed to conception and design of the study. ET, GS, IE, MF, MJ, JB, SN, MK, and MH performed laboratory experimentation. MH and ET wrote the first draft of the manuscript, and prepared the submitted version together with LS and JH. All authors contributed to editing the manuscript and approved the submitted version.

FUNDING

This work was supported by the City of Hamburg (LFF-FV75), Alexander von Humboldt Postdoctoral Fellowship (MK) and by the DFG-funded CRC/Transregio 333 (project-ID: 450149205).

ACKNOWLEDGMENTS

The authors thank Sandra Ehret, Birgit Henkel, and Meike Kroeger for excellent technical assistance.

REFERENCES

Bartelt, A., Bruns, O. T., Reimer, R., Hohenberg, H., Ittrich, H., Peldschus, K., et al. (2011). Brown Adipose Tissue Activity Controls Triglyceride Clearance. *Nat. Med.* 17 (2), 200–205. doi:10.1038/nm.2297

Bartelt, A., Weigelt, C., Cherradi, M. L., Niemeier, A., Tödter, K., Heeren, J., et al. (2013). Effects of Adipocyte Lipoprotein Lipase on De Novo Lipogenesis and white Adipose Tissue browning. *Biochim. Biophys. Acta (Bba) - Mol. Cel Biol. Lipids* 1831 (5), 934–942. doi:10.1016/j.bbalip.2012.11.011

Beigneux, A. P., Davies, B. S. J., Gin, P., Weinstein, M. M., Farber, E., Qiao, X., et al. (2007). Glycosylphosphatidylinositol-anchored High-Density Lipoprotein-Binding Protein 1 Plays a Critical Role in the Lipolytic Processing of Chylomicrons. *Cel Metab.* 5 (4), 279–291. doi:10.1016/j.cmet.2007.02.002

Blondin, D. P., Nielsen, S., Kuipers, E. N., Severinsen, M. C., Jensen, V. H., Miard, S., et al. (2020). Human Brown Adipocyte Thermogenesis Is Driven by β2-AR Stimulation. *Cel Metab.* 32 (2), 287–300. doi:10.1016/j.cmet.2020.07.005

Cannon, B., and Nedergaard, J. (2004). Brown Adipose Tissue: Function and Physiological Significance. *Physiol. Rev.* 84 (1), 277–359. doi:10.1152/physrev.00015.2003

Cero, C., Lea, H. J., Zhu, K. Y., Shamsi, F., Tseng, Y.-H., and Cypess, A. M. (2021). β3-Adrenergic Receptors Regulate Human Brown/beige Adipocyte Lipolysis and Thermogenesis. *JCI Insight* 6 (11), e139160. doi:10.1172/jci.insight.139160

Coleman, T., Seip, R. L., Gimble, J. M., Lee, D., Maeda, N., and Semenkovich, C. F. (1995). COOH-terminal Disruption of Lipoprotein Lipase in Mice Is Lethal in Homozygotes, but Heterozygotes Have Elevated Triglycerides and Impaired Enzyme Activity. *J. Biol. Chem.* 270 (21), 12518–12525. doi:10.1074/jbc.270.21.12518

Davies, B. S. J., Beigneux, A. P., Barnes, R. H., 2nd, Tu, Y., Gin, P., Weinstein, M. M., et al. (2010). GPIHBP1 Is Responsible for the Entry of Lipoprotein Lipase into Capillaries. *Cel Metab.* 12 (1), 42–52. doi:10.1016/j.cmet.2010.04.016

Davies, B. S. J., Goulbourne, C. N., Barnes, R. H., 2nd, Turlo, K. A., Gin, P., Vaughan, S., et al. (2012). Assessing Mechanisms of GPIHBP1 and Lipoprotein Lipase Movement across Endothelial Cells. *J. Lipid Res.* 53 (12), 2690–2697. doi:10.1194/jlr.M031559

Deshaies, Y., Géloën, A., Paulin, A., Marette, A., and Bukowiecki, L. (1993). Tissue-specific Alterations in Lipoprotein Lipase Activity in the Rat after Chronic Infusion of Isoproterenol. *Horm. Metab. Res.* 25 (1), 13–16. doi:10.1055/s-2007-1002036

Fischer, A. W., Cannon, B., and Nedergaard, J. (2018). Optimal Housing Temperatures for Mice to Mimic the thermal Environment of Humans: An Experimental Study. *Mol. Metab.* 7, 161–170. doi:10.1016/j.molmet.2017.10.009

Fischer, A. W., Jaeckstein, M. Y., Gottschling, K., Heine, M., Sass, F., Mangels, N., et al. (2021). Lysosomal Lipoprotein Processing in Endothelial Cells Stimulates Adipose Tissue Thermogenic Adaptation. *Cel Metab.* 33 (3), 547–564. doi:10.1016/j.cmet.2020.12.001

Fischer, A. W., Jaeckstein, M. Y., and Heeren, J. (2022). Lysosomal Acid Lipase Promotes Endothelial Proliferation in Cold-Activated Adipose Tissue. *Adipocyte* 11 (1), 28–33. doi:10.1080/21623945.2021.2013416

Fischer, A. W., Schlein, C., Cannon, B., Heeren, J., and Nedergaard, J. (2019). Intact Innervation Is Essential for Diet-Induced Recruitment of Brown Adipose Tissue. *Am. J. Physiology-Endocrinology Metab.* 316 (3), E487–E503. doi:10.1152/ajpendo.00443.2018

Furler, S. M., Cooney, G. J., Hegarty, B. D., Lim-Fraser, M. Y., Kraegen, E. W., and Oakes, N. D. (2000). Local Factors Modulate Tissue-specific NEFA Utilization: Assessment in Rats Using 3H-(R)-2-bromopalmitate. *Diabetes* 49 (9), 1427–1433. doi:10.2337/diabetes.49.9.1427

Goulbourne, C. N., Gin, P., Tatar, A., Nobumori, C., Hoenger, A., Jiang, H., et al. (2014). The GPIHBP1-LPL Complex Is Responsible for the Margination of Triglyceride-Rich Lipoproteins in Capillaries. *Cel Metab.* 19 (5), 849–860. doi:10.1016/j.cmet.2014.01.017

Haas, B., Mayer, P., Jennissen, K., Scholz, D., Diaz, M. B., Bloch, W., et al. (2009). Protein Kinase G Controls Brown Fat Cell Differentiation and Mitochondrial Biogenesis. *Sci. Signal.* 2 (99), ra78. doi:10.1126/scisignal.2000511

Heine, M., Fischer, A. W., Schlein, C., Jung, C., Straub, L. G., Gottschling, K., et al. (2018). Lipolysis Triggers a Systemic Insulin Response Essential for Efficient Energy Replenishment of Activated Brown Adipose Tissue in Mice. *Cel Metab.* 28 (4), 644–655. doi:10.1016/j.cmet.2018.06.020

Jakobsson, A., Jörgensen, J. A., and Jacobsson, A. (2005). Differential Regulation of Fatty Acid Elongation Enzymes in Brown Adipocytes Implies a Unique Role forElovl3during Increased Fatty Acid Oxidation. *Am. J. Physiology-Endocrinology Metab.* 289 (4), E517–E526. doi:10.1152/ajpendo.00045.2005

Jung, S. M., Doxsey, W. G., Le, J., Haley, J. A., Mazuecos, L., Luciano, A. K., et al. (2021). *In Vivo* isotope Tracing Reveals the Versatility of Glucose as a Brown Adipose Tissue Substrate. *Cel Rep.* 36 (4), 109459. doi:10.1016/j.celrep.2021.109459

Kersten, S. (2014). Physiological Regulation of Lipoprotein Lipase. *Biochim. Biophys. Acta (Bba) - Mol. Cel Biol. Lipids* 1841 (7), 919–933. doi:10.1016/j.bbalip.2014.03.013

Khedoe, P. P. S. J., Hoeke, G., Kooijman, S., Dijk, W., Buijs, J. T., Kersten, S., et al. (2015). Brown Adipose Tissue Takes up Plasma Triglycerides Mostly after Lipolysis. *J. Lipid Res.* 56 (1), 51–59. doi:10.1194/jlr.M052746

Klingenspor, M., Ivemeyer, M., Wiesinger, H., Haas, K., Heldmaier, G., and Wiesner, R. J. (1996). Biogenesis of Thermogenic Mitochondria in Brown Adipose Tissue of Djungarian Hamsters during Cold Adaptation. *Biochem. J.* 316 (Pt 2), 607–613. doi:10.1042/bj3160607

Kratky, D., Zimmermann, R., Wagner, E. M., Strauss, J. G., Jin, W., Kostner, G. M., et al. (2005). Endothelial Lipase Provides an Alternative Pathway for FFA Uptake in Lipoprotein Lipase-Deficient Mouse Adipose Tissue. *J. Clin. Invest.* 115 (1), 161–167. doi:10.1172/JCI1597210.1172/jci200515972

Kristensen, K. K., Leth-Espensen, K. Z., Kumari, A., Grønnemose, A. L., Lund-Winther, A.-M., Young, S. G., et al. (2021). GPIHBP1 and ANGPTL4 Utilize Protein Disorder to Orchestrate Order in Plasma Triglyceride Metabolism and Regulate Compartmentalization of LPL Activity. *Front. Cel Dev. Biol.* 9, 702508. doi:10.3389/fcell.2021.702508

Kuusela, P., Jacobsson, A., Klingenspor, M., Rehnmark, S., Heldmaier, G., Cannon, B., et al. (1997). Contrasting Adrenergic Effects on Lipoprotein Lipase Gene Expression in the Brown Adipose Tissue of Intact Mice and in Cultured Brown Adipocytes from Mice. *Biochim. Biophys. Acta (Bba) - Lipids Lipid Metab.* 1345 (3), 327–337. doi:10.1016/s0005-2760(97)00008-8

Long, J. Z., Svensson, K. J., Tsai, L., Zeng, X., Roh, H. C., Kong, X., et al. (2014). A Smooth Muscle-like Origin for Beige Adipocytes. *Cel Metab.* 19 (5), 810–820. doi:10.1016/j.cmet.2014.03.025

Merkel, M., Eckel, R. H., and Goldberg, I. J. (2002). Lipoprotein Lipase. *J. Lipid Res.* 43 (12), 1997–2006. doi:10.1194/jlr.r200015-jlr200

Mitchell, J. R., Jacobsson, A., Kirchgessner, T. G., Schotz, M. C., Cannon, B., and Nedergaard, J. (1992). Regulation of Expression of the Lipoprotein Lipase Gene in Brown Adipose Tissue. *Am. J. Physiology-Endocrinology Metab.* 263 (3 Pt 1), E500–E506. doi:10.1152/ajpendo.1992.263.3.E500

Mottillo, E. P., Balasubramanian, P., Lee, Y.-H., Weng, C., Kershaw, E. E., and Granneman, J. G. (2014). Coupling of Lipolysis and De Novo Lipogenesis in Brown, Beige, and white Adipose Tissues during Chronic β3-adrenergic Receptor Activation. *J. Lipid Res.* 55 (11), 2276–2286. doi:10.1194/jlr.M050005

Olivecrona, G. (2016). Role of Lipoprotein Lipase in Lipid Metabolism. *Curr. Opin. Lipidol.* 27 (3), 233–241. doi:10.1097/MOL.0000000000000297

Olivecrona, T., Hultin, M., Bergö, M., and Olivecrona, G. (1997). Lipoprotein Lipase: Regulation and Role in Lipoprotein Metabolism. *Proc. Nutr. Soc.* 56 (2), 723–729. doi:10.1079/pns19970072

Roh, H. C., Tsai, L. T., Lyubetskaya, A., Tenen, D., Kumari, M., Rosen, E. D., et al. (2017). Simultaneous Transcriptional and Epigenomic Profiling From Specific Cell Types Within Heterogeneous Tissues *In Vivo*. *Cell Rep.* 18 (4), 1048–1061. doi:10.1016/j.celrep.2016.12.087

Sanchez-Gurmaches, J., Tang, Y., Jespersen, N. Z., Wallace, M., Martinez Calejman, C., Gujja, S., et al. (2018). Brown Fat AKT2 Is a Cold-Induced Kinase that Stimulates ChREBP-Mediated De Novo Lipogenesis to Optimize Fuel Storage and Thermogenesis. *Cel Metab.* 27 (1), 195–209. doi:10.1016/j.cmet.2017.10.008

Schaltenberg, N., John, C., Heine, M., Haumann, F., Rinninger, F., Scheja, L., et al. (2021). Endothelial Lipase Is Involved in Cold-Induced High-Density Lipoprotein Turnover and Reverse Cholesterol Transport in Mice. *Front. Cardiovasc. Med.* 8, 628235. doi:10.3389/fcvm.2021.628235

Skottova, N., Savonen, R., Lookene, A., Hultin, M., and Olivecrona, G. (1995). Lipoprotein Lipase Enhances Removal of Chylomicrons and Chylomicron Remnants by the Perfused Rat Liver. *J. Lipid Res.* 36 (6), 1334–1344. doi:10.1016/s0022-2275(20)41141-1

Stanford, K. I., Middelbeek, R. J. W., Townsend, K. L., An, D., Nygaard, E. B., Hitchcox, K. M., et al. (2013). Brown Adipose Tissue Regulates Glucose Homeostasis and Insulin Sensitivity. *J. Clin. Invest.* 123 (1), 215–223. doi:10.1172/JCI62308

Ullrich, N. F., Purnell, J. Q., and Brunzell, J. D. (2001). Adipose Tissue Fatty Acid Composition in Humans with Lipoprotein Lipase Deficiency. *J. Investig. Med.* 49 (3), 273–275.

Weinstock, P. H., Bisgaier, C. L., Aalto-Setälä, H., Ramakrishnan, R., Levak-Frank, S., et al. (1995). Severe Hypertriglyceridemia, Reduced High Density Lipoprotein, and Neonatal Death in Lipoprotein Lipase Knockout Mice. Mild Hypertriglyceridemia with Impaired Very Low Density Lipoprotein Clearance in Heterozygotes. *J. Clin. Invest.* 96 (6), 2555–2568. doi:10.1172/JCI118319

Weinstock, P. H., Levak-Frank, S., Hudgins, L. C., Radner, H., Friedman, J. M., Zechner, R., et al. (1997). Lipoprotein Lipase Controls Fatty Acid Entry into Adipose Tissue, but Fat Mass Is Preserved by Endogenous Synthesis in Mice Deficient in Adipose Tissue Lipoprotein Lipase. *Proc. Natl. Acad. Sci. U.S.A.* 94 (19), 10261–10266. doi:10.1073/pnas.94.19.10261

Weir, G., Ramage, L. E., Akyol, M., Rhodes, J. K., Kyle, C. J., Fletcher, A. M., et al. (2018). Substantial Metabolic Activity of Human Brown Adipose Tissue during Warm Conditions and Cold-Induced Lipolysis of Local Triglycerides. *Cel Metab.* 27 (6), 1348–1355. doi:10.1016/j.cmet.2018.04.020

Worthmann, A., John, C., Rühlemann, M. C., Baguhl, M., Heinsen, F.-A., Schaltenberg, N., et al. (2017). Cold-induced Conversion of Cholesterol to Bile Acids in Mice Shapes the Gut Microbiome and Promotes Adaptive Thermogenesis. *Nat. Med.* 23 (7), 839–849. doi:10.1038/nm.4357

Young, S. G., and Zechner, R. (2013). Biochemistry and Pathophysiology of Intravascular and Intracellular Lipolysis. *Genes Dev.* 27 (5), 459–484. doi:10.1101/gad.209296.112

Conflict of Interest: The authors declare that the research was conducted in the absence of any commercial or financial relationships that could be construed as a potential conflict of interest.

Publisher's Note: All claims expressed in this article are solely those of the authors and do not necessarily represent those of their affiliated organizations, or those of the publisher, the editors, and the reviewers. Any product that may be evaluated in this article, or claim that may be made by its manufacturer, is not guaranteed or endorsed by the publisher.

Copyright © 2022 Thiemann, Schwaerzer, Evangelakos, Fuh, Jaeckstein, Behrens, Nilsson, Kumari, Scheja, Pfeifer, Heeren and Heine. This is an open-access article distributed under the terms of the Creative Commons Attribution License (CC BY). The use, distribution or reproduction in other forums is permitted, provided the original author(s) and the copyright owner(s) are credited and that the original publication in this journal is cited, in accordance with accepted academic practice. No use, distribution or reproduction is permitted which does not comply with these terms.

frontiers | Frontiers in Physiology

ORIGINAL RESEARCH
published: 07 April 2022
doi: 10.3389/fphys.2022.855193

UCHL1 Regulates Lipid and Perilipin 2 Level in Skeletal Muscle

*Ryan Antony, Katherine Aby, Hongbo Gao, Mary Eichholz, Rekha Srinivasan and Yifan Li**

Division of Basic Biomedical Sciences, University of South Dakota Sanford School of Medicine, Vermillion, SD, United States

Ubiquitin C-terminal hydrolase L1 (UCHL1) is a deubiquitinating enzyme that was originally found in neurons. We found that UCHL1 is highly expressed in slow oxidative skeletal muscles, but its functions remain to be fully understood. In this study, we observed that UCHL1 protein levels in skeletal muscle and C2C12 myotubes were downregulated by fasting or glucose starvation respectively. Skeletal muscle selective knockout (smKO) of UCHL1 resulted in a significant reduction of lipid content in skeletal muscle and improved glucose tolerance. UCHL1 smKO did not significantly change the levels of key proteins involved in oxidative metabolism such as SDHA, Akt, or PDH. Interestingly, while the levels of the major lipases and lipid transporters were unchanged, perilipin 2 was significantly downregulated in UCHL1 smKO muscle. Consistently, in C2C12 myotubes, UCHL1 siRNA knockdown also reduced perilipin 2 protein level. This data suggests that UCHL1 may stabilize perilipin 2 and thus lipid storage in skeletal muscle.

Keywords: skeletal muscle, lipid, ubiquitin C-terminal hydrolase L1, perilipin 2, mice, C2C12 cell

OPEN ACCESS

Edited by:
Tizhong Shan,
Zhejiang University, China

Reviewed by:
Jeffrey J. Brault,
Indiana University Bloomington, United States
Y. An Xiong,
Southwest Minzu University, China

****Correspondence:***
Yifan Li
yifan.li@usd.edu

Specialty section:
This article was submitted to Striated Muscle Physiology, a section of the journal Frontiers in Physiology

Received: *14 January 2022*
Accepted: *21 March 2022*
Published: *07 April 2022*

Citation:
Antony R, Aby K, Gao H, Eichholz M, Srinivasan R and Li Y (2022) UCHL1 Regulates Lipid and Perilipin 2 Level in Skeletal Muscle. Front. Physiol. 13:855193. doi: 10.3389/fphys.2022.855193

INTRODUCTION

Skeletal muscle is the largest tissue in the body and is critical for metabolism. Skeletal muscles are highly heterogenous and plastic in terms of metabolism and contractility. Based on the nature of their metabolism and contractile activities, skeletal muscle fibers are roughly classified as slow oxidative (type I), fast oxidative (type IIa and IIx), and fast glycolytic (type IIb) fibers (Schiaffino and Reggiani, 2011). The oxidative fibers can use both glucose and fatty acids as energy fuels to generate ATP. The ability of muscle fibers to shift fuel preferences due to various factors and stimuli is known as metabolic plasticity (Kelley, 2005). Skeletal muscle metabolic plasticity is attenuated or diminished in obesity, diabetes, and aging (Storlien et al., 2004), suggesting that metabolic plasticity is critical for whole body metabolic homeostasis.

Fatty acids oxidation (FAO) is the major energy source for oxidative skeletal muscles (Hirabara et al., 2007; Silveira et al., 2008; Turner et al., 2014; Lundsgaard et al., 2018). Free fatty acids (FFAs) are taken up into cells via specific fatty acid transport proteins such as CD36 and fatty acid binding protein (FABP). In the cytosol, FFAs are converted into acyl-coenzyme A (CoA), which is the substrate for FAO as well as lipid synthesis. FAO is carried out in mitochondria through a cyclic process of a series of enzymatic reactions. Muscle lipid homeostasis is determined by fatty acid uptake, β-oxidation, lipid synthesis, and lipolysis (Kelley, 2005; Houten et al., 2016). Intramuscular lipid content is increased with excess fatty acids availability or reduced fatty acid oxidation (Dyck et al., 1997). Impaired fatty acid metabolism and increases intramuscular lipid accumulation in obesity are linked to muscle inflammation (Das, 2001; Reidy et al., 2018) and insulin resistance (Stein and Wade, 2005; Koves et al., 2008; Turcotte and Fisher, 2008; Samuel et al., 2010; Dirks et al., 2016; Dominguez and Barbagallo, 2016; Lalia et al., 2016). On the other hand, endurance exercise training also increases intramuscular lipid, which does not cause insulin resistance but rather increases insulin sensitivity. This phenomenon is known as the athletic paradox

(Goodpaster et al., 2001; Dubé et al., 2008). These facts suggest that it is not the static intramuscular lipid content but the lipid mobilization of the stored lipid that is critical for muscle metabolism and insulin sensitivity. The regulation of intramuscular lipid storage and utilization remain to be fully understood.

The excess FFA in the cytosol will be converted to triglyceride (TG) and stored in lipid droplets (LDs) in the cells (Wang, 2016; Ogasawara et al., 2020) as intramuscular lipids. LDs are the dynamic organelles that control lipid synthesis, storage, mobilization, and lipolysis (Walther and Farese, 2012; Olzmann and Carvalho, 2019). LDs contain neutral lipid enveloped with a phospholipid monolayer embedded with several proteins. The most abundant LD associated proteins are perilipins (Kimmel et al., 2010). Of five members of perilipin family, perilipin 2, 3, and 5 are expressed in skeletal muscle and perilipin 2 is best characterized for its function in regulation of LDs and muscle lipid content (Conte et al., 2016). Perilipin 2 is positively correlated with muscle lipid content (Minnaard et al., 2009). Perilipin 2 protein can be degraded through chaperone-mediated autophagy pathway (Kaushik and Cuervo, 2015) or ubiquitin-proteasome pathway (Xu et al., 2005; Masuda et al., 2006).

Ubiquitin C-terminal hydrolase L1 (UCHL1) is highly expressed in the nervous system and functions as a deubiquitinating enzyme. UCHL1 is also expressed in some peripheral tissues, including pancreas, liver, some cancer tissues, as well as skeletal muscles, yet its function in skeletal muscle needs to be better understood. Our recent work showed that skeletal muscle UCHL1 is involved in mTORC1 activity (Gao et al., 2019). In this study, we report that muscle UCHL1 affects intramuscular lipid metabolism by stabilizing perilipin 2.

METHODS

Animals

All experimental protocols and use of animals in this study were reviewed and approved by the University of South Dakota Institutional Animal Care and Use Committee (IACUC) and followed the NIH guideline of animal use in research under protocol No. 1-03-19-22D. As previously mentioned (Gao et al., 2020), the mouse line carrying floxed UCHL1 was generated from a strain of "UCHL1 HEPD0603_7_h04" provided by the UK Medical Research Council on behalf of the European Mouse Mutant Archive (EMMA). The mouse strain with skeletal muscle specific knockout (smKO) of UCHL1 was generated by crossing a mouse carrying floxed UCHL1 and a mouse expressing cre under the skeletal muscle specific myosin light polypeptide promoter (The Jackson Laboratory, stock # 024713). For genotyping as well as for identification, a singular toe was taken from each new born mouse around 5 days after birth. The genome DNA was extracted from the toe tissue using protease K digestion method. The genotype of each mouse was confirmed using PCR with primers for floxed UCHL1 and Cre.

Glucose Tolerance and Insulin Tolerance Tests

Glucose tolerance testing (GTT) and insulin tolerance test (ITT) were done in 3-month-old WT and UCHL1 smKO mice. Both groups of mice were trained for several days before testing by placing the mice in a 50 ml tube for 2 minutes and allowing them to adapt to the testing environment. Food was removed from cages the night prior to testing to allow for a 12 h fasting period. Mice were placed in the tube for 1 min, a cut was made at the end of the tail and the blood glucose was measured using a OneTouch Ultra 2 blood glucose meter (LifeScan, Pennsylvania, United States). Blood glucose was taken before (baseline) and at 15, 30, 60, 90, and 120 min after intraperitoneal injection of glucose solution (2 g/kg) or insulin saline (2 U/kg). The glucose tolerance curves were generated and the areas under curve (AUC) were analyzed using GraphPad Prism 9.0.

Tissue Collection

As previously described (Gao et al., 2020), mice were anesthetized using isoflurane (3–4%). Muscles of the hind limb were exposed by removing the skin. The soleus (slow oxidative fibers) and extensor digitorum longus (EDL) (fast glycolytic fibers) muscles were collected in DNase/RNase free tubes and frozen on dry ice for Western blot assay. For tissue staining, soleus muscles were isolated and snap frozen in pre-chilled 2-methylbutane (Kumar et al., 2015), then embedded in optimal cutting temperature compound (OCT) on dry ice and stored at −70°C for future cryosectioning. Muscles were sectioned into 10-15 μm sections and adhered onto slides for staining.

Muscle Staining

Intramuscular lipid was stained using Bodipy or oil red O staining.

Bodipy staining was based on published works (Spangenburg et al., 20112011; Qiu and Simon, 2016) with minor modifications. Slides were removed from the −70°C freezer and immediately fixed with 4% paraformaldehyde (PFA) for 15 min. Slides were then washed in PBS 3 times for 5 min each, and then incubated for 30 min at room temperature in a Bodipy 493/503 (ThermoFisher, D3922) in DMSO with a concentration of 3.8 mM. Following 3 washes in PBS for 5 min each, slides were mounted with Fluoromount-G solution (Southern Biotech, 0100-01) for imaging.

The oil red o staining was performed using the oil red o kit (VitroVivo Biotech, VB-3007) following the manufacturer's protocol with modifications. Slides were brought to room temperature for 30 min and fixed in 10% formalin for 20 min, followed by 30 min of air drying at room temperature. Slides were submerged in the pre-stain solution for 5 min, then incubated in pre-warmed Oil Red O solution at 60°C for 10 min, and immediately submerged into pre-warmed differentiating solution for 5 min at 60°C. The slides were removed from the solution and rinsed in 2 changes of Milli Q pure water before submerging in Myers Hematoxylin solution for 20–30 s at room temperature. The slides were then washed with tap water for 3 min, rinsed with Milli Q pure water, then mounted with Fluoromount-G solution (Southern Biotech, 0100-01).

For fluorescent staining for type I muscle fiber and UCHL1, muscle sections were fixed with 4% paraformaldehyde, washed with PBST, and incubated overnight with mouse antibody for type I myosin heavy chain (Developmental Studies Hydridoma

Bank, BA-D5) and rabbit antibody for UCHL1 (Abcam, ab108986). Following 3 washes with PBST, the sections were incubated with secondary antibodies goat-anti-mouse conjugated with Alexa-488 and goat-anti-rabbit conjugated with Alexa-594 (Invitrogen). Following 3 washes with PBST, the sections were mounted with Fluoromount-G and imaged using a fluorescent microscope (Olympus).

Cell Culture and Gene Knockdown

As previously described (Antony and Li, 2020), C2C12 myoblasts were cultured in complete media (CM) made of dulbecco's modified eagle's medium (DMEM, ThermoFisher-Gibco) containing 10% fetal bovine serum (FBS), 1% penicillin-streptomycin, and 1% HEPES. For glucose and serum starvation experiments, fully confluent cells were switched into fresh CM, incomplete media (ICM, FBS free), or FBS-free and glucose-free media (NG) overnight and then harvested for Western blot. To achieve UCHL1 knockdown (KD), once fully confluent the cells were switched into 1 ml ICM and treated with a mixture of Lipofectamine RNAiMAX (ThermoFisher, 13,778,075) and UCHL1 siRNA (IDT) for approximately 8 h. Following this, 1 ml of differentiating media (DM) made of DMEM containing 2% horse serum, 1% penicillin-streptomycin, and 1% HEPES was added to the cells. Following the overnight incubation, cells were switched to 2 ml of fresh DM. DM was changed every 72 h for a total incubation time of 12 days before being harvested for Western blot (WB).

Total Protein Extraction and Western Blot

Soleus muscle tissues were homogenized in 1X RIPA buffer containing 1% protease inhibitor cocktail (Research Products International, P50600-1), 1% phosphatase inhibitor cocktail (Research Products International, P52104-1), 0.1% SDS, and 0.1% MG132. The muscle was placed in a 1.5 ml tube and homogenized using a plastic pestles connected to an electric driver. The tissue was crushed prior to adding the above buffer, and then continuously homogenized for about 30 s in the buffer. The homogenates were allowed to set in the buffer for approximately 30 min on ice before being homogenized one more time. Tubes were then spun down at 10,000 xg for 5 min at 4°C. Protein concentration of the supernatants of muscle homogenates was determined by a standard BCA assay. The protein concentration of all samples were normalized to the same concentration. Cells were homogenized using the same buffer and concentrations of cocktails.

Western blot was performed as described previously (Gao et al., 2020). In addition to a mass ladder (BioRad Precision Plus Protein All Blue Standard) loaded into each end lane, 15 µl of homogenized muscle/cell samples containing loading buffer at a concentration of approximately 2.5 µg/µl were subject to electrophoresis in 11–16% gradient gels at 100 V for approximately 3 h. Proteins were transferred on to 0.22 µM nitrocellulose membranes at 350 mA using a trans-blot apparatus (Bio-Rad, Hercules, CA). The membranes were fixed in 50% methanol for 30 min at 4°C followed by 30 min at 37°C. The membranes were then blocked with 3% non-fat milk in PBST for 1 h on a rocker at room temperature. The membranes were then incubated with primary antibodies and 0.5% BSA in PBST overnight at 4°C. The following antibodies were used: anti UCHL1 (Abcam, 108986), GAPDH (Santa Cruz, sc-47724), Actin (Santa Cruz, sc-47778), DGAT2 (Santa Cruz, sc-293211), ATGL (Cayman, 10,006,409), Perilipin 2 (Novus, NB110-40877), Perilipin 3 (Novus, NB110-40764), OXPAT (Novus, NB110-60509), MAGL (Cayman, 100035), CD36 (Protein tech, 18836-1-AP), Akt (Cell Signaling Technologies, 9,272), phosphor-Akt (Cell Signaling Technologies, 4,051), AMPK (Cell Signaling Technologies, 2,793), phosphor-AMPK (Cell Signaling Technologies, 2,535), SDHA (Abcam, ab14715), SDHB (Abcam, ab178423), PDH (Cell Signaling Technologies, 3,205), and HSL (Cayman, 10,006,371). Following 3 washes with PBST for 5 min each, membranes were incubated with the appropriate secondary antibodies conjugated with Alexa-680 or 800 (Invitrogen) for 1 h at room temperature followed by 2 washes with PBST and 1 wash with PBS. The protein bands on the membrane were imaged using a LICOR scanner (LICOR Biosciences, Lincoln, NE). Following the imaging, some membranes were stained for total protein load using Imperial Protein Stain solution (ThermoFisher, UF286575) and de-stained with 50% methanol and 10% glacial acetic acid. Band densities of the proteins were analyzed using NIH ImageJ software and normalized against total protein stain bands or GAPDH in tissue samples or Actin in cell samples; the ratio of UCHL1 and other proteins were then calculated and compared between KO/KD and WT/Control.

Triglyceride Assay

The triglyceride content in muscle homogenates was measured using the triglyceride colorimetric assay kit (Cayman, 10,010,303) by following the manufacturer's protocol. In a 96 well plate, a standard curve was prepared using the included standard reagents and diluents. In each well, 10 µL of sample and 150 µL of the assay enzyme solution were added, thoroughly mixed on a microplate shaker (FisherBrand, 88,861,023), and then incubated for 30 min at 37°C. The absorbance of theassay was measured using a TECAN plate reader (TECAN, Infinite m200) and Magellan software. Absorbance of samples was analyzed to determine differences between WT and KO groups.

Data Analysis

All data calculations, descriptive statistics, and graphing were performed using Microsoft Excel and GraphPad Prism 9.0. To quantify Western blot results, a protein band density was normalized by total protein stain, GAPDH or beta actin as loading controls. The mean value of the WT/Control group was calculated, followed by calculating the ratio between each individual sample to that of the WT/Control mean. The mean values of the ratio of WT/Control and KO/KD samples were compared between two groups by the two-tailed *t*-test; Statistical significance was defined as p value less than 0.05. Data was presented as mean ± SD. To quantify glucose testing results, the mean values of glucose at each time point and an area under curve for both the WT and KO groups were calculated and compared using a two-tailed *t*-test to determine the statistical significance between the two groups.

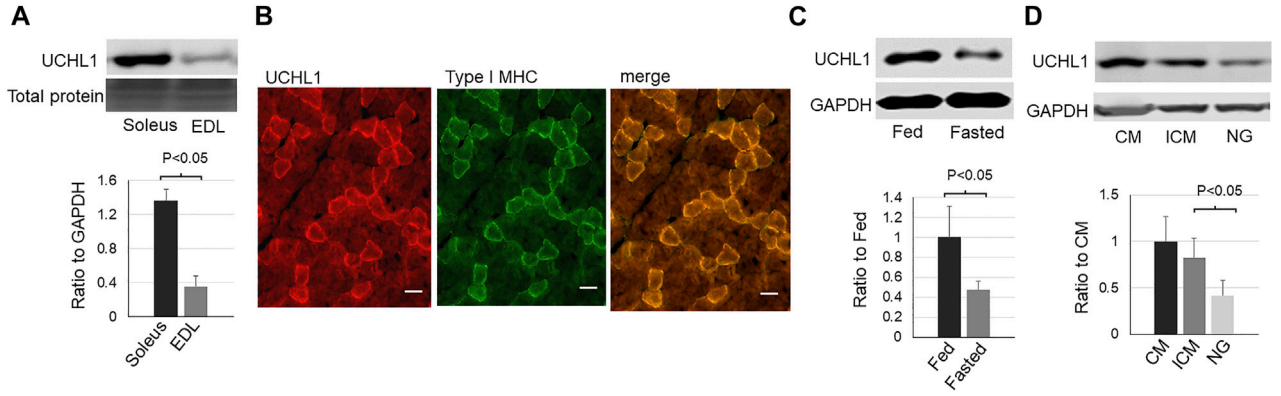

FIGURE 1 | Western blot images (top) and quantifications (bottom) of UCHL1 in mouse skeletal muscles or C2C12 myotubes. **(A)**: UCHL1 protein levels in slow oxidative muscle soleus and fast glycolytic muscle EDL (n = 4); **(B)**: Immunofluorescent staining for UCHL1 (red) and type I myosine heavy chain (green) in soleus muscle section. The scale bar = 20 μm). **(C)**: UCHL1 protein levels in soleus from fed or fasted mice (n = 3 per group); **(D)**: UCHL1 protein levels in C2C12 myotubes complete media (CM, containing 10% FBS and 4.5 g/L glucose), incomplete media (ICM, containing 4.5 g/L glucose but no FBS), or the media without FBS and glucose (NG). (n = 4 per group).

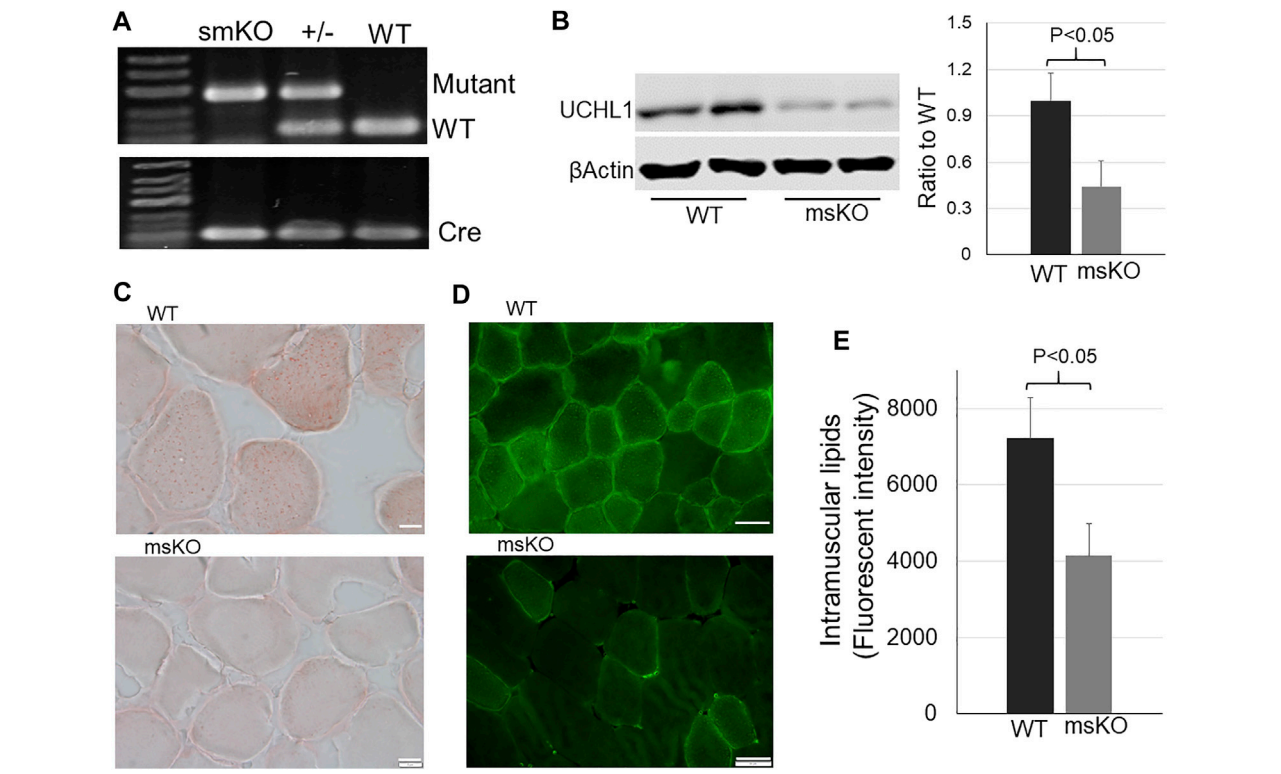

FIGURE 2 | Lipid content in skeletal muscle. **(A)**: Gel images of PCR genotyping to identify smKO, heterozygous, and WT genotypes; **(B)**: Western blot for UCHL1 in muscle from WT and UCHL1 smKO mice. n = 4. **(C)**: Oil-red-O staining for lipid in muscle from WT or UCHL1 smKO mice. The scale bar = 5 μm. **(D)**: Bodipy staining for lipid in muscle from WT or UCHL1 smKO mice. The scale bar = 20 μm. **(E)**: Lipid (triglyceride) in muscle homogenate of WT or UCHL1 smKO mice. n = 4 per group.

RESULT

UCHL1 Level is Downregulated by Fasting

In skeletal muscle, UCHL1 is highly expressed in soleus, a typical slow oxidative muscle, and is very low in EDL, a typical fast glycolytic muscle (**Figure 1A**). Immunofluorescent staining showed the colocalization of UCHL1 and type I slow oxidative fibers (**Figure 1B**). Fasting, which promotes muscles fatty acid oxidation, downregulated UCHL1 in soleus (**Figure 1C**). Consistent with this, in differentiated C2C12 myotubes,

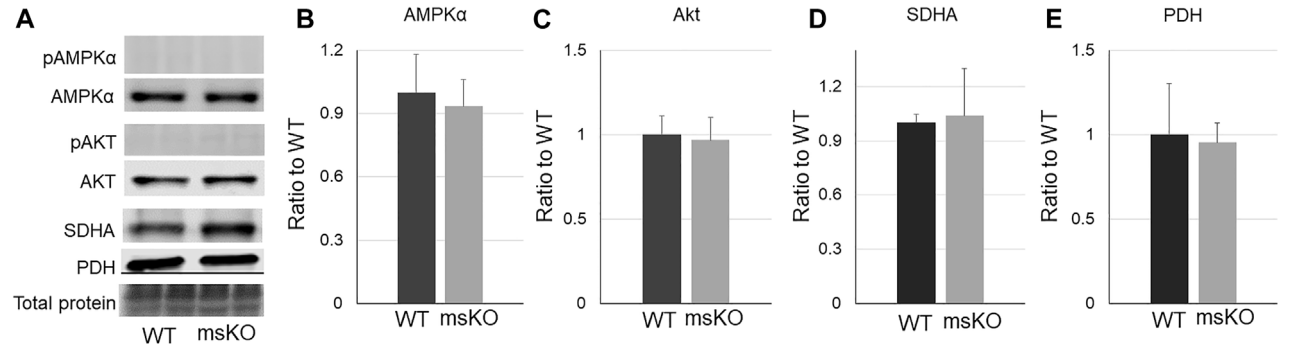

FIGURE 3 | Western blot images **(A)** and quantifications **(B–E)** of muscle samples from WT and UCHL1 smKO mice for key proteins that are involved in lipid metabolisms, including AMPKα (**(B)**, n = 5), Akt (**(C)**, n = 3), SDHA (**(D)**, n = 5), and PHD (**(E)**, n = 3).

UCHL1 level was also downregulated by glucose starvation (**Figure 1D**). Since fasting is known to shift muscle energy metabolism toward lipid oxidation, this data suggests that UCHL1 may be involved in lipid metabolism in skeletal muscle.

UCHL1 smKO Reduced Lipid Content in Skeletal Muscle

To test the functional role of UCHL1 in skeletal muscle, we have generated skeletal muscle specific knockout (smKO) of UCHL1. The genotype of homozygous floxed UCHL1 and cre transgene was confirmed by PCR and a significant reduction of UCHL1 protein level in skeletal muscle was confirmed by Western blot (**Figure 2A**). The intramuscular lipid content was measured by oil-red-o staining (**Figure 2B**), BODIPY staining (**Figure 2C**), and triglyceride assay (**Figure 2D**). As shown in these panels, the intramuscular lipid content was significantly reduced in the muscle from UCHL1 smKO mice when compared with WT. This data suggests that skeletal muscle UCHL1 may play an essential role in maintaining lipid content in skeletal muscle.

UCHL1 smKO did Not Affect the Levels of Key Proteins Involved in Metabolism

Intramuscular lipid content can be affected by overall metabolism. We then measured the level of some key proteins that regulate metabolism and mitochondrial function, including phosphorylated and total AMPKα (**Figure 3B**), phosphorylated and total Akt (C), succinate dehydrogenase (SDH) (**Figure 3D**), and pyruvate dehydrogenase (PDH) (**Figure 3E**). However, none of these proteins were altered in the UCHL1 smKO muscle. The levels of phosphorylated Akt and AMPK were nearly undetectable in both WT and UCHL1 smKO samples.

Reduced perilipin2 in UCHL1 smKO Muscle

Lipid content is determined by fatty acid transport, lipid synthesis, lipolysis, and lipid storage. We then assessed the level of proteins that are related to these functions. CD36, which is the major protein responsible for fatty acid transport, was not altered in UCHL1 smKO muscle (**Figure 4E**). The levels of three major lipases, ATGL (**Figure 4B**), HSL (**Figure 4C**), and MAGL (**Figure 4D**), also remained unchanged in UCHL1 smKO muscle, suggesting that the reduction of lipid content in UCHL1 smKO muscle is unlikely due to the increase in lipolysis activity. Interestingly, perilipin2, a key protein that is associated with and stabilize lipid droplets, was significantly reduced in UCHL1 smKO muscle (**Figure 4H**), suggesting the possibility that UCHL1 may be essential to stabilize perilipin 2 and thus lipid storage. Perilipin 3 level (**Figure 4G**) was significantly upregulated in UCHL1 smKO muscle, potentially a compensatory response to the reduction of perilipin2. The major lipid synthase DGAT2 was also upregulated in UCHL1 smKO, which may also be a compensatory response to the reduced lipid content.

Perilipin 2 Was Downregulated by UCHL1 Gene Knockdown in C2C12 Cells

To further determine whether UCHL1 regulates perilipin 2, we used siRNA to knock down (KD) UCHL1 in differentiated C2C12 myotubes. Consistent with the animal data, UCHL1 KD significantly reduced perilipin 2 protein level (**Figures 5A,B**). UCHL1 KD also upregulated CD36 (**Figure 5D**) and downregulated lipase HSL (**Figure 5E**) and MAGL (**Figure 5F**) in C2C12 cells, potentially compensatory responses to the reduced perilipin 2 and possible low lipid content. These later changes, however, were not seen in the muscle with UCHL1 KO.

UCHL1 smKO Improved Insulin Sensitivity

To test whether the reduction of intramuscular lipid affected glucose metabolism and insulin sensitivity, we conducted GTT and ITT. Mice with UCHL1 smKO have improved glucose tolerance (**Figures 6A,B**) as well as insulin tolerance (**Figure 6C**), suggesting the lower intramuscular lipid content induced by UCHL1 smKO has favorable effects on glucose metabolism and insulin sensitivity.

DISCUSSION

This study provides evidence for the first time showing that skeletal muscle UCHL1 is involved in regulation of intramuscular lipid content. In skeletal muscle, oxidative muscle uses both

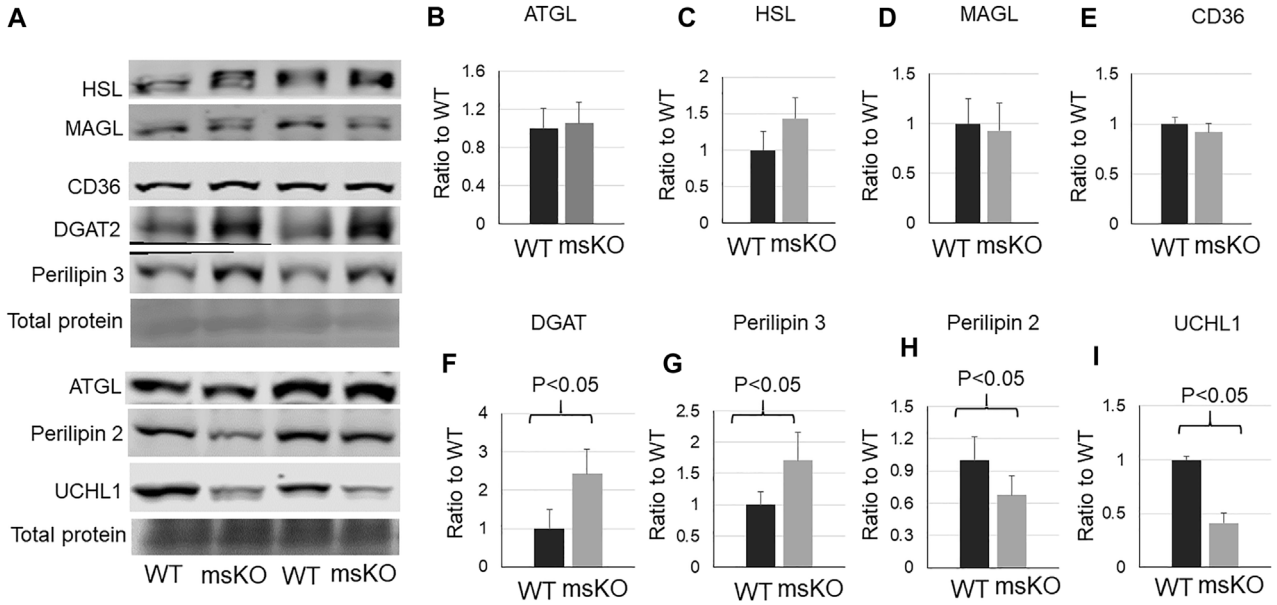

FIGURE 4 | Western blot images **(A)** and quantifications **(B–I)** of muscle samples from WT and UCHL1 smKO mice for lipase ATGL **(B)**, HSL **(C)**, and MAGL **(D)**, the fatty acid transport protein CD36 **(E)**, the key lipid synthesis enzyme DGAT2 **(F)**, perilipin 3 **(G)**, perilipin 2 **(H)**, and UCHL1 **(I)**. n = 4-5 per group.

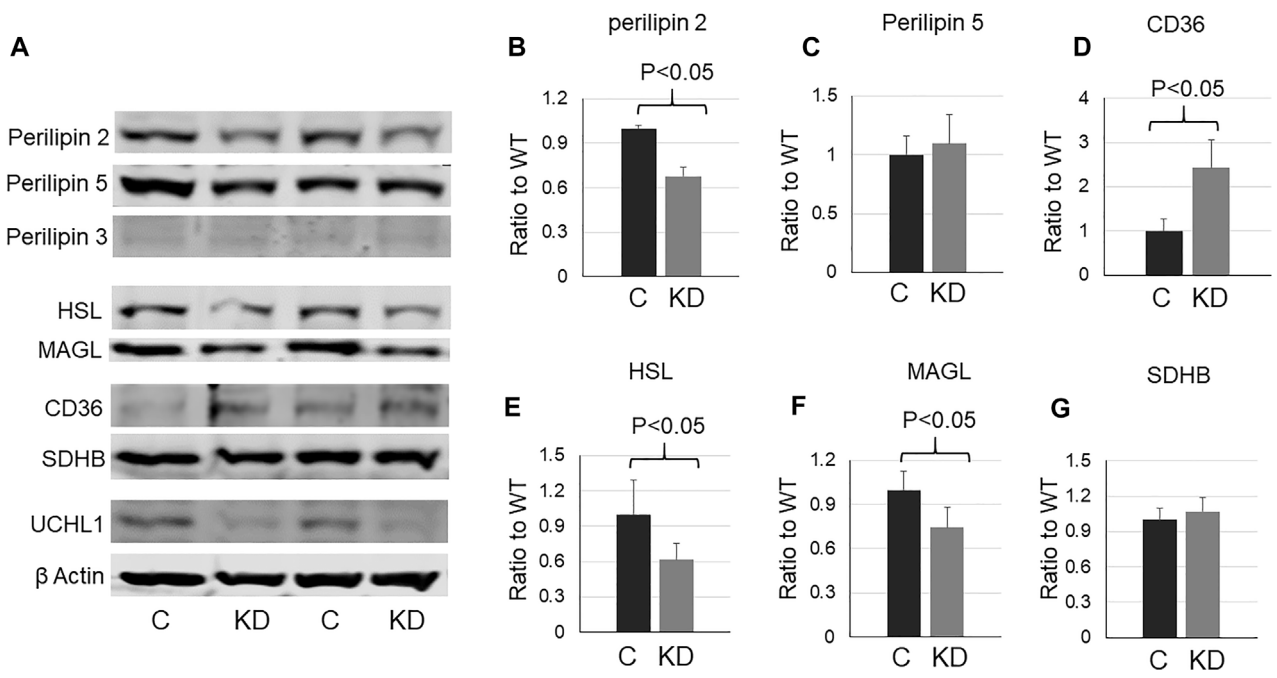

FIGURE 5 | Western blot images **(A)** and quantifications **(B–G)** of cell lysates from C2C12 myotubes with control or UCHL1 siRNA knockdown for perilipin 2 **(B)**, perilipin 5 **(C)**, CD36 **(D)**, HSL **(E)**, MAGL **(F)**, and SDHB **(G)**. n = 4 per group.

glucose and fatty acids as energy fuel, depending on the availability. When extracellular glucose levels are low, such as during fasting and exercise, the energy metabolism in oxidative muscles shifts to fatty acid oxidation. We observed that UCHL1 was highly expressed in oxidative muscle such as soleus but has very low levels in the glycolytic EDL. Moreover, skeletal muscle UCHL1 was downregulated by fasting in mice and glucose starvation in C2C12 cells, suggesting that UCHL1 may be involved in energy metabolism shift. Consistent with this, selective gene knockout of UCHL1 in skeletal muscle

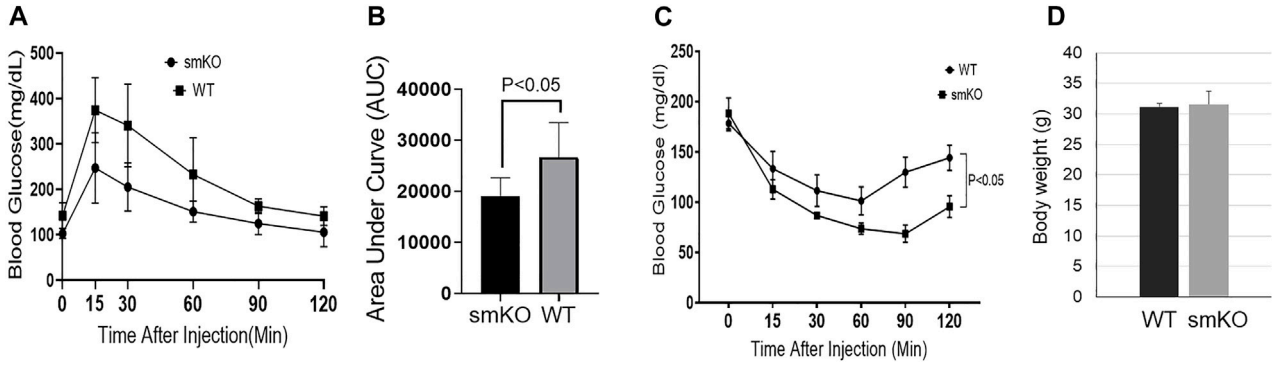

FIGURE 6 | Glucose tolerance test and insulin tolerance test. **(A–B)**: GTT curve **(A)** and area under the curve **(B)**; n = 5 per group. **(C)**: ITT curve. n = 5–6 per group. **(D)**: body weight. n = 6 per group.

significantly reduced intramuscular lipid. Together, these results suggest that UCHL1 may function to facilitate lipid storage in skeletal muscle, and downregulation of skeletal muscle UCHL1 in fasting and starvation may be essential to mobilize stored lipid for lipolysis to increase free fatty acid availability for oxidation.

The level of intramuscular lipid content can be affected by many factors, including free fatty acid uptake, lipid synthesis, lipolysis, and fatty acid oxidation. Our results showed that in UCHL1 smKO skeletal muscle there were no changes with protein levels of CD36, the major fatty acid transporter (Pepino et al., 2014), ATGL, HSL, and MAGL, the major lipases (Badin et al., 2011), suggesting that the reduced intramuscular lipid by UCHL1 smKO is unlikely due to the reduced fatty acid transport and increased lipolysis. It is also unlikely due to the reduced lipid synthesis because a major lipid synthase, DGAT2, was upregulated in muscle with UCHL1 knockout, potentially a compensatory response to the low lipid levels. AMPK and Akt pathways are major signaling pathways to promote lipolysis, mitochondrial biogenesis, and fatty acid oxidation. Our data did not show any changes in total protein level and phosphorylation of AMPK and Akt, the two major pathways that regulate lipid metabolism, in UCHL1 smKO muscle. Protein levels of SDHA and PDH, two mitochondrial markers, were also unchanged in UCHL1 smKO muscle. Together, these results suggest that the reduced lipid content in UCHL1 smKO muscle may not be due to the increased fatty acid oxidation.

Intramuscular lipids are stored into lipid droplets (LDs) (Walther and Farese, 2012). LDs are active organelles that contain and store toxic lipid as energy depots (Listenberger et al., 2003). When energy fuel runs low such as during fasting or exercise, LDs can mobilize stored lipid for lipolysis to increase free fatty acids for oxidation (Rambold et al., 2015). LD membranes are embedded with different proteins, among which is the family of perilipin proteins (Kimmel and Sztalryd, 2016). Perilipin 2 (also known as adipose differentiation-related protein, ADFP) is one of the 5 proteins in the perilipin family. Perilipin 2 is highly expressed in adipose tissues and skeletal muscle in rodents and humans (Minnaard et al., 2009). This protein is not only critical for LDs membrane integrity but can also interact with major lipases such as ATGL (MacPherson et al., 2013) or be targeted by chaperone-mediated lipophagy to mobilize stored lipid for lipolysis (Kaushik and Cuervo, 2015). Our results indicate that UCHL1 knockout in mouse skeletal muscle or knockdown in C2C12 cells result in the reduction of perilipin 2 protein level. It is plausible to propose that the downregulation of perilipin 2 may be responsible for the reduction of lipid content in UCHL1 knockout muscle. Indeed, perilipin knockout resulted in reduced lipid content in myotubes (Feng et al., 2017). UCHL1 functions as a deubiquitinating enzyme, while perilipin 2 is subjected to ubiquitin-proteasome degradation (Xu et al., 2005; Masuda et al., 2006). Therefore, UCHL1 may stabilize perilipin 2 by reducing its ubiquitination and proteasome-mediated degradation; thus, UCHL1 downregulation or deletion can lead to increased degradation of perilipin 2. Fasting-induced downregulation of UCHL1 and subsequent perilipin 2 degradation may be a mechanism for increasing access to lipids in LDs for lipolysis.

Our data showed an upregulation of perilipin 3 in UCHL1 smKO muscle. This is likely a compensatory response to the downregulation of perilipin 2 and/or low muscle lipid content. The role of perilipin 3 in skeletal muscle is not clear (Morales et al., 2017). Perilipin 3 levels in muscle biopsies from healthy human subjects are positively correlated with whole-body oxidative capacity (Covington et al., 2015). Whether this correlation is associated with lipid content is unknown. In the muscle with UCHL1 smKO, the muscle lipid is low even though perilipin 3 was upregulated, suggesting the functions of perilipin 2 and perilipin 3 may not overlap, therefore, upregulation of perilipin 3 does not compensate perilipin 2 downregulation-induced reduction of muscle lipid content.

While lipids are an essential energy depot, intramuscular lipid accumulation, as seen in obesity and aging muscle, contributes to insulin resistance. We found that mice with UCHL1 smKO exhibit improved glucose tolerance and insulin tolerance, suggesting that the reduced intramuscular lipid by UCHL1 KO is protective. This is consistent with the report that perilipin 2 KO mice showed increased insulin sensitivity in obese mice (Chang et al., 2010). Therefore, the reduced perilipin 2 by UCHL1 smKO may also contribute to the increased insulin sensitivity in this study. We would like to point out that in this study, fasting plasma insulin level was not measured. Insulin sensitivity is also regulated by many factors. Therefore, the mechanisms of the enhanced glucose tolerance and insulin tolerance in UCHL1 smKO mice remain to be further investigated.

Further studies are needed to fully understand the role of skeletal muscle UCHL1 in lipid metabolism, particularly whether upregulation

of UCHL1 in skeletal muscle is involved in metabolic disorders and insulin resistance. Interestingly, our previous work showed that UCHL1 skeletal muscle knockout reduced mitochondria oxidation activity (Gao et al., 2020), which seems contradictory to the present data because reduction of mitochondrial oxidation can increase lipid accumulation. One possibility for these seemingly contradictory results in the same UCHL1 smKO mouse model is that the reduced oxidative activity observed previously may be secondary to the reduced muscle lipid content, that is, reduced lipid and fatty acids lead to the reduced mitochondrial oxidation activity. This possibility certainly needs to be further verified.

DATA AVAILABILITY STATEMENT

The original contributions presented in the study are included in the article/**Supplementary Material**, further inquiries can be directed to the corresponding author.

ETHICS STATEMENT

The animal study was reviewed and approved by The University of South Dakota Institutional Animal Care and Use Committee.

AUTHOR CONTRIBUTIONS

RA conducted major experiments, data analysis, and writing the manuscript; KA conducted experiments, data analysis, and manuscript editing; HG conducted some experiments and data analysis; ME conducted some experiments; RS conducted some experiments; YL was responsible for the experimental design and direction, data analysis, manuscript writing and editing, and funding support.

FUNDING

This work is supported by NIH grant 1R01HL147105, which provides funding support of this study and the open publication fees.

SUPPLEMENTARY MATERIAL

The Supplementary Material for this article can be found online at: https://www.frontiersin.org/articles/10.3389/fphys.2022.855193/full#supplementary-material

REFERENCES

Antony, R., and Li, Y. (2020). BDNF Secretion from C2C12 Cells Is Enhanced by Methionine Restriction. *Biochem. Biophysical Res. Commun.* 533, 1347–1351. doi:10.1016/j.bbrc.2020.10.017

Badin, P.-M., Louche, K., Mairal, A., Liebisch, G., Schmitz, G., Rustan, A. C., et al. (2011). Altered Skeletal Muscle Lipase Expression and Activity Contribute to Insulin Resistance in Humans. *Diabetes* 60, 1734–1742. doi:10.2337/db10-1364

Chang, B. H.-J., Li, L., Saha, P., and Chan, L. (2010). Absence of Adipose Differentiation Related Protein Upregulates Hepatic VLDL Secretion, Relieves Hepatosteatosis, and Improves Whole Body Insulin Resistance in Leptin-Deficient Mice. *J. Lipid Res.* 51, 2132–2142. doi:10.1194/jlr.M004515

Conte, M., Franceschi, C., Sandri, M., and Salvioli, S. (2016). Perilipin 2 and Age-Related Metabolic Diseases: A New Perspective. *Trends Endocrinol. Metab.* 27, 893–903. doi:10.1016/j.tem.2016.09.001

Covington, J. D., Noland, R. C., Hebert, R. C., Masinter, B. S., Smith, S. R., Rustan, A. C., et al. (2015). Perilipin 3 Differentially Regulates Skeletal Muscle Lipid Oxidation in Active, Sedentary, and Type 2 Diabetic Males. *J. Clin. Endocrinol. Metab.* 100, 3683–3692. doi:10.1210/JC.2014-4125

Das, U. N. (2001). Is Obesity an Inflammatory Condition? *Nutrition* 17, 953–966. doi:10.1016/s0899-9007(01)00672-4

Dirks, M. L., Wall, B. T., van de Valk, B., Holloway, T. M., Holloway, G. P., Chabowski, A., et al. (2016). One Week of Bed Rest Leads to Substantial Muscle Atrophy and Induces Whole-Body Insulin Resistance in the Absence of Skeletal Muscle Lipid Accumulation. *Diabetes* 65, 2862–2875. doi:10.2337/db15-1661

Dominguez, L. J., and Barbagallo, M. (2016). The Biology of the Metabolic Syndrome and Aging. *Curr. Opin. Clin. Nutr. Metab. Care* 19, 5–11. doi:10.1097/MCO.0000000000000243

Dubé, J. J., Amati, F., Stefanovic-Racic, M., Toledo, F. G. S., Sauers, S. E., and Goodpaster, B. H. (2008). Exercise-induced Alterations in Intramyocellular Lipids and Insulin Resistance: the Athlete's Paradox Revisited. *Am. J. Physiology-Endocrinology Metab.* 294, E882–E888. doi:10.1152/ajpendo.00769.2007

Dyck, D. J., Peters, S. J., Glatz, J., Gorski, J., Keizer, H., Kiens, B., et al. (1997). Functional Differences in Lipid Metabolism in Resting Skeletal Muscle of Various Fiber Types. *Am. J. Physiology-Endocrinology Metab.* 272, E340–E351. doi:10.1152/ajpendo.1997.272.3.E340

Feng, Y. Z., Lund, J., Li, Y., Knabenes, I. K., Bakke, S. S., Kase, E. T., et al. (2017). Loss of Perilipin 2 in Cultured Myotubes Enhances Lipolysis and Redirects the Metabolic Energy Balance from Glucose Oxidation towards Fatty Acid Oxidation. *J. Lipid Res.* 58, 2147–2161. doi:10.1194/jlr.M079764

Gao, H., Antony, R., Srinivasan, R., Wu, P., Wang, X., and Li, Y. (2020). UCHL1 Regulates Oxidative Activity in Skeletal Muscle. *PLoS One* 15, e0241716. doi:10.1371/journal.pone.0241716

Gao, H., Freeling, J., Wu, P., Liang, A. P., Wang, X., and Li, Y. (2019). UCHL1 Regulates Muscle Fibers and mTORC1 Activity in Skeletal Muscle. *Life Sci.* 233, 116699. doi:10.1016/j.lfs.2019.116699

Goodpaster, B. H., He, J., Watkins, S., and Kelley, D. E. (2001). Skeletal Muscle Lipid Content and Insulin Resistance: Evidence for a Paradox in Endurance-Trained Athletes. *J. Clin. Endocrinol. Metab.* 86, 5755–5761. doi:10.1210/jcem.86.12.8075

Hirabara, S. M., Silveira, L. R., Abdulkader, F., Carvalho, C. R. O., Procopio, J., and Curi, R. (2007). Time-dependent Effects of Fatty Acids on Skeletal Muscle Metabolism. *J. Cel. Physiol.* 210, 7–15. doi:10.1002/jcp.20811

Houten, S. M., Violante, S., Ventura, F. V., and Wanders, R. J. A. (2016). The Biochemistry and Physiology of Mitochondrial Fatty Acid β-Oxidation and its Genetic Disorders. *Annu. Rev. Physiol.* 78, 23–44. doi:10.1146/annurev-physiol-021115-105045

Kaushik, S., and Cuervo, A. M. (2015). Degradation of Lipid Droplet-Associated Proteins by Chaperone-Mediated Autophagy Facilitates Lipolysis. *Nat. Cel Biol* 17, 759–770. doi:10.1038/ncb3166

Kelley, D. E. (2005). Skeletal Muscle Fat Oxidation: Timing and Flexibility Are Everything. *J. Clin. Invest.* 115, 1699–1702. doi:10.1172/JCI25758

Kimmel, A. R., Brasaemle, D. L., McAndrews-Hill, M., Sztalryd, C., and Londos, C. (2010). Adoption of PERILIPIN as a Unifying Nomenclature for the Mammalian PAT-Family of Intracellular Lipid Storage Droplet Proteins. *J. Lipid Res.* 51, 468–471. doi:10.1194/jlr.R000034

Kimmel, A. R., and Sztalryd, C. (2016). The Perilipins: Major Cytosolic Lipid Droplet-Associated Proteins and Their Roles in Cellular Lipid Storage, Mobilization, and Systemic Homeostasis. *Annu. Rev. Nutr.* 36, 471–509. doi:10.1146/annurev-nutr-071813-105410

Koves, T. R., Ussher, J. R., Noland, R. C., Slentz, D., Mosedale, M., Ilkayeva, O., et al. (2008). Mitochondrial Overload and Incomplete Fatty Acid Oxidation Contribute to Skeletal Muscle Insulin Resistance. *Cel Metab.* 7, 45–56. doi:10.1016/j.cmet.2007.10.013

Kumar, A., Accorsi, A., Rhee, Y., and Girgenrath, M. (2015). Do's and Don'ts in the Preparation of Muscle Cryosections for Histological Analysis. *JoVE* 99, e52793. doi:10.3791/52793

Lalia, A. Z., Dasari, S., Johnson, M. L., Robinson, M. M., Konopka, A. R., Distelmaier, K., et al. (2016). Predictors of Whole-Body Insulin Sensitivity across Ages and Adiposity in Adult Humans. *J. Clin. Endocrinol. Metab.* 101, 626–634. doi:10.1210/jc.2015-2892

Listenberger, L. L., Han, X., Lewis, S. E., Cases, S., Farese, R. V., Ory, D. S., et al. (2003). Triglyceride Accumulation Protects against Fatty Acid-Induced Lipotoxicity. *Proc. Natl. Acad. Sci. U.S.A.* 100, 3077–3082. doi:10.1073/pnas.0630588100

Lundsgaard, A.-M., Fritzen, A. M., and Kiens, B. (2018). Molecular Regulation of Fatty Acid Oxidation in Skeletal Muscle during Aerobic Exercise. *Trends Endocrinol. Metab.* 29, 18–30. doi:10.1016/j.tem.2017.10.011

MacPherson, R. E. K., Ramos, S. V., Vandenboom, R., Roy, B. D., and Peters, S. J. (2013). Skeletal Muscle PLIN Proteins, ATGL and CGI-58, Interactions at Rest and Following Stimulated Contraction. *Am. J. Physiology-Regulatory, Integr. Comp. Physiol.* 304, R644–R650. doi:10.1152/ajpregu.00418.2012

Masuda, Y., Itabe, H., Odaki, M., Hama, K., Fujimoto, Y., Mori, M., et al. (2006). ADRP/adipophilin Is Degraded through the Proteasome-dependent Pathway during Regression of Lipid-Storing Cells. *J. Lipid Res.* 47, 87–98. doi:10.1194/jlr.M500170-JLR200

Minnaard, R., Schrauwen, P., Schaart, G., Jorgensen, J. A., Lenaers, E., Mensink, M., et al. (2009). Adipocyte Differentiation-Related Protein and OXPAT in Rat and Human Skeletal Muscle: Involvement in Lipid Accumulation and Type 2 Diabetes Mellitus. *J. Clin. Endocrinol. Metab.* 94, 4077–4085. doi:10.1210/jc.2009-0352

Morales, P. E., Bucarey, J. L., and Espinosa, A. (2017). Muscle Lipid Metabolism: Role of Lipid Droplets and Perilipins. *J. Diabetes Res.* 2017, 1–10. doi:10.1155/2017/1789395

Ogasawara, Y., Tsuji, T., and Fujimoto, T. (2020). Multifarious Roles of Lipid Droplets in Autophagy - Target, Product, and what Else? *Semin. Cel Dev. Biol.* 108, 47–54. doi:10.1016/j.semcdb.2020.02.013

Olzmann, J. A., and Carvalho, P. (2019). Dynamics and Functions of Lipid Droplets. *Nat. Rev. Mol. Cel Biol* 20, 137–155. doi:10.1038/s41580-018-0085-z

Pepino, M. Y., Kuda, O., Samovski, D., and Abumrad, N. A. (2014). Structure-function of CD36 and Importance of Fatty Acid Signal Transduction in Fat Metabolism. *Annu. Rev. Nutr.* 34, 281–303. doi:10.1146/annurev-nutr-071812-161220

Qiu, B., and Simon, M. (2016). BODIPY 493/503 Staining of Neutral Lipid Droplets for Microscopy and Quantification by Flow Cytometry. *Bio-protocol* 6, e1912. doi:10.21769/BioProtoc.1912

Rambold, A. S., Cohen, S., and Lippincott-Schwartz, J. (2015). Fatty Acid Trafficking in Starved Cells: Regulation by Lipid Droplet Lipolysis, Autophagy, and Mitochondrial Fusion Dynamics. *Dev. Cel* 32, 678–692. doi:10.1016/j.devcel.2015.01.029

Reidy, P. T., McKenzie, A. I., Mahmassani, Z., Morrow, V. R., Yonemura, N. M., Hopkins, P. N., et al. (2018). Skeletal Muscle Ceramides and Relationship with Insulin Sensitivity after 2 Weeks of Simulated Sedentary Behaviour and Recovery in Healthy Older Adults. *J. Physiol.* 596, 5217–5236. doi:10.1113/JP276798

Samuel, V. T., Petersen, K. F., and Shulman, G. I. (2010). Lipid-induced Insulin Resistance: Unravelling the Mechanism. *The Lancet* 375, 2267–2277. doi:10.1016/S0140-6736(10)60408-4

Schiaffino, S., and Reggiani, C. (2011). Fiber Types in Mammalian Skeletal Muscles. *Physiol. Rev.* 91, 1447–1531. doi:10.1152/physrev.00031.2010

Silveira, L. R., Fiamoncini, J., Hirabara, S. M., Procópio, J., Cambiaghi, T. D., Pinheiro, C. H. J., et al. (2008). Updating the Effects of Fatty Acids on Skeletal Muscle. *J. Cel. Physiol.* 217, 1–12. doi:10.1002/jcp.21514

Spangenburg, E. E., Pratt, S. J. P., Wohlers, L. M., and Lovering, R. M. (20112011). Use of BODIPY (493/503) to Visualize Intramuscular Lipid Droplets in Skeletal Muscle. *J. Biomed. Biotechnol.* 2011, 1–8. doi:10.1155/2011/598358

Stein, T. P., and Wade, C. E. (2005). Metabolic Consequences of Muscle Disuse Atrophy. *J. Nutr.* 135, 1824S–1828S. doi:10.1093/jn/135.7.1824S

Storlien, L., Oakes, N. D., and Kelley, D. E. (2004). Metabolic Flexibility. *Proc. Nutr. Soc.* 63, 363–368. doi:10.1079/PNS2004349

Turcotte, L. P., and Fisher, J. S. (2008). Skeletal Muscle Insulin Resistance: Roles of Fatty Acid Metabolism and Exercise. *Phys. Ther.* 88, 1279–1296. doi:10.2522/ptj.20080018

Turner, N., Cooney, G. J., Kraegen, E. W., and Bruce, C. R. (2014). Fatty Acid Metabolism, Energy Expenditure and Insulin Resistance in Muscle. *J. Endocrinol.* 220, T61–T79. doi:10.1530/JOE-13-0397

Walther, T. C., and Farese, R. V., Jr. (2012). Lipid Droplets and Cellular Lipid Metabolism. *Annu. Rev. Biochem.* 81, 687–714. doi:10.1146/annurev-biochem-061009-102430

Wang, C.-W. (2016). Lipid Droplets, Lipophagy, and beyond. *Biochim. Biophys. Acta (Bba) - Mol. Cel Biol. Lipids* 1861, 793–805. doi:10.1016/j.bbalip.2015.12.010

Xu, G., Sztalryd, C., Lu, X., Tansey, J. T., Gan, J., Dorward, H., et al. (2005). Post-translational Regulation of Adipose Differentiation-Related Protein by the Ubiquitin/proteasome Pathway. *J. Biol. Chem.* 280, 42841–42847. doi:10.1074/jbc.M506569200

Conflict of Interest: The authors declare that the research was conducted in the absence of any commercial or financial relationships that could be construed as a potential conflict of interest.

Publisher's Note: All claims expressed in this article are solely those of the authors and do not necessarily represent those of their affiliated organizations, or those of the publisher, the editors and the reviewers. Any product that may be evaluated in this article, or claim that may be made by its manufacturer, is not guaranteed or endorsed by the publisher.

Copyright © 2022 Antony, Aby, Gao, Eichholz, Srinivasan and Li. This is an open-access article distributed under the terms of the Creative Commons Attribution License (CC BY). The use, distribution or reproduction in other forums is permitted, provided the original author(s) and the copyright owner(s) are credited and that the original publication in this journal is cited, in accordance with accepted academic practice. No use, distribution or reproduction is permitted which does not comply with these terms.

frontiers | Frontiers in Endocrinology

TYPE Mini Review
PUBLISHED 08 September 2022
DOI 10.3389/fendo.2022.866116

Check for updates

OPEN ACCESS

EDITED BY
Zhihao Jia,
Purdue University, United States

REVIEWED BY
Tongxing Song,
Huazhong Agricultural University, China
Endre Károly Kristóf,
University of Debrecen, Hungary

*CORRESPONDENCE
Yu Feng
fengyu1980@suda.edu.cn
Xiaosong Gu
xiaosonggu@hotmail.com

†These authors have contributed equally to this work

SPECIALTY SECTION
This article was submitted to Obesity, a section of the journal Frontiers in Endocrinology

RECEIVED 30 January 2022
ACCEPTED 20 July 2022
PUBLISHED 08 September 2022

CITATION
Wang Y, Wang Y, Gu J, Su T, Gu X and Feng Y (2022) The role of RNA m6A methylation in lipid metabolism. *Front. Endocrinol.* 13:866116. doi: 10.3389/fendo.2022.866116

COPYRIGHT
© 2022 Wang, Wang, Gu, Su, Gu and Feng. This is an open-access article distributed under the terms of the Creative Commons Attribution License (CC BY). The use, distribution or reproduction in other forums is permitted, provided the original author(s) and the copyright owner(s) are credited and that the original publication in this journal is cited, in accordance with accepted academic practice. No use, distribution or reproduction is permitted which does not comply with these terms.

The role of RNA m6A methylation in lipid metabolism

Yuting Wang[1†], Yujie Wang[2†], Jiarui Gu[1], Tianhong Su[3], Xiaosong Gu[3*] and Yu Feng[1*]

[1]Department of Endocrinology, The Second Affiliated Hospital of Soochow University, Suzhou, China, [2]Department of Orthopaedics, Dushu Lake Hospital Affiliated to Soochow University, Suzhou, China, [3]Department of Cardiology, the Second Affiliated Hospital of Soochow University, Suzhou, China

The m6A methylation is the most numerous modification of mRNA in mammals, coordinated by RNA m6A methyltransferases, RNA m6A demethylases, and RNA m6A binding proteins. They change the RNA m6A methylation level in their specific manner. RNA m6A modification has a significant impact on lipid metabolic regulation. The "writer" METTL3/METTL14 and the "eraser" FTO can promote the accumulation of lipids in various cells by affecting the decomposition and synthesis of lipids. The "reader" YTHDF recognizes m6A methylation sites of RNA and regulates the target genes' translation. Due to this function that regulates lipid metabolism, RNA m6A methylation plays a pivotal role in metabolic diseases and makes it a great potential target for therapy.

KEYWORDS

METTL3, obesity, FTO (fat mass and obesity-associated) gene, M6A, lipid

Introduction

Lipid metabolism exerts a profound impact on the maintenance of human physiology and health status. Adipose tissue is an important site for lipid storage, and energy homeostasis (1, 2). It is important to understand the mechanisms involved in adipose tissue development (3). Adipogenesis of the white and brown adipocytes is regulated by several endocrine hormones (1, 3). Fat mass and obesity-associated protein (FTO) pro-obesity rs1421085 T-to-C single-nucleotide polymorphism (SNP) shifts differentiation programming towards white adipocytes in subcutaneous fat (4). Meanwhile in community, unhealthy lifestyles such as nutrient surplus and unhealthy eating patterns (5) act as the main reason for the high incidence of lipid metabolism disorder. Furthermore, types of diseases caused by abnormal lipid metabolisms like diabetes (6), hyperlipidaemia (7), cardiovascular disease (8, 9), and non-alcoholic fatty liver disease (NAFLD) (10) are becoming more and more pervasive all over the world. Therefore, there is a great desire to deepen the understanding of the regulation of lipid metabolism.

In mammals, the m6A methylation is the most numerous modification of mRNA and accounts for more than sixty percent of all RNA modifications (11, 12). The RNA m6A modification is a kind of methylation modification positioned at the nitrogen atom in the sixth position of adenosine (13). The process of RNA m6A methylation is dynamically and reversibly coordinated by m6A demethylases, m6A methyltransferases, and m6A binding proteins, which are also referred to as "Writer", "Eraser", and "Reader", respectively (14). The writers methyltransferase-like 3 (METTL3), methyltransferase-like 14 (METTL14), and Wilms' tumor 1-associated protein (WTAP) have m6A methylation activity to catalyze m6A modification (15). Demethylases are predominantly made out of ALKB homolog 5 (ALKBH5) and FTO (16), catalyzing the demethylation process (17). Furthermore, m6A binding proteins are found principally in the YT521-B homology (YTH) family (18), which have the potency to recognize and specifically bind to m6A-modified transcripts (19). All kinds of RNA m6A methylation regulators are involved in different physiological processes, while many remain unknown.

In this article, we introduce the novel RNA modification and its regulatory function for RNA. We summarize the main regulators of RNA m6A methylation and describe their function and regulatory mechanism toward mRNA. The possible target gene by which RNA m6A methylation regulators affect lipid metabolism is claimed. Finally, we reviewed the RNA m6A methylation regulators on the NAFLD, diabetes, and cardiovascular diseases and its regulating pathway to provide some reference to the clinical prevention, diagnosis, and therapy research in lipid metabolism-related diseases.

Epigenetic regulatory mechanisms of RNA m6A methylation

M6A methylation is a newly discovered epigenetic regulatory mechanism in recent years. Among the more than 170 RNA modifications (20), m6A modification accounts for a large proportion in eukaryocyte (21). It is a methylation substitution reaction that takes place on the sixth nitrogen atom of the RNA molecule adenosine, which is observed enriching in 3'UTR and consensus motif RRACH in coding region (22, 23).

M6A methylation is essential in determining the fate of RNA, showing a regulatory function in multiple mRNA biological processes. Firstly, it can regulate the stability of mRNA. Facts that mRNA with lower m6A methylation level had longer half-life was first revealed in 1978 (24). The m6A reader YTHDF2 can recognize methylation sites in the coding region of mRNA and destabilized mRNA (25, 26) while, the newly identified reader Insulin-like growth factor-binding proteins (IGFBP) recognized m6A in 3'UTR inversely make the mRNA more stable (27, 28). The opposite regulatory effect may account for the different recognizing mRNA sites. Secondly, m6A facilitates the initiation of the translation process of mRNA. After reading the m6A methylation site, the m6A reader like YTHFD1/3 can recruit eIF3 to connect to mRNA. In addition, m6A at 5'UTR can directly connect to eIF3 to enhance mRNA translation (29–31). Furthermore, it also regulates mRNA splicing, processing, and nuclear export (32, 33). Recent research also shows it to to exist in lncRNA, microRNA, and non-coding RNA (32, 34, 35), considered a widespread RNA modification.

In RNA molecules, methylation levels are regulated by a series of enzymes reversibly and dynamically, which can be identified as "Writer", "Eraser", and "Reader" and all specifically interact with the m6A methylation site as follow.

The writer of m6A can catalyze mRNA methylation

METTL3 is a high molecular weight subcomplex whose component is still not fully understood, and METTL14 is its homologues (21, 36). WTAP is the regulatory subunit of methyltransferase by which METTL3 and METTL14 anchor to mRNA to methylate subsequent target adenosine residues. WTAP recruits METT3 and METT14, enabling the METTL3-METT14 complex to perform m6A methyltransferase activity, affecting m6A methylation, and thus RNA shearing (37). Junho Choe's team found that METTL3-elF3h interacts with each other to mediate mRNA cycling and translation through the association between the elF3h subunit at the mRNA 5'end and METTL3 binding to the specific site near the translation termination codon. METTL3-elF3h mediates mRNA cyclization. Thus, efficient translation of target mRNA was promoted (38).

The eraser of m6A can remove m6A from RNA

FTO was the first eraser to be identified, in 2011 (21). Since its discovery, much research on its regulation in enormous physiological and pathological processes has been carried out. FTO in humans is an approximate 400 kb gene, containing 8 introns and 9 exons, located on 16q12.2 (39). FTO can remove the m6A methylation from multiple mRNAs through an α-Ketoglutarate (α-KG) and Fe (II)-dependent manner (40). Its modification process is claimed in detail in previous research. In brief, initially, FTO oxidizes m6A methylation to the intermediate N6-hydroxymethyl adenosine (hm6A). In the second step, FTO

oxidizes metastable hm6A in the same way as m6A, forming further oxidized production N6 -formyladenosine (f6A) (41). As a result, hm6A and f6a spontaneously break down to adenine and the m6A methylation in RNA is removed (41, 42).

ALKBH5 is another eraser identified later which demethylates the RNA efficiently (43). Research has shown its regulator function in many regulator pathways by mRNA methylation. However, the underlying mechanism remains mysterious.

The reader of m6A can capture mRNA methylation

YTH domain is a module recognizing the methylation of m6A dependently, consisting of YTHDC1, YTHDC2, YTHDF1, YTHDF2, and YTHDF3 (25). The stability of m6A methylation modified mRNA is regulated by YTHDF2 in the way of recognizing m6A methylation and reducing the stability of the target transcript. In addition, another m6A reading protein, YTHDF1, was found to interact with the translation machinery of the related genes and promote protein synthesis. The m6A mRNA modification enforces rapid response of gene expression and controlled protein production, improved translation efficiency through YTHDF1-mediated translation, and controls target transcripts' lifetime through YTHDF2-mediated degradation (29).

RNA m6A methylation regulates the lipid metabolism

Lipid, which mainly consists of triglycerides, cholesterol, phospholipids, and glycolipid, is involved in body energy metabolism and is the component of the cell membrane. It is also the precursor of various molecules that play important biological roles. Thus, lipid metabolism, such as digestion, absorption, synthesis, and decomposition is essential for the maintenance of cellular homeostasis (44, 45).

The RNA m6A methylase METTL3 and METTL4 are also involved in the regulation of lipid accumulation in cells. METTL3-mediated m6A methylation makes the metabolism-related gene's mRNA more unstable, leading to metabolic disorders and lipid accumulation in the liver (46). Likewise, in cardiac cells, METTL3 deficiency decreases the RNA m6A methylation and the triglyceride deposition (47). Fatty acid synthase (FASN), acetyl-CoA carboxylase (ACCY), and stearoyl-CoA desaturase 1 (SCD1) are the regulator targets, as recently reported (Figure 1). Mechanistically, METTL3/METTL14 complex induces the increase of mRNA to accelerate the production of lipid (48, 49). Consistently, METTL3 and the recognizing and binding protein YTHDF2 increase the m6A methylation level of peroxisome proliferator-activated receptorα(PPARα) and its expression, impacting the

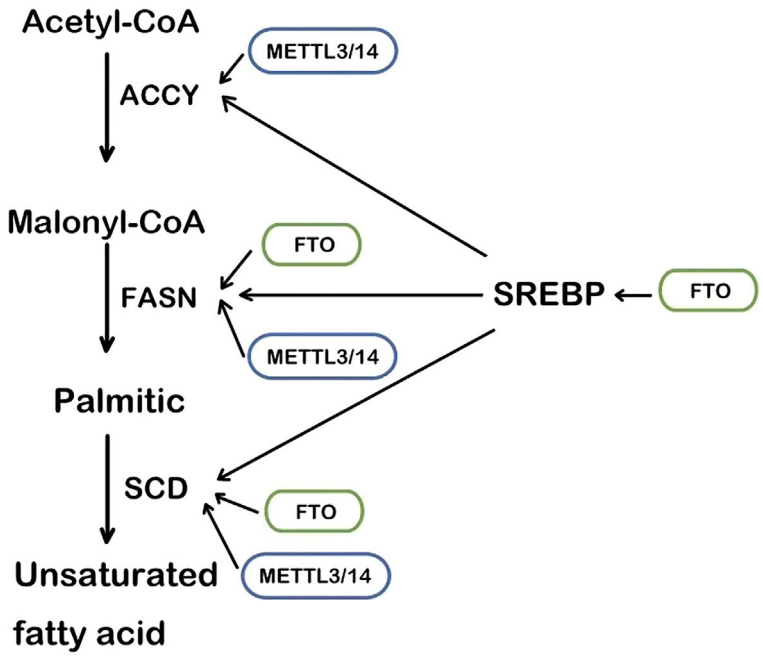

FIGURE 1
The main steps of lipogenesis and the regulation of FTO and METTL3/14. SREBP, sterol regulatory element-binding protein; FASN, fatty acid synthase; ACCY, acetyl-CoA carboxylase; SCD, stearoyl-CoA desaturase.

downstream lipid accumulation (50). Inflammation is also involved in the lipid accumulation procedure. METTL3 deficiency induces a lower level of m6A methylation of TNF receptor-associated factor 6 (TRAF6) and therefore the transcripts are entrapped in the nucleus, leading to the downstream mitogen-activated protein kinase (MAPK) and nuclear factor κ-B (NF-κB) to be suppressed. In consequence, inflammation and the absorption of long-chain fatty acids (LCFA) are reduced (51).

Once introduced in 1974 (52), RNA m6A methylation modification was found to affect diverse physiological and pathological progressions in cardiomyocytes (53), hepatocyte (54), axoneuron (11), and so on. Its regulation function in the lipid metabolism is revealed over decades. In general, its regulation function depends on the enhancement or reduction of the m6A level and recognition of the m6A site by various regulatory enzymes. But its interaction with genes related to lipid synthesis and decomposition is complicated and remains to be elucidated by research.

The first identified RNA m6A demethylase, FTO, is strongly connected with lipid accumulation in multiple cells and tissues. In the obesity group, high FTO level is positively correlated with Body Mass Index (BMI) and body fat (55, 56). *In vitro*, it promotes intracellular lipid accumulation by RNA demethylation while FTO knockdown did not (57, 58).

As an enzyme that demethylates m6A (59), FTO regulates m6A methylation levels of multiple RNA in lipid anabolism and catabolism. The process of lipid synthesis can be improved by FTO-mediated RNA demethylation. In the 3'UTR region of multiple lipogenic genes' mRNA such as SCD, PPARγ, and sterol regulatory element-bindin protein-1 (SREBP1), which are all involved in the triacylglycerol and Cholesterol Synthesis. (Figure 1) FTO decreases their level of m6A methylation to improve the stability of mRNA (60, 61). In the hepatocyte, the m6A methylation level in FASN mRNA is enhanced and lipogenesis is inhibited by the FTO knockdown and YTHDF2 recognition (62). Angiopoietin-like protein 4 (ANGPTL4) is also the key target of triglycerides synthesis and hydrolysis intracellularly and extracellularly. It inhibits lipoprotein lipase(LPL), leading to inhibiting extracellular lipolysis (63). FTO decreases the level of the translation of ANGPTL4, hence hydrolysis of extracellular triglycerides is promoted. The fatty acid is transported into adipocytes, inducing lipid accumulation (39, 63). Conversely, ANGPTL4 promotes intracellular lipolysis (64). Evidence has shown knockout of FTO affects intracellular ANGPTL4 level and intracellular lipolysis (65). The different results may account for the different mRNA sites where the m6A methylation is located. It is an interesting issue to explore.

Nevertheless, the role played by FTO in lipolysis remains disputed. FTO decreases the expression of interleukin 6 (IL-6) mRNA in adipose tissues (66) and consequently inhibits the lipolysis genes (67). In addition, FTO reduces lipolysis and fatty acid oxidation by reducing the adipose triglyceride lipase (ATGL), hormone-sensitive lipase (LIPE), and carnitine palmitoyltransferase 1 (CPT1) mRNA expression (68).

Interestingly, another FTO regulator pathway revealed that the promotion of FTO downregulated the obesity-related gene iroquois homeobox protein 3 (IRX3) level in the hypothalamus and macrophage. So, lipolysis was inhibited through affecting whole body modulated energy expenditure and metabolic inflammation (69, 70). However, it should be noted that the interaction of FTO and IRX3 is not the traditional m6A methylation modification, but the noncoding regions of FTO serve as a long-range regulatory element to influence the expression of IRX3 (71).

Furthermore, FTO-mediated RNA m6A methylation shows a close correlation with cellular triglyceride (TG) uptaking that is regulated by adenosine 5'-monophosphate-activated protein kinase (AMPK) (72, 73). AMPK suppresses the expression of FTO to upregulate the m6A level of Parkin2 mRNA and promote its decay. Then CD36 was translocated to the membrane and LCFA uptaking of cells is increased (74, 75).

In summary, both FTO and METTL3 play vital regulatory roles in lipid metabolism and can promote the accumulation of lipids in various cells, affecting the decomposition and synthesis of lipids. The regulation pathways of FTO and METTL3/METTL14 are complex and diverse, which can methylate or demethylate the RNA m6A of targets in multiple pathways such as inflammation, energy homeostasis, nerve-related lipid regulation, lipid metabolism balance, resulting in corresponding high or low gene expression (Figure 2). In addition, YTHDF protein plays an epigenetic role in recognizing m6A methylation sites of RNA and regulates the translation. Although the area of RNA m6A methylation is a popular spot in recent years, a convincing and authoritative theory is urgently needed. The function of RNA m6A methylation in many genes remains controversial and the deeply regulation process requires further investigation.

m6A methylation and lipid-related metabolic diseases

When the cellular lipid metabolism is disordered, excessive lipid accumulation or lipid accumulation in ectopic tissues due to the imbalance of lipid uptake, decomposition, and synthesis in the cell, can result in a series of intracellular pathophysiological reactions. Inflammation (76), oxidative stress (77), chromatin histone modification (78), etc. caused by lipid accumulation can lead to cellular dysfunction, apoptosis, and even death. As mentioned above, RNA m6A methylation is involved in multiple pathways in lipid metabolism, and it also shows a vital function in the occurrence and development of lipid metabolic diseases (Table 1). Over the past decades, studies have investigated some possible targets for the diagnosis, physiopathology process,

10.3389/fendo.2022.866116

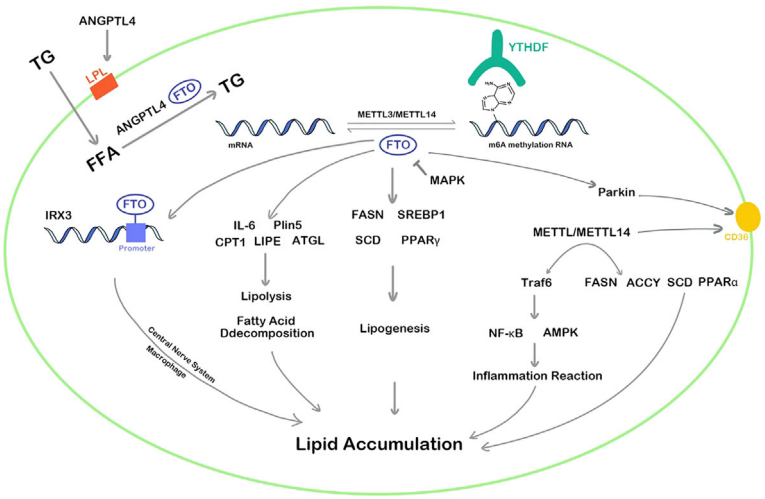

FIGURE 2
RNA m6A regulators influence lipid cellar accumulation in various ways. TG, triglyceride; ANGPTL4, angiopoietin-like protein 4; IRX3, iroquois homeobox protein 3; MAPK, mitogen-activated protein kinase; FFA, free fatty acid; IL-6, interleukin 6; Plin5, perilipin5; CPT1, carnitine palmitoyltransferase 1; LIPE, hormone-sensitive lipase; ATGL, adipose triglyceride lipase; PPAR, peroxisome proliferator-activated receptor; FASN, fatty acid synthase; LPL, lipoprotein lipase; SREBP1, sterol regulatory element-bindin protein-1; SCD, stearoyl-CoA desaturase; Traf6, TNF receptor associated factor 6; ACCY, acetyl-CoA carboxylase; NF-κb, nuclear factor kappa-B; AMPK, adenosine 5'-monophosphate-activated protein kinase.

TABLE 1 Multiple functions of RNA m6A methylation regulator in lipid metabolic disease.

Regulator	Disease	Influence towards disease	Target	Function	Year	Ref.
METTL3	NAFLD	NEGATIVE	DDIT3	Loss of METTL3 results in increasing in DDIT	2021	(79)
METTL3	NAFLD	NEGATIVE	Rubicon axis	METTL3 and its partner YTHDF1 promote the stability of Rubicon mRNA	2021	(80)
METTL3	NAFLD/NASH	POSITIVE	CD36,CCL2	METTL3 inhibits the expression of CD36 and CCL2	2015	(81)
FTO	NAFLD	NEGATIVE	SREBP1c, CIDEC	Knockdown of FTO down-regulates the expression of SREBP1c and CIDEC	2018	(82)
FTO	NAFLD	NEGATIVE	FASN, SCD, MGAT1, MTTP, APOB, LIPC	FTO overexpression in HepG2 cells positively regulate FASN, SCD1, MAGT1 while negatively regulate MTTP, APOB, LIPC	2018	(57)
IGF2BP2	NAFLD	NEGATIVE	CCL2	Overexpression of p62/IMP2-2/IGF2BP2-2 elevated CCL2 expression levels	2014	(83)
IGF2BP1/ IGF2BP3	NAFLD/HCC	NEGATIVE	LINC01138	IGF2BP1/IGF2BP3 stabilized LINC01138 transcript	2018	(84)
METTL3	T2DM	NEGATIVE	FASN	METTL3 silencing could decrease the m6A mRNA levels of FASN	2019	(48)
METTL3	HCC	NEGATIVE	SOCS	YTHDF2 cooperates with METTL3 depressing the level of SOCS	2018	(85)
YTHDC2	NAFLD	CRITICAL	SREBP1c, FASN, SCD1, and ACCY1	YTHDC2 decreases the stability of mRNA of SREBP1c, FASN, SCD1, and ACCY1 and inhibit gene expression	2020	(86)
FTO	HYPERLIPIDAEMIA	NEGATIVE	–	the secretion of inflammatory factors IL-1βand the expression of FTO was high in dyslipidemia induced by LPS	2016	(87)
METTL14	ATHEROSCLEROSIS	NEGATIVE	ZFAS1/RAB22a	METTL14 mediated m6A modification to LncRNA ZFAS1/RAB22a	2020	(88)

and therapy of metabolic diseases such as NAFLD, diabetes, hyperlipidemia, and atherosclerosis (Figure 3).

m6A methylation and the lipid metabolism in NAFLD

The liver is one of the most significant organs in fatty acid synthesis and decomposition. Recent studies have revealed that RNA m6A methylation happened in hepatocyte matters in lipid metabolism disorder. Patients who suffered from NAFLD were detected to have a higher level of FTO mRNA in the liver (46). Similar results were observed in several studies (89–91), which have been widely acknowledged by researchers.

Thus, exploring the further mechanism is imperative. The "writer" METTL3 is also considered to be related to liver lipid accumulation (50, 92). Forkhead box O1 (FOXO1), Enoyl-CoA Hydratase And 3-Hydroxyacyl CoA Dehydrogenase (EHHADH), PPARα, FASN, and Sirtuin 1 (SIRT1) were the regulator targets that had been reported (93). Furthermore, in the recent 2 years of research, some other regulation targets have been put forward. METTL3, as the m6A writer, improves DNA damage-inducible transcript 4 (DDIT4) mRNA the methylation level, as a result, affects its stability. When METTL3 is knocked down, DDIT4 reduces the level of lipid accumulation and the activity of inflammation in hepatocytes of the NAFLD patients by the signaling pathway of the mechanistic target of rapamycin complex 1 (mTORC1) and NF-κB (79). Autophagy also plays a role in RNA m6A methylation of the NAFLD progression. METTL3 and its partner YTHDF1 inhibit the autophagic flux in hepatocytes and block the clearance of lipid droplets by the means of promoting the stability of Rubicon mRNA, which inhibited the autophagy process of autophagosome-lysosome fusion (80).

Conversely, METTL3 knockdown increased the free fatty acid uptake mediated by CD36, and the inflammation reaction induced by C-C motif chemokine ligand 2 (CCL2), as the result, lead to the progression from NAFLD to non-alcoholic steatohepatitis (NASH) (81). The regulation of METTL3 on NAFLD may be diverse.

FTO can affect the expression of FASN, SCD, Monoacylglycerol acyltransferase (MAGAT), SREBP1c, and cell death-inducing DFF45-like effector C (CIDEC) (82) to regulate the lipogenesis in hepatocytes. Meanwhile, FTO up/down-regulates the lipid transport protein of microsomal triglyceride transfer protein (MTTP), hepatic lipase (LIPC), apolipoprotein B (APOB) (57), inducing the process of lipid transport (93). As a result, excessive lipid deposition in hepatocytes results in hepatocyte steatosis.

Furthermore, the "reader" YTHDF2 is also involved in the regulation of TG homeostasis and lipogenesis in NAFLD, and SREBP1c, FASN, and SCD1, and ACCY1 is the gene related to the process (86). In the next section, IGF2BP2, a recently identified m6A reader, was also reported to be a promoter of NAFLD (83), which can promote the stability of mRNA (28), and IGF2BP1/IGF2BP3 was also reported to be associated with poor outcomes of liver cancer (84).

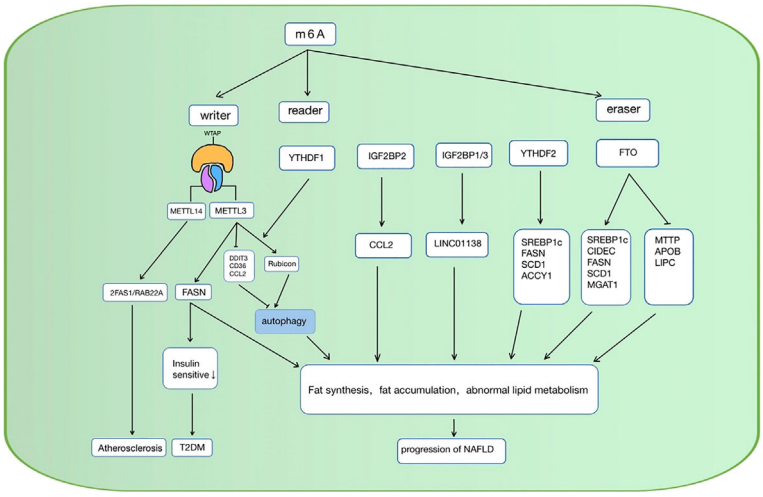

FIGURE 3
RNA m6A regulators are involved in the regulation of lipid metabolic diseases in various ways. NAFLD, non-alcoholic fatty liver disease; CCL, C-C motif chemokine ligand 2; SREBP1c, sterol regulatory element-bindin protein-1; FASN, Fatty acid synthase; SCD1, stearoyl-CoA desaturase; ACCY1, acetyl-CoA carboxylase, CIDEC, cell death-inducing DFF45-like effector C; MAGAT, monoacylglycerol acyltransferases; LIPC, hepatic lipase; APOB, apolipoprotein; ZFAS1/RAB22a, zinc finger antisense 1/ras-related protein rab-22a; DDIT3, DNA damage-inducible transcript 4; T2DM, diabetes mellitus type 2; METTL, methyltransferase-like 3; YTHFD, YT521-B homology domain family; FTO, fat mass and obesity-associated protein; IGFBP, Insulin-like growth factor-binding proteins; MTTP, microsomal triglyceride transfer protein.

NAFLD is a complex metabolic disease and many pathological changes happened in liver tissue (94).The RNA m6A methylation regulator FTO, METTL3, and the recognition protein family YTHDF affect the progression of NAFLD to hepatocellular carcinoma (HCC) by the means of disorder lipid metabolism, oxidative stress (87), and autophagy (80), making it an important potential treatment target. Altering the RNA m6A methylation level of various proteins reduces the hepatic abnormal lipid accumulation, thereby further relieving the abnormal state of cells. This epigenetic regulation may significantly improve the development of NAFLD and even reverse hepatocyte degeneration.

m6A methylation and lipid metabolism in diabetes

Diabetes is one of the highest prevalence diseases and over 400 million patients live with this disease worldwide. Its complication causes severe disease burden (95, 96). It has been revealed that multiple m6A methylations target pathways like Insulin-like growth factor 1-protein kinase B-pancreatic and duodenal homeobox 1(IGF1-AKT-PDX1) and genes like diacylglycerol acyltransferase 2 (DGAT2), glucose-6-phsophatase catalytic subunit (G6PC), and FOXO1, are involved in the glucose and insulin secretion regulation of pancreatic islet B cell (97, 98). Besides, lipid metabolism disorder related to m6A methylation also plays an important part in insulin resistance.

FASN, the key protein in lipid metabolism, has proved to be closely connected to insulin resistance by research that in adipose tissue, FASN expression was increased and insulin sensitivity was impaired (99). METTL3 also inhibits insulin sensitivity *via* the modification of FASN mRNA. Along with the overexpression or the METTL3 deficiency in high-fat diet (HFD) rats, the level of FASN mRNA and lipid content in the liver is higher or lower accordingly, and the insulin sensitivity is improved (46, 48). However, further studies are still needed to claim how exactly m6A interacts with insulin sensitivity.

RNA m6A methylation and lipid metabolism in cardiovascular diseases

Cardiovascular disease is the leading cause of death worldwide, while hyperlipidemia is responsible for about one-third of all cardiovascular diseases (100, 101). The RNA m6A methylation involved lipid metabolism disorder and chronic inflammation reaction has been reported as a possible mechanism in the past few years. Research has revealed that hyperlipidemia level is highly connected with m6A-SNPs (102) and FTO-associated inflammatory factor IL-1β, IL-6, and LPS which induce hyperlipidemia may be the factors in the development of chronic heart disease (38, 87). Additionally, 6-phosphogluconate dehydrogenase (6PGD) is also considered a key point. YTHDF2 binds to 6PGD mRNA and promotes its translation, while 6PGD deficiency can lead to lower blood cholesterol making YTHDF2 a possible target for lowering blood cholesterol (103–105). Moreover, very recent research mentioned that the METTL14 mediating lncRNA zinc finger antisense 1/ras-related protein rab-22a (ZFAS1/RAB22a) m6A methylation modification is also a possible pathway to atherosclerosis (88).

Conclusion and discussion

After decades of research, RNA m6A methylation remains a broad research space that structures functions and regulation mechanisms of many regulators remain critical and unknown (106). RNA m6A methylation is an important and novel regulatory manner in epigenetics. It has a regulatory role in adipogenicity differentiation and adipogenesis in adipose tissue (107, 108). In addition, it also exerts vital functions in lipid metabolism, which is interwoven with human health. A greater understanding of the regulatory mechanism of lipid metabolism also leads to advances in life science research.

In the process of RNA m6A methylation regulating the lipid metabolism, the m6A "writers", "erasers", and "readers" can add, remove, or recognize the RNA m6A methylation sites in mRNA and affect its translation, decay, splicing, and export, leading to thousands of biological processes (109). Inflammation is one of the parts, and it has proved closely connected with obesity and fatty acid absorption (110, 111). In the process of RNA m6A methylation regulating lipid metabolism, IL-6, CCL2, IRX3, TRAF6, and many inflammation factors-related proteins become the central regulatory targets. The lipid synthesis and decomposition genes such as FASN, SREBP, and CES2 (112) are also affected by mRNA m6A methylation and demethylation. Lipogenesis and lipolysis are directly regulated. In addition, some other cell signaling pathways are also involved. The regulation of RNA m6A methylation is a complex process that involves a variety of mechanisms in multiple cells. Research in this area still has much to be done.

Disorder of the global or partial lipid metabolism causes intractable chronic diseases. In the occurrence and development of NAFLD, abnormal lipid accumulation in hepatocytes is one of the major pathological changes, and METTL3, METTL14, FTO, and YTHDF mediated key gene mRNA m6A methylation are all related to it. Furthermore, lipid metabolism disorder is responsible for insulin resistance, hyperlipidemia, and atherosclerosis (113), in which RNA m6A methylation all plays a critical part, making it a great potential therapeutic target.

At the present stage, further research on m6A mRNA methylation in its effective metabolism is needed. Many studies remain controversial, and m6A mRNA methylation

may affect the expression of mRNA or protein levels of different key positive or negative regulatory factors in different pathophysiological processes, so, likely, the "Writer", "Eraser", and "Reader" of the same RNA m6A methylation regulators may coregulate two pathophysiological processes with opposite effects. Moreover, future studies on the regulatory mechanism of m6A mRNA methylation on adipose metabolism should not be limited to METTL3, FTO, and YTHDF2, and other "Writer", "Eraser", and "Reader" of m6A mRNA methylation may also participate in the occurrence of lipid metabolism through different pathways while researches remain limited. In summary, RNA m6A methylation regulates many targets, including lipid synthesis, breakdown, as well as accumulation. Moreover, RNA m6A methylation has the therapeutic potential to be a target for metabolic diseases like obesity, NAFLD, and diabetes which will foster the treatment of them and related diseases better in humans in the future.

Author contributions

YF conceived the study and designed the study protocol. YTW and YJW conducted the literature review and drafted the manuscript. TS and JG reviewed the manuscript for intellectual content, and XG made revisions as needed. All authors contributed to the article and approved the submitted version.

Funding

This work was supported by the National Natural Science Foundation of China (Grant numbers 82070838 to FY, 82170831 to GX), National Tutorial System Training Project for Youth Key Talents in the Suzhou Health system(Grant numbers Qngg2021007 to FY), Project of medical application of nuclear technology in discipline construction(Grant numbers XKTJ-HRC2021007 to GX).

Conflict of interest

The authors declare that the research was conducted in the absence of any commercial or financial relationships that could be construed as a potential conflict of interest.

Publisher's note

All claims expressed in this article are solely those of the authors and do not necessarily represent those of their affiliated organizations, or those of the publisher, the editors and the reviewers. Any product that may be evaluated in this article, or claim that may be made by its manufacturer, is not guaranteed or endorsed by the publisher.

References

1. Gohlke S, Zagoriy V, Cuadros Inostroza A, Méret M, Mancini C, Japtok L, et al. Identification of functional lipid metabolism biomarkers of brown adipose tissue aging. *Mol Metab* (2019) 24:1–17. doi: 10.1016/j.molmet.2019.03.011

2. Cheng L, Zhang S, Shang F, Ning Y, Huang Z, He R, et al. Emodin improves glucose and lipid metabolism disorders in obese mice *via* activating brown adipose tissue and inducing browning of white adipose tissue. *Front Endocrinol (Lausanne)* (2021) 12:618037. doi: 10.3389/fendo.2021.618037

3. Wang QA, Tao C, Gupta RK, Scherer PE. Tracking adipogenesis during white adipose tissue development, expansion and regeneration. *Nat Med* (2013) 19:1338–44. doi: 10.1038/nm.3324

4. Tóth BB, Arianti R, Shaw A, Vámos A, Veréb Z, Póliska S, et al. FTO intronic SNP strongly influences human neck adipocyte browning determined by tissue and PPARγ specific regulation: A transcriptome analysis. *Cells* (2020) 9:987. doi: 10.3390/cells9040987

5. Zhang Y, Ma KL, Ruan XZ, Liu BC. Dysregulation of the low-density lipoprotein receptor pathway is involved in lipid disorder-mediated organ injury. *Int J Biol Sci* (2016) 12:569–79. doi: 10.7150/ijbs.14027

6. Watt MJ, Miotto PM, De Nardo W, Montgomery MK. The liver as an endocrine organ-linking NAFLD and insulin resistance. *Endocr Rev* (2019) 40:1367–93. doi: 10.1210/er.2019-00034

7. Xenoulis PG, Steiner JM. Lipid metabolism and hyperlipidemia in dogs. *Vet J* (2010) 183:12–21. doi: 10.1016/j.tvjl.2008.10.011

8. Deprince A, Haas JT, Staels B. Dysregulated lipid metabolism links NAFLD to cardiovascular disease. *Mol Metab* (2020) 42:101092. doi: 10.1016/j.molmet.2020.101092

9. Aryal B, Price NL, Suarez Y, Fernández-Hernando C. ANGPTL4 in metabolic and cardiovascular disease. *Trends Mol Med* (2019) 25:723–34. doi: 10.1016/j.molmed.2019.05.010

10. Zakaria Z, Othman ZA, Nna VU, Mohamed M. The promising roles of medicinal plants and bioactive compounds on hepatic lipid metabolism in the treatment of non-alcoholic fatty liver disease in animal models: molecular targets. *Arch Physiol Biochem* (2021) 21, 1–17. doi: 10.1080/13813455.2021.1939387

11. Zhang Y, Geng X, Li Q, Xu J, Tan Y, Xiao M, et al. m6A modification in RNA: biogenesis, functions and roles in gliomas. *J Exp Clin Cancer Res* (2020) 39:192. doi: 10.1186/s13046-020-01706-8

12. Chen M, Nie ZY, Wen XH, Gao YH, Cao H, Zhang SF, et al. m6A RNA methylation regulators can contribute to malignant progression and impact the prognosis of bladder cancer. *Biosci Rep* (2019) 39:BSR20192892. doi: 10.1042/BSR20192892

13. Li J, Pei Y, Zhou R, Tang Z, Yang Y. Regulation of RNA N(6)-methyladenosine modification and its emerging roles in skeletal muscle development. *Int J Biol Sci* (2021) 17:1682–92. doi: 10.7150/ijbs.56251

14. Du Y, Ma Y, Zhu Q, Liu T, Jiao Y, Yuan P, et al. An m6A-related prognostic biomarker associated with the hepatocellular carcinoma immune microenvironment. *Front Pharmacol* (2021) 12:707930. doi: 10.3389/fphar.2021.707930

15. Wang Y, Zheng Y, Guo D, Zhang X, Guo S, Hui T, et al. m6A methylation analysis of differentially expressed genes in skin tissues of coarse and fine type liaoning cashmere goats. *Front Genet* (2019) 10:1318. doi: 10.3389/fgene.2019.01318

16. Yang J, Chen J, Fei X, Wang X, Wang K. N6-methyladenine RNA modification and cancer. *Oncol Lett* (2020) 20:1504–12. doi: 10.3892/ol.2020.11739

17. Feng ZY, Gao HY, Feng TD. Immune infiltrates of m(6)A RNA methylation-related lncRNAs and identification of PD-L1 in patients with primary head and neck squamous cell carcinoma. *Front Cell Dev Biol* (2021) 9:672248. doi: 10.3389/fcell.2021.672248

18. Zhang L, Chen S, Ma J, Liu Z, Liu H. REW-ISA V2: A biclustering method fusing homologous information for analyzing and mining epi-transcriptome data. *Front Genet* (2021) 12:654820. doi: 10.3389/fgene.2021.654820

19. Bai Y, Yang C, Wu R, Huang L, Song S, Li W, et al. YTHDF1 regulates tumorigenicity and cancer stem cell-like activity in human colorectal carcinoma. *Front Oncol* (2019) 9:332. doi: 10.3389/fonc.2019.00332

20. Wei CM, Gershowitz A, Moss B. Methylated nucleotides block 5' terminus of HeLa cell messenger RNA. *Cell* (1975) 4:379–86. doi: 10.1016/0092-8674(75)90158-0

21. Fu Y, Dominissini D, Rechavi G, He C. Gene expression regulation mediated through reversible m6A RNA methylation. *Nat Rev Genet* (2014) 15:293–306. doi: 10.1038/nrg3724

22. Dominissini D, Moshitch-Moshkovitz S, Schwartz S, Salmon-Divon M, Ungar L Osenberg S, Cesarkas K, et al. Topology of the human and mouse m6A RNA methylomes revealed by m6A-seq. *Nature* (2012) 485:201–6. doi: 10.1038/nature11112

23. Meyer KD, Saletore Y, Zumbo P, Elemento O, Mason CE, Jaffrey SR. Comprehensive analysis of mRNA methylation reveals enrichment in 3' UTRs and near stop codons. *Cell* (2012) 149:1635–46. doi: 10.1016/j.cell.2012.05.003

24. Sommer S, Lavi U, Darnell JEJr. The absolute frequency of labeled n-6-methyladenosine in HeLa cell messenger RNA decreases with label time. *J Mol Biol* (1978) 124:487–99. doi: 10.1016/0022-2836(78)90183-3

25. Wang X, Lu Z, Gomez A, Hon GC, Yue Y, Han D, et al. N6-methyladenosine-dependent regulation of messenger RNA stability. *Nature* (2014) 505:117–20. doi: 10.1038/nature12730

26. Zaccara S, Ries RJ, Jaffrey SR. Reading, writing and erasing mRNA methylation. *Nat Rev Mol Cell Biol* (2019) 20:608–24. doi: 10.1038/s41580-019-0168-5

27. Feng M, et al. YBX1 is required for maintaining myeloid leukemia cell survival by regulating BCL2 stability in an m6A-dependent manner. *Blood* (2021) 138:71–85. doi: 10.1182/blood.2020009676

28. Huang H, Weng H, Sun W, Qin X, Shi H, Wu H, et al. Recognition of RNA N(6)-methyladenosine by IGF2BP proteins enhances mRNA stability and translation. *Nat Cell Biol* (2018) 20:285–95. doi: 10.1038/s41556-018-0045-z

29. Wang X. N(6)-methyladenosine modulates messenger RNA translation efficiency. *Cell* (2015) 161:1388–99. doi: 10.1016/j.cell.2015.05.014

30. Liu T, Wei Q, Jin J, Luo Q, Liu Y, Yang Y, et al. The m6A reader YTHDF1 promotes ovarian cancer progression *via* augmenting EIF3C translation. *Nucleic Acids Res* (2020) 48:3816–31. doi: 10.1093/nar/gkaa048

31. Shi H, Wang X, Lu Z, Zhao BS, Ma H, Hsu PJ, et al. YTHDF3 facilitates translation and decay of N(6)-methyladenosine-modified RNA. *Cell Res* (2017) 27:315–28. doi: 10.1038/cr.2017.15

32. Roundtree IA, Luo GZ, Zhang Z, Wang X, Zhou T, Cui Y, et al. YTHDC1 mediates nuclear export of N(6)-methyladenosine methylated mRNAs. *Elife* (2017) 6:BSR20192892. doi: 10.7554/eLife.31311

33. Sun T, Wu R, Ming L. The role of m6A RNA methylation in cancer. *BioMed Pharmacother* (2019) 112:108613. doi: 10.1016/j.biopha.2019.108613

34. Liu N, Pan T. N6-methyladenosine–encoded epitranscriptomics. *Nat Struct Mol Biol* (2016) 23:98–102. doi: 10.1038/nsmb.3162

35. Liu N, Zhou KI, Parisien M, Dai Q, Diatchenko L, Pan T, et al. N6-methyladenosine alters RNA structure to regulate binding of a low-complexity protein. *Nucleic Acids Res* (2017) 45:6051–63. doi: 10.1093/nar/gkx141

36. Bokar JA, Shambaugh ME, Polayes D, Matera AG, Rottman FM. Purification and cDNA cloning of the AdoMet-binding subunit of the human mRNA (N6-adenosine)-methyltransferase. *Rna* (1997) 3:1233–47.

37. Ping XL, Sun BF, Wang L, Xiao W, Yang X, Wang WJ, et al. Mammalian WTAP is a regulatory subunit of the RNA N6-methyladenosine methyltransferase. *Cell Res* (2014) 24:177–89. doi: 10.1038/cr.2014.3

38. Zhong H, Tang HF, Kai Y. N6-methyladenine RNA modification (m(6)A): An emerging regulator of metabolic diseases. *Curr Drug Targets* (2020) 21:1056–67. doi: 10.2174/1389450121666200210125247

39. Yang Z, Yu GL, Zhu X, Peng TH, Lv YC. Critical roles of FTO-mediated mRNA m6A demethylation in regulating adipogenesis and lipid metabolism: Implications in lipid metabolic disorders. *Genes Dis* (2022) 9:51–61. doi: 10.1016/j.gendis.2021.01.005

40. Su R, Dong L, Li Y, Gao M, Han L, Wunderlich M , et al. Targeting FTO suppresses cancer stem cell maintenance and immune evasion. *Cancer Cell* (2020) 38:79–96.e11. doi: 10.1016/j.ccell.2020.04.017

41. Zhao X, Yang Y, Sun BF, Zhao YL, Yang YG. FTO and obesity: mechanisms of association. *Curr Diabetes Rep* (2014) 14:486. doi: 10.1007/s11892-014-0486-0

42. Jia G, Fu Y, Zhao X, Dai Q, Zheng G, Yang Y, et al. N6-methyladenosine in nuclear RNA is a major substrate of the obesity-associated FTO. *Nat Chem Biol* (2011) 7:885–7. doi: 10.1038/nchembio.687

43. Zheng G, Dahl JA, Niu Y, Fu Y, Klungland A, Yang YG, et al. Sprouts of RNA epigenetics: The discovery of mammalian RNA demethylases. *RNA Biol* (2013) 10:915–8. doi: 10.4161/rna.24711

44. Bian X, Liu R, Meng Y, Xing D, Xu D, Lu Z, et al. Lipid metabolism and cancer. *J Exp Med* (2021) 218:e20201606. doi: 10.1084/jem.20201606

45. Röhrig F, Schulze A. The multifaceted roles of fatty acid synthesis in cancer. *Nat Rev Cancer* (2016) 16:732–49. doi: 10.1038/nrc.2016.89

46. Li Y, Zhang Q, Cui G, Zhao F, Tian X, Sun BF, et al. m(6)A regulates liver metabolic disorders and hepatogenous diabetes. *Genomics Proteomics Bioinf* (2020) 18:371–83. doi: 10.1016/j.gpb.2020.06.003

47. Xu Z, Qin Y, Lv B, Tian Z, Zhang B. Intermittent fasting improves high-fat diet-induced obesity cardiomyopathy *via* alleviating lipid deposition and apoptosis and decreasing m6A methylation in the heart. *Nutrients* (2022) 14:251. doi: 10.3390/nu14020251

48. Xie W, Ma LL, Xu YQ, Wang BH, Li SM. METTL3 inhibits hepatic insulin sensitivity *via* N6-methyladenosine modification of fasn mRNA and promoting fatty acid metabolism. *Biochem Biophys Res Commun* (2019) 518:120–6. doi: 10.1016/j.bbrc.2019.08.018

49. Yang Y, Cai J, Yang X, Wang K, Sun K, Yang Z, et al. Dysregulated m6A modification promotes lipogenesis and development of non-alcoholic fatty liver disease and hepatocellular carcinoma. *Mol Ther* (2022) 30:2342–53. doi: 10.1016/j.ymthe.2022.02.021

50. Zhong X, Yu J, Frazier K, Weng X, Li Y, Cham CM, et al. Circadian clock regulation of hepatic lipid metabolism by modulation of m(6)A mRNA methylation. *Cell Rep* (2018) 25:1816–1828.e1814. doi: 10.1016/j.celrep.2018.10.068

51. Zong X, Zhao J, Wang H, Lu Z, Wang F, Du H, et al. Mettl3 deficiency sustains long-chain fatty acid absorption through suppressing Traf6-dependent inflammation response. *J Immunol* (2019) 202:567–78. doi: 10.4049/jimmunol.1801151

52. Desrosiers R, Friderici K, Rottman F. Identification of methylated nucleosides in messenger RNA from novikoff hepatoma cells. *Proc Natl Acad Sci U.S.A.* (1974) 71:3971–5. doi: 10.1073/pnas.71.10.3971

53. Qin Y, Li L, Luo E, Hou J, Yan G, Wang D, et al. Role of m6A RNA methylation in cardiovascular disease (Review). *Int J Mol Med* (2020) 46:1958–72. doi: 10.3892/ijmm.2020.4746

54. Chen M, Wong CM. The emerging roles of N6-methyladenosine (m6A) deregulation in liver carcinogenesis. *Mol Cancer* (2020) 19:44. doi: 10.1186/s12943-020-01172-y

55. Tews D, Fischer-Posovszky P, Wabitsch M. Regulation of FTO and FTM expression during human preadipocyte differentiation. *Horm Metab Res* (2011) 43:17–21. doi: 10.1055/s-0030-1265130

56. Czogała W, Czogała M, Strojny W, Wątor G, Wołkow P, Wójcik M, et al. Methylation and expression of FTO and PLAG1 genes in childhood obesity: Insight into anthropometric parameters and glucose-lipid metabolism. *Nutrients* (2021) 13:1683. doi: 10.3390/nu13051683

57. Kang H, Zhang Z, Yu L, Li Y, Liang M, Zhou L, et al. FTO reduces mitochondria and promotes hepatic fat accumulation through RNA demethylation. *J Cell Biochem* (2018) 119:5676–85. doi: 10.1002/jcb.26746

58. Wu R, Liu Y, Yao Y, Zhao Y, Bi Z, Jiang Q, et al. FTO regulates adipogenesis by controlling cell cycle progression *via* m(6)A-YTHDF2 dependent mechanism. *Biochim Biophys Acta Mol Cell Biol Lipids* (2018) 1863:1323–30. doi: 10.1016/j.bbalip.2018.08.008

59. Huang Y, Su R, Sheng Y, Dong L, Dong Z, Xu H, et al. Small-molecule targeting of oncogenic FTO demethylase in acute myeloid leukemia. *Cancer Cell* (2019) 35:677–691.e610. doi: 10.1016/j.ccell.2019.03.006

60. Hu Y, Feng Y, Zhang L, Jia Y, Cai D, Qian SB, et al. GR-mediated FTO transactivation induces lipid accumulation in hepatocytes *via* demethylation of m(6)A on lipogenic mRNAs. *RNA Biol* (2020) 17:930–42. doi: 10.1080/15476286.2020.1736868

61. Sun L, Gao M, Qian Q, Guo Z, Zhu P, Wang X, et al. Triclosan-induced abnormal expression of miR-30b regulates fto-mediated m(6)A methylation level to cause lipid metabolism disorder in zebrafish. *Sci Total Environ* (2021) 770:145285. doi: 10.1016/j.scitotenv.2021.145285

62. Sun D, Zhao T, Zhang Q, Wu M, Zhang Z. Fat mass and obesity-associated protein regulates lipogenesis *via* m(6) a modification in fatty acid synthase mRNA. *Cell Biol Int* (2021) 45:334–44. doi: 10.1002/cbin.11490

63. Yoshida K, Shimizugawa T, Ono M, Furukawa H. Angiopoietin-like protein 4 is a potent hyperlipidemia-inducing factor in mice and inhibitor of lipoprotein lipase. *J Lipid Res* (2002) 43:1770–2. doi: 10.1194/jlr.C200010-JLR200

64. Dijk W, Kersten S. Regulation of lipoprotein lipase by Angptl4. *Trends Endocrinol Metab* (2014) 25:146–55. doi: 10.1016/j.tem.2013.12.005

65. Wang CY, Shie SS, Wen MS, Hung KC, Hsieh IC, Yeh TS, et al. Loss of FTO in adipose tissue decreases Angptl4 translation and alters triglyceride metabolism. *Sci Signal* (2015) 8:ra127. doi: 10.1126/scisignal.aab3357

66. Terra X, Auguet T, Porras JA, Quintero Y, Aguilar C, Luna AM, et al. Anti-inflammatory profile of FTO gene expression in adipose tissues from morbidly obese women. *Cell Physiol Biochem* (2010) 26:1041–50. doi: 10.1159/000323979

67. Zeng B, Wu R, Chen Y, Chen W, Liu Y, Liao X, et al. FTO knockout in adipose tissue effectively alleviates hepatic steatosis partially *via* increasing the secretion of adipocyte-derived IL-6. *Gene* (2022) 818:146224. doi: 10.1016/j.gene.2022.146224

68. Mizuno TM. Fat mass and obesity associated (FTO) gene and hepatic glucose and lipid metabolism. *Nutrients* (2018) 10:1600. doi: 10.3390/nu10111600

69. de Araújo TM, Velloso LA. Hypothalamic IRX3: A new player in the development of obesity. *Trends Endocrinol Metab* (2020) 31:368–77. doi: 10.1016/j.tem.2020.01.002

70. Yao J, Wu D, Zhang C, Yan T, Zhao Y, Shen H., et al. Macrophage IRX3 promotes diet-induced obesity and metabolic inflammation. *Nat Immunol* (2021) 22:1268–79. doi: 10.1038/s41590-021-01023-y

71. Smemo S, Tena JJ, Kim KH, Gamazon ER, Sakabe NJ, Gómez-Marín C, et al. Obesity-associated variants within FTO form long-range functional connections with IRX3. *Nature* (2014) 507:371–5. doi: 10.1038/nature13138

72. Zhao L, Zhang C, Luo X, Wang P, Zhou W, Zhong S, et al. CD36 palmitoylation disrupts free fatty acid metabolism and promotes tissue inflammation in non-alcoholic steatohepatitis. *J Hepatol* (2018) 69:705–17. doi: 10.1016/j.jhep.2018.04.006

73. Jeppesen J, Albers PH, Rose AJ, Birk JB, Schjerling P, Dzamko N, et al. Contraction-induced skeletal muscle FAT/CD36 trafficking and FA uptake is AMPK independent. *J Lipid Res* (2011) 52:699–711. doi: 10.1194/jlr.M007138

74. Wu W, Wang S, Liu Q, Shan T, Wang X, Feng J, et al. AMPK facilitates intestinal long-chain fatty acid uptake by manipulating CD36 expression and translocation. *FASEB J* (2020) 34:4852–69. doi: 10.1096/fj.201901994R

75. Zhou X, Chen J, Chen J, Wu W, Wang X, Wang Y, et al. The beneficial effects of betaine on dysfunctional adipose tissue and N6-methyladenosine mRNA methylation requires the AMP-activated protein kinase α1 subunit. *J Nutr Biochem* (2015) 26:1678–84. doi: 10.1016/j.jnutbio.2015.08.014

76. Boulangé CL, Neves AL, Chilloux J, Nicholson JK, Dumas ME. Impact of the gut microbiota on inflammation, obesity, and metabolic disease. *Genome Med* (2016) 8:42. doi: 10.1186/s13073-016-0303-2

77. McGarry JD, Mannaerts GP, Foster DW. A possible role for malonyl-CoA in the regulation of hepatic fatty acid oxidation and ketogenesis. *J Clin Invest* (1977) 60:265–70. doi: 10.1172/JCI108764

78. McDonnell E, Crown SB, Fox DB, Kitir B, Ilkayeva OR, Olsen CA, et al. Lipids reprogram metabolism to become a major carbon source for histone acetylation. *Cell Rep* (2016) 17:1463–72. doi: 10.1016/j.celrep.2016.10.012

79. Qin Y, Li B, Arumugam S, Lu Q, Mankash SM, Li J, et al. m(6)A mRNA methylation-directed myeloid cell activation controls progression of NAFLD and obesity. *Cell Rep* (2021) 37:109968. doi: 10.1016/j.celrep.2021.109968

80. Peng Z, Gong Y, Wang X, He W, Wu L, Zhang L, et al. METTL3-m(6)A-Rubicon axis inhibits autophagy in nonalcoholic fatty liver disease. *Mol Ther* (2021). doi: 10.1016/j.ymthe.2021.09.016

81. Li X, Yuan B, Lu M, Wang Y, Ding N, Liu C, et al. The methyltransferase METTL3 negatively regulates nonalcoholic steatohepatitis (NASH) progression. *Nat Commun* (2021) 12:7213. doi: 10.1038/s41467-021-27539-3

82. Chen A, Chen X, Cheng S, Shu L, Yan M, Yao L, et al. FTO promotes SREBP1c maturation and enhances CIDEC transcription during lipid accumulation in HepG2 cells. *Biochim Biophys Acta Mol Cell Biol Lipids* (2018) 1863:538–48. doi: 10.1016/j.bbalip.2018.02.003

83. Simon Y, Kessler SM, Bohle RM, Haybaeck J, Kiemer AK. The insulin-like growth factor 2 (IGF2) mRNA-binding protein p62/IGF2BP2-2 as a promoter of NAFLD and HCC? *Gut* (2014) 63:861–3. doi: 10.1136/gutjnl-2013-305736

84. Li Z, Liu X, Li S, Wang Q, Di Chen . The LINC01138 drives malignancies *via* activating arginine methyltransferase 5 in hepatocellular carcinoma. *Nat Commun* (2018) 9:1572. doi: 10.1038/s41467-018-04006-0

85. Chen M, Wei L, Law CT, Tsang FH, Shen J, Cheng CL, et al. RNA N6-methyladenosine methyltransferase-like 3 promotes liver cancer progression through YTHDF2-dependent posttranscriptional silencing of SOCS2. *Hepatology* (2018) 67:2254–70. doi: 10.1002/hep.29683

86. Zhou B, et al. N(6) -methyladenosine reader protein YT521-b homology domain-containing 2 suppresses liver steatosis by regulation of mRNA stability of lipogenic genes. *Hepatology* (2021) 73:91–103. doi: 10.1002/hep.31220

87. Zhang Y, Guo F, Zhao R. Hepatic expression of FTO and fatty acid metabolic genes changes in response to lipopolysaccharide with alterations in m(6)A modification of relevant mRNAs in the chicken. *Br Poult Sci* (2016) 57:628–35. doi: 10.1080/00071668.2016.1201199

88. Gong C, Fan Y, Liu J. METTL14 mediated m6A modification to LncRNA ZFAS1/ RAB22A: A novel therapeutic target for atherosclerosis. *Int J Cardiol* (2021) 328:177. doi: 10.1016/j.ijcard.2020.12.002

89. Guo J, Ren W, Li A, Ding Y, Guo W, Su D, et al. Fat mass and obesity-associated gene enhances oxidative stress and lipogenesis in nonalcoholic fatty liver disease. *Dig Dis Sci* (2013) 58:1004–9. doi: 10.1007/s10620-012-2516-6

90. Chen J, Zhou X, Wu W, Wang X, Wang Y. FTO-dependent function of N6-methyladenosine is involved in the hepatoprotective effects of betaine on adolescent mice. *J Physiol Biochem* (2015) 71:405–13. doi: 10.1007/s13105-015-0420-1

91. Sun L, Ling Y, Jiang J, Wang D, Wang J, Li J, et al. Differential mechanisms regarding triclosan vs. bisphenol a and fluorene-9-bisphenol induced zebrafish lipid-metabolism disorders by RNA-seq. *Chemosphere* (2020) 251:126318. doi: 10.1016/j.chemosphere.2020.126318

92. Heng J, Wu Z, Tian M, Chen J, Song H, Chen F, et al. Excessive BCAA regulates fat metabolism partially through the modification of m(6)A RNA methylation in weanling piglets. *Nutr Metab (Lond)* (2020) 17:10. doi: 10.1186/s12986-019-0424-x

93. Zhao Z, et al. Epitranscriptomics in liver disease: Basic concepts and therapeutic potential. *J Hepatol* (2020) 73:664–79. doi: 10.1016/j.jhep.2020.04.009

94. Eslam M, Valenti L, Romeo S. Genetics and epigenetics of NAFLD and NASH: Clinical impact. *J Hepatol* (2018) 68:268–79. doi: 10.1016/j.jhep.2017.09.003

95. Chatterjee S, Khunti K, Davies MJ. Type 2 diabetes. *Lancet* (2017) 389:2239–51. doi: 10.1016/S0140-6736(17)30058-2

96. Vijan S. In the clinic. type 2 diabetes. *Ann Intern Med* (2015) 162:Itc1–16. doi: 10.7326/AITC201503030

97. De Jesus DF, Zhang Z, Kahraman S, Brown NK, Chen M, Hu J, et al. m(6)A mRNA methylation regulates human β-cell biology in physiological states and in type 2 diabetes. *Nat Metab* (2019) 1:765–74. doi: 10.1038/s42255-019-0089-9

98. Yang Y, Shen F, Huang W, Qin S, Huang JT, Sergi C, et al. Glucose is involved in the dynamic regulation of m6A in patients with type 2 diabetes. *J Clin Endocrinol Metab* (2019) 104:665–73. doi: 10.1210/jc.2018-00619

99. Menendez JA, Vazquez-Martin A, Ortega FJ, Fernandez-Real JM. Fatty acid synthase: association with insulin resistance, type 2 diabetes, and cancer. *Clin Chem* (2009) 55:425–38. doi: 10.1373/clinchem.2008.115352

100. Zhao D, Liu J, Wang M, Zhang X, Zhou M. Epidemiology of cardiovascular disease in China: current features and implications. *Nat Rev Cardiol* (2019) 16:203–12. doi: 10.1038/s41569-018-0119-4

101. Gazzola K, Reeskamp L, van den Born BJ. Ethnicity, lipids and cardiovascular disease. *Curr Opin Lipidol* (2017) 28:225–30. doi: 10.1097/MOL.0000000000000412

102. Mo X, Lei S, Zhang Y, Zhang H. Genome-wide enrichment of m(6)A-associated single-nucleotide polymorphisms in the lipid loci. *Pharmacogenomics J* (2019) 19:347–57. doi: 10.1038/s41397-018-0055-z

103. Sheng H, Li Z, Su S, Sun W, Zhang X, Li L, et al. YTH domain family 2 promotes lung cancer cell growth by facilitating 6-phosphogluconate dehydrogenase mRNA translation. *Carcinogenesis* (2020) 41:541–50. doi: 10.1093/carcin/bgz152

104. Batetta B, Bonatesta RR, Sanna F, Putzolu M, Mulas MF, Collu M, et al. Cell growth and cholesterol metabolism in human glucose-6-phosphate dehydrogenase deficient lymphomononuclear cells. *Cell Prolif* (2002) 35:143–54. doi: 10.1046/j.1365-2184.2002.00231.x

105. Zheng N. Research progress of N6-methyladenosine in the cardiovascular system. *Signal Transduct Target Ther* (2020) 26:. doi: 10.12659/MSM.921742

106. Jiang X, Liu B, Nie Z, Duan L, Xiong Q, Jin Z, et al. The role of m6A modification in the biological functions and diseases. *Signal Transduct Target Ther* (2021) 6:74. doi: 10.1038/s41392-020-00450-x

107. Song T, Yang Y, Wei H, Xie X, Lu J, Zeng Q, et al. Zfp217 mediates m6A mRNA methylation to orchestrate transcriptional and post-transcriptional regulation to promote adipogenic differentiation. *Nucleic Acids Res* (2019) 47:6130–44. doi: 10.1093/nar/gkz312

108. Song T, Yang Y, Jiang S, Peng J. Novel insights into adipogenesis from the perspective of transcriptional and RNA N6-Methyladenosine-Mediated post-transcriptional regulation. *Adv Sci (Weinh)* (2020) 7:2001563. doi: 10.1002/advs.202001563

109. Wu S, Zhang S, Wu X, Zhou X. m(6)A RNA methylation in cardiovascular diseases. *Mol Ther* (2020) 28:2111–9. doi: 10.1016/j.ymthe.2020.08.010

110. Vogel A, Brunner JS, Hajto A, Sharif O, Schabbauer G. Lipid scavenging macrophages and inflammation. *Biochim Biophys Acta Mol Cell Biol Lipids* (2022) 1867:159066. doi: 10.1016/j.bbalip.2021.159066

111. Cox AJ, West NP, Cripps AW. Obesity, inflammation, and the gut microbiota. *Lancet Diabetes Endocrinol* (2015) 3:207–15. doi: 10.1016/S2213-8587(14)70134-2

112. Takemoto S, Nakano M, Fukami T, Nakajima M. m(6)A modification impacts hepatic drug and lipid metabolism properties by regulating carboxylesterase 2. *Biochem Pharmacol* (2021) 193:114766. doi: 10.1016/j.bcp.2021.114766

113. Bäck M, Yurdagul AJr., Tabas I, Öörni K, Kovanen PT. Inflammation and its resolution in atherosclerosis: mediators and therapeutic opportunities. *Nat Rev Cardiol* (2019) 16:389–406. doi: 10.1038/s41569-019-0169-2

Advantages of publishing in Frontiers

OPEN ACCESS
Articles are free to read for greatest visibility and readership

FAST PUBLICATION
Around 90 days from submission to decision

HIGH QUALITY PEER-REVIEW
Rigorous, collaborative, and constructive peer-review

TRANSPARENT PEER-REVIEW
Editors and reviewers acknowledged by name on published articles

Frontiers
Avenue du Tribunal-Fédéral 34
1005 Lausanne | Switzerland

Visit us: www.frontiersin.org
Contact us: frontiersin.org/about/contact

REPRODUCIBILITY OF RESEARCH
Support open data and methods to enhance research reproducibility

DIGITAL PUBLISHING
Articles designed for optimal readership across devices

FOLLOW US
@frontiersin

IMPACT METRICS
Advanced article metrics track visibility across digital media

EXTENSIVE PROMOTION
Marketing and promotion of impactful research

LOOP RESEARCH NETWORK
Our network increases your article's readership